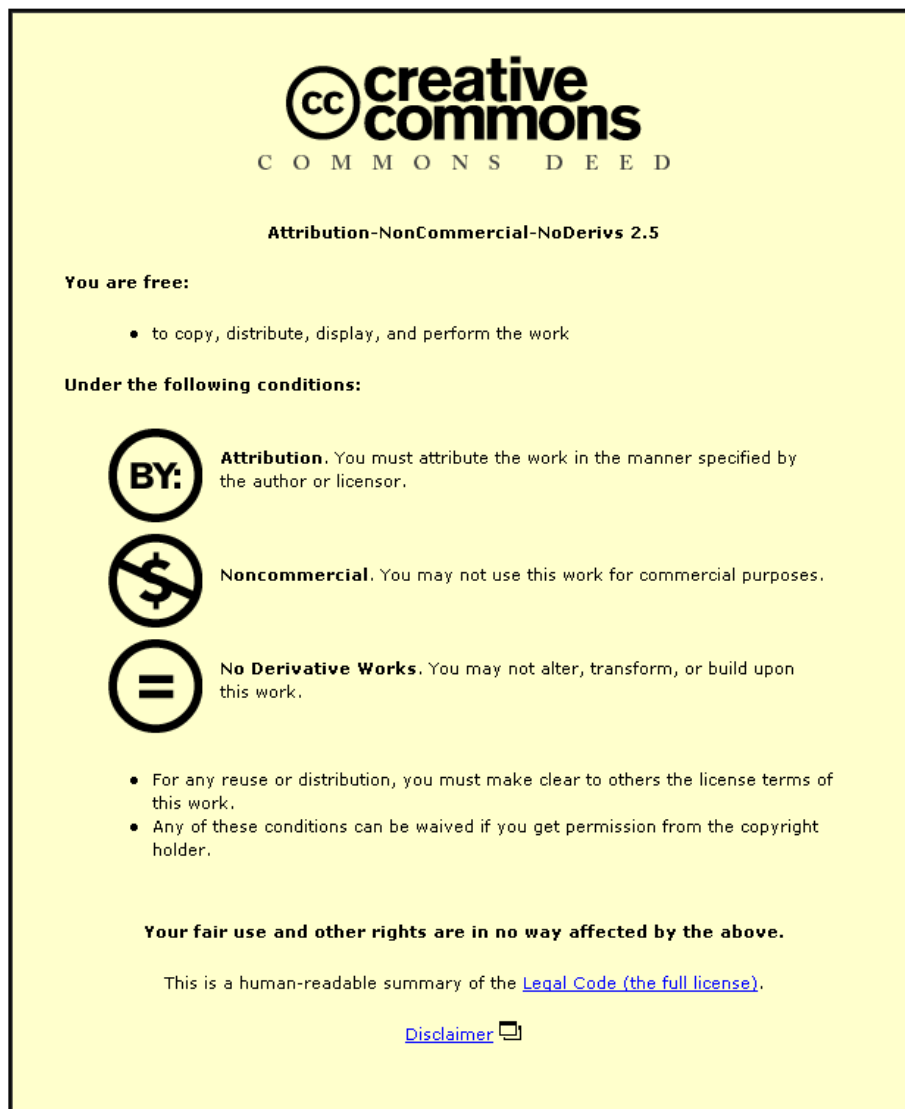


This item was submitted to Loughborough University as a PhD thesis by the author and is made available in the Institutional Repository (<https://dspace.lboro.ac.uk/>) under the following Creative Commons Licence conditions.



For the full text of this licence, please go to:  
<http://creativecommons.org/licenses/by-nc-nd/2.5/>

BLLID No: D 31055/80

LOUGHBOROUGH  
UNIVERSITY OF TECHNOLOGY  
LIBRARY

AUTHOR/FILING TITLE

SILVA-NIETO, R

ACCESSION/COPY NO.

113696/02

VOL. NO.

CLASS MARK

~~1 JUL 1981~~

LOAN COPY

09 MAR 82

~~10 MAR 82~~

- 6 JUL 1990

15 MAR 85

- 5 JUL 1991

03 MAY 83

03

29 JUL 1991

11 OCT 1991

0113696 02





PREDICTION AND CHARACTERIZATION  
OF COMPRESSION MOULD FLOW  
FOR UNSATURATED POLYESTER  
RESIN SHEET MOULDING COMPOUND

by

Roberto Javier Silva-Nieto  
Institute of Polymer Technology 1980

A thesis submitted in partial fulfilment of the requirements for  
the award of Doctor of Philosophy of the  
Loughborough University of Technology

January 1980

Director of Research: Professor B Downs  
Department of Mechanical Engineering  
Supervisors: Professor A W Birley  
Director, Institute of Polymer Technology  
Dr. B C Fisher  
Department of Mechanical Engineering

Loughborough University of Technology Library	
Date	Mar 80
Class	
Acc. No.	113696/02

Certificate of Originality

This is to certify that I am responsible for the work submitted in this thesis, that the original work is my own except as specified in acknowledgements or in footnotes, and that neither the thesis nor the original work contained therein has been submitted to this or any other institution for a higher degree.

## SUMMARY

During the past twenty years there has been considerable interest in developing the technology for manufacturing engineering articles from sheet moulding compound (SMC) by compression moulding. Some of the problems with this technology are associated with the flow of SMC during moulding.

This research work proposes methods for characterising the rheological behaviour of SMC and predicting the shape of charges for moulding articles free of weld-lines without substantially altering the initial fibre orientation of the matrix.

The theoretical development of the charge shape prediction procedure for moulding symmetrical and unsymmetrical plates includes a mathematical model of the compression flow process, which is used to determine flow front development, and mould cavity pressure and velocity distributions. The mathematical model assumes a Newtonian flow behaviour.

An instrumented mould was designed, manufactured and used to test the mathematical model of the compression flow process. The analysis of the experimental work includes: moulding conditions (such as mould cavity pressure, platen displacement and ram-force); fibre orientation measurements (using X-ray techniques); quantification of fibre glass distribution by chemical methods; and, material mechanical properties (e.g. tensile strength). There was good agreement between the theoretical and experimental results for moulded symmetrical and unsymmetrical plates.

A theoretical and experimental analysis of the rheological behaviour of SMC was carried out as a second stage of the research work to test the validity of the Newtonian flow assumption. The work analyses squeeze flow of SMC discs with the aim of obtaining a better understanding of the basic rheological behaviour of SMC during compression moulding.

The theoretical analysis treats the SMC as a viscoelastic material having an equation of state with equal viscous, elastic and yield strain components. The time variation of compression force when squeezing the SMC discs between two parallel plates (one fixed and one mobile) has been derived from the equation of state. The values of the elastic, viscous and yield components were determined by using a least-squares method of curve fitting to the experimental results.

The last part of the research work includes the application of the charge shape prediction procedure to mould an engineering article under industrial compression-moulding conditions. The results of this practical application of the theory are discussed.

## ACKNOWLEDGEMENTS

The author wishes to acknowledge:

- ICI Petrochemicals Division and the Science Research Council for their financial support
- Dr B C Fisher for his supervision and helpful advice on this work
- Professor A W Birley, Director of the Institute of Polymer Technology, for his encouragement during this work
- The technical staff involved in the manufacture of the mould and instrumentation
- BTR-Permal RP Ltd for the material supplied and facilities provided for the case study applications
- John J Morris (ICI Petrochemicals Division) for his helpful comments

Finally, the author gives a special recognition to his wife Lety, who supported him during the development of this work in spite of the difficulties which arose.

TABLE OF CONTENTS

	Page No
SUMMARY .....	i
ACKNOWLEDGEMENTS .....	iii
TABLE OF CONTENTS .....	iv
NOTATION .....	vii
CHAPTER 1: INTRODUCTION .....	1
CHAPTER 2: DEVELOPMENT OF SMC - THE STATE OF THE ART	4
2.1 SMC Manufacture .....	4
2.2 SMC Chemistry .....	6
CHAPTER 3: DESIGNING WITH SMC - THE STATE OF THE ART	14
3.1 Introduction .....	14
3.2 Strength and Form Design .....	14
3.3 SMC Rheology .....	18
3.4 Moulding Production Problems .....	23
3.5 Design Applications .....	31
CHAPTER 4: RHEOLOGICAL CHARACTERIZATION OF SMC .....	35
4.1 Introduction .....	35
4.2 Equation of State .....	36
4.3 Compression Force General Analysis	39
4.4 Final Equation .....	46
CHAPTER 5: EXPERIMENTAL WORK ON RHEOLOGY .....	47
5.1 Experimental Work .....	47
5.2 Determination of Material Parameters for 20°C Tests .....	67
5.3 Discussion of Results .....	69
CHAPTER 6: THEORY FOR TWO-DIMENSIONAL COMPRESSION- MOULD FLOW .....	76
6.1 Introduction .....	76

	Page No
6.2 Flow Theory for Compression Moulding	78
6.3 Assumptions .....	79
6.4 Theoretical Analysis .....	81
6.5 Boundary Conditions .....	85
 CHAPTER 7: THE PREDICTION OF CHARGE SHAPES FOR TWO-DIMENSIONAL PRODUCTS .....	 86
7.1 Introduction .....	86
7.2 General Approach .....	86
7.3 Computer Solution .....	92
7.4 Numerical Example .....	97
 CHAPTER 8: DESIGN OF COMPRESSION-MOULD AND ASSOCIATED INSTRUMENTATION .....	 107
8.1 Introduction .....	107
8.2 Mould Design Considerations .....	107
8.3 Mould Instrumentation and Control Equipment .....	118
8.4 Calibration Procedure Before Moulding	120
 CHAPTER 9: EXPERIMENTAL WORK .....	 125
9.1 Introduction .....	125
9.2 Analysis of SMC Before Moulding ....	126
9.3 Measurements During SMC Moulding ....	129
9.4 Analysis of Moulded SMC .....	140
9.5 Discussion .....	148
 CHAPTER 10: CASE STUDY USING CHARGE SHAPE PREDICTION PROCEDURE .....	 158
10.1 Introduction .....	158
10.2 Charge Shape Prediction ..	158
10.3 Discussion of Moulding Results .....	164
10.4 Conclusions ....	171
 CHAPTER 11: GENERAL CONCLUSIONS AND FUTURE WORK .....	 172

	Page No
REFERENCES .....	174
APPENDIX 1: PROGRAM USED TO RECORD RHEOLOGY DATA (3 Channels) .....	186
APPENDIX 2: PROGRAM USED TO ANALYSE DATA ... ..	190
APPENDIX 3: SAMPLE PREPARATION FOR THE ANALYSIS OF THE CROSS-SECTION OF UNCURED SMC BY REFLECTIVE LIGHT .....	197
APPENDIX 4: COMPUTER PROGRAM FOR EVALUATING THE CHARGE SHAPE .....	198
APPENDIX 5: SAMPLE PREPARATION FOR X-RAY ANALYSIS OF THE CROSS-SECTION .....	208
APPENDIX 6: METHOD USED FOR THE EVALUATION OF FIBRE-GLASS CONTENT .....	209
APPENDIX 7: PROGRAM USED TO RECORD MOULDING DATA (20 Channels) .....	211
APPENDIX 8: USEFUL DATA CONCERNING THE WHOLE PROJECT (FOR FUTURE WORK) .....	215
APPENDIX 9: MOULD DRAWINGS .....	220
APPENDIX 10: RHEOLOGICAL DATA .....	239

NOTATIONSymbol

A	Area
D	Diameter
d	Distance along a stream-line
F	Force
f	Yield stress
$f_i$	Body forces
G	Pressure gradient
g	Acceleration due to gravity
H	Initial plate separation
h	Plate separation
$\dot{h}$	Plate speed
h	Distance between nodes
i,j,k	Unit vector in Cartesian coordinates, directions x, y, z.
K	Elasticity modulus
$K_{\alpha\beta}$	Factor of proportionality
L	A parameter which characterises flow length
n	Exponent of the power law equation
p	Pressure
R	Radius at the boundary
Re	Reynolds number
r	Radius
$T_{ij}$	Stress tensor
t	Time
U,V,W	Velocity in x, y and z directions respectively
U	Velocity along a stream-line
V	Volume
$v_i$	Velocity
x,y,z	Cartesian coordinate axes
$\gamma$	Shear strain
$\dot{\gamma}$	Shear rate
$\Delta\bar{p}$	Pressure difference
$\Delta x$	Constant interval in x direction
$\nabla$	Differential operator
$\delta_{ij}$	Kronecker delta
$\mu$	Viscosity
$\rho$	Density

$\sigma$  Normal stress  
 $\tau$  Shear stress

## CHAPTER 1

INTRODUCTION

In recent years there has been a large increase in the use of fibre reinforced polyester compounds for manufacturing engineering products. Applications in the transportation (particularly for road vehicles), business equipment and electrical appliance industries have resulted in significant replacement of the more conventional design materials (especially in the USA), and the current forecast for the fibre reinforced polyester compounds continues to be one of moderate growth.

Sheet moulding compound (SMC) is a polyester prepreg reinforced with fibre glass, chemically thickened, and manufactured as a sheet. Products are made from SMC by using matched metal compression moulds. The SMC flows during compression moulding under the action of pressure and heat, and then sets to the actual shape because of cure.

The research and development work associated with SMC technology covers a period of approximately 20 years, and some aspects of the technology have received more attention than others. There has been a large amount of SMC chemical formulation work: for example, recent developments in the use of thermoplastic additives to compensate for polymerization shrinkage during curing have been largely responsible for making possible the wide scale engineering applications of this material, where product shrink, warp and surface finish may now be controlled. Other chemical formulation work has concentrated on producing stronger and tougher SMC materials.

As a result research and development effort is tending now to concentrate on the problems associated with the engineering applications of SMC materials. These problems range from those of automating the production process (both for SMC manufacture and product moulding) to those concerned with the effects of the moulding process variables on SMC flow and finished product quality. A major need of SMC technology at the moment is for a better understanding of how mould flow affects the structural characteristics of moulded parts. The shape and position of the charge is important in determining the formation of flow faults (e.g. weld-lines), distribution of mechanical properties, and product stiffness.

The work of this thesis has been concerned with the conception and development of a method of predicting and characterizing two-dimensional compression-mould flow for an unsaturated polyester resin SMC. The SMC used in this thesis has 25% glass fibre content and 15% of low profile additive (diluted in Styrene).

Chapters 2 and 3 place this work in perspective against current knowledge for the engineering use of SMC. Chapter 2 reviews the developments in SMC chemistry and manufacture which have led to the situation where SMC is now a viable design material. Chapter 3 discusses the state of the art for designing with SMC materials, including the aspects of rheology and modelling of compression mould flow.

The *first* stage of the work (see Chapter 6) involved developing a mathematical model for SMC flow which could be applied to the compression-moulding of flat products. The aim of doing this was to be able to predict the position and shape of the charge for moulding products without weld-lines. Chapter 7 explains the charge shape prediction procedure, together with a computer procedure and a numerical example.

The experimental programme which was designed to test the validity of the charge shape prediction procedure is given in Chapters 8 and 9. Chapter 8 describes the design of a compression mould, and the associated instrumentation, for moulding plates of various shapes, while Chapter 9 presents the results of the experimental programme.

Then the procedure, which is explained in Chapter 7, was used to predict the position and geometry of the SMC charge for a commercial product, and mouldings were made in an industrial production-process situation. Chapter 10 describes the results of this case study.

Clearly mathematical assumptions about the nature of flow were necessary for the modelling of such a complex process as the compression-moulding of SMC. Thus the aim of the *second* stage of the work was to develop a better understanding of SMC flow. This work was carried out using a parallel plate plastometer. Chapter 4 develops the mathematical theory for the rheological characterization of SMC at 200°C, treating SMC as a viscoelastic material. Chapter 5 describes the experimental work which tests the theory, and in addition shows how the plastometer can give useful information related with the compression moulding process.

Thus the theme of the work in this thesis centres on the prediction and characterization of flow during the compression-moulding of SMC. Chapter 11 presents the conclusions and recommendations for further work. The work presented in this thesis is only part of an effort which is required to obtain a better understanding of how compression mould flow affects the structural characteristics for the design of SMC products.

## CHAPTER 2

DEVELOPMENT OF SMC - THE STATE OF THE ART2.1 SMC Manufacture

The development of SMC materials spans approximately 20 years, stemming from the invention in 1958 of the process to manufacture premix (L1), the first handleable polyester pre-impregnated fibre-glass material. Until then, products made in polyester resin fibre-glass reinforced materials were produced by wet-moulding techniques, involving separate applications of fibre and resin. These techniques were only suitable for producing large simple shapes, e.g. cylindrical tanks, flat trays, boat hulls etc.

Previously in 1951 and 1953, Frillette and Fisk (K2) respectively had patented chemical processes for thickening unsaturated polyester resins, but the potential importance of their work to the development of SMC technology was not to be realised until the mid-1960's. Frillette's thickening reaction used either magnesium oxide or calcium hydroxide, and Fisk's patent used magnesium hydroxide.

The advance made by the premix material was that it contained resin, fillers and fibre-glass together. This material introduced the possibility of wider applications of reinforced polyester resin compounds, but a disadvantage was that the mechanical properties of the premix material were lower than those given by the wet-moulding techniques. Therefore premix was used only for small articles.

By 1960 prepregs were being manufactured in the USA. These prepregs were composed of polyester resin plus a solvent diallyl phthalate which lowered the viscosity (L1). There were two important stages in their manufacture. For the first stage the viscosity was very low so that the fibre-glass material was easily impregnated with resin; during the second stage the viscosity was increased so that it was easy to handle and so that the flow during moulding would be more uniform. To increase the viscosity the solvent was removed by placing the prepreg into an oven. Definitely the idea of the two-stage process was right, but the way in which it was achieved was very expensive and dangerous.

It was not until 1965 that a new technique was developed in Germany (L1) for achieving the two-stage thinning-thickening mechanism for a polyester resin by using the early work of Frillette and Fisk. The polyester resin was dissolved in styrene and a small percentage of calcium or magnesium oxide was added. The oxides reacted with the carboxyl endings of the polyester resin, producing an increase in the viscosity of the material. Then metal coordination complexes are formed by linking the metal with the ester oxygen in the linear polymer. Therefore the liquid resin is transformed into a handleable paste.

The type of reinforcement used at that time was in the form of fibre-glass mat. However the SMC material obtained by this technique had the disadvantage of being expensive, giving a poor surface finish, having a brittle behaviour, and showing large shrinkage on curing.

In 1966 Owens-Corning replaced the fibre-glass mat with chopped glass, to reduce the cost of manufacture. This modification to the manufacturing process of using a belt system for resin impregnation (B1) allowed for more flexibility in the manufacture of the material.

In 1968 the low shrink (LS) and low profile (LP) moulding compounds were patented in the USA, which reduced the shrinkage from 7% (typical of unsaturated polyester resin alone) to almost zero (from +0.5 mm/m to -0.5 mm/m). This modification also improved the surface finish of the moulded products. These improvements have been responsible for the increased number of moulding compound applications. It was not until 1970 that the LS and LP moulding compounds were used in industry, but since then the technology has evolved very quickly.

Thus there have been many developments in SMC manufacture since the process innovation introduced by Owens-Corning in 1966. The different types of SMC now available include:

HMC	High-strength moulding compound
LMC	Low-pressure moulding compound
SMC	Sheet moulding compound
SMC-C	Continuous-fibre SMC
SMC-D	Directional-fibre SMC
SMC-R	Random-fibre SMC

SPMC	Solid polyester moulding compound
TMC	Thick moulding compound
UMC	Unidirectional moulding compound
XMC	Directionally-reinforced moulding compound

Combinations of SMC-C, SMC-D and/or SMC-R may be produced using the same belt-type impregnator, or for example by feeding continuous glass-fibre yarn and chopped glass-fibre into a roll-type impregnator machine (Prepreg-Harzmatte-SMC, S13). All these processes are continuous, except XMC manufacture (A1).

Modifications to SMC production machines have resulted in better quality SMC materials. Specially profiled kneading-rollers have been used for fibre compaction to ensure that SMC is produced with essentially planar-isotropic properties, i.e. with random fibre orientation and uniform fibre distribution in the plane of the sheet (T5). Also, twin bed double steel chain compaction using a staggered arrangement of kneading-rollers in tandem, can reduce the volume of trapped air and increase wet-out (A3). Heated conveyors have been used to reduce the maturation time from 4 to 10 days to 3 to 8 minutes (L4).

A very important improvement has been the development of a new machine to produce a thicker SMC (TMC) while at the same time improving the impregnation of the glass-fibre, for an increased production rate and reduced cost.

SMC technology is now moving towards a completely automated process system in which the mixing room is controlled in line with the SMC production machine, and even in some cases the SMC production machine feeds the compression moulding press directly (W6, Y1).

## 2.2 SMC Chemistry

This section deals with the developments in SMC chemistry in four parts by describing: the chemical components found in typical SMC formulations; the main chemical reactions associated with the manufacture and moulding of SMC; and the effect of variations in SMC composition on mechanical properties, and also viscosity and flow.

### 2.2.1 Chemical Composition

The approximate composition by weight of a sheet moulding compound is as follows:

Resin	25 - 35%
Catalyst	0.5 - 1.5%
LS or LP additive	2 - 5%
Filler	40 - 65%
Thickener	0.5 - 1.5%
Release agent	0.5 - 2.0%
Pigments	3 - 5%
Fire retardants	2 - 5%
Reinforcements	20 - 30%

The role and type of components used in the manufacture of SMC are as follows.

The resin is the key component in the matrix of the moulding compound, and since it is unsaturated, it allows the formation of a permanent three-dimensional cross-linked network. An unsaturated polyester resin was used in the work of this thesis. For unsaturated polyester resins, the main resin systems are (B9):

- Orthophthalic* - general purpose resin because of its price and properties. It has low thermal stability and absorbs water.
- Isophthalic* - used for impact resistance, crack resistance, resistance to humidity and environments containing oil, paraffin, etc.
- Terephthalic* - has very similar behaviour to the isophthalic resins.
- Biphenolic* - used for its chemical resistance, mainly in aqueous environments and resistant to high temperatures.

Other types of unsaturated polyester resin systems have been developed from combinations of these four resins (H4), to obtain more economical systems with better corrosion resistance and lower density.

However vinyl esters (J1) are also used; they improve chemical resistance and tensile strength. Epoxy resins combined with unsaturated polyester resins (E1) reduced SMC manufacturing costs, cure times and increase shelf life, but there is an accompanying reduction in some mechanical properties.

The factors affecting the consistency of the resin were analysed by Brown (B9).

The catalyst initiates the polymerisation reaction. It determines gel and cure times, and shelf-life. The most commonly used catalyst is the t-butyl-perbenzoate (B5). However other types of catalyst can be used, like the peroxyketals which cure faster and give to the moulding compound a longer shelf-life than the t-butyl-perbenzoate (T3); the best results are obtained with peroxyketals when the resin system is isophthalic (C1). Other catalysts are the so called AZO-initiators which reduce sink-marks and cure faster than the peroxyketals (K1), but they produce blisters (B6). Catalyst selection is explained by Bowyer (B5) and Seamark (S3).

LS and LP additives are used to control the 7% shrinkage of the polyester resin. The difference between the two additives is the shrinkage control achieved (B13). LS gives approximately 0.001 mm/mm, while LP gives +0.0005 to -0.0005 mm/mm.

The amount of additive is about 2-5% by weight, but it is 7-20% by weight when mixed with styrene (A7). Generally the LS and LP additives are syrups of a thermoplastic in styrene, such as PE, PS, PVA, PVC, PMMA and so on (B5). The LP additives which allow very small shrinkage and good pigmentability are bakelite LP-100 (for MgO at 1%) or PVA (for  $Mg(OH)_2$  at 4%) (A7). The factors affecting the selection of a LS and LP system were analysed by Atkins (A7) and Bowyer (B5).

Fillers are used to control the viscosity of the mixture and gloss surface on the final product, to reduce shrinkage and price, and to improve chemical resistance and physical properties. The fillers can be sulphates, silica and silicates and carbonates (B5). One of the most

commonly used is calcium carbonate. The factors affecting the selection of the filler were studied by Murfitt (M12).

Thickeners increase the viscosity of the moulding compound from 1000-3500 cps to  $20 - 30 \times 10^6$  cps after maturation (M9), making the moulding compound easy to handle. The more common thickeners used are the oxides and hydroxides of calcium and magnesium. The following factors which affect the thickening reaction have been examined: the acid/alcohol ratio of the resin, the concentration and degree of distribution of the thickener (L3); the type, morphology and specific surface of the thickener (F3); the presence of a dihydroxyl in the resin and the water content (B11); the thixotropy and temperature (A2); and LP additive, filler and internal release agent (S3).

Recently a new thickening reaction has been developed (F1), which is based on the chemistry of the urethanes. It eliminates many of the problems associated with the use of alkaline earth oxides and hydroxides.

Release agents ease the extraction of the moulded article from the mould. Low percentages of release agents must be used, because they affect the paintability and the mechanical properties. The more common release agents are stearates of Al, Ca and Zn. However mixtures of Zn and Al stearate give good results, but not in LP SMC (K2). A new Ca/Zn stearate shows better properties than Ca or Zn stearates alone (S15). The selection of release agents is explained by Seamark (S3).

Pigments are used to modify the colour of the moulding compound. Pigments can be organic or inorganic. They are generally diluted in a carrier (M7). The factors affecting the efficiency of the pigment are explained by Seamark (S3).

Fire retardants provide the moulding compound with self-extinguishing properties. The more commonly used are aluminium trihydrate (ATH), or organic fire retardants containing halogens or phosphorus (M7). The use of a ATH/carbonate/bromine system improves the dispersion of the fire retardant and the ignition resistance, reduces cost and allows higher quantities of filler to be used for the same viscosity compared with ATH systems (D2).

Reinforcements improve the mechanical properties of the moulding compound and reduce shrinkage. Fibre-glass is the most commonly used in bundles of 108 strands, with fibre diameters ranging from 9 to 14 $\mu$  and lengths from 12 to 50 mm, although nowadays there are SMC's with continuous fibres (B13). Graphite is also used as reinforcement, or combinations of graphite and glass-fibres, which are known as hybrid moulding compounds (A4). However, not only glass in the form of fibres is used; hollow microspheres of glass reduce the density and improve impact resistance (C3, M8).

The fibres are covered with a size which protects the fibres and increases their affinity with the resin (B5). The properties of the compound can be modified by changing the solubility of the size (A2, B13, S3). Insoluble size - also known as low solubility fibres, hard glass or soft finish fibres - improve impact properties, but reduces surface finish quality and interlaminar strength. Soluble size - also known as high solubility fibres, soft glass or hard finish fibres - improve wet-out, surface finish quality, flexural strength and interlaminar strength.

### 2.2.2 Chemical Reactions

There are four main reactions associated with SMC manufacture and moulding.

First the linear polymer is formed. This reaction is in two stages to permit a degree of mobility in the final thermoset (R1). Initially a prepolymer forms from a saturated diacid and glycol; then the linear polymer is obtained when the prepolymer reacts with maleic anhydride.

Secondly there is the thickening reaction. This reaction is in three stages (F3, L3, M3, W1). First basic salts form between the carboxyl endings of the linear polymer and the thickener. Water content is very important at this stage. It is necessary to prevent the formation of diacids between two linear polymers, but too much water will give a fast reaction speed.

The water acts as a catalyst in the second stage, during the formation of neutral salts. But in the case of  $Mg(OH)_2$ , the water produced from the formation of basic salts is used as the second stage catalyst.

The last stage of the thickening reaction is the formation of metal coordination complexes, between the alkaline earth element of the neutral salt and the oxygen of the ester links. A weak three-dimensional cross-linking is created, but this is strong enough to increase the viscosity of the moulding compound. Another factor which influences the increase in viscosity is the formation of bridges between the hydrogen of the carbonyl end groups and the ester oxygen of two linear polymers.

The shrinkage control and cross-linking reactions occur during moulding. The mechanisms of the shrinkage control and cross-linking are described in references (A7, B13, P1). The material is placed in the mould and heated. This causes the whole moulding compound to expand and at a certain temperature the initiator is activated into free radicals. Then the free radicals activate the styrene and the linear polymer, the styrene becomes fixed between two linear polymers, thus starting the cross-linking (which defines the gel time).

The shrinkage control additive (thermoplastic) becomes incompatible with the cross-linked resin due to increasing molecular weight of the "solvent". Therefore the thermoplastic together with the rest of uncured polyester form a separate phase. It is this precipitation of the thermoplastic which controls the shrinkage of the moulding compound.

The residues of uncured polyester still within the thermoplastic start curing and shrink, forming the first voids. The polyester starts cooling, but when its temperature reaches the glass transition temperature the shrinkage almost stops, which is not the case with the thermoplastic (it has a lower glass transition temperature). A second formation of voids occurs while the thermoplastic is cooling and therefore shrinking, but the dimensions of the moulding are already set by this time.

### 2.2.3 Effects of Composition on Flow and Viscosity

One of the important factors in the manufacture of SMC is the analysis of the combined effects of the many compound elements (see Section 2.2.1) to determine the flow behaviour and viscosity of the material. There is much current work in this area of SMC development, but the following main effects have emerged.

The viscosity of SMC is important because it directly affects mouldability, and also homogeneity and isotropy after moulding. Where the viscosity of SMC at 200C is less than  $2 \times 10^6$  cps the product will have resin-rich regions, but when it is higher than  $50 \times 10^6$  cps, the flow properties will be very poor (S9), and the moulding of complicated shapes will be very difficult.

Initially the resin alone has a low viscosity and shows Newtonian behaviour (T4). The main effect of adding the catalyst is to modify the time allowed for flow (before gel occurs) and not to alter the mixture viscosity. The catalyst also affects the shelf-life.

The thickener has a direct effect on the viscosity of the compound; therefore its selection must be studied carefully (F3, S3). The use of MgO instead of  $Mg(OH)_2$  reduces the shelf-life (M3), but when using  $Mg(OH)_2$  at 3% a lower viscosity can be achieved ( $10 \times 10^6$  cps) than that obtained with MgO at 1% ( $100 \times 10^6$  cps) (L9). However, the use of an additive called Paraplex CM-201 combined with MgO allows the viscosity plateau of the SMC to be chosen (A2).

Fillers are used to reduce the mobility of the resin in the resin/fibre matrix, but in certain cases special fillers must be used to reduce the viscosity to keep the SMC within mouldability limits (M11). LS or LP additives increase the viscosity of the compound (A7), due to interaction between the additive and the thickener. Viscosity also increases with the use of aluminium trihydrate (G2), and with increases in the content of fibres, the length to diameter ratio of the fibres, and the solubility of the fibre coating (B12, G1, H1, O2).

#### 2.2.4 Effects of Composition on Mechanical Properties

The fibre-glass is the main element affecting the mechanical properties of moulded products. Increasing the length of the fibres improves the mechanical properties, e.g. tensile strength (B13). The type of fibre coating also affects mechanical properties: a soluble coating increases flexural strength, and an insoluble one increases impact and tensile strength (B13).

However, other elements can affect significantly the mechanical properties of the moulding compound. The use of HAR-MICA as filler improves the mechanical properties (W7), but the use of clay, combined with wetting-agents, as a filler, reduces the mechanical properties and affects the thickening reaction (S12). The use of aluminium trihydrate as fire retardant combined with silane-special improves the mechanical properties and surface finish (A7).

The ways in which the lack of toughness of SMC can be improved have been studied recently. Certainly part of the problem can be solved by reducing the degree of the cross-linking in the final product, thus increasing molecule mobility and flexibility (C4). Other methods of increasing the mobility and flexibility are the addition to the moulding compound of special additives such as hydroxyl terminated polyesters (HTP) or copolymers of butadiene and acrylonitrile (known as Hycar VTBNX). HTP can toughen the compound (G3, R3), but in some cases it reduces other mechanical properties (R3). The so called Hycar VTBNX shows better toughness than that obtained with HTP's (M5, T2), without a reduction in other mechanical properties. Also a toughened material can be achieved using the resin manufactured by Freeman Chemicals, known as Stypol 40-3910 (A5).

The identification of the effects of variations in the SMC formulation on mechanical properties is still an area of much current activity especially where design applications are involved (Collister SPI Conference 1979, Ferrarini SPI Conference 1979). The main trend is to formulate SMC composition to suit the product requirements. However some standard SMC's are being produced, as evidenced by the considerable amount of mechanical properties characterisation work of Denton (D5) on Owens-Corning's SMC-R50.

## CHAPTER 3.

DESIGNING WITH SMC - THE STATE OF THE ART3.1 Introduction

Because SMC materials are relatively new, design procedures for using them to manufacture engineering products have not been formalised to the same extent as have the procedures for designing with the older conventional engineering materials. Designing with SMC still depends largely on experience: the designer needs to work closely with the moulder to seek his advice and experience, to use laboratory test facilities to get design data for the actual moulded material, and to use prototype testing before committing to production.

Designing SMC structural components is particularly difficult. Figure 3.1 shows schematically the steps which might be followed in the design procedure and the knowledge needed. The problem is complex but may be stated simply as a need to understand for a given SMC material formulation how mould flow determines the properties of the finished component. Moulding-process and charge shape geometry and placement considerations are associated with this problem. They are cosmetic (e.g. surface waviness, sink marks, blisters, and paintability) as well as structural (e.g. isotropy of mechanical properties, strength and stiffness prediction weld-line formation).

There is much current work in this field, but the following sections have been chosen as being appropriate to review the present state of knowledge:

- 3.2 *Strength and Form Design*
- 3.3 *SMC Rheology*
- 3.4 *Moulding Production Problems*
- 3.5 *Design Applications*

3.2 Strength and Form Design

There are two general approaches to determining the mechanical properties data needed for structural design. One is based on predictive methods, which were reviewed by Chamis (C2) in 1972, but more

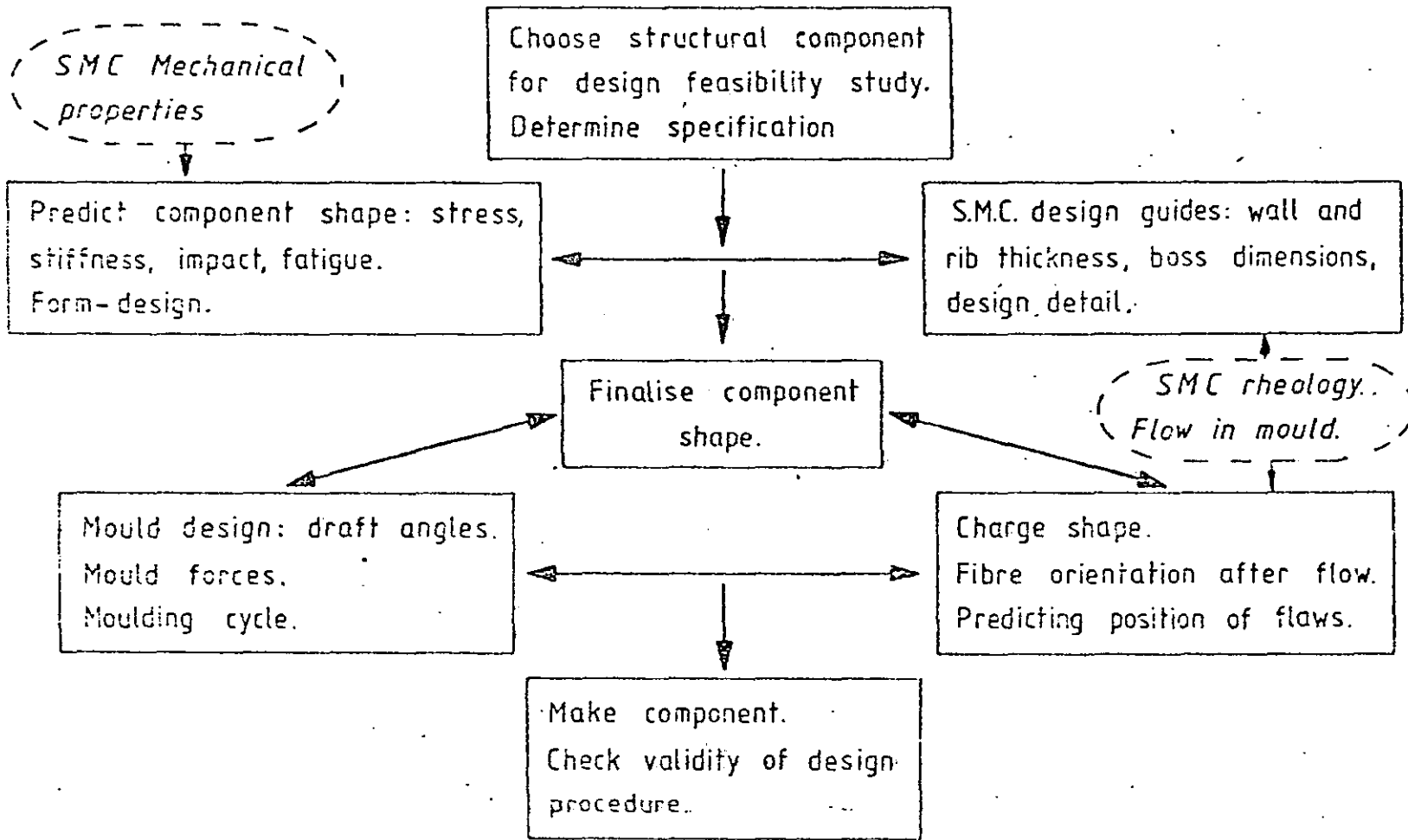


Fig.3.1  
 DESIGN PROCEDURE FOR S.M.C. STRUCTURAL COMPONENTS: CASE STUDY DEVELOPEMENT.

recently by Bert (B3). There are now established theories for predicting the linear-elastic and thermal-expansion behaviour for planar-random fibre composites. However work still needs to be done to achieve better agreement with experimental results, and to predict fatigue and impact properties.

By contrast the approach taken by Dow Chemicals (E4) and Owens-Corning (D5) has been to mount substantial test programmes to provide SMC data needed by designers. Denton's work is the first comprehensive attempt to characterize the mechanical properties of one SMC material at various temperatures.

SMC manufacturers have also published guides to product-design (B10, F4, O3). These give guidelines for shaping ribs and bosses, stiffening edges, moulding inserts, selecting shapes to avoid flow faults, positioning flash lines, etc. Table 3.1 shows examples of these recommendations.

Generally product stress and strain calculations are based on classical methods for linear-elastic uniform homogeneous planar-isotropic materials. Design approaches can use formulae (L8) or finite-element methods (D3). Generally over design results from the former approach, although the latter approach may reduce this. For example reference (D3) describes how a finite-element computer model can be used to fix thickness values for the stress distribution, and then final design modifications (e.g. rib reinforcements) may be decided from prototype testing.

More work is needed to develop a finite-element method which incorporates the variation of mechanical properties induced by flow. Eisenberg's work (E3) at General Motors is a step in this direction; it predicts preferential stiffness directions from charge-shape flow.

Therefore it is not surprising that prototype manufacture plays an important part in proving the initial design dimensions of SMC products. Moulding prototypes is not only necessary to provide products for strength testing, but also to ensure that desired patterns of mould flow are achieved. Five different ways of making SMC prototypes are described in references D1, L8, N2, O4, S5.

TABLE 3.1  
ARTICLE DESIGN RECOMMENDATIONS

Draft angle	1-1.5° for less than 200 mm depth; 2-3° for more than 200 mm depth and with texture 1° for each 0.025 mm of texture depth
Corners	Minimum inside radius is 1.5 mm; design with generous radii always
Wall thickness	Minimal and constant, range from 1.5 to 25 mm; normal thickness variation $\pm 0.1$ mm and maximum thickness built-up as required
Component support	Mould as column maintaining the nominal thickness
Flanges	Make them thicker or with changes in direction to increase the strength. For wall thickness of 2-3 mm make the flanges twice the wall thickness
Ribs	Rib base 2.3-9.4 mm, top of the rib at least 1.75 mm; radius on the ribs 0.1-0.25 mm to reduce sink marks, but low strength. Design rib shorter and wider in such a way that the section stiffness is the same along the rib; height to width ratio recommended 5:1, although 15:1 can be used
Bosses	Equal to the nominal thickness, length of the screw 2.5 x diameter, use safety factors to determine the dimensions of the boss, strengthen it with ribs and webs in the case of lateral loads, but in tension load the ribs and webs could be the cause of failure. Use self-tapping screws for the cases when the screw will be removed less than 4 times, for other cases use inserts. See reference (g) for holes diameter selection
Radii of edges	Minimum (concave or convex) 0.5 mm
Undercuts	Not recommended, however they can be moulded by selecting the parting line

#### REFERENCES

- a. BTR-Permalit RP Ltd, "GRP Technology and Practice", 1974
- b. C C Boner, 30th Annual Tech. Conf., SPI, 1975, Section 16-A.
- c. C A Charters, *Plast. Eng.*, 32, 2, (1976), 38-40.
- d. Freeman Chemicals Ltd., "Freeman Chemicals SMC DMC & You", 1976
- e. A Luchini, Int. Symposium on Polyester Moulding Compounds, Geneva 1977, paper 10
- f. F Mandy, *Reinf. Plast. Congr.*, Proc. Brighton Engl. 1974, p.33-39.
- g. F L Massey, 32nd Annual Tech Conf., SPI, 1977, Section 2-F
- h. C G Nenadal, 30th Annual Tech Conf., SPI, 1975, Section 20-C.

### 3.3 SMC Rheology

There has been a considerable amount of work directed towards the general aim of understanding the nature of SMC compression flow. This section reviews that work in three parts. Firstly there are the standard rheological tests which have been developed in an attempt to measure the viscosity or to understand the flow behaviour of SMC during compression moulding. The second part presents work which outlines how SMC flows during the compression-moulding cycle, and finally work concerned with modelling flow behaviour is presented in the last part. (The effects of variations in SMC formulation on rheology were described in Chapter 2, Section 2.1).

#### 3.3.1 Rheological Tests

The need for improved experimental techniques which can be used either to analyse the effect of the different components in the compound or to characterize the rheological behaviour of fibre reinforced polyester compounds has been emphasised during recent years by the increased engineering usage of these materials. Rheological measurements are needed which better describe material characteristics under flow conditions that are directly relevant to the actual moulding process (W4). A characteristic of the many conventional flow tests (see Table 3.2) is that none provides such data directly. Additionally they cannot handle the complications of flow behaviour introduced by long fibre reinforcement and cross-linking reactions.

Much recent work into the rheological behaviour of SMC has been done with the Rheometrics Dynamic Spectrometer (R2), which provides data on the viscous and elastic components at different strain rates. The testing principle involves subjecting SMC discs to variable frequency oscillatory shear and measuring phase difference between the shear and elastic components. Early work was by Maker and Ford (M2), and also Maxel (M3), who did work at compression moulding temperatures. Powell (P3) is using the equipment to examine effects of formulation. However the problem remains of linking the results in a meaningful way to the compression moulding process. The test is not a physical representation of the moulding process, and ultimately a less expensive and simpler test will be needed.

TABLE 3.2  
FLOW TESTS FOR SHEET MOULDING COMPOUND

<u>Name of Test</u>	<u>Parameters Measured</u>	<u>Remarks</u>	<u>Ref</u>
Audrey dielectric spectrometer	Dielectric losses vs time	Relates the dielectric losses with viscosity	a
Brookfield HBT viscometer	Viscosity	Measures viscosity of SMC without glass fibres	b
Cup flow test	Time	Measures flow time for a given moulding pressure and temperature	c
Dynamic mechanical testing	Viscosity & moduli vs time, temperature, strain and frequency	Testing often uses a Rheometrics Dynamic Spectrometer	d
Parallel cylinder shear rheometer	Shear stress vs time	Sensitive to fibre orientation in complete SMC	e
Parallel plate plastometer	Force vs time	Based on Scott's work (f) Limited to certain viscosities	g
Platen movement test	Displacement vs time	Used to determine approximate gel and cure times	h
Platen displacement flow test	Force vs time	Measures the ability to flow	i
Renault test	Flow length	Useful for Renault SMC only	c
Serpentine flow test	Flow length	Measures effect of moulding pressure on flow length	c
Spiral flow test	Flow length	Measures effects of moulding pressure on flow length	c

#### REFERENCES

- a. D C Hylton and M R McCormick, 34th Annual Tech.Conf., SPI, 1979, Section 23-E
- b. J T O'Reilly, 20th Annual Tech. Conf., SPI, 1965, Section 14-B.
- c. J Methven, *Plastics & Rubber: Processing*, 1, 4, (1976) 149-157.
- d. R Powell, 34th Annual Tech. Conf., SPI, 1979, Section 7-D.
- e. D H Thomas, 33rd Annual Tech. Conf., SPI, 1978, Section 19-F.
- f. J R Scott, *Trans. Inst. Rubber Ind.*, 7, (1931), 169-186.
- g. R Burns and K S Gandhi, 32nd Annual Tech. Conf., SPI, 1977, Section 7-C.
- h. S J Thompson, *Plastics and Rubber Int.*, 3, 4 (1978), 159-161.
- i. H Okuto, H Hirand and M Yotsuzuka, *Plast. Tech.*, 19, 9, (1973), 43-45.

### 3.3.2 SMC Flow During Compression-Moulding

It is important to know and understand what happens inside the mould during the compression process. The nature of the process is shown by the typical compression-force versus time and platen displacement versus time variations in Figures 3.2 and 3.3 respectively.

The compression of the SMC starts with an increase in the ram-force and the whole charge is deformed, but as soon as the material is plasticized on the surfaces in contact with the mould (hot layers) the ram-force decreases (O2). The hot layers of SMC will flow filling the cavity while the cold layers present a resistance to flow (M2). The flow of SMC is more like a sheet than a liquid. Hence the way in which ribs and bosses are filled in a compression mould is by folding the material into them. Initially the ribs and bosses are by-passed by the flow front and when the cavity is filled the material will be forced into the ribs and bosses (M2).

During moulding the material will pass through three stages: the first one is an endothermic reaction. The material is plasticized and expands thermally in the areas of plastification. The second stage is the polymerization and gelling of the material after which no further homogeneous flow can take place. The gel time (see Figure 3.4) can be identified on a temperature-time curve as the first knee (F2). The second stage is an exothermic reaction and finishes at the end of the polymerization. This time is known as the curing time, and it can be identified on a temperature-time curve at the time of the maximum recorded temperature (see Figure 3.4). Immediately after curing the material shrinks, but in the case of LS or LP SMC's the thermoplastic will come out of solution and compensate for the shrinkage. This corresponds to the third stage.

These stages can also be approximately determined in time by recording the movement of the ram during moulding (M7, T8), but platen displacement recordings are difficult to relate to gel and cure times (B13).

The way in which the material cures inside the mould is from the edges towards the centre, because of the way in which the material flows due to the method of heating (M2). A problem associated with this phenomenon is the difference in density through the moulded article.

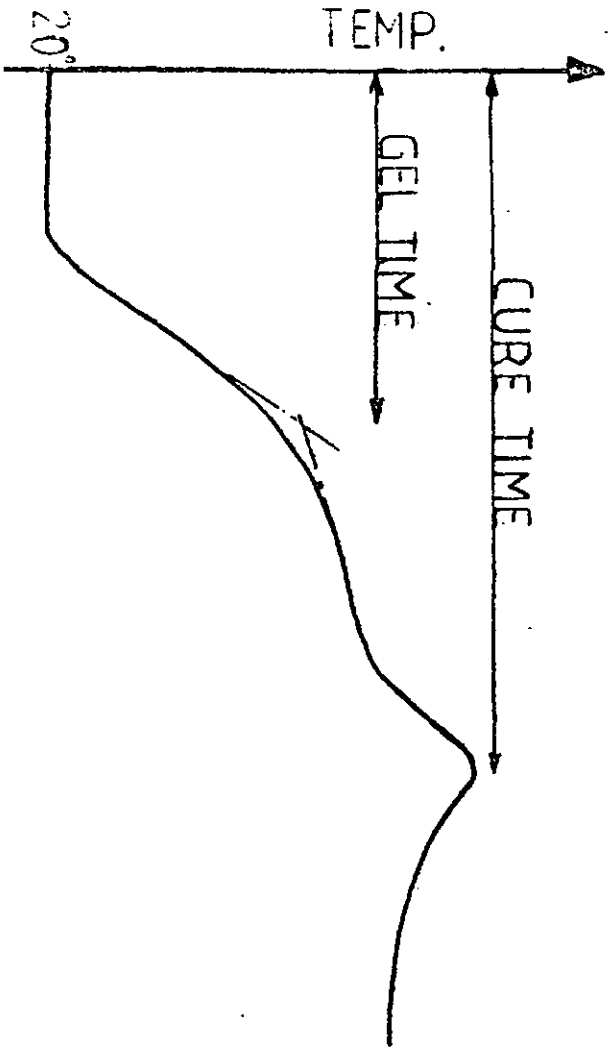


Fig.3.4

TIME

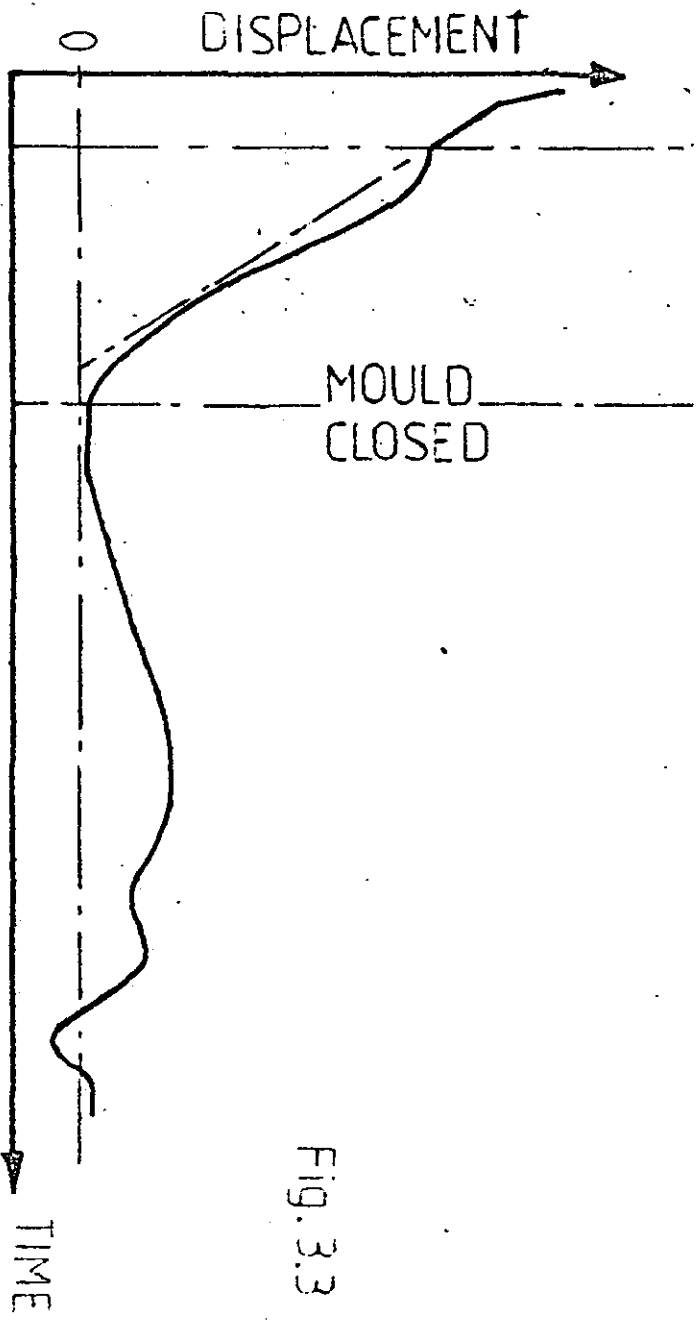


Fig. 3.3

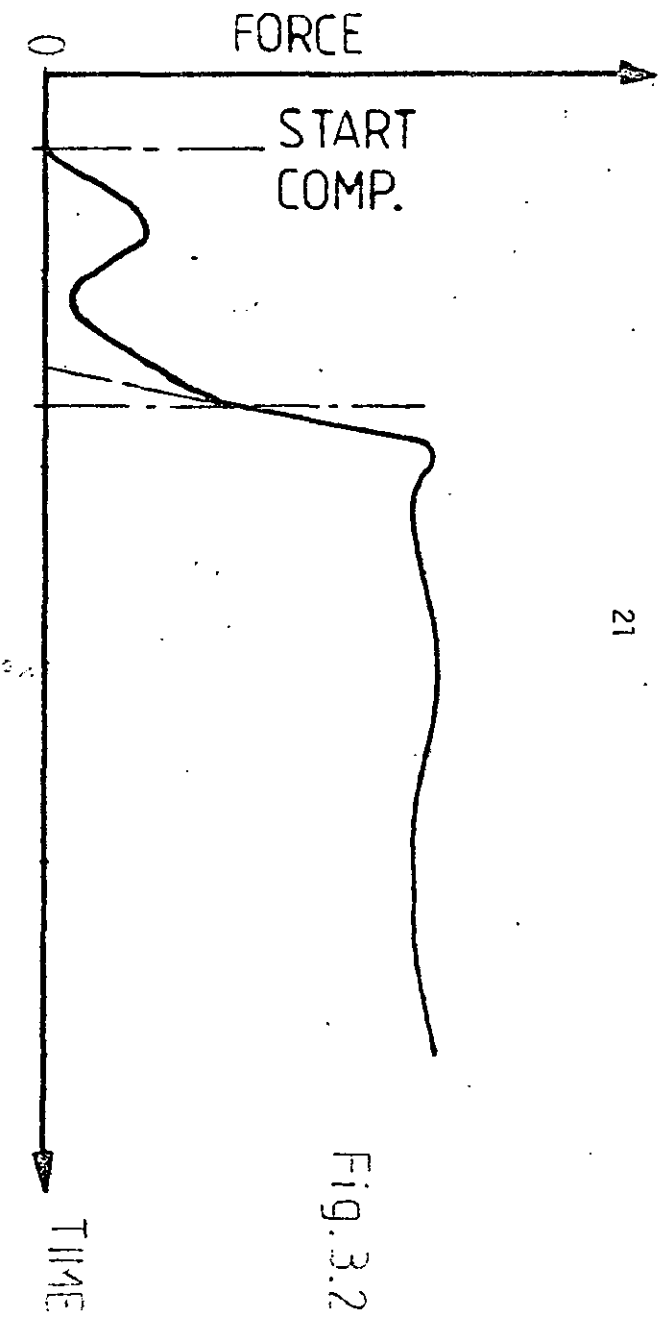


Fig.3.2

However if the heat required during moulding is calculated for different sections from the edges of the mould to the centre, thermal equilibrium can be achieved for the final article (H3). The combination of a heat conduction equation, a curing equation, and suitable boundary conditions will make it possible to predict product curing and determine the optimum thermal equilibrium (W4). Unfortunately this has not yet been thoroughly explored.

The flow of SMC during compression-moulding is also affected by the material's viscoelastic nature (S6). Sieglaff found that if the moulding process is fast, the flow stresses and strains become important near curved sections. Voids and residual stresses may be created because of the dependence of elastic response on moulding speed. If the moulding is slow the elastic response may be disregarded and a more complete and uniform flow will be achieved.

Another important flow consideration concerns the choice of the charge area. Two completely opposed theories exist: one suggests choosing a small charge area - between 11 to 50% (G4, T8) - and the other a large area, between 70 to 84% (D4, H3, M7, S7).

Using a small charge area helps to expel trapped air, thus reducing blister formation (G4), but the variation in the mechanical properties is increased (S11). Also longer flow lengths give better surface finishes. On the other hand thermal equilibrium is improved by increasing the charge area (H3).

Therefore the choice of one or the other theory depends on the requirements of the final article. However, the optimum compromise between random fibre distribution and blister and voids formation can be achieved with a charge of 74% (D4).

### 3.3.3 Mathematical Models for SMC Flow

One of the first workers to recognise the viscoelastic nature of SMC flow behaviour was Sieglaff (S6); Maxwell's later work (M3, M13) confirmed this, but neither worker tried to establish an equation of state for their SMC materials. Thomas (T4) used a parallel cylinder shear rheometer to establish a mathematical equation of state with elastic and viscous components (based on a Voigt model) for matured SMC at room temperature, but that work was not mathematically rigorous.

Gandhi and Burns (B12, G1) were the first to apply the mathematical theory of squeeze flow to the problem of determining an equation of state for a fibre reinforced polyester resin compound. They used a parallel plate plastometer and assumed a power law equation to characterise the behaviour of a dough moulding compound (DMC) at room temperature for limited shear rate conditions.

One of the ideas proposed by the work of this thesis is that the parallel plate plastometer provides a good physical representation of the compression moulding process when moulding flat components from SMC. Chapters 4 and 5 (and also S8) show how a mathematical analysis for the squeeze flow of SMC discs between parallel plates can be developed and used to determine the equation of state at room temperature. Extending that analysis to actual compression moulding conditions - with all the attendant SMC material changes - is at the moment mathematically too complex; however the squeeze flow experimental technique itself may be used to provide data which show the relationship between moulding-process conditions and SMC gel and cure times (see Chapter 5 and reference S8).

But the work of this thesis has also developed a way of modelling SMC compression-flow during moulding at 160°C. By assuming that the SMC flow is Newtonian, a mathematical analysis has been derived which can be used to predict charge shapes for moulding two-dimensional SMC components free from weld-lines (see Chapters 6, 7 and 9, and also reference S7).

The only other reported modelling work has been by Smith (S10) who made a similar Newtonian assumption when he recently established a mathematical model for the flow of SMC into ribs, in order to investigate the formation of sink marks. He obtained good agreement between theoretical and experimental work.

### 3.4 Moulding Production Problems

An important part of the success of an SMC article is the design of the mould. Two types of moulds can be used: either a positive one or a semi-positive one. Positive moulds close onto the SMC itself and do not produce flash. However they are difficult to operate, so generally SMC compression moulds are now semi-positive. Moulding is usually off-the-stops. The advantages of the semi-positive moulds are that they are

cheaper and last longer than the positive ones. Principles for the design of SMC moulds are given in references B14, L8, 03. Table 3.3 summarises the main points.

Initially SMC was moulded using compression moulded presses for thermoset materials, but as the technology has developed, special presses have been built to meet the requirements of the SMC moulding process (B14, L8, 03). The ram initial speed must be fast (500 mm/sec) to avoid a possible pre-curing of the SMC, but the mould closure speed must be relatively slow (0 to 25 mm/sec) to avoid material segregation problems. Table 3.4 lists other desirable press characteristics.

To speed up press cycle times, semi-automatic (R4) or completely automatic (W6) press loading and unloading is being used. The idle time during curing has been bypassed by using a compression-mould transfer line system (Y1), although this new technology is only economic at high production rates (e.g. 700 000 parts/year).

It is important that press operation is repeatable from the set moulding conditions; therefore it is recommended to monitor process conditions by installing pressure and speed transducers (W6). Platen parallelism will tend to decrease with use (from about 0.3 mm/m when new), but Todd (T9) at General Motors has developed a servohydraulic programmable force/velocity control (PVFC) which maintains the parallelism of the mould surface during closure, and also controls the speed and force on the SMC such that the flow during closure is laminar. PVFC has been used both at General Motors and also General Tyre and Rubber Company, Akron, Ohio, together with an in-mould coating system to improve moulded article surface finish (Y1).

Additional considerations to those of mould design and press operation are moulding process conditions. Correct setting of these conditions to avoid variability in moulded article physical properties usually calls for good moulding experience. The conditions which need to be considered are:

- the mould temperature must be kept within the required tolerances
- the pressure build-up must be fast and high enough to ensure the compaction of the material

TABLE 3.3

## MOULD DESIGN RECOMMENDATIONS

Material	P-20 steel pre-toughened to 300 Brinell (Ni-steel), but Just (d) suggested the use of AISI-4041 cast steel for which porosity can be controlled. Cast steel is used with large and complex moulds
Block thickness	The mould cavity must be surrounded by enough material to avoid any possible deformation during moulding
Flash	Vertical flash is always preferred although in some cases it could be necessary to use a horizontal one. The disadvantage of a horizontal flash is that it wears out quickly (e).
Flash Clearance	Between 0.05 to 0.1 mm
Telescopic Length	Between 8 to 40 mm depending on the size and complexity of the article
Shear edge taper	A 2-3° taper for semipositive moulds along 3-10 mm depending on the complexity of the cavity
Wear plates	The areas with important wear, such as shut-off faces should be made from separate inserts (e)
Stops	The mould must be equipped with stops, but moulding off-stops
Surface Finish	A surface finish of 800 grit must be achieved. The use of chrome plating increases the mould-life and eases the extraction of the moulded article, it does not increase surface finish. A mould cavity blasted with 80 grit glass beads can produce a uniform flow (f). Use nickel-plating in deep moulds
Guidance	Use guide-pins with bushes. In the case of large moulds (more than 450 mm square) rectangular guides are placed beside the guide-pins to increase rigidity. These rectangular guides have hardened shoes fitted into the mould
Ejection	Ejector-pins are the more common method, but in some cases it could be necessary to use ejector-plates. The number of ejectors depends on type of article and material. Ejectors permit the escape of air and gases avoiding voids-formation.

(CONTINUED)

TABLE 3.3

## MOULD DESIGN RECOMMENDATIONS (Continued)

Heat	<p>Three types of heat can be used:</p> <p><i>steam</i>: it is cheap, but limited in temperature and it depends on the pressure variations of the system.</p> <p><i>oil</i>: it is cheap, it does not depend on pressure variations and it has unlimited temperature possibilities</p> <p><i>electric</i>: more uniform and unlimited in temperature possibilities, but expensive</p> <p>See references (g) and (h) to evaluate the required heat.</p>
Isolation	Use silico-aluminate to reduce the heat losses of convection and radiation (i). Such losses are about 60 to 70% of the total losses

REFERENCES

- a. M J Buttler, Int. Symposium on Polyester Moulding Compounds, Geneva 1977, paper 11.
- b. A Luchini, Ibid, paper 10
- c. Owens-Corning Fibreglas, Pub. No. 5-TM-6991-A, 1976.
- d. H A Just and W H Englehart, 33rd Annual Tech. Conf., SPI, 1978, Section 21-D.
- e. Polyester Comp. Group, Reinf. Plast. Cong., Brighton 1978, 32/211-215.
- f. A J Rudy, 33rd Annual Tech. Conf., SPI, 1978, Section 4-D.
- g. J H DuBois and D W Riley, Nat. Symp. Plast. Mould/Dies-Des/Const., SPE-1977, paper 11
- h. E A Herman, 33rd Annual Tech. Conf., SPI, 1978, Section 14-F.
- i. I J Čatić, Plast. & Rubber: Processing, 3, 1, (1978) 21-23.

TABLE 3.4  
PRESS CHARACTERISTICS

Parallelism of the platens	The parallelism must be about 0.3 mm/m
Sufficient moulding pressure	The moulding pressure varies from 4 to 15 MN/m <sup>2</sup> depending on the mould complexity
Pressure build-up	The pressure build-up must be in 2 seconds
Bending deflection	The maximum bending deflection must be of about 0.1 mm/m
Opening force	A 20% of the moulding force is required for opening the mould
Slow opening speed	A slow opening speed of about 1 mm/sec is required to avoid any damage on the final article
Fast opening speed	A minimum of 500 mm/sec is required to reduce the moulding cycle
Ejection system	An ejection system in both top and low platens is recommended

#### REFERENCES

- a. M J Buttler, Int. Symposium on Polyester Moulding Compounds, Geneva 1977, paper 11.
- b. A Luchini, Ibid, paper 10
- c. Owens-Corning Fibreglas, Pub. No. 5-TM-6991-A, 1976

TABLE 3.5  
MOULDING PROBLEMS

<u>Problem</u>	<u>Cause</u>	<u>Findings</u>
Blisters	Fracturing process due to low interlaminar strength where air and gases are trapped (a)	Use vacuum moulding and reduce the charge up to 11%, use vinylester as binder and low solubility roving size (a). 74% of area covered is the optimum compromise between blister formation and fibre orientation (b) Use high pressure to eliminate blisters, but increase macroporosity due to excessive styrene (c)
Cracks	During flow the fibre glass migrates to the mid-thickness of the article creating regions of the article poor in resin (d)	Use liquid rubber, copolymer of butadiene and acrylnitrile with terminal and pendant reactive vinyl groups (e)
Delamination	Non-shear stress between two layers (f)	Use always an odd number of layers for the SMC charge. An even number of layers has zero shear stress between the mid-thickness layers (f)
Orientation	Fibre glass tends to orient during flow (f)	Use between 60 to 80% of charge area covered (f) Use Prepreg-Harzmatte-SMC instead of SMC (g)
Porosity	During flow the low profile additive migrates to the surface of the SMC and the f.g. to the mid-thickness (d). It can also be due to excessive styrene (white areas) or losses in styrene (black areas) (c)	Use an acrylic primer to improve surface finish (d). Use the mould coating system immediately after curing (h) Use vacuum moulding to reduce white areas, but it increases black areas. Slow closing increases also black areas, while high pressure increases white areas (c). Change the order at which the SMC components are mixed and substitute some of them also.

(CONTINUED)

TABLE 3.5  
MOULDING PROBLEMS (Continued)

Problem

Sink marks	Surface depression, generally opposite to massive areas (e.g. ribs) where a non-uniform shrinkage has taken place	Use moulding temperature of about 150°C, apply the pressure in two steps (5.76 and 2.72 MN/m <sup>2</sup> ) and select accurately the position and shape of the SMC charge. Use SMC sandwiches, placing long fibres with high viscosity in the finish surface and short fibres with low viscosity in the rib side (j) Use the optimum heat transfer in the mould (k) Reduce the fibre length from 25 to 12 mm, increase the fibre content from 20 to 35% or more and use short thick ribs with minimum radius (l) Use the mould coating system immediately after curing (h) Determine the shape of the rib and wall thickness with a mathematical model. Use protruding ribs, but only in cosmetic applications (m).
Voids	Air trapped between SMC layers	Use a maximum of 74% charge area to increase flow (b)
Warpage	Non-uniform curing	Use either Cu-Be inserts or determine the heat transfer required for a uniform curing (k)
Waviness	Non-parallel compression moulding	Use a programmable force/velocity control system (n)
Weld lines	Where two flow fronts meet forming a resin rich line and there are not f.g. crossing the line	Use the mould cavity blasted with 80 grit-glass beads (o). Use Prepreg-Harzmatte-SMC to produce a turbulent flow (g). Predict the shape of the SMC charge using a mathematical model (p).

(CONTINUED)

TABLE 3.5  
MOULDING PROBLEMS (Continued)

REFERENCES

- a. R M Griffith and H Shanosky, *Plast. Des. Process*, 17, 2, (1977), 10-12.
- b. D L Denton, 34th Annual Tech. Conf., SPI, 1979, Section 11-F.
- c. J D Gorsuch, R M Griffith and H Shanosky, 33rd Ibid, 1978, Section 9-F
- d. G D Cheever, *J Coatings Tech.*, 5, 645, (1978), 36-49
- e. F J McGarry, E H Rowe and C K Riew, 32nd Annual Tech. Conf., SPI, 1977, Section 16-C.
- f. P Roubinet, *Verre Textile Plastiques Renforces*, 17, 6, (1979), 5-20.
- g. A Spaay, 33rd Annual Tech. Conf., SPI, 1978, Section 9-G.
- h. B Miller, *Plast. World*, 36, 3, (1978), 48-51.
- i. R Lottig, T Niemann and D Stevenson, *Nat. Tech. Conf.*, SPE, Louisville, Ky, 1975, 214-5.
- j. F J Amphor, *Plast. World*, 36, 5, (1978), 48-51.
- k. E A Herman, 33rd Annual Tech. Conf., SPI, 1978, Section 14-F.
- l. F Mandy, *Reinf. Plast. Cong. Proc. Brighton Engl.* 1974, p.33-39.
- m. K L Smith and N P Suh , 36th Annual Tech. Conf., SPE , 1979, p.796-799.
- n. W H Todd, *Modern Plastics*, 53, 6, (1976) 54-56.
- o. A J Rudy, 33rd Annual Tech. Conf., SPI, 1978, Section 4-D.
- p. R J Silva-Nieto, B C Fisher and A W Birley, 34th Ibid, 1979, Section 7-B.

- the charge must be positioned correctly in the mould
- the amount of charge material must be always the same.  
Multi-layer charges should consist of an odd number of layers.
- the shape of the charge must be carefully studied
- the compression speed must be compatible with the material viscosity, and gel and cure times

The problems associated with SMC moulding are blisters, cracks, delamination, fibre orientation, porosity, sink-marks, voids, warpage, waviness, and weld-lines. There are many techniques which are used to detect these moulding faults; six of the more common ones are listed below (Table 3.5 lists the moulding problems):

- 1) None-destructive radiography - used to detect voids, porosity, entrapped air, fibre orientation and microcracks (E2, P2).
- 2) Cross-section radiography - used to detect delamination, and blisters (E2, P2).
- 3) Contact photography - used to analyse the fibre-structure (E2, P2).
- 4) Silver coat process - used to detect resin separation, microcracks, porosity, glass fibre filaments, flow lines, waviness and internal voids near the surface of the article (E2, P2).
- 5) Burning technique - used to analyse the fibre orientation due to flow (N1).
- 6) Non-destructive infra-red thermography - used to detect weld-lines and subsurface cracking (M6).

### 3.5 Design Applications

The applications of SMC are in the transport, electrical and business equipment, building, chemical and furniture industries. The most important is the transport industry, with applications mainly in the automotive field.

The following list shows examples of applications of SMC (L7, M1, N3, T10).

- 1) Transport industry. The applications are for cars, trucks, trailers, motorcycles, trains, buses, caravans, boats and planes, such as: ERF - truck-cab, front ends, bumpers, hard tops, hoods, spoilers, doors, boots, wheel openings, wheel covers, drip pans, radiator housings, boat motor housing, seat sheels for trains, snowmobile and shrouds.
- 2) Electrical and business equipment industry. Switch boxes, electrical cabinets, telephone cabinets, lamp-housing, insulators, battery racks, computer terminal housing, motor interior components and housings for cash registers, scientific recorders, medical testers, typewriters, air conditioners and humidifiers.
- 3) Building industry. Window frames, doors, cladding panels, walls, water containers, tubs, shower trays, sinks, basins and bath tubs.
- 4) Chemical industry. Storage tank panels and load-bearing structures with concrete bases.
- 5) Furniture industry. Chairs, tables, desks and stadium seats.

Not all these applications use the same SMC formulation. For example, load-bearing applications tend to have high fibre glass content (or even use unidirectional reinforcements. Reference W5 describes the development of the compression moulded RP/C (reinforced plastics and composites) wheel for which a 50% fibre glass content with either polyester or vinyl ester resin systems is being used. Reference M4 describes the 1980 bumper system, for which the face and diagonal members of the bumper are of 65% fibre glass SMC. Reference H5 describes the development of RP bumpers moulded using a 50% glass vinyl ester resin system. Reference S14 describes the use of SMC with 26% of continuous fibres and 9% of random fibres (SMC-C26/R9) in bus wheel wells. Reference A1 describes the advantages of a 26% chopped glass plus 49% continuous glass XMC (total glass content is 75%) and the possible applications due to the high mechanical properties of this material. However for general use, in low stressed applications, a conventional LP SMC with low percentages of glass fibre is suitable (see Chapter 10, Case Study).

This analysis of design applications shows the success which SMC has enjoyed over a relatively short period of time. The reason for this success is the number of advantages offered to the designer when compared with other materials. The following two lists show the advantages and disadvantages of SMC materials.

### 3.5.1 Advantages of SMC

- design flexibility
- dimensional stability
- parts consolidation
- high strength to weight ratio
- light weight (compared with steel and aluminium)
- low tooling cost ( $\frac{1}{4}$  of the price for steel and aluminium)
- chemical corrosion resistance
- moderate finishing costs
- good electrical properties
- good thermal properties
- semi-automatic manufacturing process
- less dependence on oil prices, due to its composition
- self extinguishing fire properties
- easy to glue or drill
- easy to repair
- possibility of formulating the SMC material to suit the final product
- SMC can be pigmented and moulded
- SMC is economic when annual production is in the range of 15,000 to 300,000 parts (A6).
- comparing the price on a weight basis for SMC with respect to steel and aluminium, SMC is more expensive; but comparing the price on a volume basis, steel and aluminium are about  $1\frac{1}{2}\%$  more expensive than SMC (L1).

### 3.5.2 Disadvantages of SMC

- high raw material costs
- low flexural modulus
- long production cycle times compared with thermoplastics
- viscosity variation with age of the material

- not economic for production runs smaller than 15,000 parts or more than 300,000 parts
- special surface treatment needed before painting
- higher density than thermoplastics
- styrene losses during manufacture and consequent pollution problems
- residual styrene after moulding
- isotropy dependence on flow
- special storing conditions needed
- maturation requirements before moulding
- strict quality control during SMC production and product moulding
- formation of weld-lines during moulding
- non recycleable material
- economical only for articles with ribs and bosses. For very simple articles the use of a continuous strand mat technique is cheaper.

## CHAPTER 4

RHEOLOGICAL CHARACTERIZATION OF SMC4.1 Introduction

The increased engineering use of SMC during the last 15 years has highlighted the need for an improved understanding of SMC flow behaviour. Part of that need is for improved experimental techniques which characterize SMC behaviour in a straightforward manner under conditions directly relevant to the compression moulding process (W4). Chapter 3 has explained that some of the many presently used conventional flow tests have this problem.

A physical representation of the compression-moulding process for producing flat parts is the squeeze flow of material between parallel plates, and it was for this reason that the squeeze flow technique was chosen in this work as a method for characterizing SMC behaviour. The aim was to gain further understanding of the rheological behaviour of SMC during moulding, but also to determine the form of the equation of state since this information can be used to improve the charge shape prediction procedure described in Chapters 6 and 7.

The basis of the squeeze flow method of flow characterization is given by Scott's original work (S1, S2); many workers (B4, B7, B12, L5, L6, G5) have followed his approach to examine the squeeze flow behaviour of Newtonian and non-Newtonian materials. Although Scott was the first to establish the equation for compression squeezing of Newtonian and non-Newtonian materials he did not define the range of applicability of his work.

Attempts by subsequent workers (B7, L5) to define the range of applicability have been in terms of the characteristic relaxation time ( $\lambda$ ) for the fluid.  $\lambda$  has been defined by Leider (L5, L6) in an equation form, the parameters involved in such equations were measured with a Weissenberg R-16 rheogoniometer. Brindley et al (B7) used a parameter called Deborah number (De) to characterise the flow behaviour of the fluid.  $De = \lambda/t_{\frac{1}{2}}$ , where  $t_{\frac{1}{2}}$  is the time needed for the plates to attain half their initial separation, under a constant compression force.

A power law equation of state can be used as the equation when  $De < 1$ , i.e. when the material is submitted to a light load (B7) or slow

squeezing (G5). Then the material behaviour is purely viscous.  $De > 1$  indicates viscoelastic behaviour, for example during fast squeezing or for heavy compressive forces. Unfortunately, it is not possible to use this characterization technique directly with fibre reinforced polyester compounds because their viscosities are too high for the delicate equipment used to determine  $\lambda$ .

Nevertheless by assuming dough moulding compound (DMC) was a power law fluid, Burns and Gandhi (B12) used Scott's equation for the rheological characterization of DMC. They showed that this was a realistic assumption for the low fibre content, short fibre length DMC. However applications of squeeze flow theory to the higher fibre content, long fibre length SMC need to account for the significant viscoelastic response shown by these materials during the compression moulding process (M2, S6).

Thus the basic idea behind the work reported in this Chapter, and Chapter 5, is that the squeeze flow of SMC discs between two parallel plates (one fixed and one mobile) provides a good foundation for the theoretical and experimental analysis of the rheological behaviour of SMC during compression moulding. The approach of the squeeze flow analysis is to characterize the flow behaviour by the time variation of compressive force during squeezing, using an equation of state which describes the viscoelastic nature of SMC flow. This mathematical analysis has been developed here only for flow at 20°C (room temperature). At the higher temperatures used for compression moulding, SMC flow becomes more complex, for example, due to non-uniform temperature and viscosity distributions within the SMC. Mathematical modelling of flow is therefore more complicated.

#### 4.2 Equation of State

Fundamentally the flow analysis for the plastometer depends on knowing the equation of state for the SMC. At present such an equation does not exist. The concept for the equation of state used in this work was formulated from ideas reported in the literature together with the interpretation of the flow behaviour shown by some preliminary work with the parallel plate plastometer.

The three main aspects of the time dependent behaviour of the material during compression flow which the equation of state needs to take into account are the viscoelastic nature of flow, the breaking of molecular bonds formed during thickening, and the increasing resistance to deformation which is shown as the fibre bundles become compacted together. The concept of viscoelastic flow is mentioned by Sieglaff (S6) and Maxwell (M3), and Thomas (T4) has suggested the following equation of state from his empirical studies with a parallel cylinder shear rheometer:

$$\tau = \mu \dot{\gamma}^n + K\gamma$$

where:  $\tau$  = shear stress  
 $\mu$  = viscosity modulus  
 $\gamma$  = shear strain ( $\dot{\gamma}$  is shear rate)  
 $K$  = elasticity modulus  
 $n$  = exponent

I have introduced a yield element into this equation to account for the effects of fibre interaction and molecular bond breakage during the later stages of compression flow. Thus:

$$\tau = \mu \dot{\gamma}^n + K\gamma + f \quad (4.1)$$

where:  $f$  = yield stress

In general it has been found that the physical interpretation of  $f$  is not straightforward (S8). For example, the experimental work shows  $f$  to have a small negative value at the beginning of compression. This may be attributable to the compression of voids in the SMC.

Figure 4.1 shows the analogue for the equation of state. Linear viscoelasticity is assumed, and since there is equal strain in each element, the total compression force is the sum of the forces acting on each of the viscous, elastic and yield elements. This is the basis for the analysis.

$$F_T = F_v + F_e + F_y \quad (4.2)$$

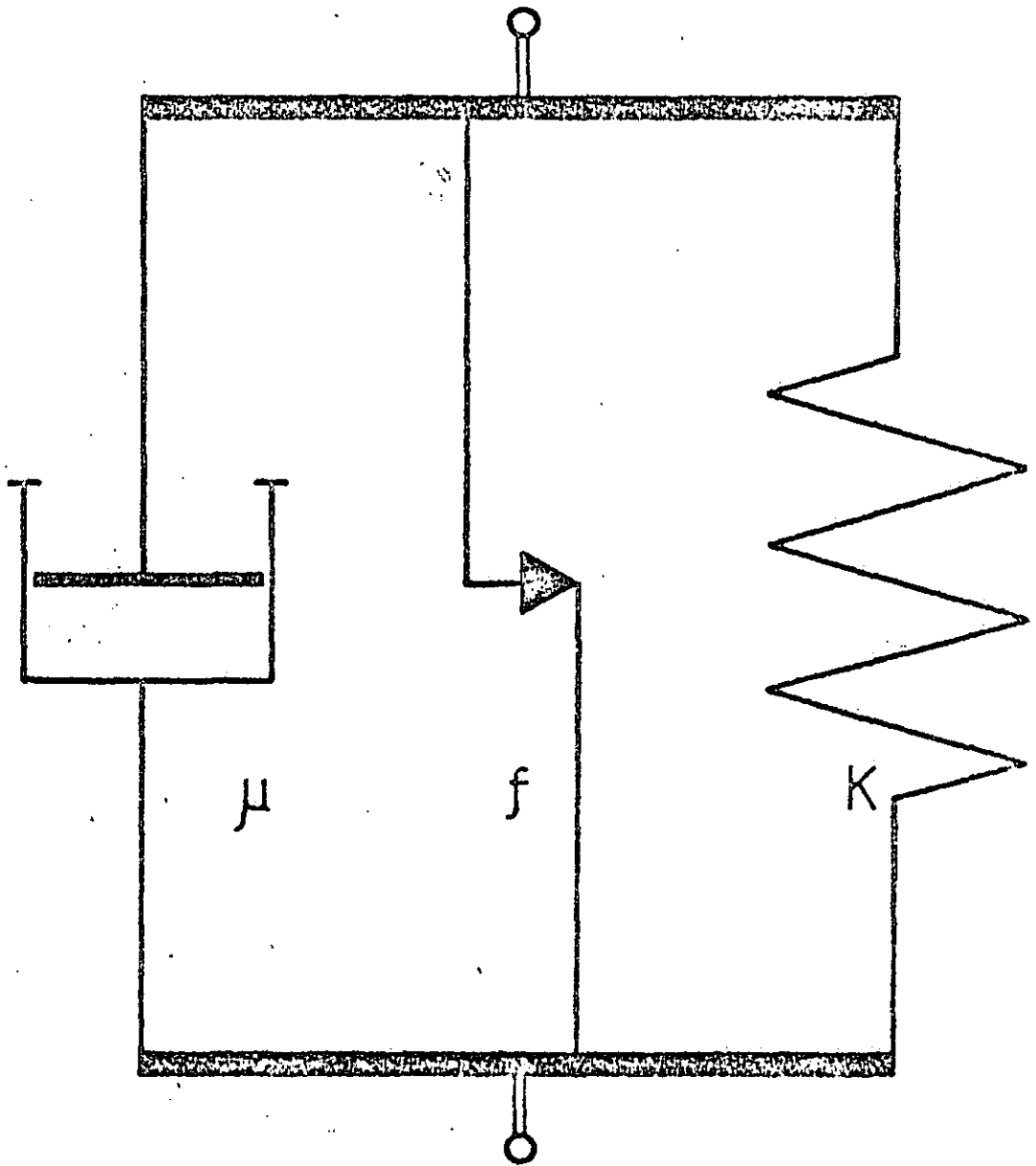


Fig.4.1 ANALOGUE MODEL FOR SMC  
EQUATION OF STATE.

where:  $F_T$  = total compression force  
 $F_v$  = viscous force  
 $F_e$  = elastic force  
 $F_y$  = yield force

#### 4.3 Compression Force General Analysis

The analysis begins by using the momentum and continuity equations, which have the following general form (T1):

$$\rho \frac{Dv}{Dt} = - \nabla p - (\nabla \cdot \tau) + \rho g \quad (4.3)$$

$$\frac{\partial \rho}{\partial t} + (\nabla \cdot \rho v) = 0 \quad (4.4)$$

where:  $\rho$  = density  
 $t$  = time  
 $\nabla$  = differential operator  
 $v$  = velocity tensor  
 $\tau$  = stress tensor  
 $p$  = pressure  
 $g$  = acceleration due to gravity

These equations may be written in cylindrical coordinates (T1) for the system shown in Figure 4.2, where the origin of the axes lies in the surface of a rigidly fixed lower plate.

To apply equations 4.3 and 4.4 to the analysis of compression flow of SMC in the parallel plate plastometer, the following assumptions were made:

- 1) The material is uniform, homogeneous, isotropic in the  $r-\theta$  plane, and incompressible. Body forces have been disregarded.
- 2) The Reynolds number is very small and hence the inertia terms of the momentum equation have been disregarded.
- 3) The plate separation is smaller than the diameter ( $D > H$ ), i.e. not greater than about one quarter of the diameter.

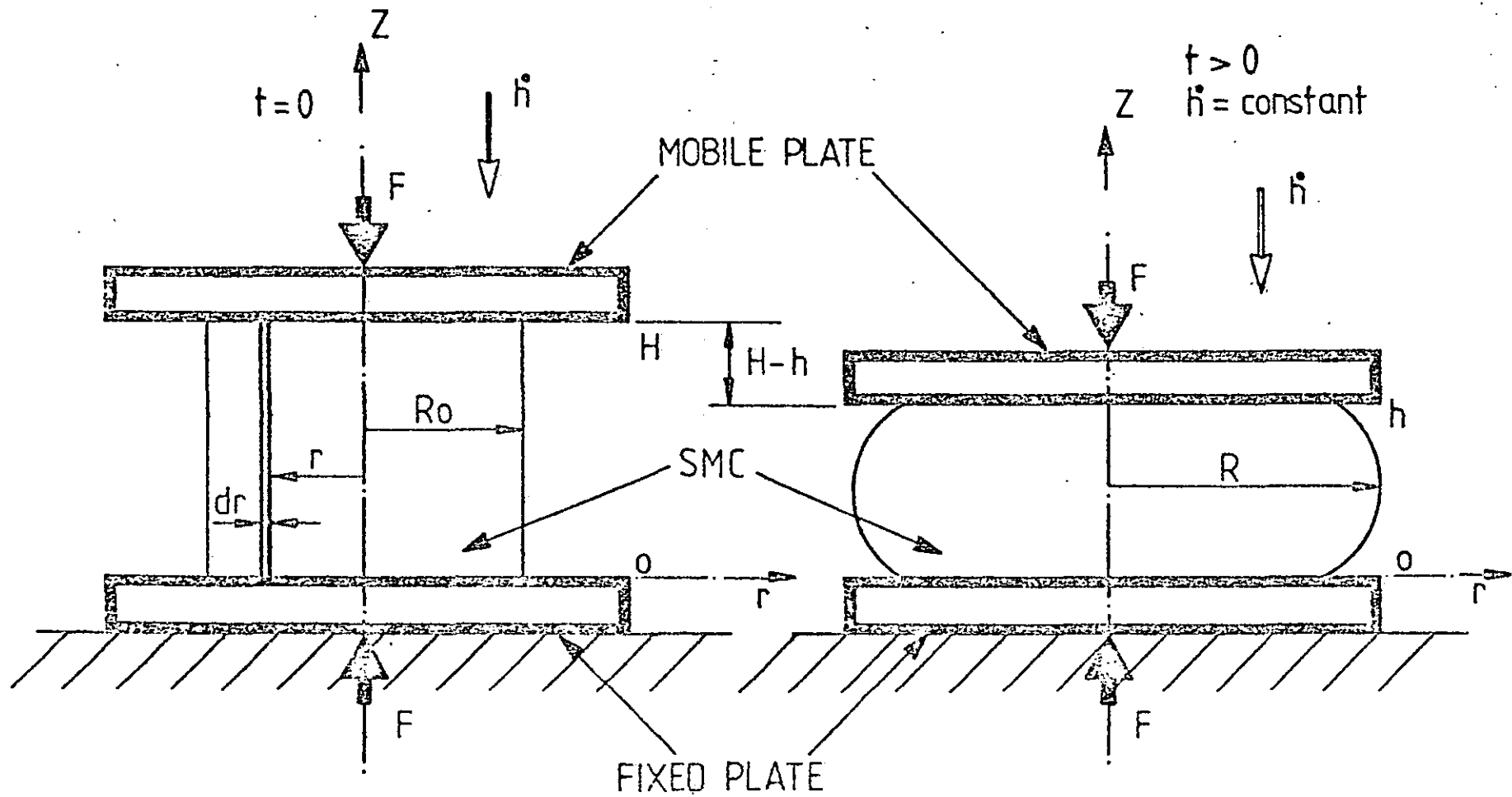


Fig.4.2 CYLINDRICAL COORDINATE SYSTEM

- 4) the material flows radially outwards in layers.
- 5) There is no surface-slip effect during flow, i.e. the thin layer of SMC which touches the plastometer plates has zero speed.
- 6) Fibre reorientation due to flow is small, which usually applies when the final compressed thickness is not less than about 70% of the SMC original thickness, (D4, M7).

Using these assumptions, equations 4.3 and 4.4 may be written as:

$$\frac{1}{r} \frac{\partial}{\partial r} (r \cdot v_r) + \frac{\partial v_z}{\partial z} = 0 \quad (4.5)$$

$$\frac{\partial \tau_{rz}}{\partial z} = - \frac{\partial p}{\partial r} \quad (4.6)$$

where:  $v_r$  = radial speed  
 $v_z$  = normal speed  
 $\tau_{rz}$  = shear stress  
 $p$  = pressure

For constant volume of SMC, equation 4.5 becomes:

$$\frac{\dot{h}r}{2} = \int_0^{h(t)/2} v_{r1} dz + \int_{h(t)/2}^{h(t)} v_{r2} dz \quad (4.7)$$

where:  $h(t)$  = instantaneous value of plate separation  
 $h(t) = H - \dot{h}t$   
 $H$  = initial plate separation  
 $\dot{h}$  = plate speed  
 $v_{r1}, v_{r2}$  = radial speed

The radial shear strain  $\gamma_r$  is related to the plastometer plate closure by:

$$\gamma_r = \ln(r/r_0) = (1/2) \ln(H/h(t)) \quad (4.8)$$

The governing equation for the force variation vs time is obtained by combining equations 4.1, 4.6 and 4.7, for the conditions of constant compressive speed and constant SMC volume. (These were the conditions for the tests reported in this thesis).

For simplicity of derivation, the analysis for the time variation of compressive force equation was carried in three parts. Firstly equations 4.6 and 4.7 were combined with the viscous element only of equation 4.1, then with the elastic element, and finally the analysis was for the viscous and yield elements together.

The boundary conditions for the three analyses are as follows:

$$\begin{aligned} v_r &= 0 \text{ at } t \leq 0 \text{ for all } r \text{ and } z \\ v_r &= 0 \text{ at } z = 0 \text{ and } z = H \text{ for } t \geq 0 \\ v_r &= v_{r\max} \text{ at } z = h(t)/2 \text{ for } t \geq 0 \\ p &= \text{atmospheric pressure at } r = R \text{ for all } t \\ h(t) &= H \text{ at } t = 0 \end{aligned}$$

$$\frac{\partial v_r}{\partial r} \text{ is negligible compared with } \frac{\partial v_r}{\partial z} .$$

#### 4.3.1 Analysis for a Viscous Element

This analysis is based on the principles outlined by Scott's work (S1), but with one important difference: Scott's work was for two plates moving towards the mid-thickness, but for the work reported here, one plate is mobile and one fixed. This fact alters the force equation.

At this stage it is instructive to point out that some workers (e.g. L5) have used Scott's theory (i.e. the theory for two plates moving towards the centre) but applied it to experimental work with one plate fixed and one mobile.

The three equations required are 4.6, 4.7 and the equation of state 4.9 together with the boundary conditions:

$$\tau_{rz} = \mu \dot{\gamma}^n = \mu \left( \frac{\partial v_r}{\partial z} \right)^n \quad (4.9)$$

Assuming that  $\tau_h$  is the shear stress at  $z = h$

$$\tau_{rz} = 2 \tau_h (z - h(t)/2)/h(t) \quad h(t) \geq z \geq h(t)/2 \quad (4.10)$$

$$\tau_{rz} = 2 \tau_h (h(t)/2 - z)/h(t) \quad h(t)/2 \geq z \geq 0$$

Substituting 4.10 in 4.9 and integrating  $v_r$

$$v_r = \left| \left( \frac{2 \tau_h}{\mu h(t)} \right) \left( \frac{n}{n+1} \right) \left[ (h(t)/2)^{(n+1)/n} - (z - h(t)/2)^{n+1} \right] \right| \quad (4.11)$$

Substituting in 4.7 and integrating

$$(2 \tau_h / \mu h(t))^{1/n} = (2n+1)(2/h(t))^{(n+1)/n} (\dot{h}r/2h(t)) \quad (4.12)$$

Substituting 4.12 in 4.11

$$v_r = \left| \left( \frac{\dot{h}r}{2 h(t)} \right) \left( \frac{2n+1}{n+1} \right) \left[ 1 - \left( \frac{2z}{h(t)} - 1 \right)^{(n+1)/n} \right] \right| \quad (4.13)$$

Derivating 4.13 in  $z$  and substituting in 4.9

$$\tau_{rz} = \mu \left[ \left( \frac{\dot{h}r (2n+1)}{h(t)^2 n} \right)^n \left[ \left( \frac{2z}{h(t)} - 1 \right) \right] \right] \quad (4.14)$$

Using equation 4.6, integrating it and then equating it to 4.14.

Integrating the pressure

$$p = - 2\mu \frac{\dot{h}^n R^{n+1} (2n+1)^n}{n^n (n+1) (h(t))^{2n+1}} \left[ 1 - (r/R)^{n+1} \right] \quad (4.15)$$

Evaluating the force:

$$F = 2\pi \int_0^R p r dr = - 2\mu \frac{\dot{h}^n R^{n+3} (2n+1)^n \pi}{n^n (n+3) (h(t))^{2n+1}} \quad (4.16)$$

Knowing that the speed of compression and the volume (V) are constants:

$$F = \mu f_1(t) \quad (4.17)$$

$$f_1(t) = - \frac{2 \dot{h}^n V^{(n+3)/2} (2n+1)^n}{n^n (n+3) \pi^{(n+1)/2} (h(t))^{(5n+5)/2}} \quad (4.18)$$

#### 4.3.2 Analysis for an Elastic Element

The three equations required in this analysis are 4.6, 4.7 and the equation of state 4.19 together with the boundary conditions

$$\tau_{rz} = K\gamma \quad (4.19)$$

Equation 4.19 may be written as

$$\tau_{rz} = K \ln (r/r_0) \quad (4.20)$$

Assuming the equation of radial speed of the form:

$$v_r = Az^2 + Bz + c \quad (4.21)$$

Combining equation 4.21 with the boundary conditions

$$v_r = 4 v_{\max} (zh(t) - z^2)/h(t)^2 \quad (4.22)$$

Substituting equation 4.22 in equation 4.7 and integrating,  $v_{r\max}$  is found as a function of  $r$ ,  $\dot{h}$ , and  $h(t)$ . Then substituting  $v_{r\max}$  in equation 4.22

$$v_r = 3 r \dot{h} (zh(t) - z^2)/h(t)^3 \quad (4.23)$$

Equation 4.23 may be written as:

$$dr = 3r (zh(t) - z^2) dh/h(t)^3 \quad (4.24)$$

Integrating equation 4.24 and then substituting in equation 4.20

$$\tau_{rz} = 3K [z (1/H - 1/h(t)) + z^2(1/h(t)^2 - 1/H^2)/2] \quad (4.25)$$

Differentiating 4.25 in z, substituting in equation 4.6 and integrating gives:

$$p = 3K [(1/H - 1/h(t)) + h (1/h(t)^2 - 1/H^2)/2] (R - r) \quad (4.26)$$

Integrating the pressure, as in equation 4.16, and considering that the volume of material is always constant:

$$F = K f_2(t) \quad (4.27)$$

$$f_2(t) = [V^{3/2}/(\pi^{1/2} h(t)^{5/2}H) (h(t)-H) + (H^2-h(t)^2)/2h(t)] \quad (4.28)$$

### 4.3.3 Analysis of Viscous and Yield Elements Together

This analysis is based on the work of Oka (01) and on the analysis of section 4.3.1. Oka has developed an equation for the force variation vs time of a Bingham body.

$$\tau_{rz} = \mu \dot{\gamma} + f \quad (4.29)$$

$$F_{vy} = -\frac{3}{2} \mu \frac{V^2 \dot{h}}{\pi h(t)^5} + \frac{2}{3} f \frac{V^{3/2}}{\pi^{1/2} h(t)^{5/2}} \quad (4.30)$$

Equation 4.30 is the one obtained by Oka. This equation can be written as:

$$F_{vy} = F_v + F_y \quad (4.31)$$

The viscous force obtained by Oka is the same as the one obtained in section 4.3.1 when  $n = 1$ . Assuming that the strain in both elements is the same, the equation for a viscous and yield elements with variable  $n$  can be written as follows:

$$F_{vy} = \mu f_1(t) + f f_3(t) \quad (4.32)$$

$$f_3(t) = (2 V^{3/2}) / (3 \pi^{1/2} h(t)^{5/2}) \quad (4.33)$$

#### 4.4 Final Equation

The governing equation for the compression force has the following form:

$$F_T = \mu f_1(t) + K f_2(t) + f f_3(t) \quad (4.34)$$

where  $f_1(t)$ ,  $f_2(t)$  and  $f_3(t)$  are the time dependent factors defined in equations 4.18, 4.28, 4.33.

## CHAPTER 5

EXPERIMENTAL WORK ON RHEOLOGY5.1 Experimental Work

There were two main aims for the experimental programme. One was to check if the three element model for the equation of state provided a realistic mathematical basis for characterizing the rheological behaviour of SMC at 20°C and at 160°C. The other aim was to show how the parallel plate plastometer can be used to give data which characterize SMC flow behaviour under conditions similar to those of the actual moulding process.

The experimental work involved squeezing discs of SMC between parallel plates mounted in an Instron TT-CM machine. Figure 5.1 shows a general view of the parallel plate plastometer in the Instron machine, Figure 5.2 shows a close-up of the plastometer and Figure 5.3 shows the drawing for the manufacture of the plastometer.

The experimental work was split into two main parts, depending on the temperature at which the tests were carried out. The first part was carried out at 20°C. Discs of 40 mm diameter were cut from a LP-SMC (SY-19/25L, see section 9.1 for material composition). One month old and 3 month old batches of SMC were used for the tests. The discs were stacked in 1, 2 or 3 layers and compressed at constant speeds ranging from 0.1 cm/min to 5.0 cm/min. The compression tests were stopped when 70% of the initial thickness was achieved. The second part was carried out at 160°C. Otherwise the material was tested under the same conditions as in the first part.

The following equipment was used in addition to the parallel plate plastometer. Cr-Al thermocouples measured the temperature of the plastometer and also the temperatures of the SMC discs. The movement of the mobile plate was measured by one displacement transducer (DC-LVDT type). A Digital Equipment PDP-11/05 16 bit length computer collected displacement, compressive force and temperature (of the SMC discs) data on-line during each test (Appendix 1 shows the program used to record the data).

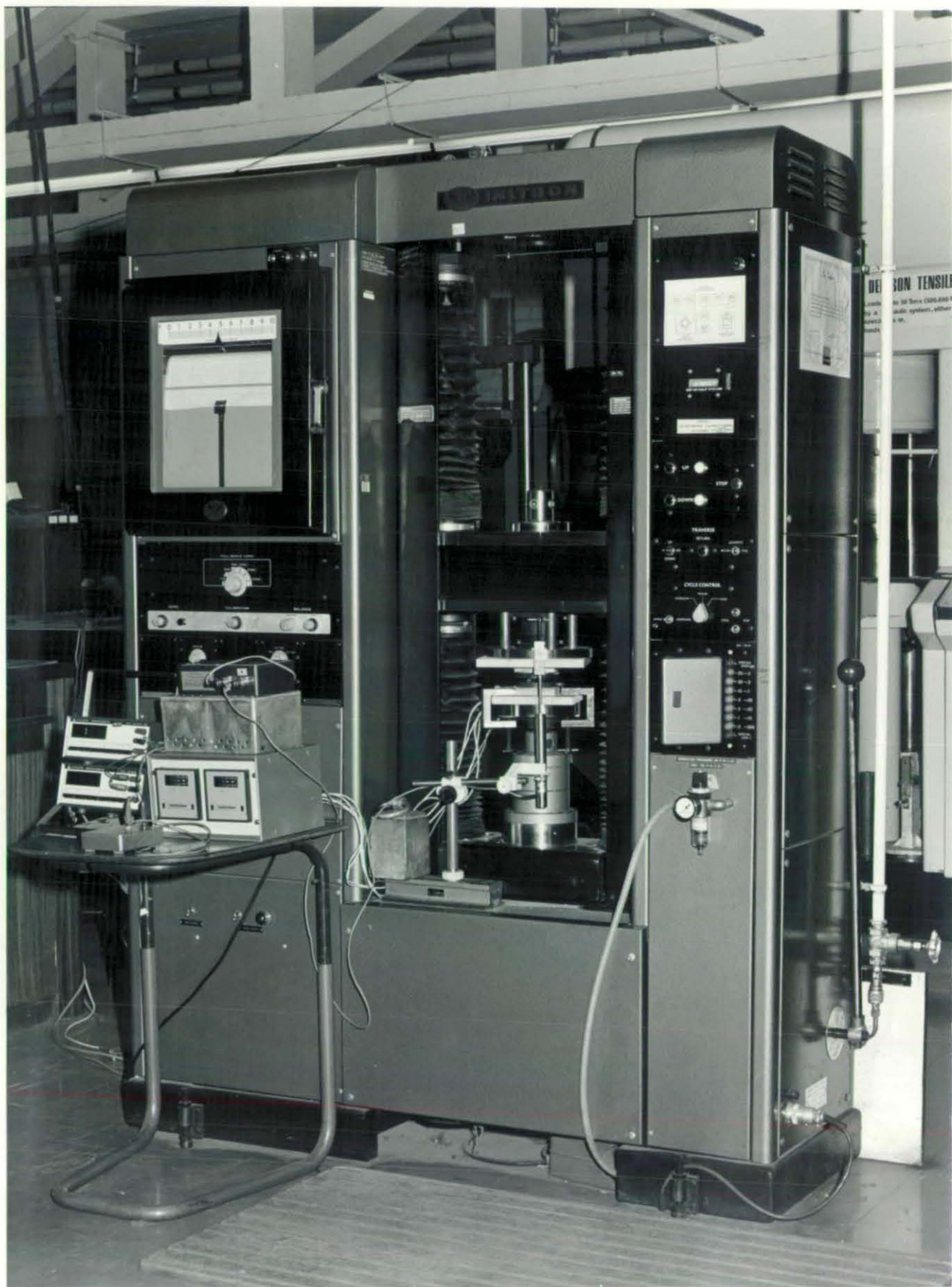


FIGURE 5.1 General view of plastometer

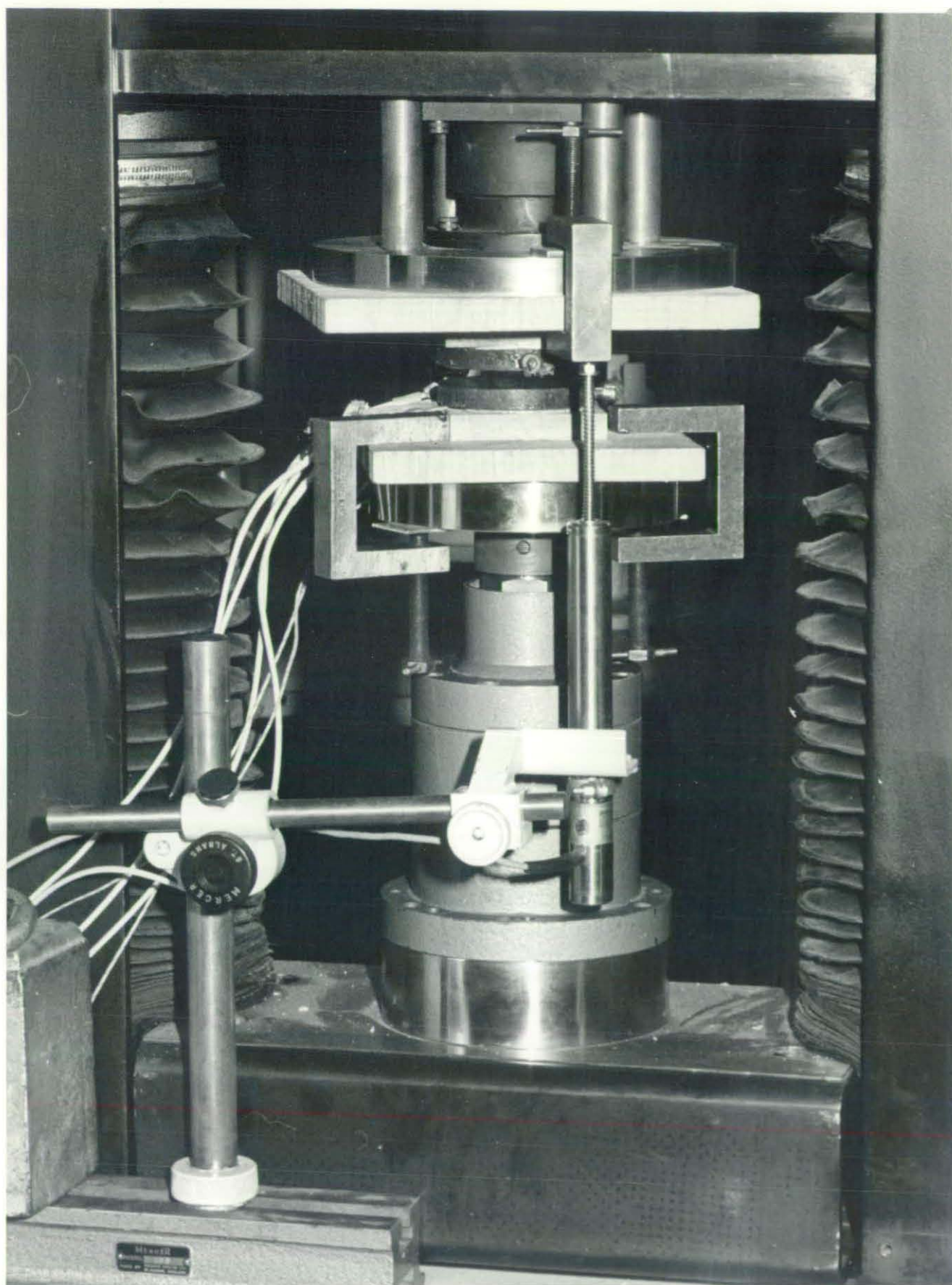


FIGURE 5.2 Close-up of plastometer



### 5.1.1 Squeeze Tests at 20°C

Figures 5.4 to 5.6 show the time variation of compression force for tests at 20°C. The curves in these figures have been fitted using the model of equation 4.34. Figure 5.6 compares the flow behaviour of one month old and three month old SMC, stored under manufacturer's recommended conditions (in a cool place, and out of direct light).

The variation of the compression force with shear strain for the data from Figures 5.4 to 5.6 for different volumes of SMC and plate closure speeds is shown in Figure 5.7 for the one month old SMC.

Although most of the discs were squeezed to 70% of their initial thickness, some tests were carried out further than 70%, some samples were squeezed to 40% of their SMC initial thickness. Figure 5.8 shows the force variation with time up to a 60% reduction of the initial thickness. Figures 5.9 to 5.11 are photographs of sections through the SMC discs taken at points 1 to 3 respectively in Figure 5.8, showing how the fibre spacing varies during compression. (Appendix 3 explains the sample preparation for cross-section analysis with reflective light).

### 5.1.2 Squeeze Tests at 160°C

For these tests, the temperature of the plastometer plates was controlled to 160°C ± 1.25 deg C. Disc compression started immediately after the discs had been placed on the lower plate. SMC temperature for each test was measured by a Cr-Al thermocouple in the middle of the disc.

Figures 5.12 to 5.14 show the experimental force versus time data for these tests, and temperature-time variation is shown in Figures 5.15 and 5.16.

Marker and Ford (M2) found that the SMC in contact with the mould flows easier than that at mid-thickness (see Figure 5.17). Figure 5.18 shows the flow front profile of a sample compressed at 160°C. Such a flow front profile is due to the difference in temperature from the surface to the mid-thickness.

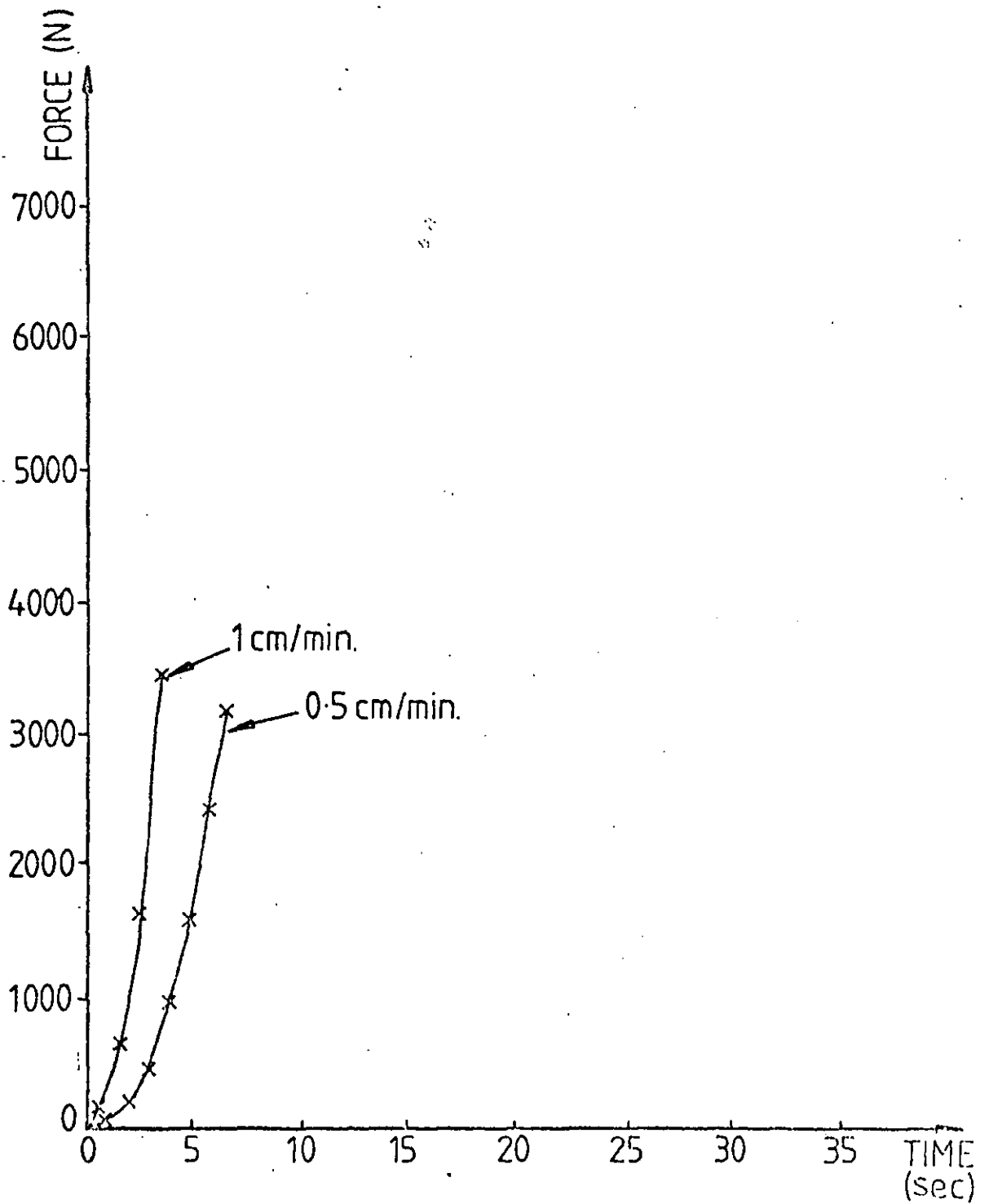


Fig.5.4 FORCE-TIME VARIATION AT 20°C  
(1 LAYER OF 1 MONTH OLD SMC ).

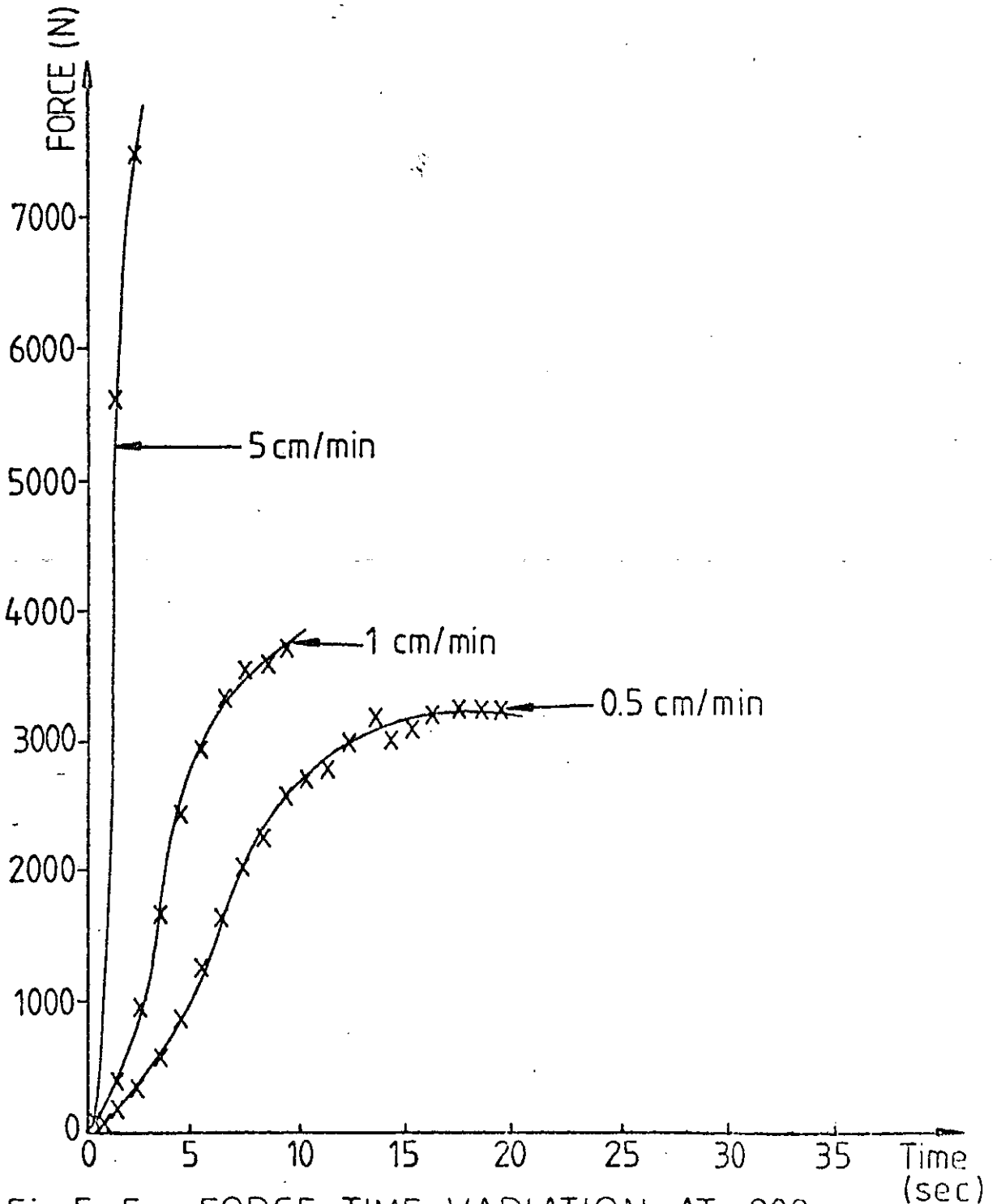


Fig.5.5 FORCE-TIME VARIATION AT 20°C  
(3 LAYERS OF 1 MONTH OLD SMC).

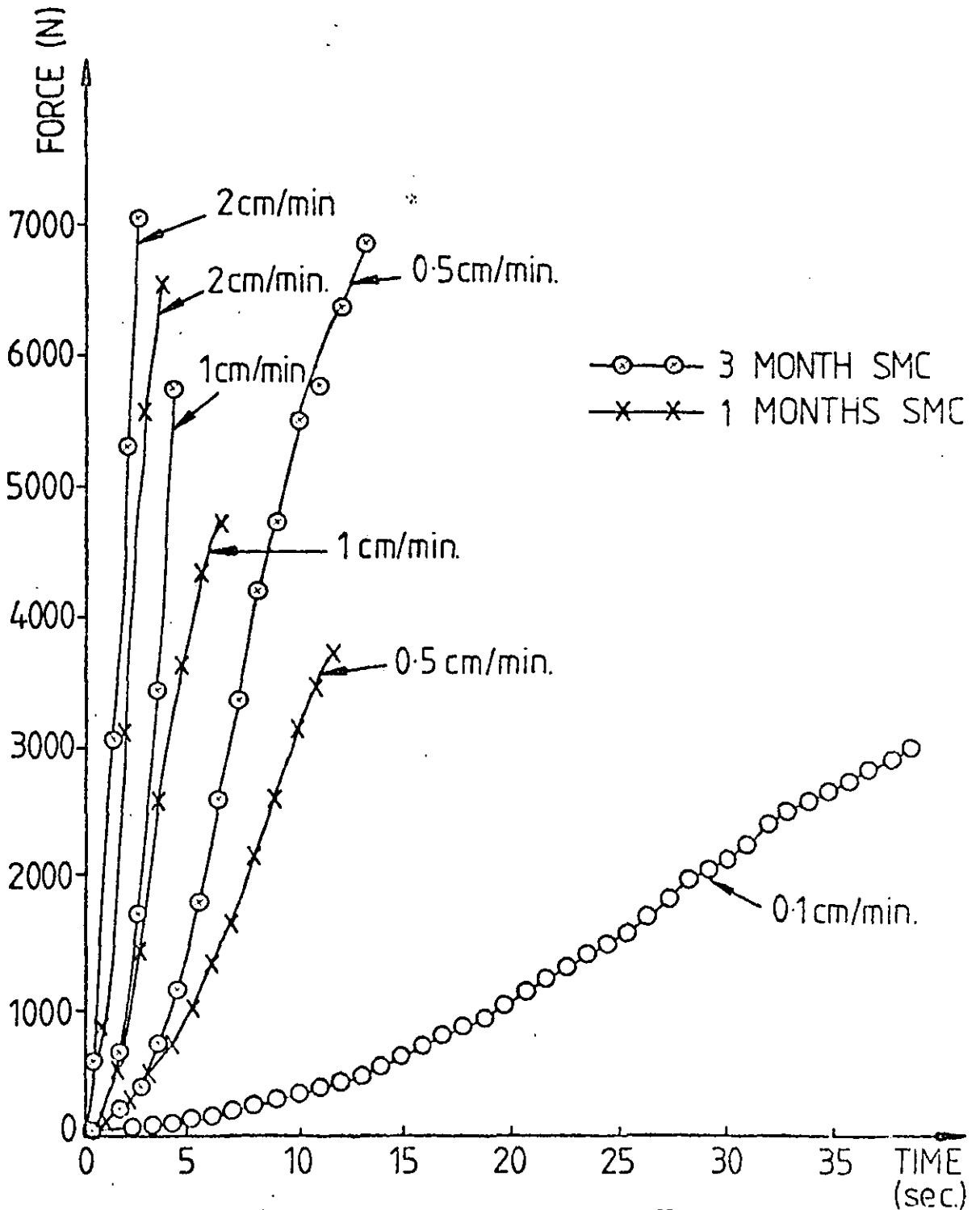


Fig.5.6 COMPARISON OF FORCE-TIME VARIATION AT 20°C (2 LAYERS OF 1 MONTH OLD AND 3 MONTH OLD SMC).

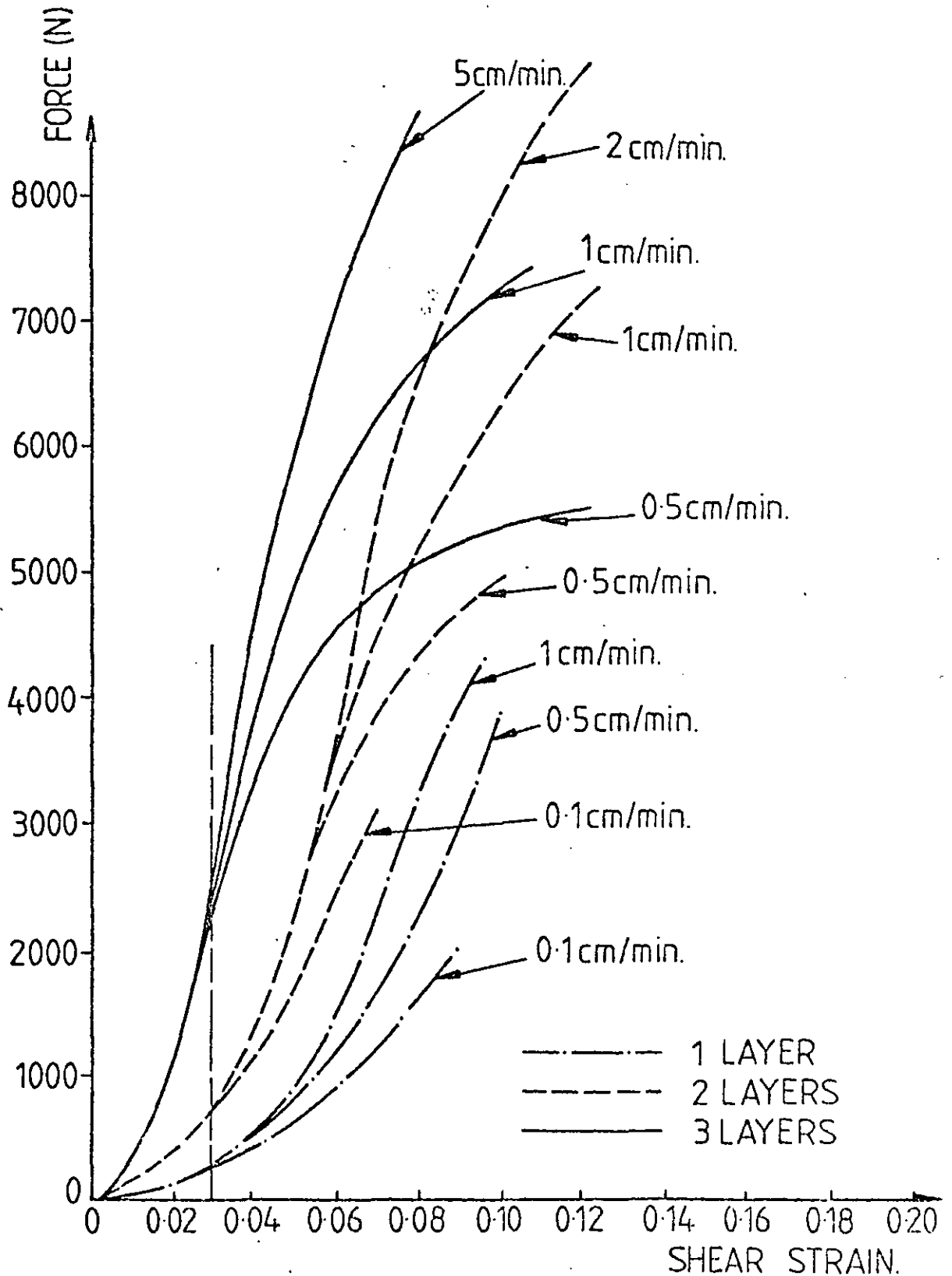


Fig.5.7 FORCE-STRAIN VARIATION AT 20°C  
(1,2 AND 3 LAYERS OF 1 MONTH OLD  
SMC).

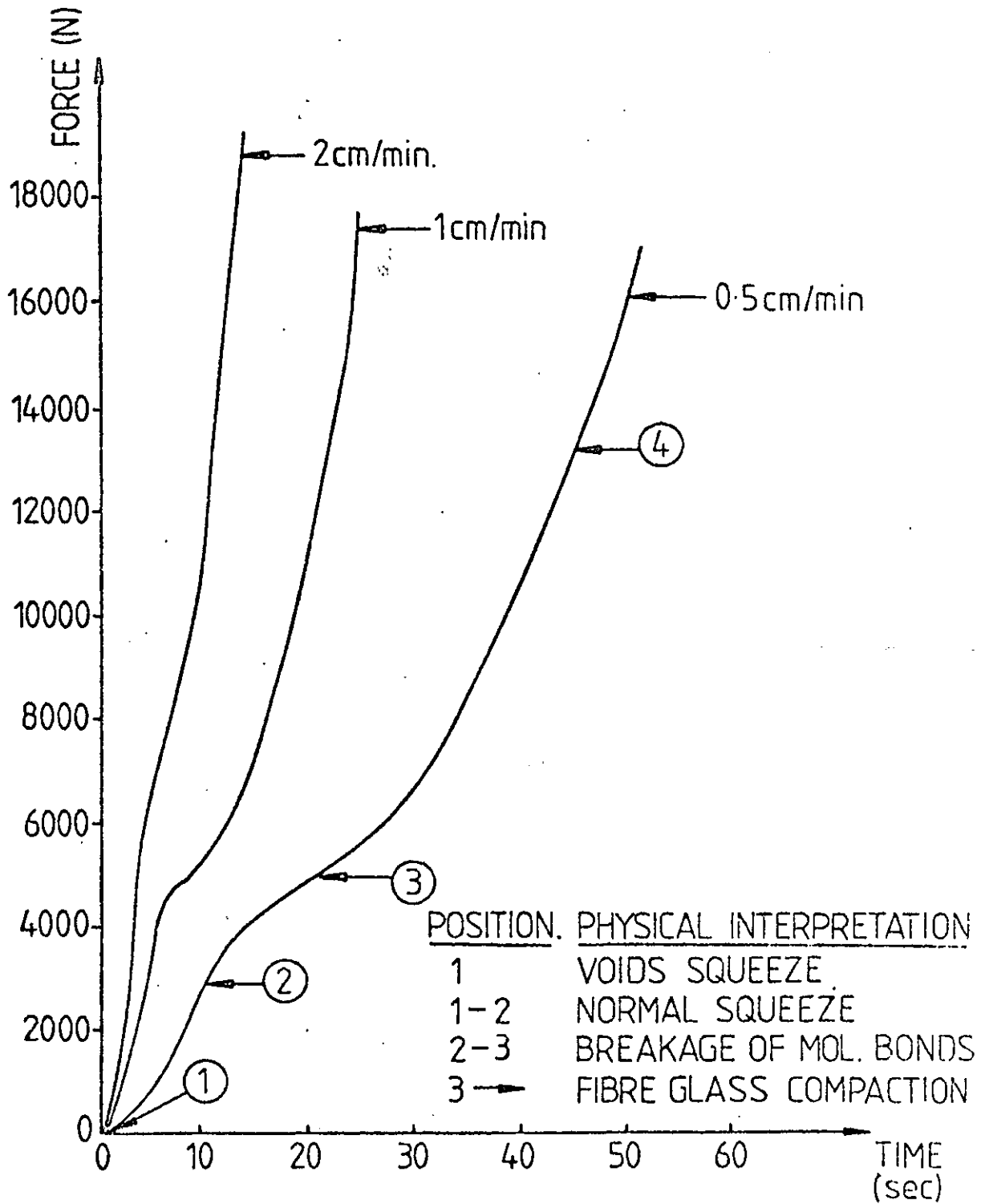


Fig. 5.8 FORCE-TIME VARIATION AT 20°C SHOWING DIFFERENT STAGES OF FLOW BEHAVIOUR (2 LAYERS OF 1 MONTH OLD SMC).

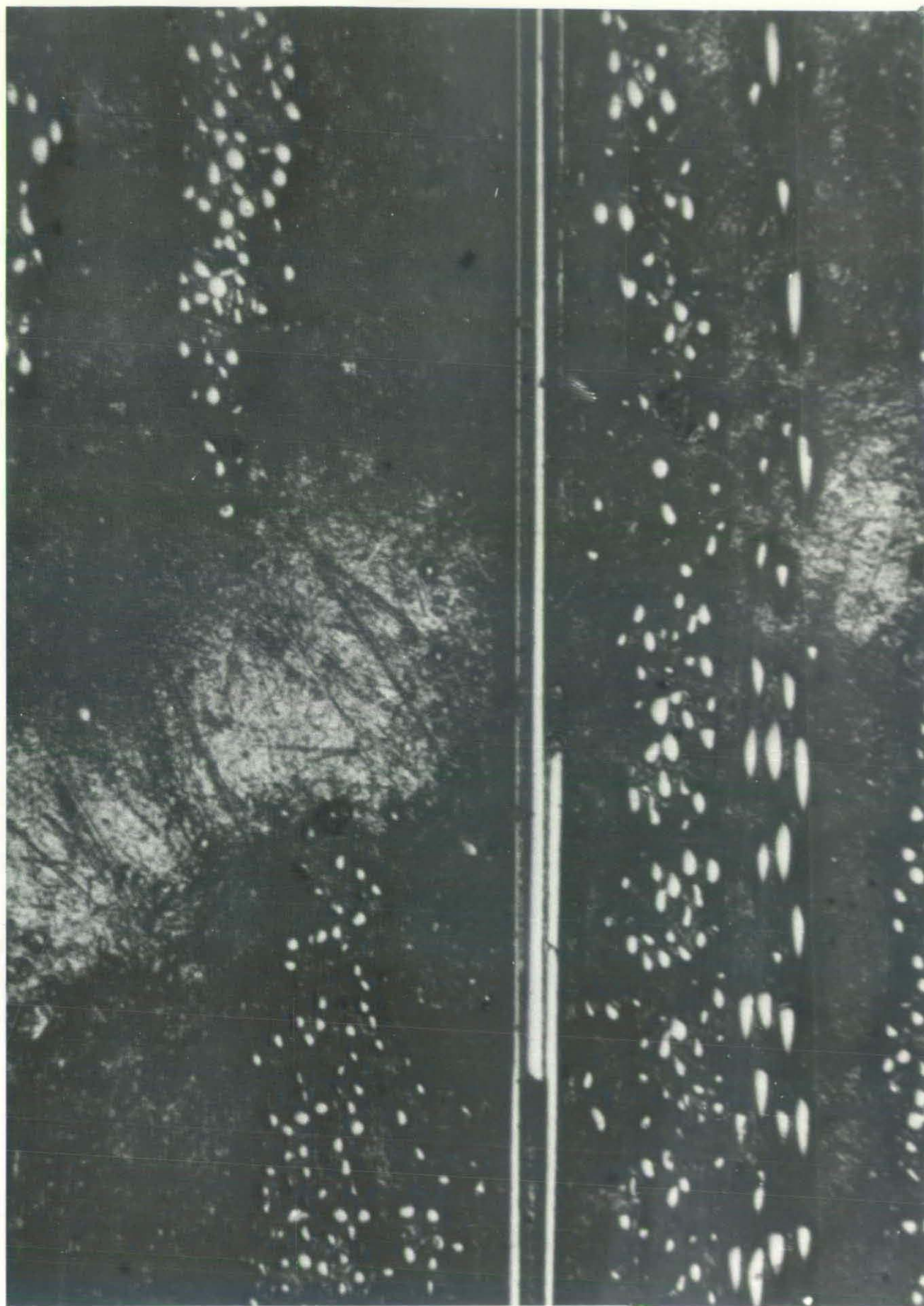


FIGURE 5.9 Cross-section of SMC disc at point 1 in Figure 5.8 (2 layers of 1 month old SMC). Magnification x 6.3

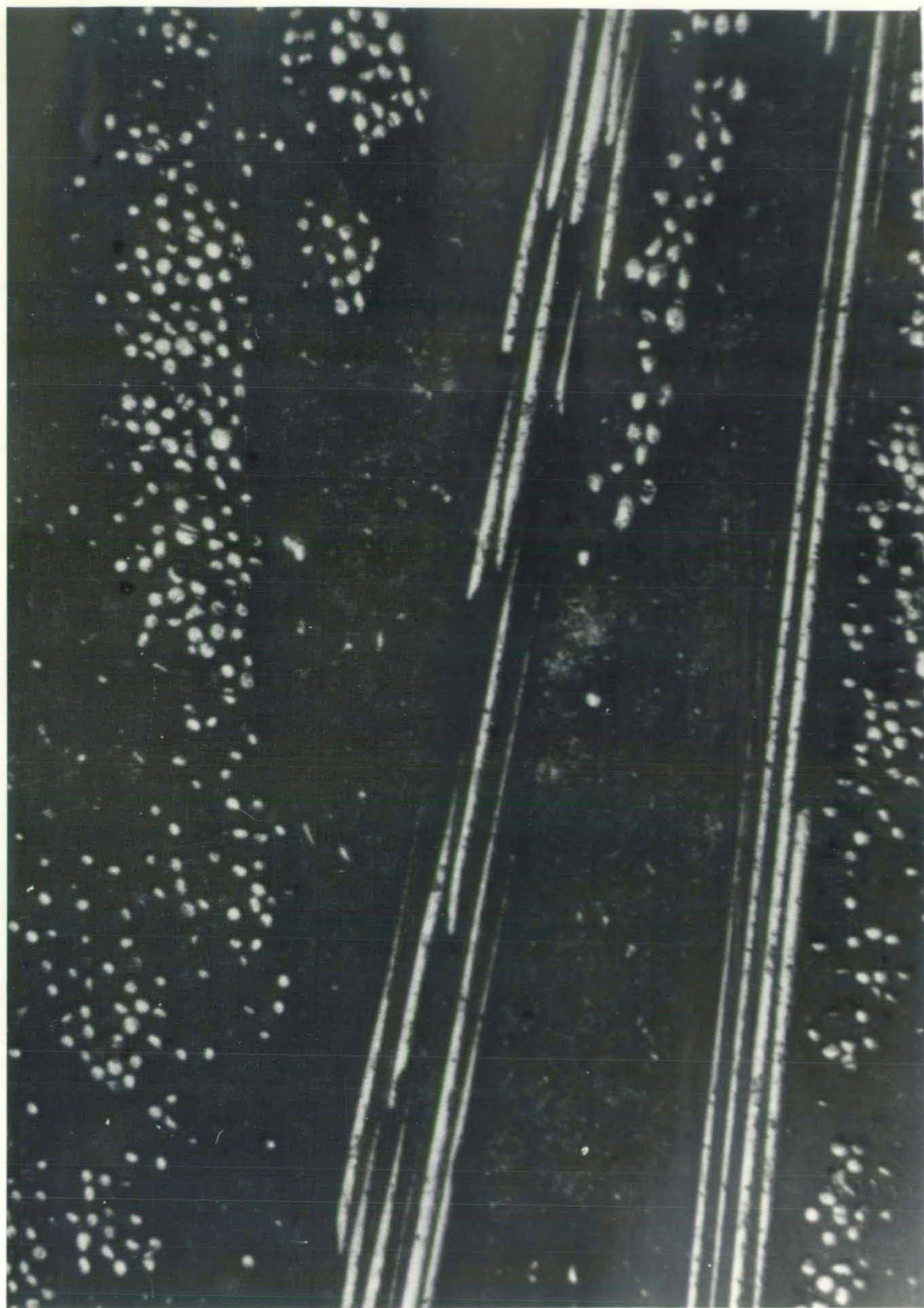


FIGURE 5.10 Cross-section of SMC disc at point 2 in Figure 5.8 (2 layers of 1 month old SMC). Magnification x 6.3.

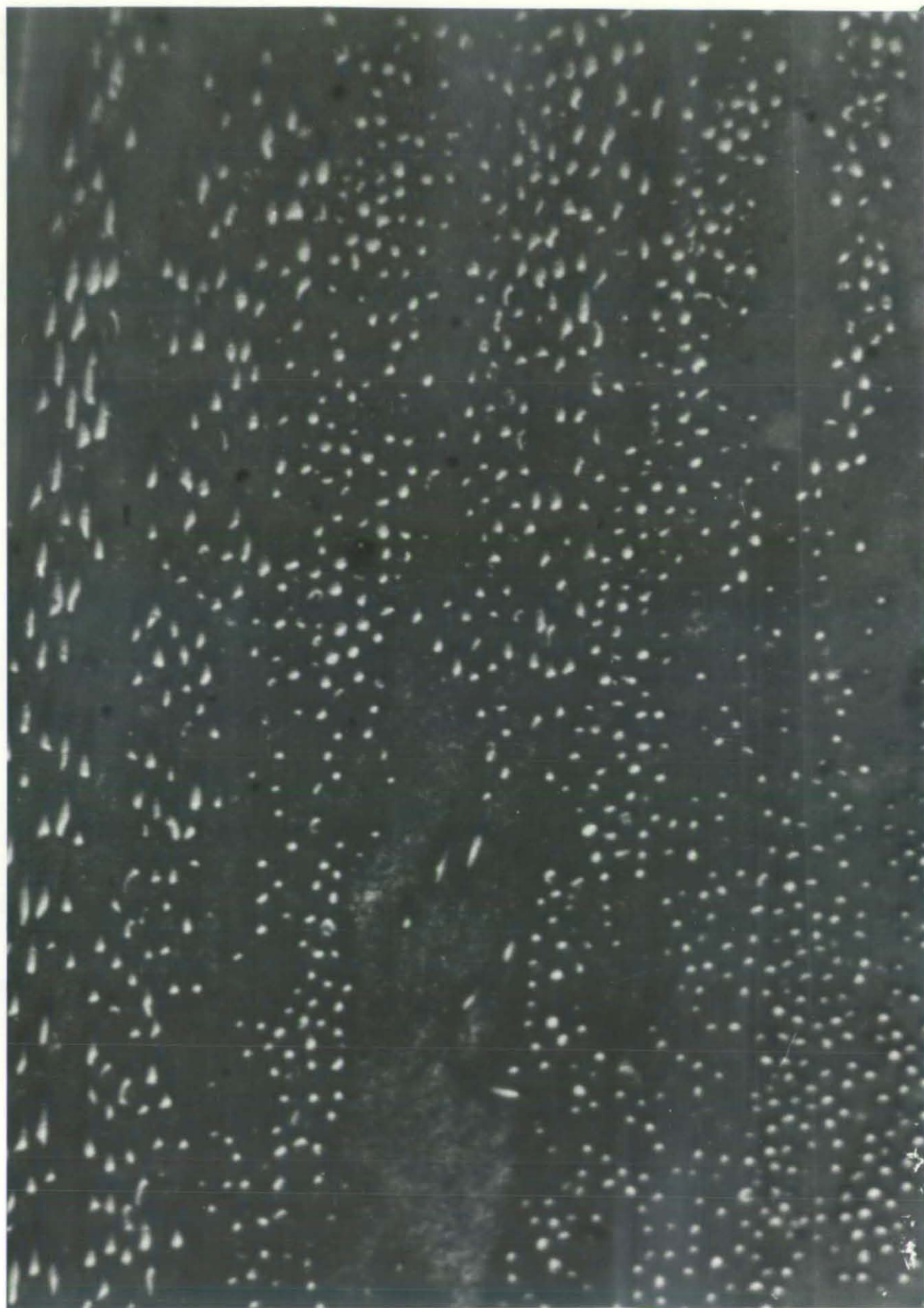


FIGURE 5.11 Cross-section of SMC disc at point 3 in Figure 5.8 (2 layers of 1 month old SMC). Magnification x 6.3.

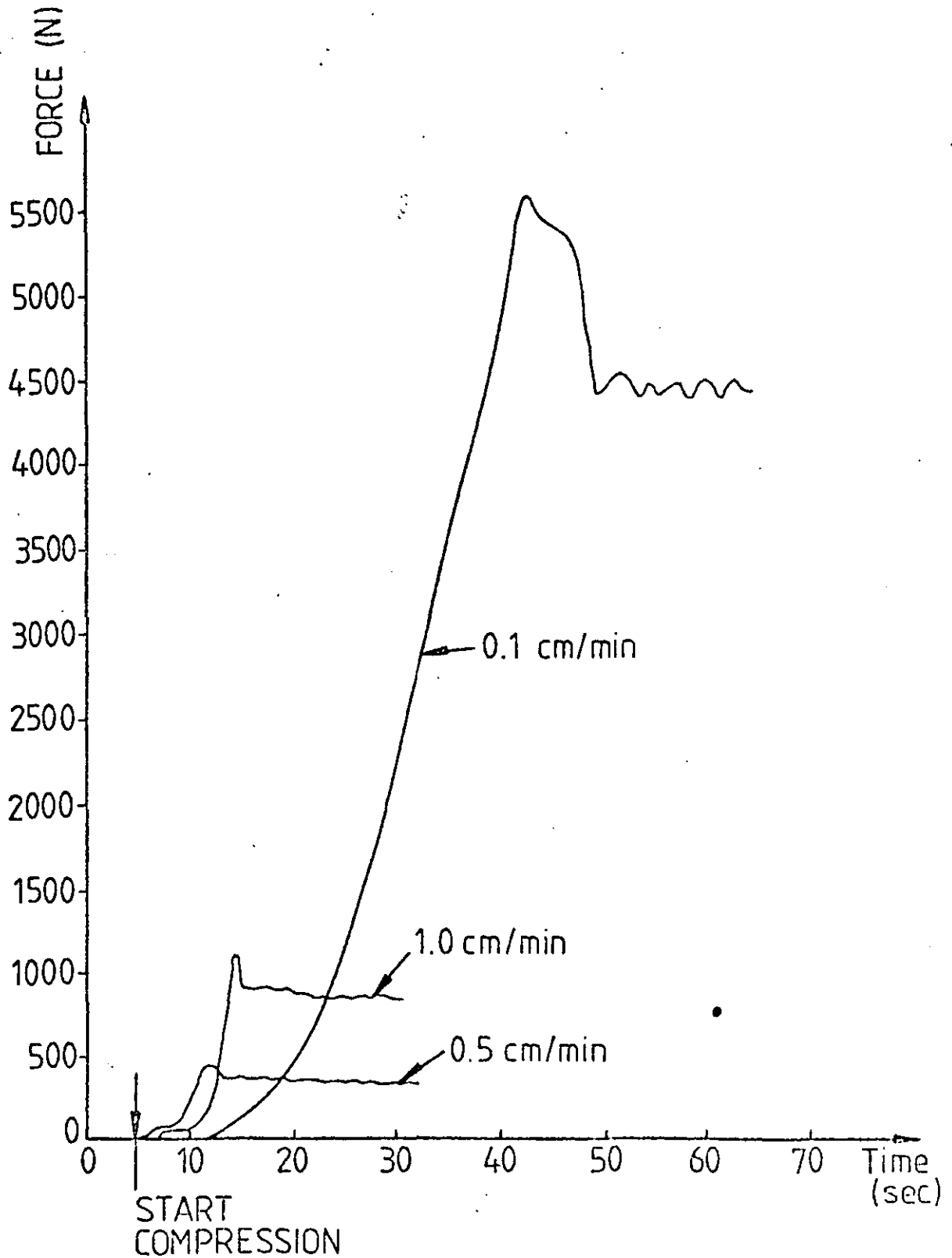


Fig.5.12 FORCE-TIME VARIATION AT 160°C  
(1 LAYER OF 1 MONTH OLD SMC).

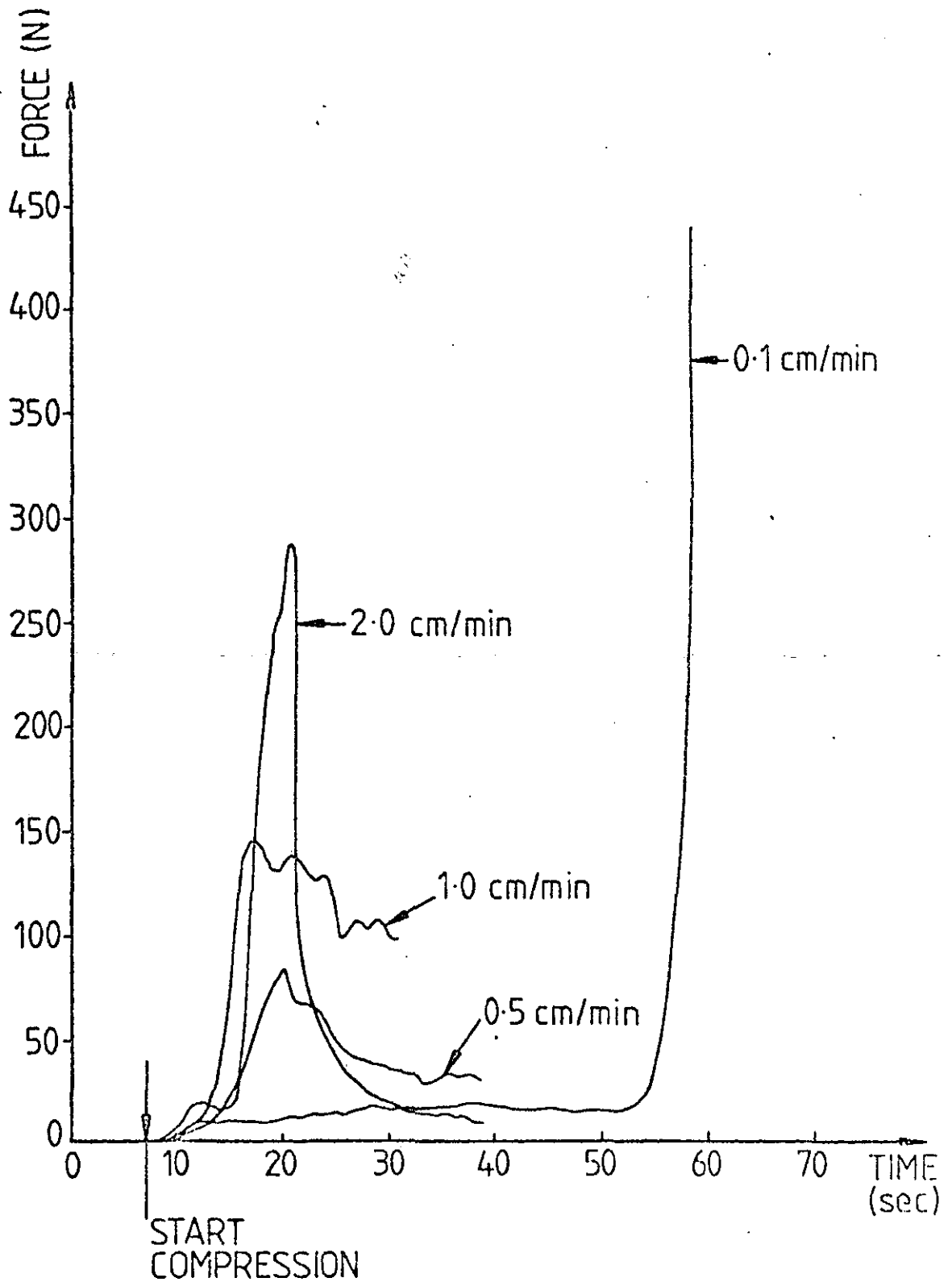


Fig.5.13 FORCE-TIME VARIATION AT 160°C  
(2 LAYERS OF 1 MONTH OLD SMC).

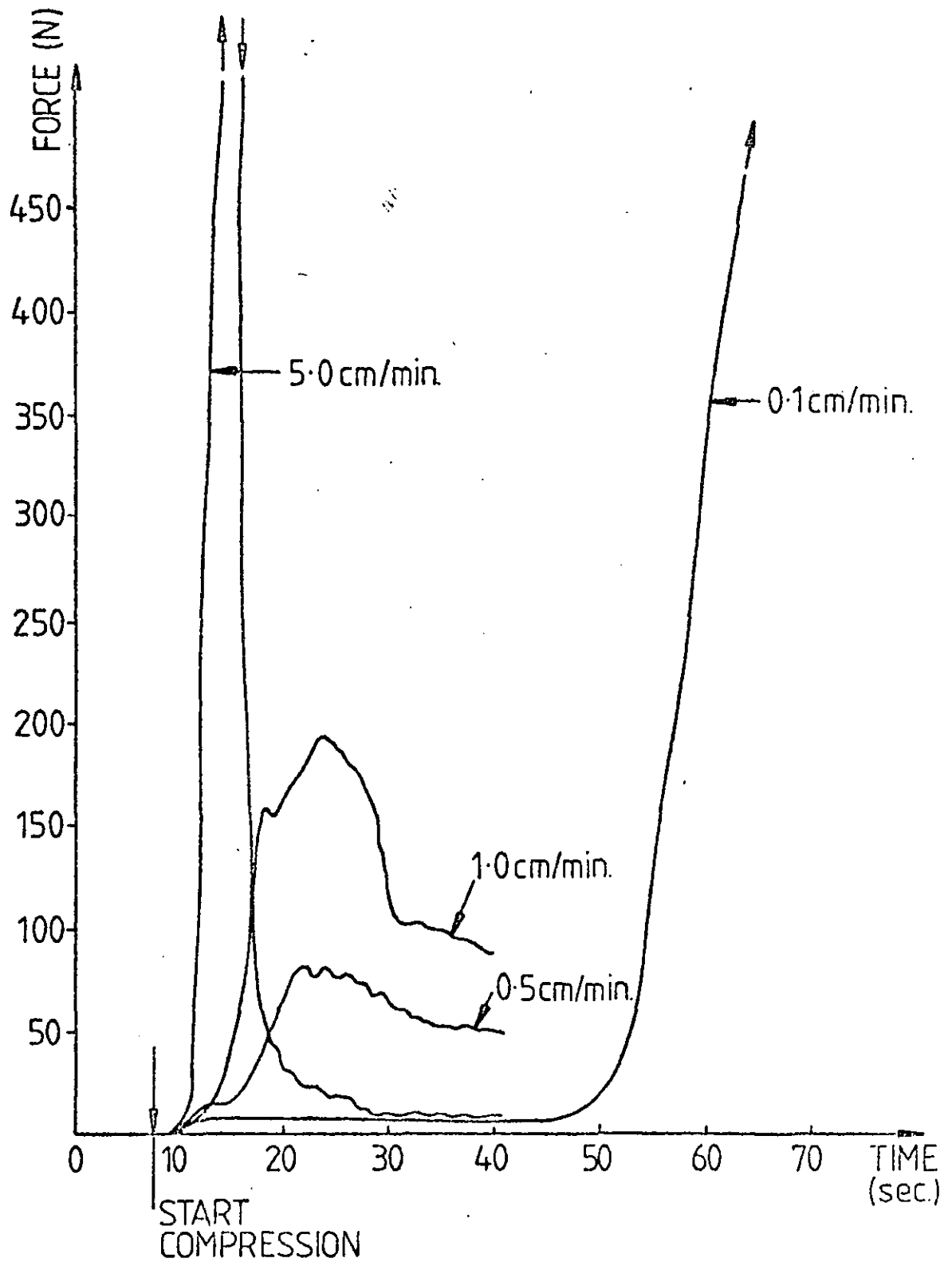


Fig.5.14 FORCE-TIME VARIATION AT 160°C  
(3 LAYERS OF 1 MONTH OLD SMC).

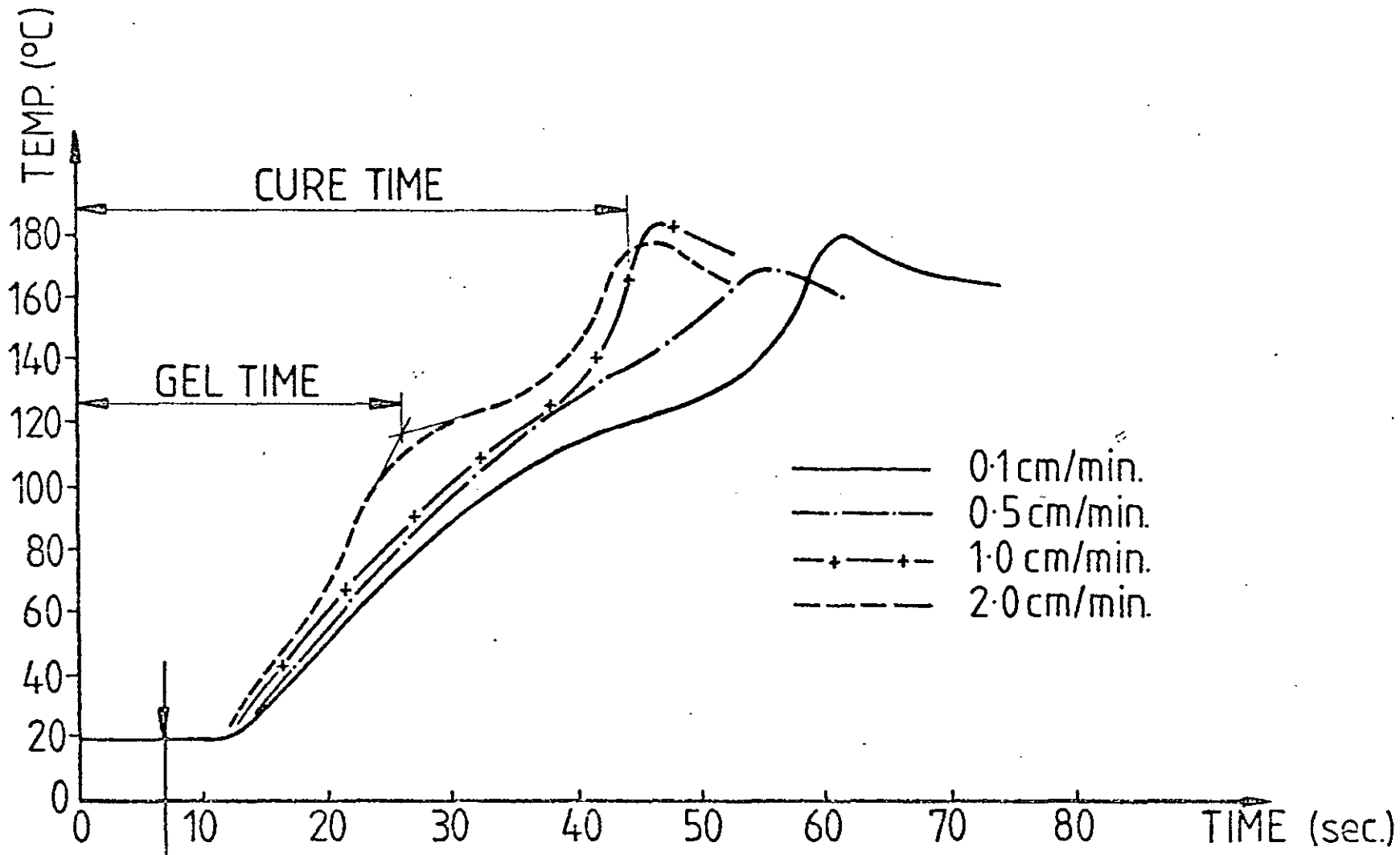


Fig. 5.15 TEMPERATURE-TIME VARIATION WITH CLOSURE SPEED AT 160°C (2 LAYERS OF 1 MONTH OLD SMC).

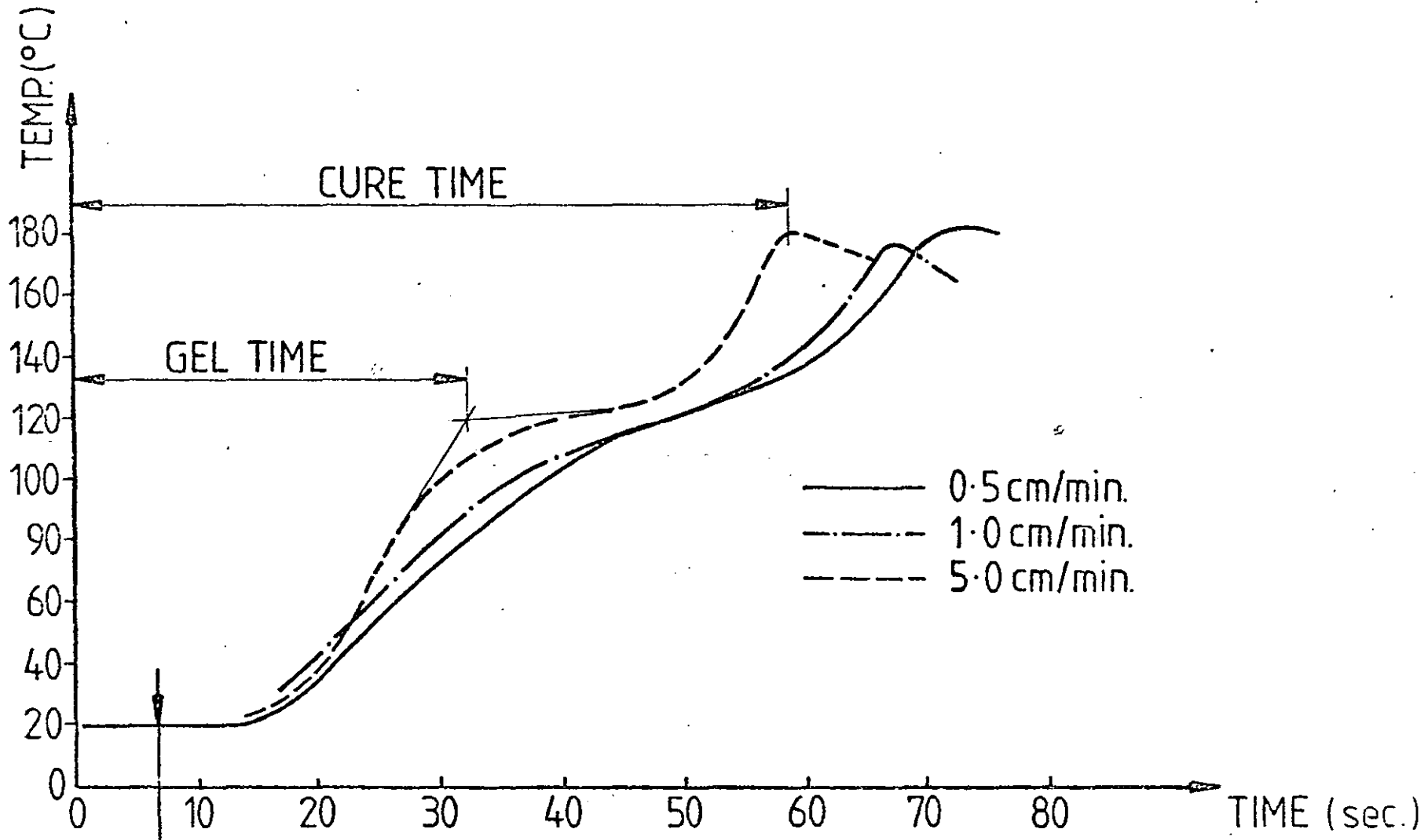


Fig.5.16 TEMPERATURE-TIME VARIATION WITH CLOSURE SPEED AT 160°C (3 LAYERS OF 1 MONTH OLD SMC).

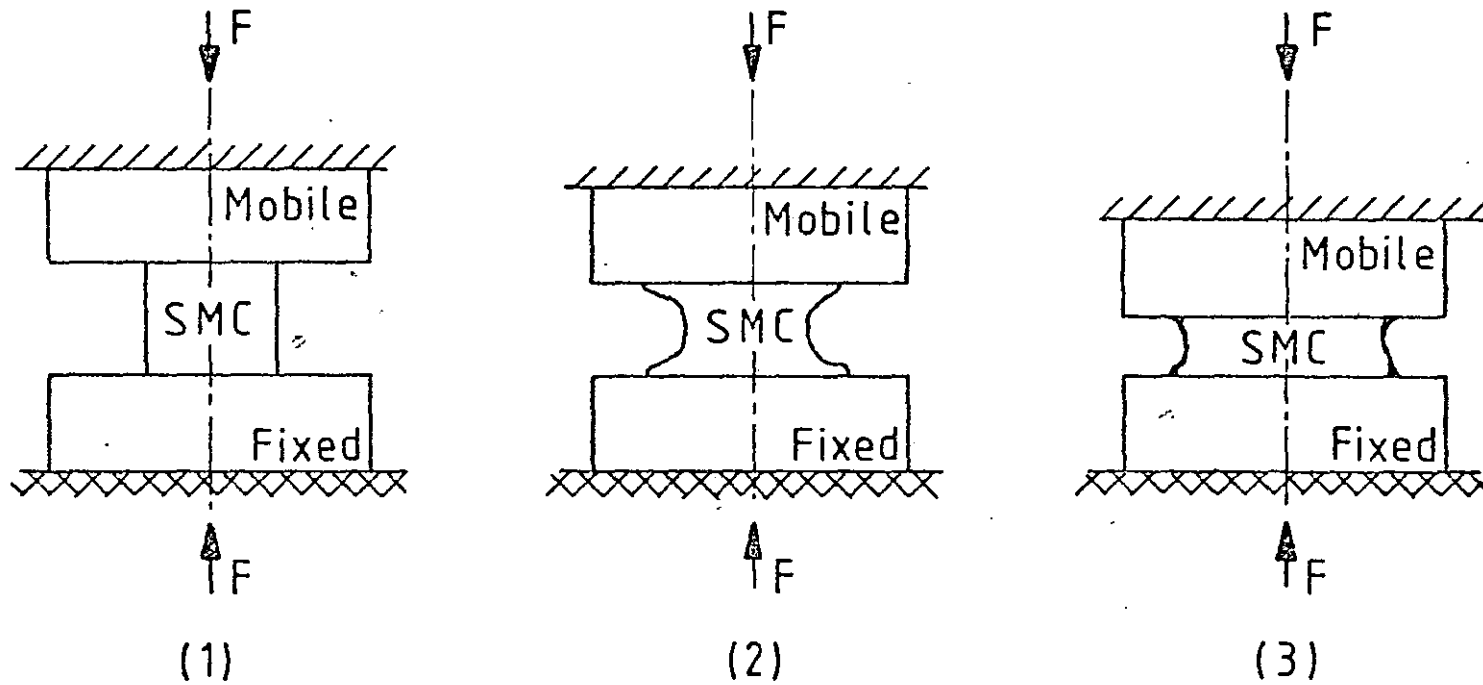
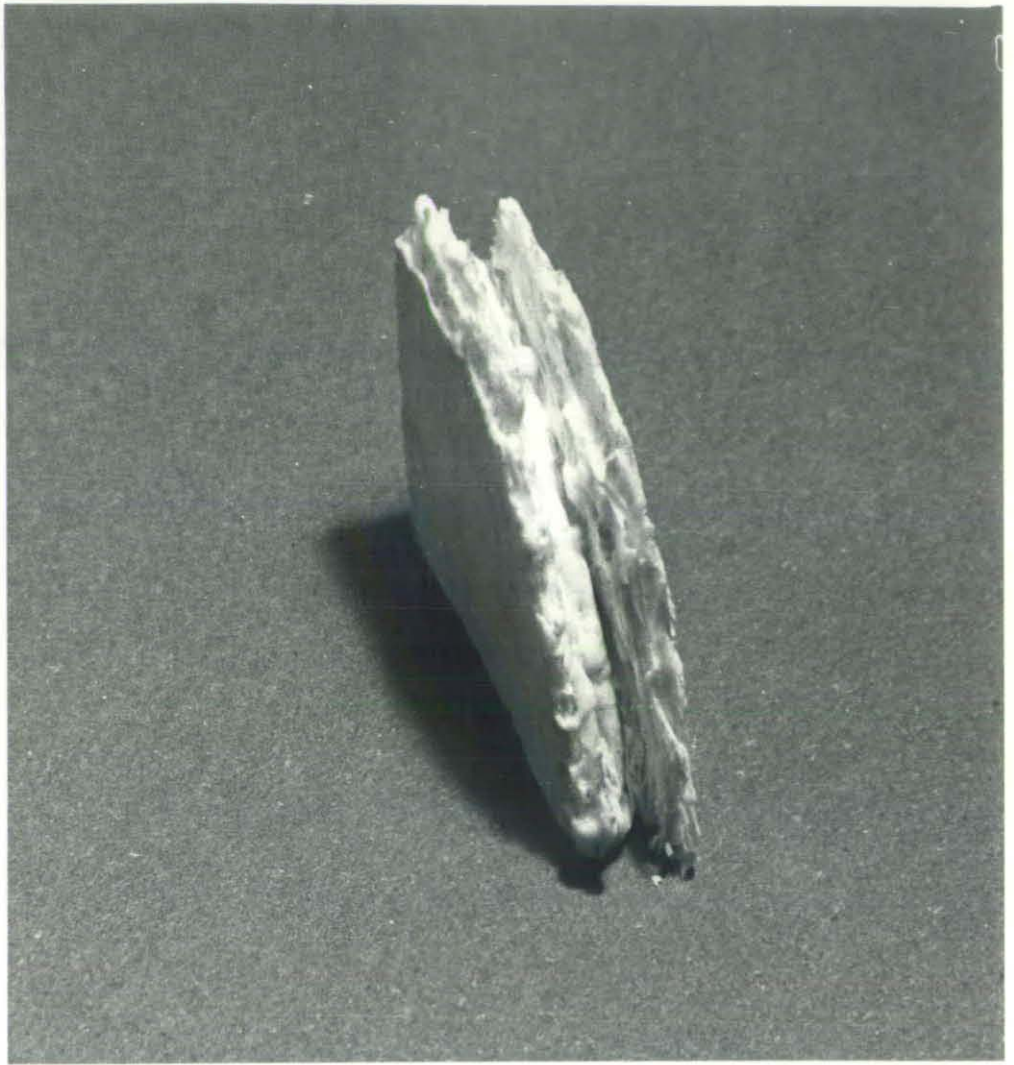


Fig.5.17 FLOW FRONT (THICKNESS) ADVANCE  
PARALLEL DISC WORK



---

FIGURE 5.18 Compressed sample at 160°C, showing the flow front profile. (2 layers of 1 month old SMC).

---

Two similar tests were run to measure the temperature variation through the SMC disc thickness during compression, in order to check if the SMC temperature could be considered to be approximately uniform. For each test two thermocouples were placed at the centre of the disc, one approximately 0.3 mm from the SMC surface and the other at the mid-thickness. Figure 5.19 shows the results. For one test the thermocouples were directly in contact with the SMC, while for the other they were between cellophane discs 0.2 mm thick (following the technique described by Okuto (02)).

## 5.2 Determination of Material Parameters for 20°C Tests

The viscosity, elasticity and yield parameters  $\mu$ ,  $K$  and  $f$  (see equation 4.34) were determined from the experimental data by using a least-squares solution to an over-determined set of equations (D7). The force-time experimental data for each test were substituted in turn into equation 4.34 and the functions  $f_1(t)$ ,  $f_2(t)$  and  $f_3(t)$  were evaluated for a range of values of  $n$ , the exponent of the shear rate. The functions  $f_1(t)$ ,  $f_2(t)$  and  $f_3(t)$  were each standardised to the range 0 to 1 for the fitting. The computer program used for the curve fitting is outlined in Appendix 2.

From the basis of the best fit to data, one value of  $n$  was chosen for the complete series of tests for the one month old SMC and one value was chosen for the series of tests with 3 month old SMC. These values of  $n$  were equal to unity for both batches of SMC. Previous work (T4) has shown that  $n$  is generally close to unity.

General relationships for the parameters  $\mu$ ,  $K$  and  $f$  were developed by fitting log-log plots to the values of  $\mu$ ,  $K$  and  $f$  given for each test by the fits to experimental data. For a range of shear strain, the parameters depend on shear rate and SMC initial thickness (see Figure 5.8). The standard error of fit was almost zero for low ranges of shear strain, e.g. from 0 to 0.04, but increased to about 20 when fitting was made over the complete strain range covered by the tests.

The values of  $\mu$ ,  $K$  and  $f$  for 1 month old SMC for a strain range of 0 to 0.04 are given by:

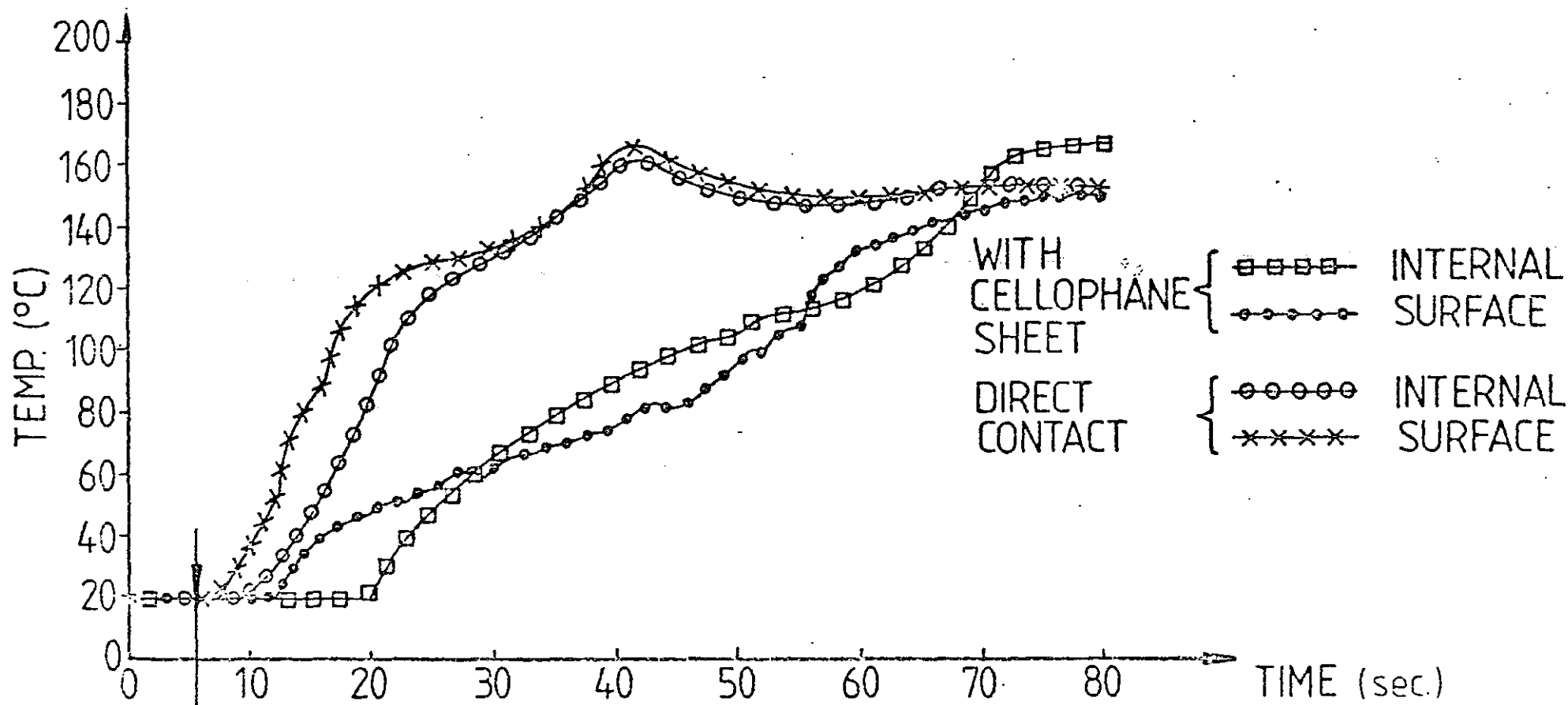


Fig.5.19 TEMPERATURE-TIME VARIATION THROUGH SMC THICKNESS  
 AT 160°C (2 LAYERS OF 1 MONTH OLD SMC AT 2cm/min).

$$\mu = (2.485 \times 10^{-7} H^{6.2} + 9.027 \times 10^{-3}) / \dot{\gamma}^{0.6189} \quad (5.1)$$

$$K = (8.730 \times 10^{-3} H^{2.2} + 8.067 \times 10^{-2}) / \dot{\gamma}^{0.3675} \quad (5.2)$$

$$f = (-3.653 \times 10^{-6} H^{5.7} - 1.425 \times 10^{-1}) \dot{\gamma}^{0.3141} \quad (5.3)$$

Figure 5.20 shows the variation predicted by equations 5.1 to 5.3 for the shear rates used in the tests. For the range of strains covered by the experiments, the  $\mu$  and  $f$  relationships give log-log lines with approximately the same slope but which give decreased values of  $\mu$  and  $f$  as the strain range over which the fitting is made is increased. On the other hand, the  $K$  relationships give values of  $K$  which decrease with shear rate for small ranges of shear strain (e.g. Figure 5.20), but which increase with shear rate when fitting is over larger strain ranges, e.g. from 0 to 0.1 and above.

### 5.3 Discussion of Results

#### 5.3.1 Tests at 200C

The time variations of compressive force at the various shear rates for 1 month old and 3 month old SMC were predicted from equation 4.34 using the appropriate values of  $H$ ,  $\dot{h}$ , SMC volume, and  $\mu$ ,  $K$  and  $f$  (e.g. obtained by the curve fitting program of Appendix 2). The predicted flow behaviour, shown by the curves in Figures 5.4 to 5.6, compares well with the experimental data. The standard error of fit varies with the strain range over which the fit is made. Its value increases from zero for the range 0 to 0.04 up to 20 for the range 0 to 0.16. Appendix 10 show the force obtained in the experiment, the fitted force using the program of Appendix 2, and the predicted force using the equations 5.1 to 5.3.

The shape of the force vs time responses is similar for compression of three different volumes of SMC at various shear rates (or plate closure speeds). SMC viscosity is shear rate dependent, and hence compression force is a function of shear rate. The force response is also a function of SMC age. Older SMC is stiffer (see Figure 5.6) because of styrene losses and the increased structure formation which

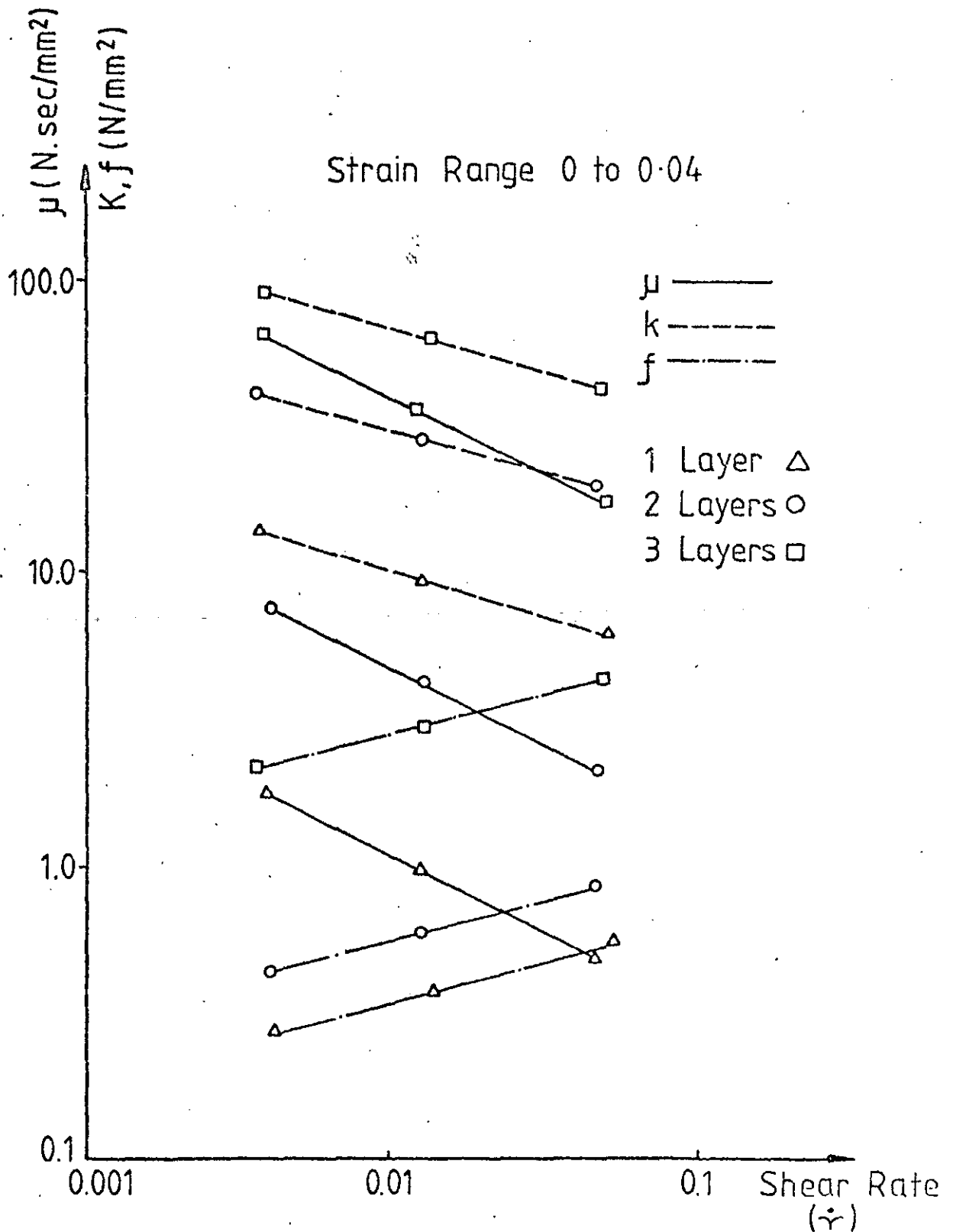


Fig.5.20 VARIATION OF PARAMETERS  $\mu, k$  AND  $f$  WITH SHEAR RATE. (1 MONTH OLD SMC AT 20°C).

has occurred with age.

The general concept of resistance to biaxial elongation has been put forward (M2, W4) as an explanation of the flow behaviour of "cold" SMC during squeezing. The work here suggests that this resistance arises partly from the glass fibre network, but mainly from the provisional network of bonds within the mature SMC created by the thickening agent (see section 2.2). The effect of adding thickener is to produce a high viscosity paste, whereas the viscosity (and hence resistance to flow) of a resin/fibre mixture alone remains low. This explanation is important for the following interpretation of the squeeze flow test data (S8).

Although insufficient evidence exists at present to provide a full understanding of matrix-fibre interaction during flow, a four stage physical model of flow can be used to explain the flow behaviour shown in Figures 5.7 and 5.8. The points 1 to 3 on the 0.5 cm/min curve in Figure 5.8 mark the beginning of these stages. Figures 5.9 to 5.11 show respectively the spacing between fibre bundles at these points during disc compression. Disc thickness at point 3 is approximately 70% of the initial thickness.

The initially flat or slowly increasing part of the curves in Figures 5.7 and 5.8 is the voids compression stage - for example, see the white "clouds" on the photograph of Figure 5.9. This behaviour is shear rate independent.

The next stage, between points 1 and 2 in Figure 5.8 is the visco-elastic biaxial elongation of the fibre and matrix networks together. In this work it has been called normal squeezing. Material stiffness increases with shear rate (see Figure 5.7), as implied by Marker and Ford (M2). It has been found also that this behaviour is dependent on SMC thickness.

The next stage from points 2 to 3 in Figure 5.8, is marked by a fall in the resistance to flow. Figures 5.10 and 5.11 show the fibre spacings at points 2 and 3 respectively. A yield effect starts at point 2 in Figure 5.8 and towards the end of the curves in Figure 5.7. This yield is associated mainly with the metal coordination complex bonds breaking due to increased shear strain. That this yield effect depends primarily on bond strength is shown by the curves in Figure 5.6 where

higher forces are needed to break the stronger bonds of the older SMC. The effect is strain rate dependent, as indicated by the curves in Figure 5.8. Another effect associated with lower flow resistance, perhaps towards the end of this flow stage, would be fibres beginning to align with flow direction. Bond strength probably also contributes to the layer dependent stiffness behaviour in Figure 5.7. The lack of prepolymer bonds between the layers of multilayer discs makes flow easier and hence give these discs lower stiffnesses than for the single layer material. However a reduced stiffness would also be expected due to the series connection of individual layer-stiffnesses.

During the fibre interaction stage of flow after point 3, compressive stiffness increases rapidly due to fibre bundles coming into contact with each other. The disc thickness at point 4 in Figure 5.8 corresponds to a 60% reduction of initial thickness.

It is likely therefore that the parameters  $\mu$ ,  $K$  and  $f$  have different values for each of the four stages of flow, and that general equations of the form shown by equations 5.1 to 5.3 (see Figure 5.20), should be derived for each stage of flow behaviour. It is also important to notice that due to the non-homogeneity of SMC, when composed of two or more layers, the parameters obtained by curve fitting were different for every case (e.g. 1, 2 and 3 layers). The main difficulties of obtaining general equations like those shown by equations 5.1 to 5.3 which describe the parameters  $\mu$ ,  $K$  and  $f$  for all the squeezing conditions, arise because of the stage behaviour (see Figure 5.8) as well as the non-uniform layer behaviour - i.e. 3 layers of SMC behave differently to 1 layer of the equal thickness. The discrepancies which can arise by using equations 5.1 to 5.3 to calculate compression force compared with the experimental and fitted forces are shown in Appendix 10.

### 5.3.2 Tests at 160°C

No modelling of this high temperature behaviour was attempted. The aim is to show empirically the interrelation of the time variation of plate closure speed, temperature and compression force with SMC gel and cure times.

Compression of the SMC discs for these tests started immediately after the SMC discs had been placed on the lower plate of the plasto-

meter. Figures 5.12 to 5.14 show the force vs time variation for 1, 2 and 3 layers of SMC. The general shape of the curves follows that given by Okuto (02). The small peaks at the start of each curve result from compression while the SMC is at 20°C, before heating has taken effect. The initial effect of heating is to decrease the viscosity of the material immediately adjacent to the hot plates. This is shown by the fall in force before the steep rise associated with compression. The final plateau region of all the curves occurs when plate closure is stopped (at 70% of initial thickness for all tests). The associated drop in force is due to material relaxation.

Greater compressive forces will be needed to compress to a given thickness if the gel time occurs during compression. The gel time for this SMC material is about 25 seconds (see Figure 5.15). For example, a high force is needed to achieve a 30% thickness reduction for the 0.1 cm/min test in Figure 5.12. If the compression speed is increased, the 30% thickness reduction occurs before the gel time and hence the overall force level is less. However the compressive force does not continue to decrease with increase in closure speed, e.g. see 1.0 cm/min curve in Figure 5.12. Figures 5.13 and 5.14 also show this behaviour.

The explanation for this behaviour lies in the variation of viscosity through the SMC thickness due to heating. Heat transfer from the plastometer plates forms layers of low viscosity SMC next to the plates and these layers can accommodate the majority of flow (and hence thickness reduction) if the heat transfer rate and compression speed are so matched. The compression force will be low if the gel time is not exceeded, and discs flow with deeply concave edges due to the outer layers flowing more easily than the centre ones (see Figures 5.17 and 5.18). If the heat transfer rate is not rapid enough, not only will the low viscosity layers flow but also the higher viscosity layers (i.e. colder material in the middle) will undergo more deformation, thus requiring higher compression forces. Then disc edges advance with a jagged but fairly uniform shape during flow.

The different temperatures at the middle and surface of the SMC discs (see Figure 5.19) during compression are evidence for the thickness variation of viscosity. Figure 5.15 shows how tangents drawn to curves give gel times. The internal layers have slightly longer gel times than the surface ones, but the temperature becomes uniform through

the SMC sample towards the end of the cure time. Okuto's technique (02) of sandwiching thermocouples between cellophane sheets enables thermocouples to be reused, but it has been found in this work that the temperature measurements were in error compared with those measured by thermocouples placed directly in the SMC material.

Gel and cure times decrease with increasing closure speed (see Figures 5.15 and 5.16) for a given SMC thickness because the disc to plate contact area increases more quickly at the higher speeds. Consequently there is a higher heat transfer rate into the SMC.

Finally, the interrelation between the time variation of compression force, SMC temperature and plate closure displacement is shown in Figure 5.21 for the compression of 2 layers of SMC at 2 cm/min. The temperature vs time curve shows the gel and cure times. For correct moulding, the end of compression (for 30% thickness reduction) must be reached before the gel time. The force-time graph gives the approximate magnitude of the required compression force for the particular speed of closure, temperature and material used. (Note that for this test, plate closure stopped at the end of compression and the consequent drop in force is due to relaxation of the SMC).

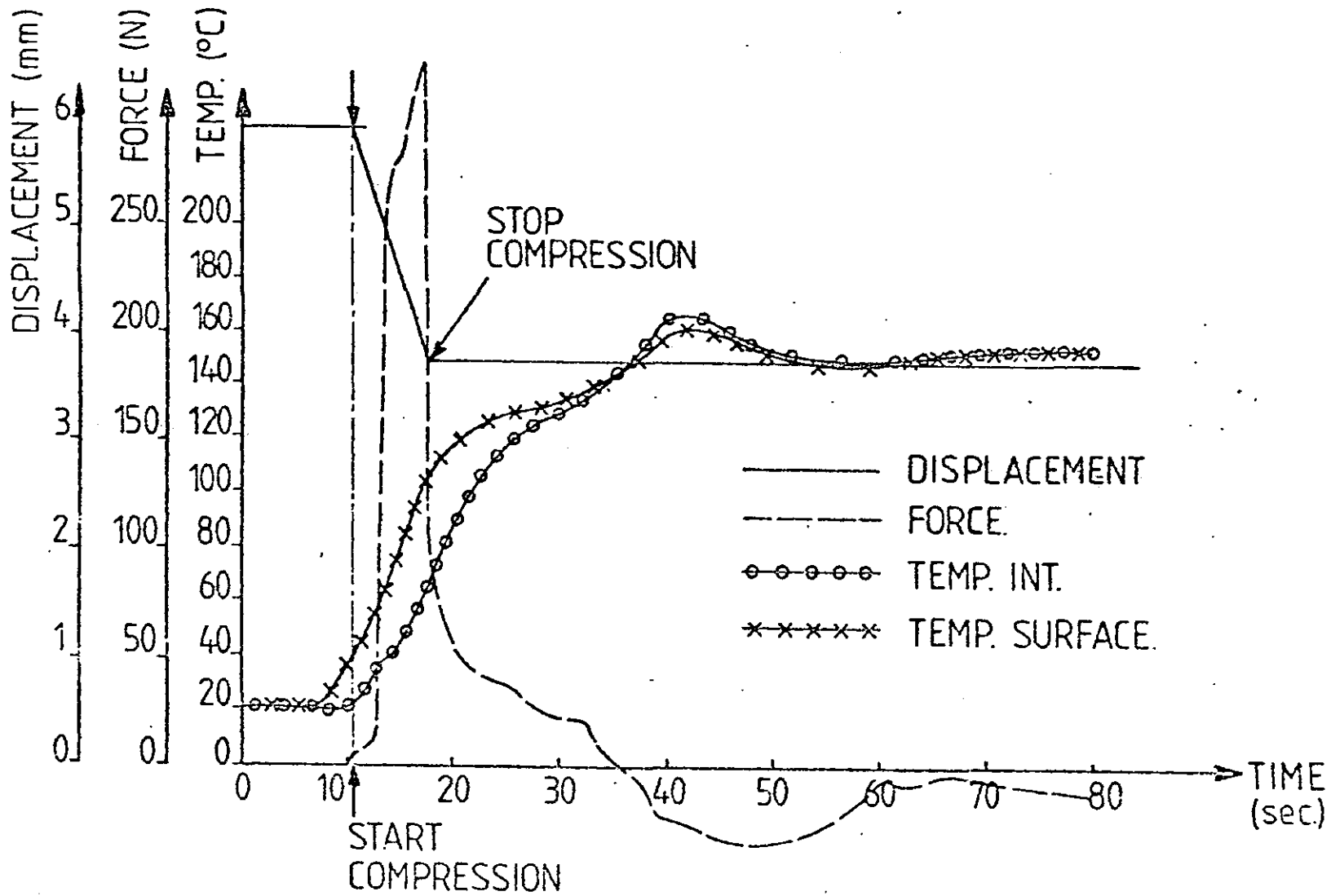


Fig.5.21 INTERRELATION OF FORCE, SMC TEMPERATURE AND DISPLACEMENT DURING PLASTOMETER CLOSURE.

## CHAPTER 6

THEORY FOR TWO DIMENSIONAL COMPRESSION-MOULD FLOW6.1 Introduction

One of the engineering needs associated with designing components from sheet moulding compound (SMC) is to understand more completely the flow behaviour during compression moulding. Initial considerations before moulding, such as geometry, size and positioning of the charge relative to the mould cavity shape, are important in determining the formation of weld-lines and the reorientation of fibres within the SMC matrix during flow. Therefore it would be very useful to be able to model SMC flow, so that these effects might be predicted and the structural properties of SMC products improved.

In Chapter 3 it was pointed out that apart from the work of Marker and Ford (M2) and Thompson (T8), there is little work in this area; no unified approach to modelling SMC flow exists. Certainly the problem is complex. To be useful in an engineering sense, a flow model must realistically describe the effects of moulding-process variables on the SMC material, e.g. pressure, temperature, mould closure cycle etc. The equation of state must take into account the effects of SMC composition and the extent to which the rheological behaviour of SMC is modified during flow.

Thus a rigorous approach to providing a theoretical basis for SMC flow is complex. By contrast, the approach taken here is mathematically more straightforward. The model for flow developed in this chapter, assumes that SMC flow behaviour is essentially Newtonian, and that the fibre reorientation effects are small. It analyses the case of compression flow for flat parts of uniform thickness, without bosses, ribs or lips. Even though bosses, ribs and lips are formed during compression flow, the way in which the SMC flows into these features is different to the way in which SMC flows for flat parts.

A main reason for assuming Newtonian flow was to make the mathematical analysis sufficiently manageable so that the feasibility of flow modelling could be examined. The actual nature of SMC flow is

Momentum  
Equation

Continuity  
Equation

Assumptions



Mould-Cavity Pressure Distribution  
(Poisson's Equation):

$$\frac{\partial^2 \bar{p}}{\partial X^2} + \frac{\partial^2 \bar{p}}{\partial Y^2} = - \frac{12\mu W h}{h^3}$$

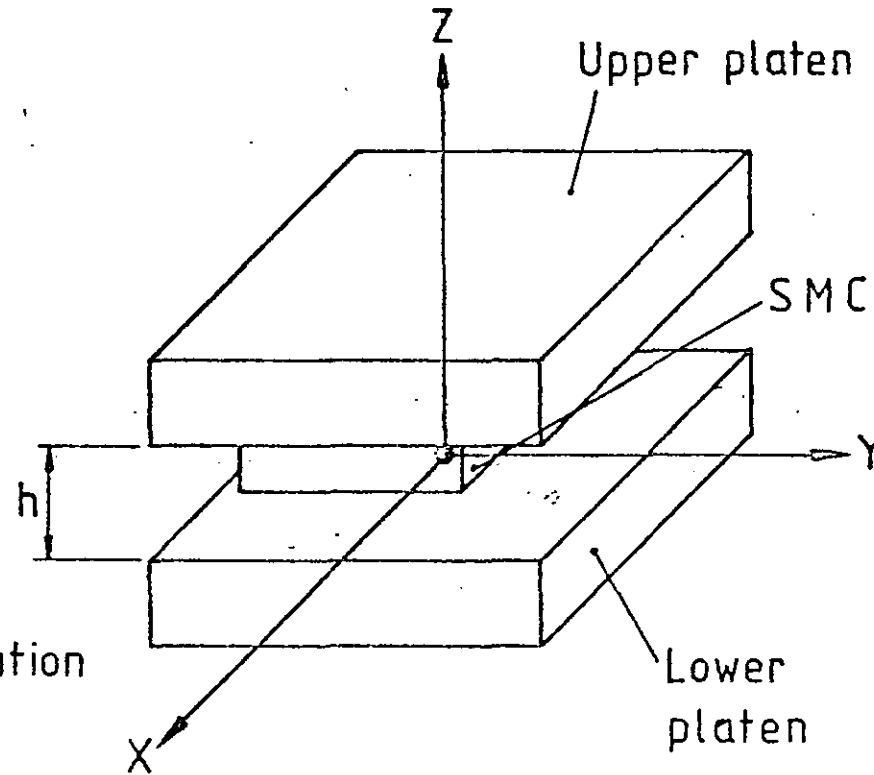


Fig.6.1

## FLOW THEORY FOR COMPRESSION MOULDING

viscoelastic and it has not been disregarded by the work in this thesis (see Chapters 4 and 5). At the moment however, the state-of-the-knowledge is that the exact contributions of the viscous and elastic elements during mould flow are not yet fully understood.

## 6.2 Flow Theory for Compression Moulding

The analysis begins by using the momentum and the continuity equations, for the Cartesian coordinate system shown in Figure 6.1, where the origin of the axes lies in the surface of a rigidly fixed lower platen. These equations may be written using tensor notation (B2, L2):

$$\rho \frac{Dv_i}{Dt} = \rho f_i + \frac{\partial T_{ji}}{\partial x_j} \quad (6.1)$$

$$\frac{D\rho}{Dt} + \rho \frac{\partial v_i}{\partial x_i} = 0 \quad (6.2)$$

where:

- $v_i$  = velocity
- $t$  = time
- $\rho$  = density
- $f_i$  = body forces
- $T_{ji}$  = stress tensor
- $x_j$  = distance
- $i, j, k$  = directions x, y, z

Defining  $T_{ii} = \sigma_{xx}, \sigma_{yy}, \sigma_{zz}$  and  $T_{ij} = \tau_{xy}$ , etc. then equations 6.1, 6.2 may be written in Cartesian axis form for the velocities U, V, W in the x, y, z directions.

$$\rho \frac{DU}{Dt} = \rho f_x + \frac{\partial \sigma_{xx}}{\partial x} + \frac{\partial \tau_{yx}}{\partial y} + \frac{\partial \tau_{zx}}{\partial z} \quad (6.3)$$

$$\rho \frac{DV}{Dt} = \rho f_y + \frac{\partial \sigma_{yy}}{\partial y} + \frac{\partial \tau_{xy}}{\partial x} + \frac{\partial \tau_{zy}}{\partial z} \quad (6.4)$$

$$\rho \frac{DW}{Dt} = \rho f_z + \frac{\partial \sigma_{zz}}{\partial z} + \frac{\partial \tau_{xz}}{\partial x} + \frac{\partial \tau_{yz}}{\partial y} \quad (6.5)$$

and:

$$\frac{D\rho}{Dt} + \rho \frac{\partial U}{\partial x} + \rho \frac{\partial V}{\partial y} + \rho \frac{\partial W}{\partial z} = \dot{\rho} \quad (6.6)$$

### 6.3 Assumptions

To apply equations 6.3 - 6.6 to the analysis of compression flow of SMC, we have made the following assumptions:

1. The material is homogeneous.
2. The material is uniform
3. The material is planar-isotropic in the X-Y plane
4. The material is incompressible
5. There are no body forces acting on the material
6. The material has constant viscosity during moulding and the flow is Newtonian, i.e.  $n$  is nearly unity in the power law equation. The constant viscosity assumption is justified if the moulding temperature remains constant during mould closure.
7. The surface of the lower plate remains rigidly fixed. The origin of the axes lies in the surface of the lower plate and only the upper plate moves.
8. The area covered by the material before moulding ( $A_I$ ) must be between the following limits to prevent significant fibre re-orientation during flow:

$$65\% A_F < A_I < 100\% A_F \quad (6.7)$$

where:  $A_I$  is the area covered by the charge  
 $A_F$  is the area of the cavity mould.

Therefore the limits for the thickness of the charge are  $1.42h_F > h_I > h_F$  (where  $h_F$  is the final thickness and  $h_I$  is the initial one). The limitations of the plate separation can be ignored if  $h_I \ll r$ , where  $r$  is the charge shape radius. Diens (D6) found that if  $h_I \leq 0.1r$  the effect of plate separation can be disregarded, which is the case for SMC mouldings.

Also, it should be mentioned here that there is a compromise for the selection of percentage or area covered by the SMC charge. This compromise is between the amount of fibre orientation occurring during flow and the quality of surface finish

required. The work of this thesis is more concerned to avoid fibre reorientation during flow:

9. The speed of moulding is constant and very small (10 mm/sec) compared with other manufacturing-processes for plastics. There has to be a compromise between the segregation of the SMC matrix and the cycle time. Fast cycle times cause segregation of the SMC matrix. Since the speed of the upper plate of the mould is small, and the distance that the upper plate has to pass through is very small, the acceleration of the upper plate can be disregarded.
10. The Reynolds number ( $R$ ) is very small. Therefore the inertia terms of the momentum equation may be disregarded. Knowing that  $R = \rho L U/\mu$  (6.8)
 

where:  $\rho$  = density  
 $\mu$  = viscosity  
 $L$  = a parameter which characterises flow length  
 $U$  = radial speed

A typical value for SMC density is  $1.8\text{g/cm}^3$  (03) and viscosity (without fibres) is 15 - 70 mm cps (03). Even for large values of  $L$ ,  $R$  will be always small. This inertia terms may be ignored.
11. It is assumed that as soon as the SMC touches the mould surface a thin layer with zero speed will be formed (zero wall-slip) and that the flow front will be convex (see boundary conditions equation 6.23). However it should be pointed out that during moulding the flow front tends to have a concave form because the speed of the material near the plates is high and the speed of the mid-thickness is almost zero (depending on the compression speed). However the zero wall-slip and convex flow front assumptions were made to reduce the complexity of the mathematical model.
12. The material flows in layers as Marker and Ford have demonstrated (M2), and as we have shown in Chapter 5. Thus:

$$\frac{\partial \tau_{xz}}{\partial x} = \frac{\partial \tau_{yz}}{\partial y} = 0 \quad (6.9)$$

#### 6.4 Theoretical Analysis

From all these assumptions equations 6.3 - 6.6 become:

$$\frac{\partial \sigma_{xx}}{\partial x} + \frac{\partial \tau_{yx}}{\partial y} + \frac{\partial \tau_{zx}}{\partial z} = 0 \quad (6.10)$$

$$\frac{\partial \sigma_{yy}}{\partial y} + \frac{\partial \tau_{xy}}{\partial x} + \frac{\partial \tau_{zy}}{\partial z} = 0 \quad (6.11)$$

$$\frac{\partial \sigma_{zz}}{\partial z} = 0 \quad (6.12)$$

$$\frac{\partial U}{\partial x} + \frac{\partial V}{\partial y} + \frac{\partial W}{\partial z} = 0 \quad (6.13)$$

From assumption 6, the stress for Newtonian flow may be expressed in tensor notation as (B2):

$$T_{ij} = -p \delta_{ij} + 2 \mu (e_{ij} - (1/3) \Delta \delta_{ij}) \quad (6.14)$$

$$e_{ij} = (1/2) \left( \frac{\partial v_i}{\partial x_j} + \frac{\partial v_j}{\partial x_i} \right) \quad (6.15)$$

$$\Delta = \frac{\partial v_i}{\partial x_i} \quad (6.16)$$

Using equation 6.14 the normal and shear stresses may be defined as:

$$T_{ii} = -p + \frac{4}{3} \mu \frac{\partial v_i}{\partial x_i} \quad (6.17)$$

$$T_{ii} = \sigma_{xx}, \sigma_{yy}, \sigma_{zz}$$

$$\tau_{ij} = \mu \left( \frac{\partial v_i}{\partial x_j} + \frac{\partial v_j}{\partial x_i} \right) \quad (6.18)$$

$$\tau_{ij} = \tau_{xy}, \dots$$

Expressing equations 6.10 - 6.11 in tensor notation and substituting into 6.17 - 6.18

$$\frac{\partial p}{\partial x_i} = (4/3) \cdot \mu \frac{\partial^2 v_i}{\partial x_i^2} + \mu \left( \frac{\partial^2 v_i}{\partial x_j^2} + \frac{\partial^2 v_j}{\partial x_i \partial x_j} \right) \quad (6.19)$$

From the continuity equation since  $\rho$  is constant:

$$\frac{\partial v_i}{\partial x_i} = 0 \quad (6.20)$$

Equation 6.19 becomes

$$\frac{\partial p}{\partial x_i} = \mu \nabla^2 v_i \quad (6.21)$$

This equation is called the equation of *creeping viscous flow*. In order to solve equation 6.21, it will be expressed in Cartesian form. In the x direction the equation is:

$$\frac{\partial p}{\partial x} = \mu \left( \frac{\partial^2 U}{\partial x^2} + \frac{\partial^2 U}{\partial y^2} + \frac{\partial^2 U}{\partial z^2} \right) \quad (6.22)$$

To integrate equation 6.22, let  $\partial p / \partial x = G$  and use the following boundary conditions:

$$\text{at } z = 0 \quad U = 0 \quad (6.23)$$

$$\text{at } z = h/2 \quad \partial U / \partial z = 0$$

Note that  $h$  is the thickness at the instant of mould closure and is time independent. Assuming that the two first terms at the right hand side of equation 6.22 are small compared with the last one, equation 6.22 becomes

$$U = - G (hz - z^2)/2\mu \quad (6.24)$$

Integrating  $U$  along the thickness (from 0 to  $h$ )

$$\bar{U} = - G h^2/12\mu \quad (6.25)$$

where  $\bar{U}$  is the average velocity in the  $x$  direction.

Evaluating the maximum speed (at  $z = h/2$ )

$$U_{\max} = - G h^2/4\mu \quad (6.26)$$

$$G = - 4U_{\max}\mu/h^2 \quad (6.27)$$

$$\therefore U_{\max} = 3\bar{U} \quad (6.28)$$

Integrating equation 6.22 from 0 to  $h$  (since  $h$  is constant it is independent of  $x$  and  $y$ ).

$$\frac{\partial}{\partial x} \int_0^h \bar{p} dz = \mu \left( \frac{\partial^2}{\partial x^2} \int_0^h U dz + \frac{\partial^2}{\partial y^2} \int_0^h U dz + \left[ \frac{\partial U}{\partial z} \right]_0^h \right) \quad (6.29)$$

Knowing that  $\bar{p} = p_{z=h} = p_{z=0}$ , equation 6.29 can be expressed as:

$$\frac{\partial}{\partial x} (h\bar{p}) = \mu \left( \frac{\partial^2}{\partial x^2} (h\bar{U}) + \frac{\partial^2}{\partial y^2} (h\bar{U}) \right) + \mu \left[ \frac{\partial U}{\partial z} \right]_0^h \quad (6.30)$$

Then:

$$\frac{\partial \bar{p}}{\partial x} = \mu \left( \frac{\partial^2 \bar{U}}{\partial x^2} + \frac{\partial^2 \bar{U}}{\partial y^2} \right) - \frac{12 \mu \bar{U}}{h^2} \quad (6.31)$$

$$\frac{\partial \bar{p}}{\partial y} = \mu \left( \frac{\partial^2 \bar{V}}{\partial x^2} + \frac{\partial^2 \bar{V}}{\partial y^2} \right) - \frac{12 \mu \bar{V}}{h^2} \quad (6.32)$$

Integrating the continuity equation 6.20 in  $z$ , and using average values:

$$\frac{\partial \bar{U}}{\partial x} + \frac{\partial \bar{V}}{\partial y} + \frac{\partial W}{\partial z} = 0 \quad (6.33)$$

$$- \int_0^h \frac{\partial W}{\partial z} dz = \int_0^h \left( \frac{\partial \bar{U}}{\partial x} + \frac{\partial \bar{V}}{\partial y} \right) dz \quad (6.34)$$

Knowing that  $W = 0$  at  $z = 0$ ,  $W = -W_h$  at  $z = h$  and that  $W_h = \text{constant}$ .

$$\frac{W_h}{h} = \frac{\partial \bar{U}}{\partial x} + \frac{\partial \bar{V}}{\partial y} \quad (6.35)$$

Combining equations 6.31, 6.32, 6.35 after first differentiating equations 6.31, 6.32 with respect to  $x$  and  $y$  respectively

$$\frac{\partial^2 \bar{p}}{\partial x^2} = \mu \left( \frac{\partial^3 \bar{U}}{\partial x^3} + \frac{\partial^3 \bar{U}}{\partial x \partial y^2} \right) - \frac{12 \mu}{h^2} \frac{\partial \bar{U}}{\partial x} \quad (6.36)$$

$$\frac{\partial^2 \bar{p}}{\partial y^2} = \mu \left( \frac{\partial^3 \bar{V}}{\partial x^2 \partial y} + \frac{\partial^3 \bar{V}}{\partial y^3} \right) - \frac{12 \mu}{h^2} \frac{\partial \bar{V}}{\partial y} \quad (6.37)$$

$$\therefore \frac{\partial^2 \bar{p}}{\partial x^2} + \frac{\partial^2 \bar{p}}{\partial y^2} = \mu \frac{\partial^2}{\partial x^2} \left( \frac{\partial U}{\partial x} + \frac{\partial V}{\partial y} \right) + \mu \frac{\partial^2}{\partial y^2} \left( \frac{\partial U}{\partial x} + \frac{\partial V}{\partial y} \right) - \frac{12\mu}{h^2} \left( \frac{\partial U}{\partial x} + \frac{\partial V}{\partial y} \right) \quad (6.38)$$

Equation 6.38 is the governing equation for the pressure distribution over the mould cavity. It has the form of Poisson's equation:

$$\frac{\partial^2 \bar{p}}{\partial x^2} + \frac{\partial^2 \bar{p}}{\partial y^2} = -12 \mu W_h / h^3 \quad (6.39)$$

$$\nabla^2 \bar{p} = -12 \mu W_h / h^3 \quad (6.40)$$

### 6.5 Boundary Conditions

The approach for solving equation 6.39 has been to assume a free surface boundary condition up to the instant before completion of mould closure, i.e. the SMC flow meets all edges of the mould simultaneously. We have taken the boundary pressure value as atmospheric, with pressure acting normal to the SMC free surface. There are no other boundary forces.

This approach neglects the effects on boundary conditions of material viscosity and friction of the flow front. (See example in Chapter 7).

CHAPTER 7  
THE PREDICTION OF CHARGE SHAPES FOR  
TWO-DIMENSIONAL PRODUCTS

### 7.1 Introduction

The idea of using an equation which governs compression mould flow to predict charge shapes for moulding flaw free SMC products was originally suggested by Thomas (T7). The work of Chapter 6 of this thesis shows that this governing equation for mould flow describes the mould pressure distribution at the instant of mould closure. The equation applies to the compression moulding of flat parts of uniform thickness. The step by step procedure suggested here shows how this equation may be used to calculate a charge shape for a given mould geometry. The fundamental hypothesis is that the resulting mould flow from the charge occurs without the formation of weld-lines, and without significant fibre reorientation if the charge area is not less than approximately 70% of the mould cavity area.

### 7.2 General Approach

The method of calculating the charge shape is to evaluate the pressure distribution over the mould-cavity area at the instant of mould closure by solving equation 6.39 over this area. Then knowing the pressure contours and the velocity distribution, the stream-lines can be drawn. The flow is "reversed" along the stream-lines, taking into account the pressure gradient, to obtain the position of the flow front during the SMC flow.

Figures 7.1 and 7.2 show schematically the steps which would be followed for a finite difference solution of the equations, to determine the charge shape for moulding a square plate. These steps are outlined below for a hand calculation to show the general approach. Computer solutions can be used, and because the solution of the set of finite difference equations is likely to be straightforward a matrix inversion approach to their solution can be used rather than an

iterative one (see Section 7.4). The following eight steps outline the approach for a hand solution by iteration:

1. Form a square mesh pattern over the component. If the component has one or more axes of symmetry, then only the part of the component lying between axes need to be covered by a mesh. If the component does not have axes of symmetry, then it has to be covered completely.
2. Number the rows and letter the columns.
3. Assume a pressure of 1 bar at the boundary. This constitutes the boundary condition.
4. Solve the finite difference form of Poisson's equation by iteration (S4)

$$\nabla^2 \bar{p} = -12 \mu W_h / h^3 \quad (7.1)$$

In finite difference form equation 7.1 at node  $n$  of the mesh shown in Figure 7.2 becomes:

$$p_1 + p_2 + p_3 + p_4 - 4 p_0 = (-12 \mu W_h / h^3) h^2 \quad (7.2)$$

where:  $p_0$  is the pressure of the node  $n$   
 $p_1, p_2, p_3, p_4$  are the pressures on the four surrounding nodes  
 $h$  is the distance between nodes

Move through the mesh points in order, row by row (or column by column) starting from the centre. Iterate until the difference between pressures at a node on successive iterations is not greater than 0.5.

5. Plot the pressure variation for each column (as a percentage of pressure at the centre) and interpolate from this graph to obtain

the pressure contours on the component, e.g. 80%, 60%, 40% etc.

6. Draw the stream-lines perpendicular to the pressure contours. Calculate the pressure gradient at selected points (about 3) along every stream-line and use the form of equation 6.25 to determine the velocity at each point. For the x and y directions this equation gives:

$$\bar{U} = (h^2/12\mu) \frac{\partial \bar{p}}{\partial x} \quad (7.3)$$

$$\bar{V} = (h^2/12\mu) \frac{\partial \bar{p}}{\partial y} \quad (7.4)$$

Combining equations 7.3 and 7.4 the resultant velocity at each point. Check that the stream-lines do follow the directions of the resultant velocities. Stream-lines need only to be drawn over the part of the component which is of interest. It is not necessary to draw them to the centre since the work here uses a minimum charge area of 70%.

7. Calculate a flow front position for each stream-line using the following procedure. The form of equation 6.25 shows that the resultant velocity at a point on a stream-line may be written:

$$\bar{U}_R \propto \frac{\partial \bar{p}}{\partial s} \quad (7.5)$$

Thus along two stream-lines  $\alpha$  and  $\beta$ , the resultant velocities may be expressed (without the 'R' subscripts):

$$\bar{U}_\alpha \propto \left(\frac{\partial \bar{p}}{\partial s}\right)_\alpha \quad (7.6)$$

$$\bar{U}_\beta \propto \left(\frac{\partial \bar{p}}{\partial s}\right)_\beta \quad (7.7)$$

Take the stream-line  $\alpha$  as the reference, and define a factor  $K_{\alpha\beta}$  as:

$$K_{\alpha\beta} = \bar{U}_\beta / \bar{U}_\alpha \quad (7.8)$$

Hence, since at an instant of time the constants of proportionality (see equations 7.3 and 7.4) have the same value along each stream-line:

$$K_{\alpha\beta} = (\frac{\partial \bar{p}}{\partial s})_\beta / (\frac{\partial \bar{p}}{\partial s})_\alpha \quad (7.9)$$

Let  $d_\alpha$  be a small distance between points 0 and 1 on the stream-line  $\alpha$ , where point 0 is at the edge of the mould cavity and point 1 is inside the cavity. If  $\Delta \bar{p}_\alpha$  is the pressure difference between these points,  $(\partial \bar{p} / \partial s)_\alpha$  may be approximated to  $\Delta \bar{p}_\alpha / d_\alpha$ . By "reversing the flow", the flow front will move back to point 1 from point 0; there will be correspondingly small movements along other stream-lines. As the first step in calculating these movements it is necessary to estimate the associated values of  $\partial \bar{p} / \partial s$ . For example for the stream-line  $\beta$   $\partial \bar{p} / \partial s$  may be approximated by  $\Delta \bar{p}_\beta / d_\beta$  where  $d_\beta$  is a small distance along the stream-line from the mould cavity edge.

Hence a value for  $K_{\alpha\beta}$  may be calculated by using equation 7.9 in the form:

$$K_{\alpha\beta} = (\frac{\Delta \bar{p}}{d})_\beta / (\frac{\Delta \bar{p}}{d})_\alpha \quad (7.10)$$

Thus the actual value of  $d_\beta$ , which gives the flow front position on stream-line  $\beta$ , is given by:

$$d_\beta = K_{\alpha\beta} d_\alpha \quad (7.11)$$

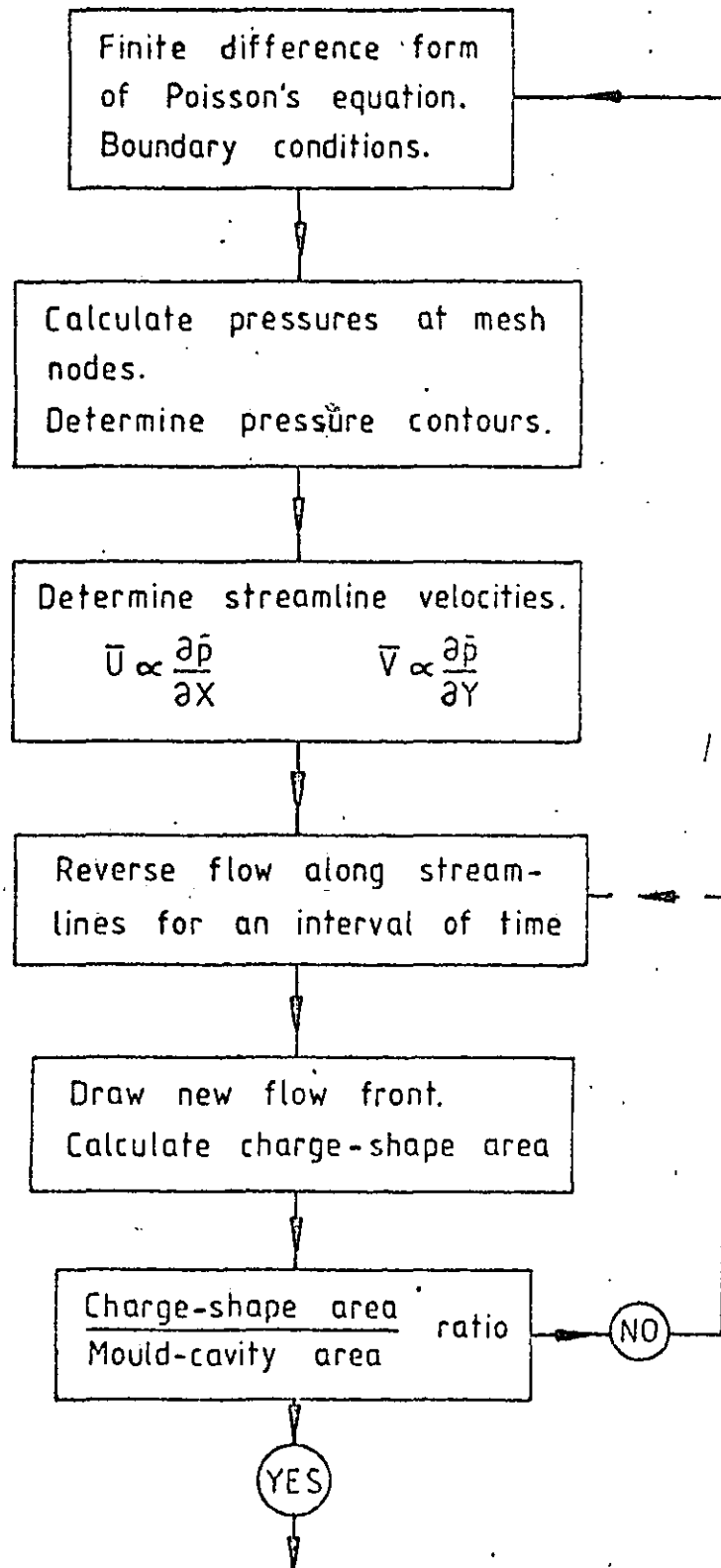
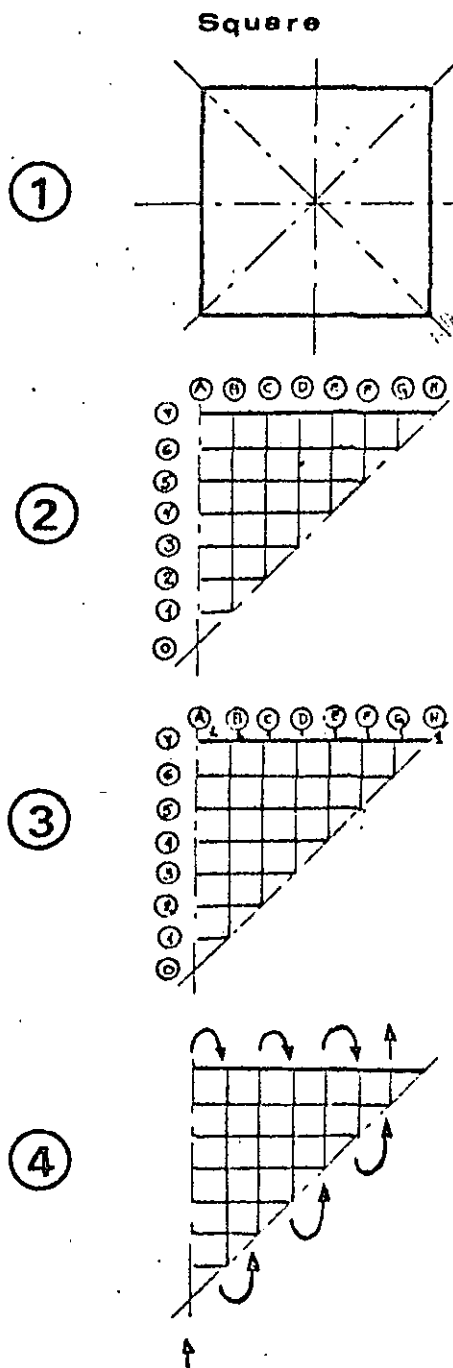


Fig.7.1 CHARGE SHAPE CALCULATION

STEP



STEP

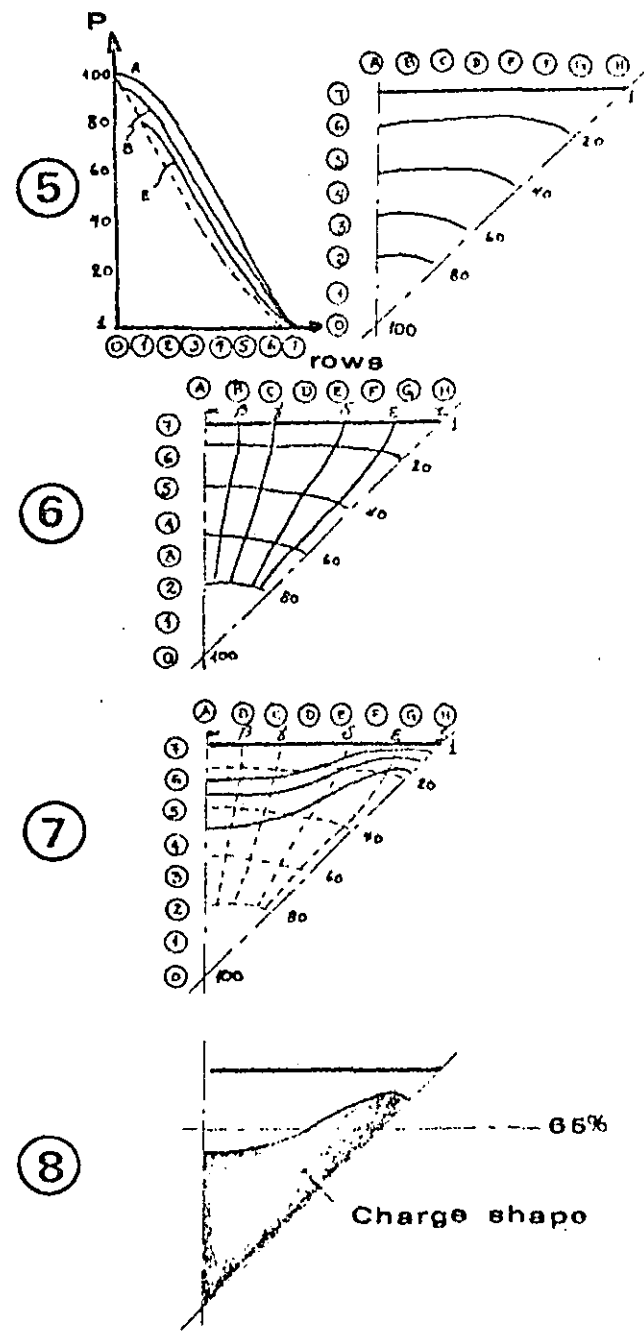


Fig.7.2 DIAGRAM SHOWING THE PROCEDURE

Repeat this procedure for the other stream-lines, keeping  $d_{\alpha}$  as the reference distance. Draw the locus through the calculated points to obtain the flow front position. When the flow front position has been determined, the pressure field must be corrected for subsequent calculations by assuming that the new flow front now has the pressure boundary conditions of 1 bar.

8. Repeat the procedure from steps 4 to 7 until 70% of the mould surface is covered by the SMC. When this is so the last flow front defines the charge shape which will give moulded products without weld-lines. In the case of hand calculations, it will be difficult to evaluate the pressure field for a new flow front because the mesh is a pattern of squares, whereas the flow front will usually be curved. Then the procedure is to repeat step 7 but with a difference  $d_{\alpha}$ , until 70% coverage is obtained. (In the cases analysed in this work the calculations have always been based on the first pressure distribution, i.e. the pressure gradients referred to the product edge).

Note: This method may be used to predict the shape of charges less than 70% mould cavity coverage. In such cases significant fibre reorientation may occur because of increased flow. This will cause variations in mechanical properties throughout the moulded item, but weld-lines should still not form. For the calculations of less than 70% area it is recommended to evaluate the pressure distribution for every new flow front.

### 7.3 Computer Solution

A computer program was written to ease the calculation of the charge shape geometry. The program is outlined in this section, but a more complete description of the program is given in Appendix 4.

#### 7.3.1 Structure of the Program

The computer program is divided into four sections:

1. Calculation of pressure contours
2. Calculation of stream-lines

3. Calculation of flow-front position
4. Calculation of the area covered by the new flow front.

The computer program requires input data at the beginning of every section. It prints the results at the end of every section. The reason for this program structure is that it was more straightforward in this project to carry out by hand the interpretation and refinement associated with data interpolation before passing into the next stage of calculation. The additional work which would have been needed to computerise completely the calculation procedure could not be justified in the context of the work for this thesis. Thus the practical approach of using the computer as an aid to calculation has been followed.

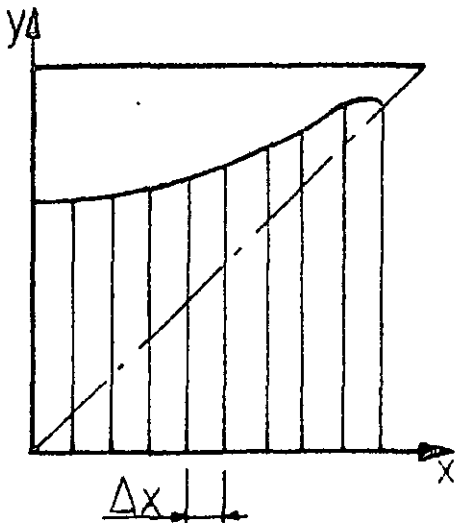
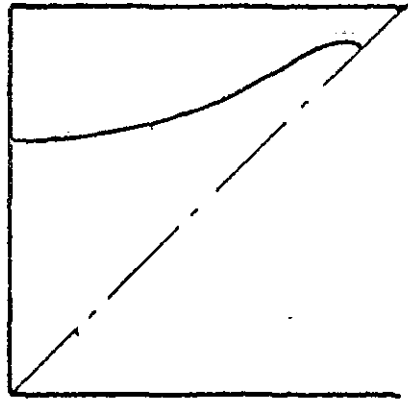
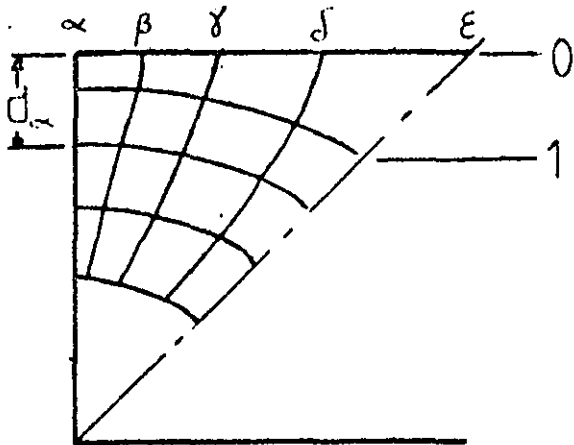
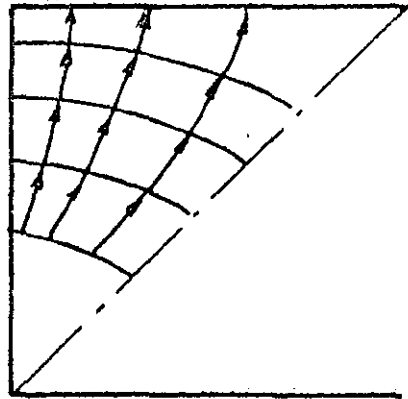
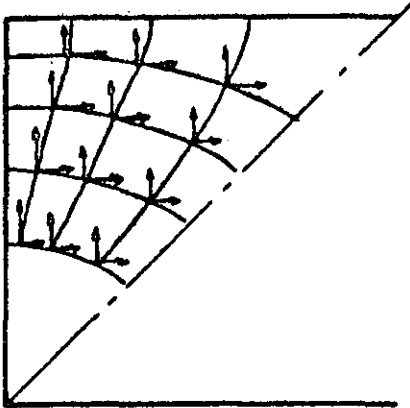
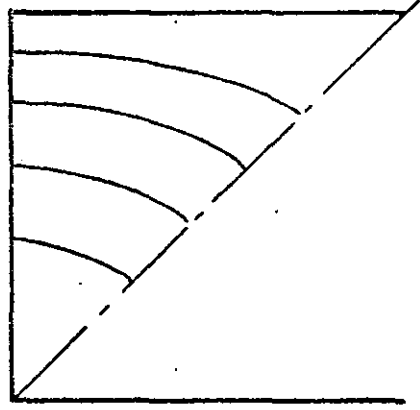
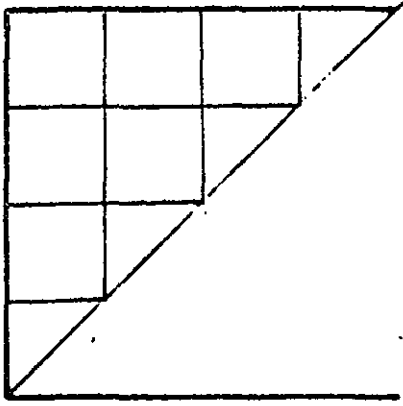
### 7.3.2 General Description of the Method

The program follows the method outlined in section 7.2. The general step by step procedure for using the computer program is shown in Figure 7.3 for the example of calculating the charge shape of a square plate. This is given as a numerical example in the next section, but the general procedure is as follows:

1. Use steps 1 and 2 from section 7.2. These steps are carried out by hand. Supply the node characteristics, the boundary conditions and the moulding conditions as specified in Appendix 4. The computer will generate the finite difference equations of the Poisson's equation 7.1 for every node and solve this set of equations by matrix inversion (W3). Then the pressure contours will be evaluated by interpolation. The computer will print the pressure distribution at each node and plot the pressure contours. The contours surround the centre of pressure.
2. By hand draw the stream-lines perpendicular to the pressure contours and select a number of points (about 3), on every stream-line. By hand calculate the pressure gradient from the results of step 1 for the x and y directions for every point. Supply these data to the computer. The computer will evaluate the resultant flow speed with its direction at every node.

INPUT

OUTPUT



CHARGE AREA  
AND  
% OF AREA

Fig.7.3 SECTIONS OF COMPUTER PROGRAM

3. By hand, plot the directions of velocity vectors from step 2, and check that the stream-lines follow the velocity vectors. Supply to the computer the distances  $d_{\alpha 1}$ ,  $d_{\beta 1}$  and so on (see step 7, section 7.2), and the pressure differences  $\Delta \bar{p}_{\alpha 1}$ ,  $\Delta \bar{p}_{\beta 1}$ , and so on (see step 7, section 7.2). The computer will calculate the point on each stream-line of the new flow front using equations 7.10 and 7.11.

4. By hand plot the new flow front. Position the points calculated in step 3 on their corresponding stream-lines and joint the points to obtain the flow front line. Locate the origin for a set of x-y axes at the centre of pressure of the charge shape (the centre of pressure was given from step 1) and supply to the computer the y-coordinates of points on the new flow front for constant intervals  $\Delta x$ . The computer will evaluate the area covered by the new flow front and the percentage of area covered related to the mould cavity area.

There are four calculation routines to choose depending on the number of axes of symmetry (from four axes to unsymmetrical shapes, see Appendix 4).

5. It will be necessary to repeats steps 3 and 4 if the percentage area does not correspond to that required. Increase or reduce the distances  $d_{\alpha}$ ,  $d_{\beta}$  and so on, taking into account the variation in  $\Delta \bar{p}_{\alpha}$ ,  $\Delta \bar{p}_{\beta}$ , etc.

As a general comment, it is appropriate to mention here that the difficulties associated with using the finite-difference method with curvilinear shapes have not been overlooked by this work. For such cases it may be more convenient to use finite-element methods (M10, V1), although no attempt was made to use finite-element methods for this work.

However, the computer program has been written to deal with unsymmetrical articles, for which the regular form (star) of the finite-difference method becomes irregular at the boundary (S4) as shown in Figure 7.4.

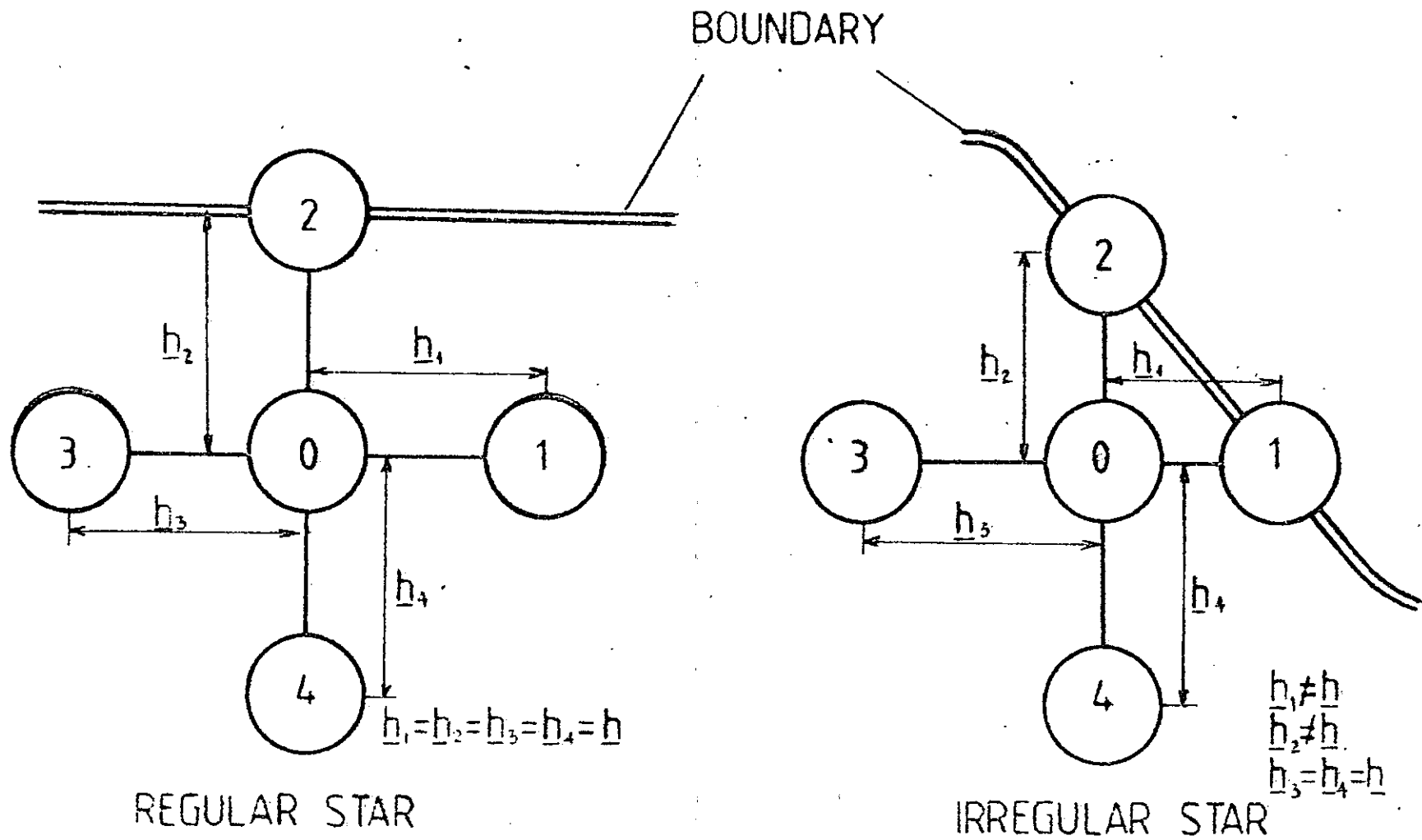


Fig.7.4

## 7.4 Numerical Example

In this section the calculation procedure outlined in Figure 7.3 is applied to determine the charge shape for a square plate.

### 7.4.1 The Problem

Determine the charge shape for the square plate shown in Figure 7.5. The plate is to be made from a low profile sheet moulding compound (LP-SMC) which has a viscosity of  $0.03 \text{ N-sec/mm}^2$  ( $30 \times 10^6 \text{ cps}$ ) and is to be moulded at a speed of  $0.83 \text{ mm/sec}$ . The plate thickness is  $3.0 \text{ mm}$ . The percentage of the cavity area covered by the SMC charge should be  $70\%$ .

### 7.4.2 Calculation Procedure

As the square has 4 axes of symmetry, only the shaded area in Figure 7.5 needs be considered. Make a  $10 \times 10$  mesh over one quarter of the plate and number all nodes except those on the boundary (see Figure 7.6). Take the value of the pressure at boundary as  $100 \text{ KN/m}^2$  (1 bar). Table 7.1 shows the node characteristic (as specified in Appendix 4) for each node of Figure 7.6.

The  $x$  and  $y$  coordinates of every node at which the pressure value needs to be calculated must be supplied as input data. The computer will print the pressure values and plot the pressure contours (see Figure 7.7).

Use the pressure contours to determine the pressure gradient in the  $x$  and  $y$  directions for some points along the stream-lines (see section 7.2 step 6). Supply the pressure gradients (see Table 7.2) as input to the second section of the computer program.

The computer program evaluates and prints the resultant speed and direction at every node supplied. Figure 7.8 shows the resultant speeds with their directions (plotted by hand).

The next step is to select the reference stream-line ( $\alpha$ ). For this example, select the stream-line which coincides with row 10 and supply the distances  $d$ , (including the reference  $d_\alpha$  and initial estimates of  $d_\beta$ ,  $d_\gamma$ , etc), and the associated pressure differences of each stream-line. These data are shown in Table 7.3 for the stream-lines of Figure 7.8.

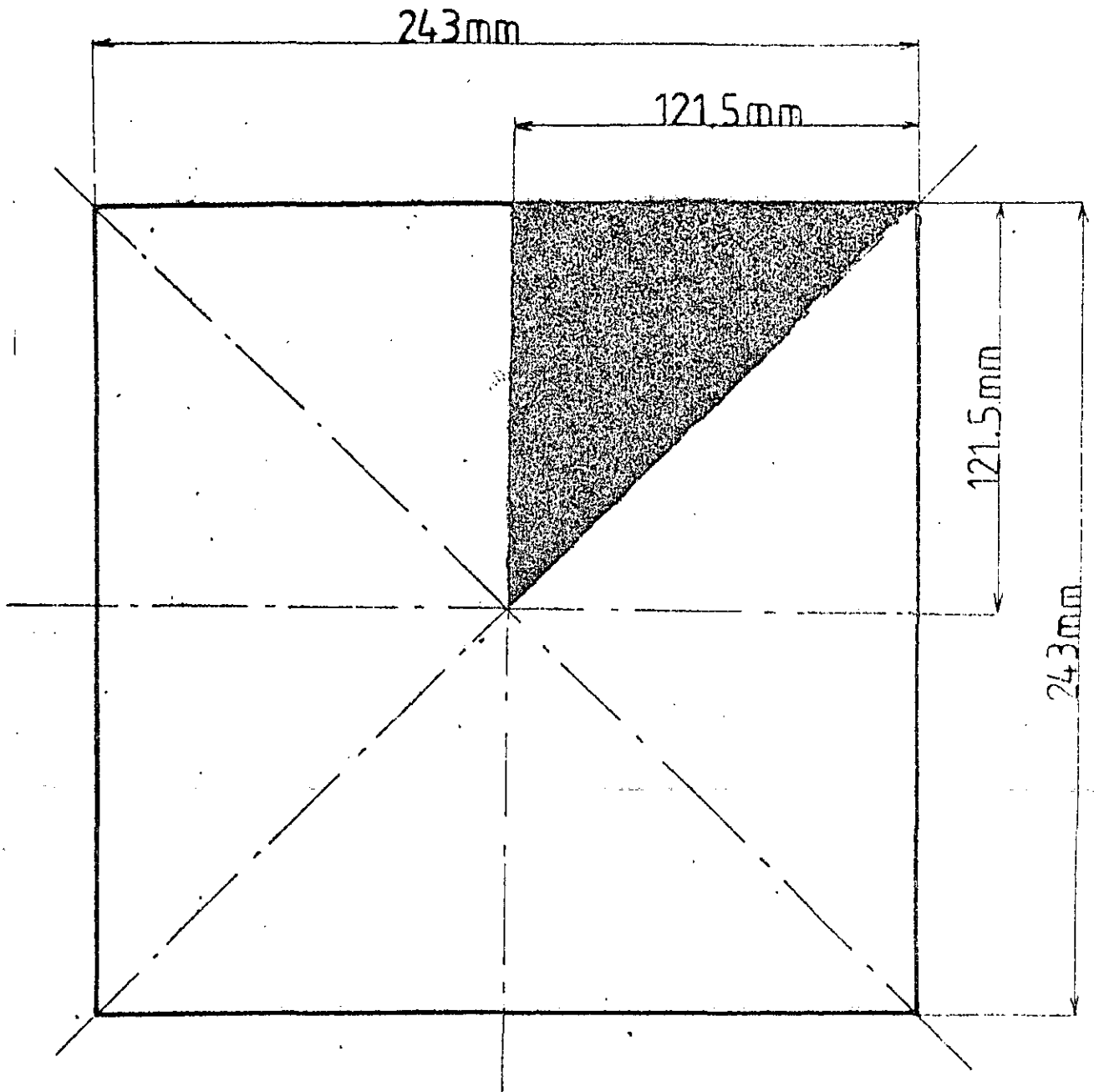


Fig.7.5 DIMENSIONS OF SQUARE PLATE

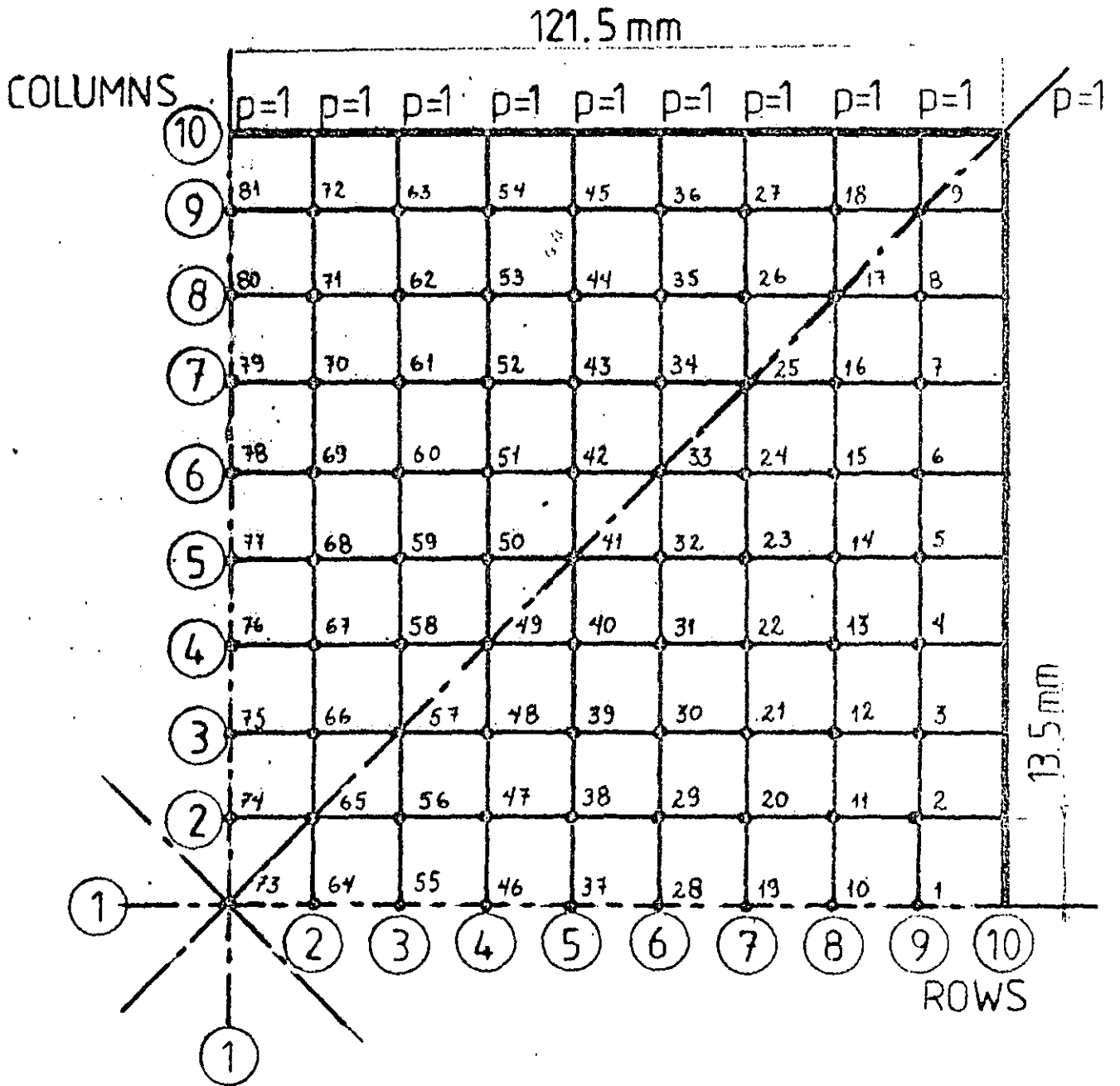


Fig.7.6 MESH NODES AND NUMBERING



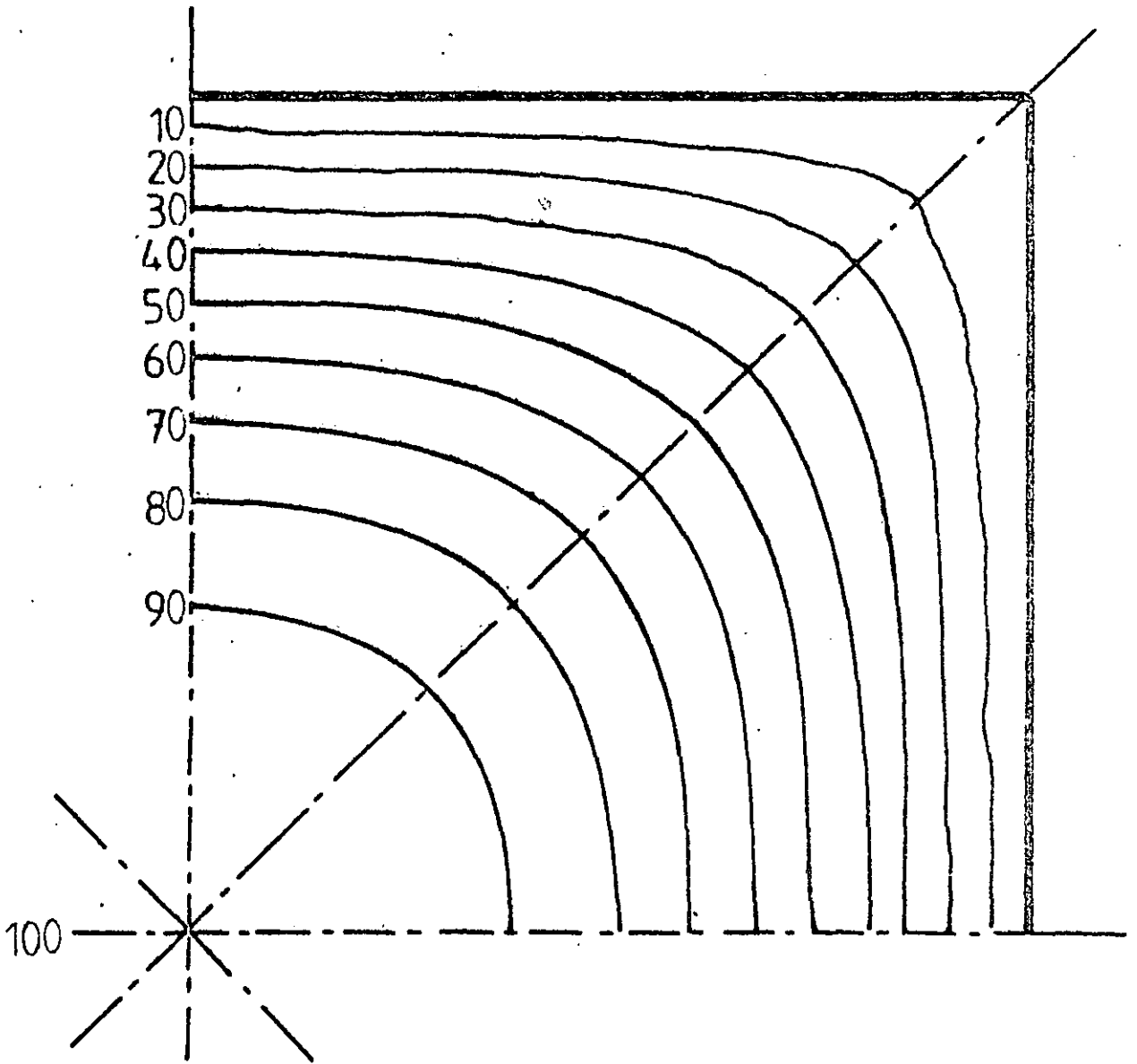


Fig.7.7 PRESSURE CONTOURS IN PERCENTAGE

TABLE 7.2

Streamline	$\partial\bar{p}/\partial x$ (%/mm)	$\partial\bar{p}/\partial y$ (%/mm)
$\beta$	0.05	2.0
$\beta$	0.05	1.53
$\beta$	0.08	1.25
$\gamma$	0.08	1.66
$\gamma$	0.15	1.42
$\gamma$	0.21	1.25
$\delta$	0.11	1.66
$\delta$	0.17	1.33
$\delta$	0.26	1.05
$\epsilon$	0.2	1.25
$\epsilon$	0.43	0.95
$\epsilon$	0.52	0.83

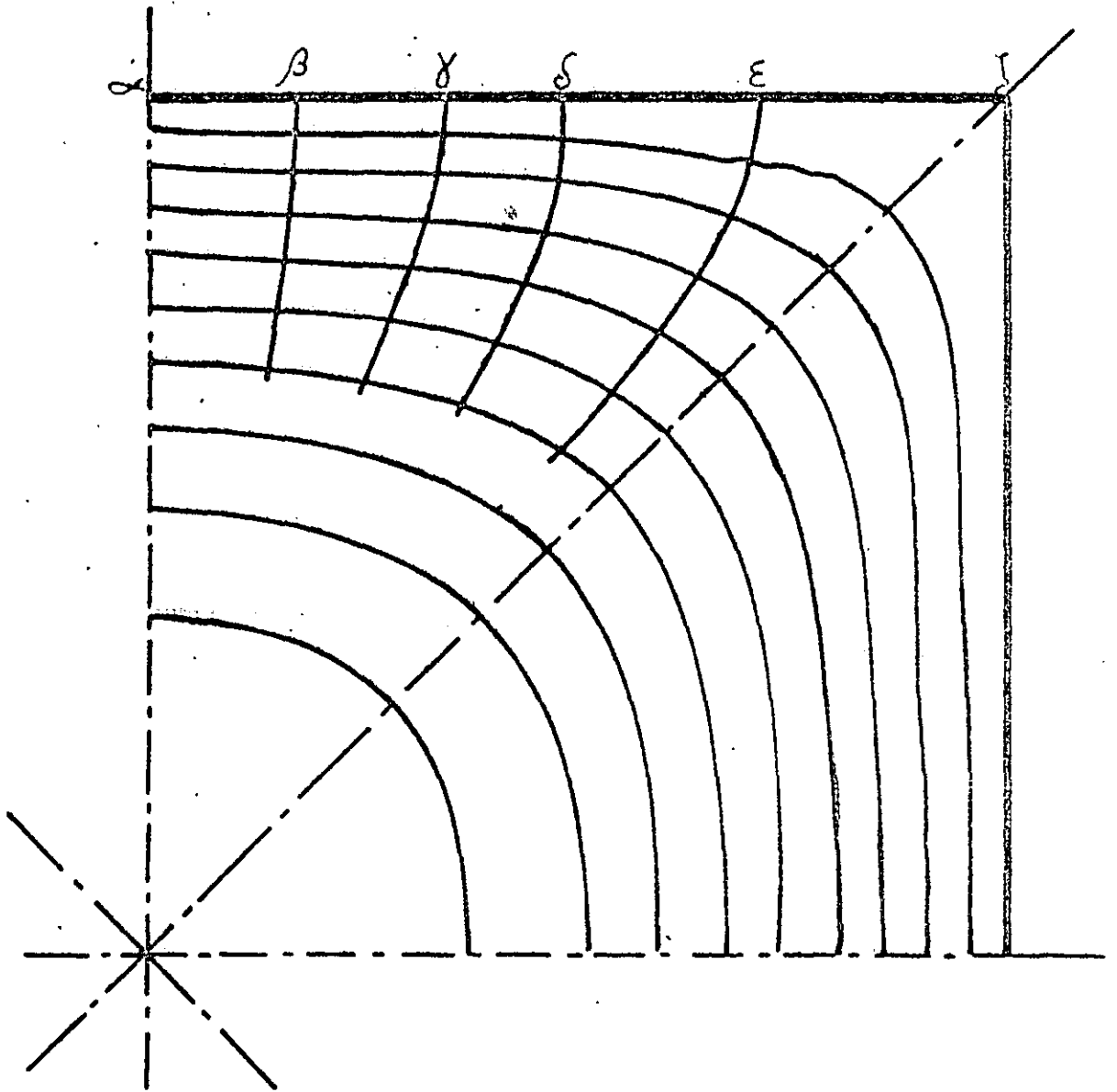


Fig.7.8 STREAM-LINES AND PRESSURE  
CONTOURS

TABLE 7.3

Stream-line	$d_i$ (mm)	$\Delta \bar{p}$ (%)
$\alpha$ (Reference)	25	43
$\beta$	26	43
$\gamma$	28	43
$\delta$	32	43
$\epsilon$	40	43
$\zeta$	60	43

The computer will revise the estimates  $d_\beta$ ,  $d_\gamma$  etc to their correct values for a flow front which passes through the point defined by  $d_\alpha$ . Figure 7.9 shows the flow front.

The next step is to measure the distance from the x-axis to the flow front at intervals  $\Delta x$  of 11.15 mm (the value selected for this case) to supply the data for the last section of the program. Table 7.4 shows these data. The selection of the width  $\Delta x$  depends on the degree of variation in the flow front shape.

TABLE 7.4

Interval No	y Distance (mm)
1	96.50
2	97.50
3	99.00
4	100.75
5	101.75
6	103.75
7	105.5
8	106.5
9	109.5
10	112.5
11	114.0

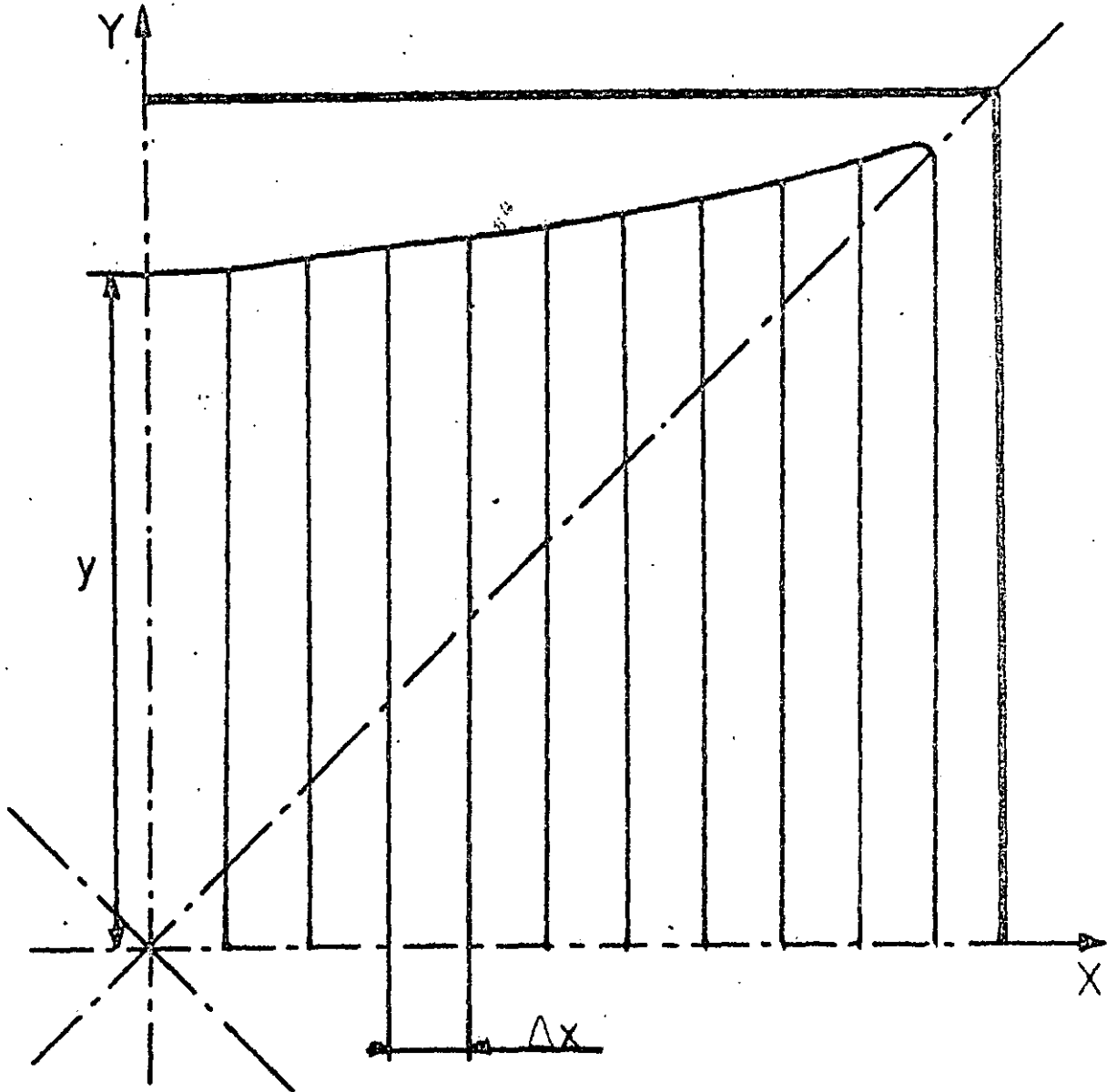


Fig.7.9 SHAPE OF THE CHARGE AND SECTIONS  
FOR CALCULATING THE AREA

The area obtained for the complete charge is 5166 mm<sup>2</sup> which corresponds to 70% of the mould cavity area. Generally the desired value of area is not obtained from the first calculation. The distances  $d$  and the pressure differences  $\Delta\bar{p}$  have to be either increased or reduced respectively, according to whether the charge area needs to be reduced or increased, and the new position of the flow front formed. It is usually possible to obtain the required area to within  $\pm 2\%$  from two or three calculations.

## CHAPTER 8

DESIGN OF COMPRESSION-MOULD AND  
ASSOCIATED INSTRUMENTATION8.1 Introduction

A semi-positive compression mould, together with associated instrumentation and control equipment, was designed and manufactured as part of the experimental programme to test the charge shape calculation method. The mould was equipped with pressure transducers to measure the mould cavity pressure distribution, since the governing equation for flow is in terms of the pressure distribution (see Chapter 6). The moulded plates were also X-rayed to give further information on flow.

The mould instrumentation provided data which enabled comparisons to be made with previous moulding-process investigations (M2, T8). These checks on the moulding-process conditions for the work in this thesis ensured that realistic compression moulding conditions were maintained during the experiments even though a compression moulding press was not used. Compression moulding was carried out using the compression crosshead of a 500 kN capacity Denison hydraulic materials-testing machine.

The variables which were measured (in addition to mould cavity pressures) were mould cavity temperature, platen parallelism during closure, and closure speed. These data were collected on-line using a Digital Equipment PDP-11/05 16 bit length computer. Figure 8.1 shows a general arrangement of the mould and the instrumentation. <sup>45</sup>

The following sections give specific details of the mould design and instrumentation:

- 8.2 *Mould design consideration*
- 8.3 *Mould instrumentation and control equipment*
- 8.4 *Calibration procedure before moulding*

8.2 Mould Design Considerations

Figures 8.2 and 8.3 show the mould in the closed and fully open positions with the electronic control box next to it. A drawing of

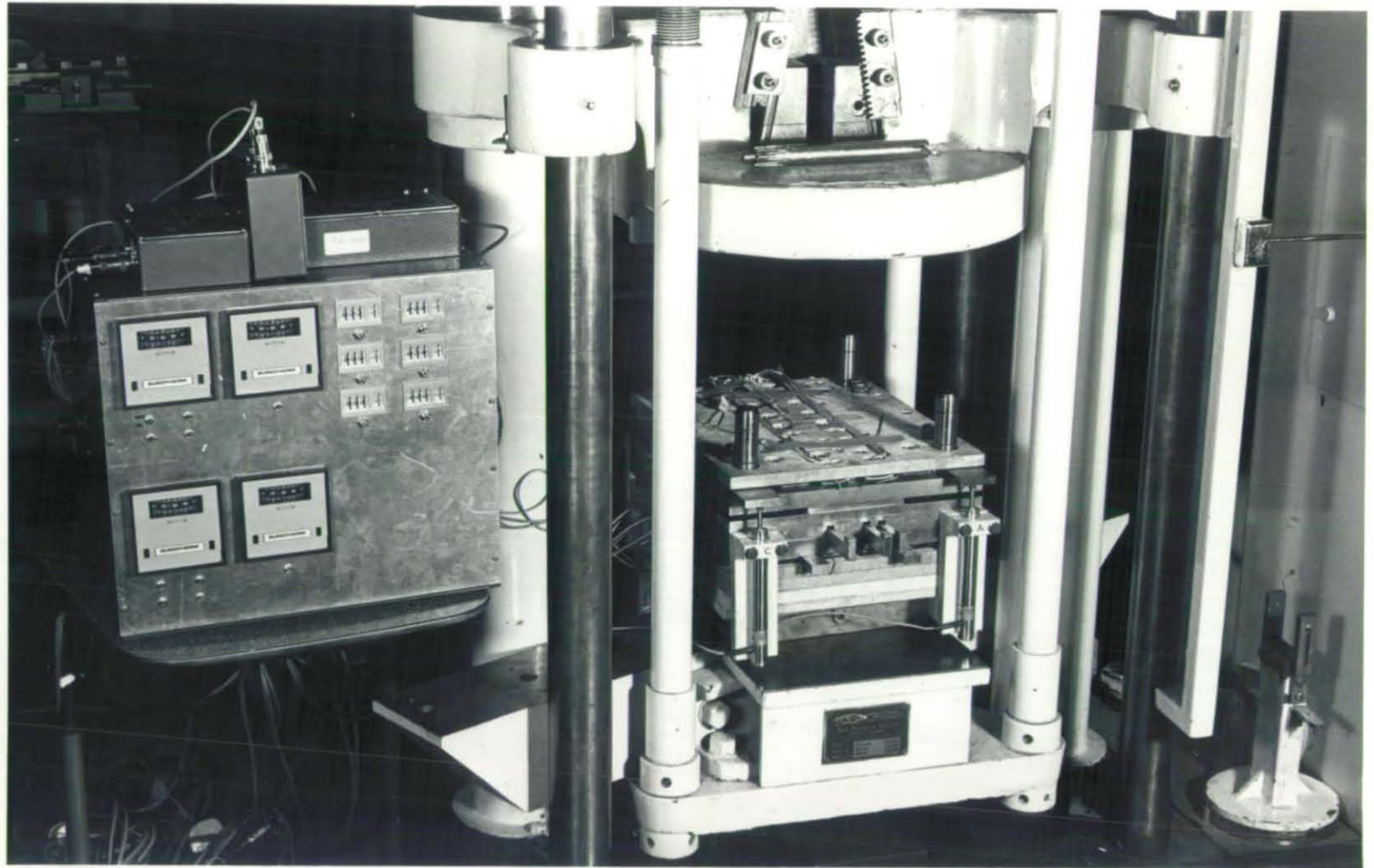


FIGURE 8.1 General view of mould and instrumentation

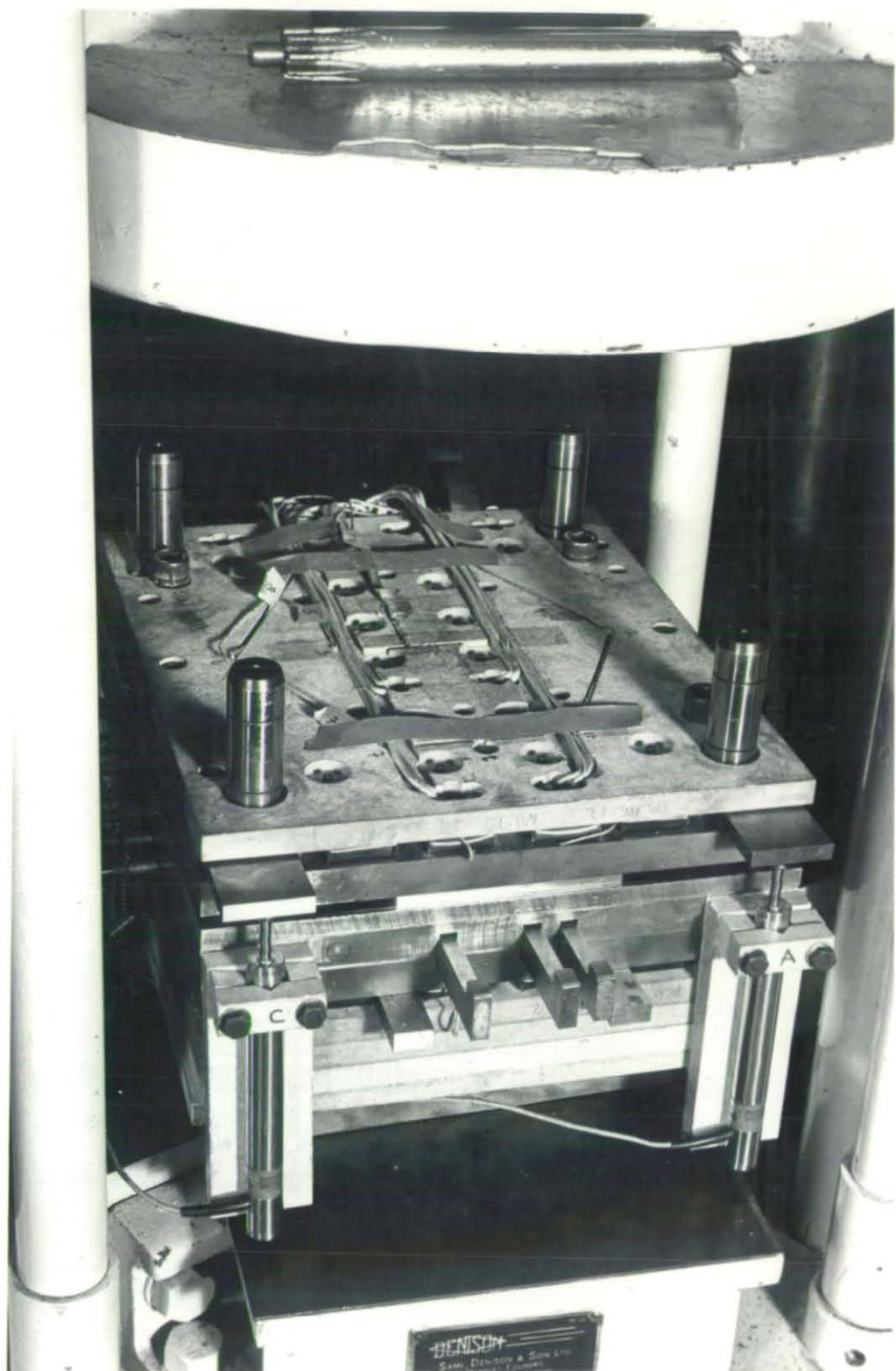


FIGURE 8.2 Close-up of the mould closed

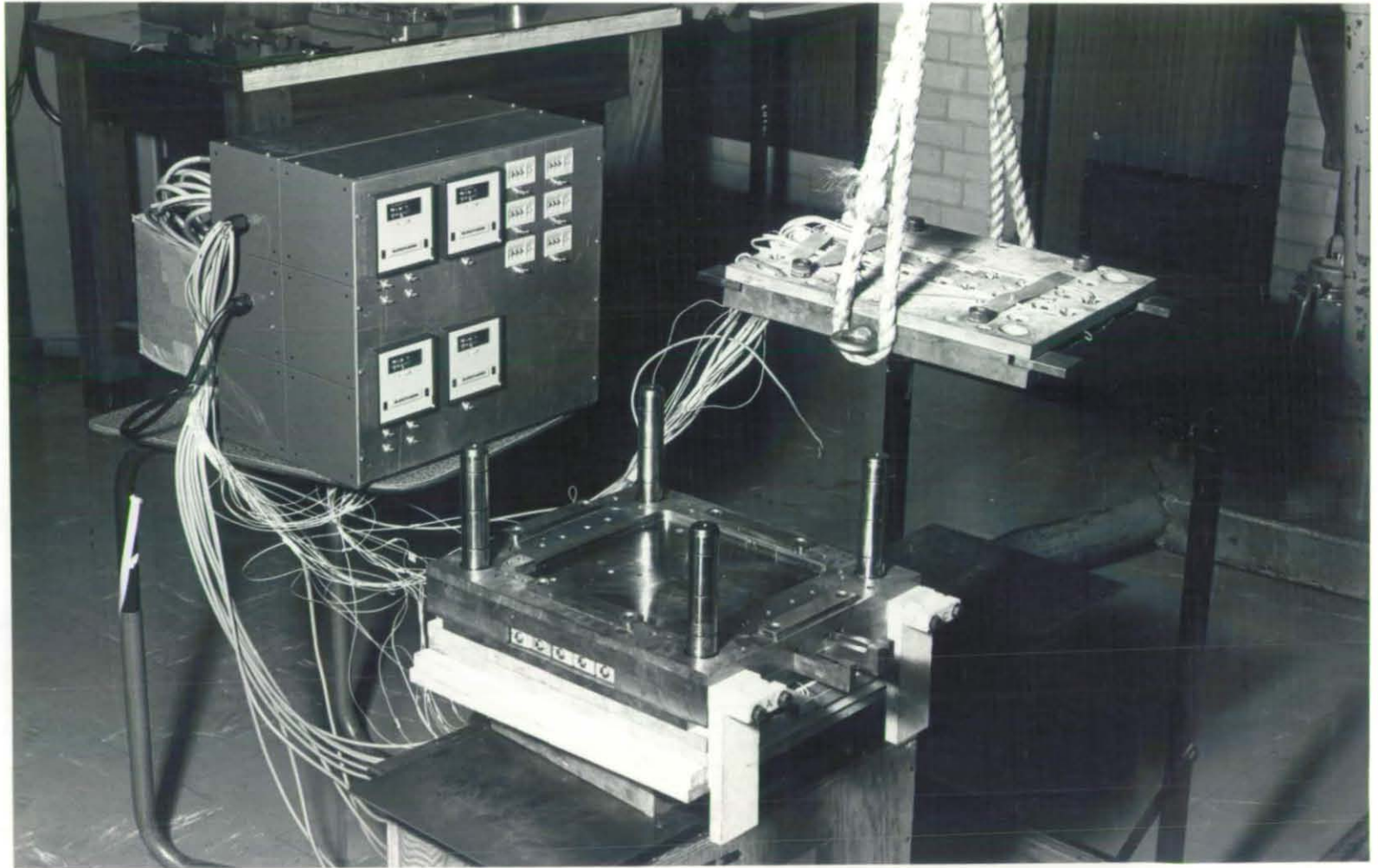


FIGURE 8.3 Mould open with instrumentation

the mould is in Appendix 9 together with the set of plans required for its manufacture.

Mould selection was based on the type of moulds commonly used in industry. Therefore a semi-positive mould was selected with a shear-edge with  $5^{\circ}$  slope and a fit between the punch and cavity of g6H7. This fit must be maintained. If excessive clearance develops between the punch and cavity side, flash will result during moulding and preferential orientation of the fibre glass will be induced in the material near the shear edges.

The mould was designed to make four different plate shapes. These shapes were based on considerations of symmetry and positions of centre of area (see Figures 8.4 to 8.7). The relationship between symmetry and shape are:

square	4 axes of symmetry
rectangle	2 axes of symmetry
triangle and square	1 axis of symmetry
trapezoid	unsymmetrical

This versatility of being able to manufacture differently shaped plates with one mould was achieved by using mould inserts, so that the cavity shape could be altered by adding or taking out inserts. The punch was made from steel plates screwed to a top plate so that its shape could be altered correspondingly.

The cavity was made from two plates (one plate for the cavity walls and the other for the base of the cavity) plus the inserts. Figures 8.8 to 8.11 show the arrangements of inserts to make the four different mould cavity shapes. There are four matching punch shapes.

Although it is possible with this tool to mould four differently-shaped plates, the manufacture problem was that all the inserts had to fit perfectly into the cavity to avoid flash during moulding and fibre orientation near shear edges. The necessary closeness of fit was achieved by machining the inserts approximately to their dimensions (about 1 mm oversize) and then grinding them to the required cavity shape. When the cavity was finished the punch was fitted to the cavity.

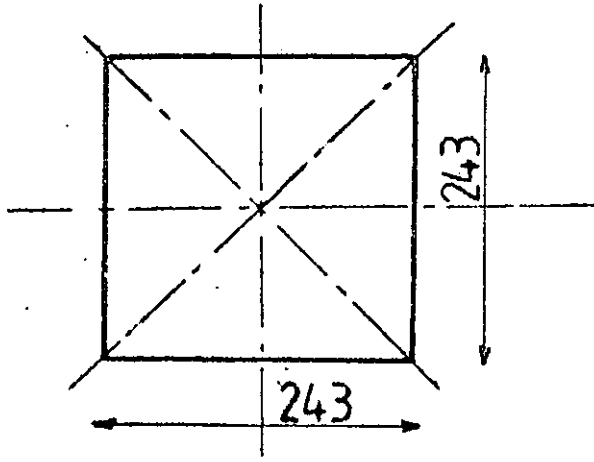


Fig. 8.4

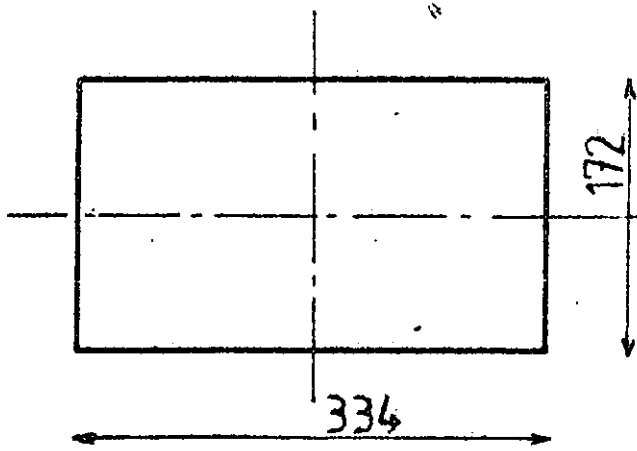


Fig. 8.5

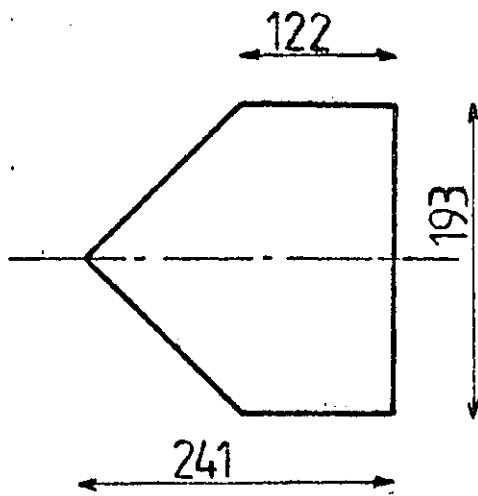
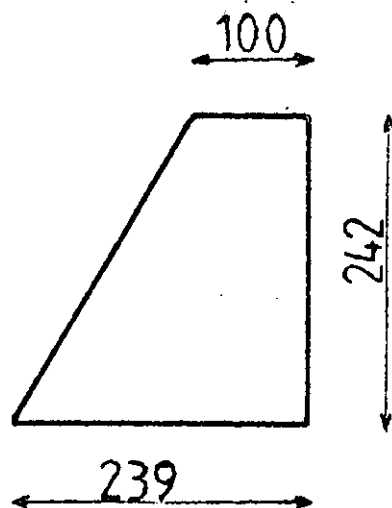


Fig. 8.6



DIM. IN mm.

Fig. 8.7

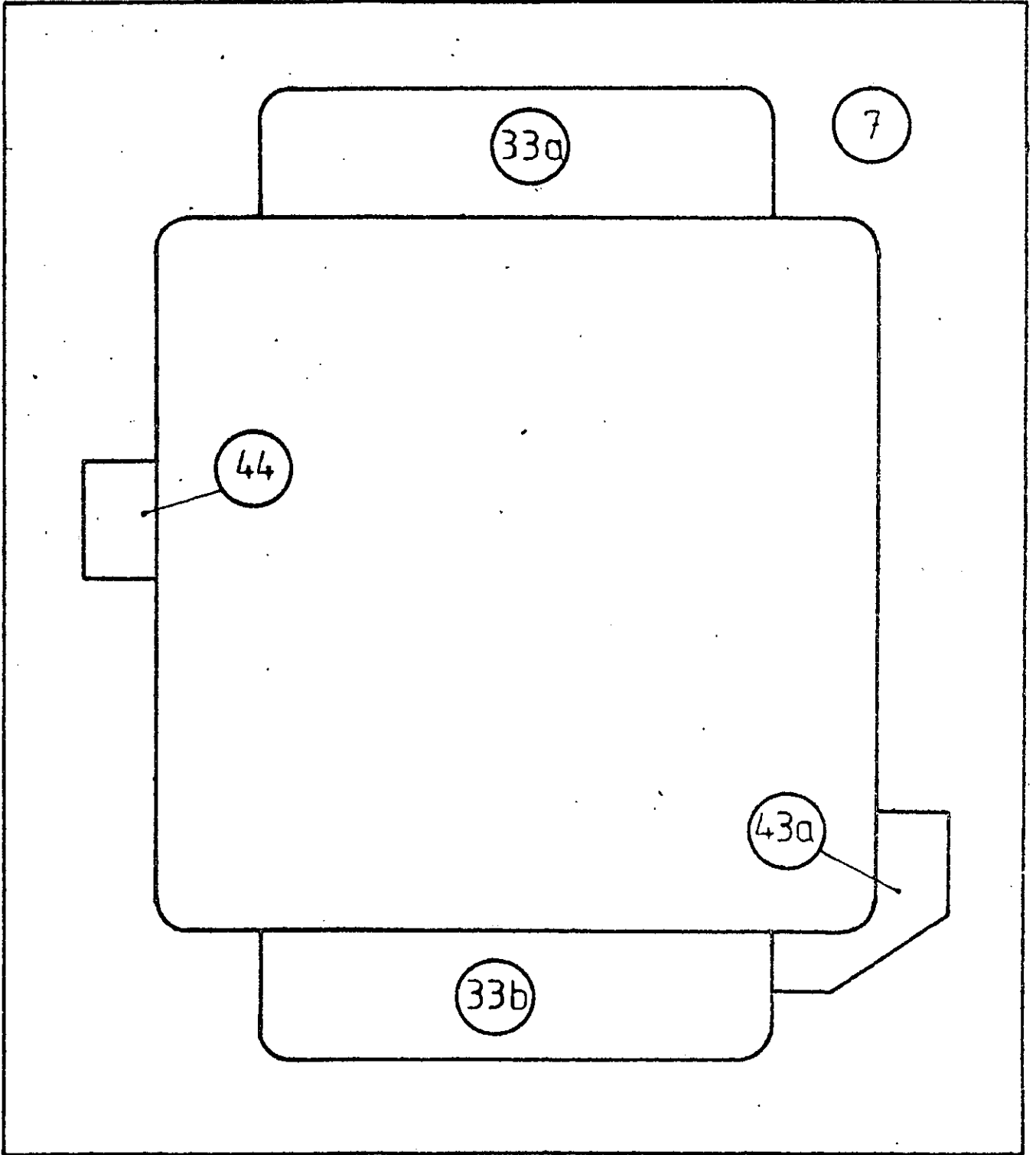


Fig. 8.8 INSERTS FOR SQUARE CAVITY

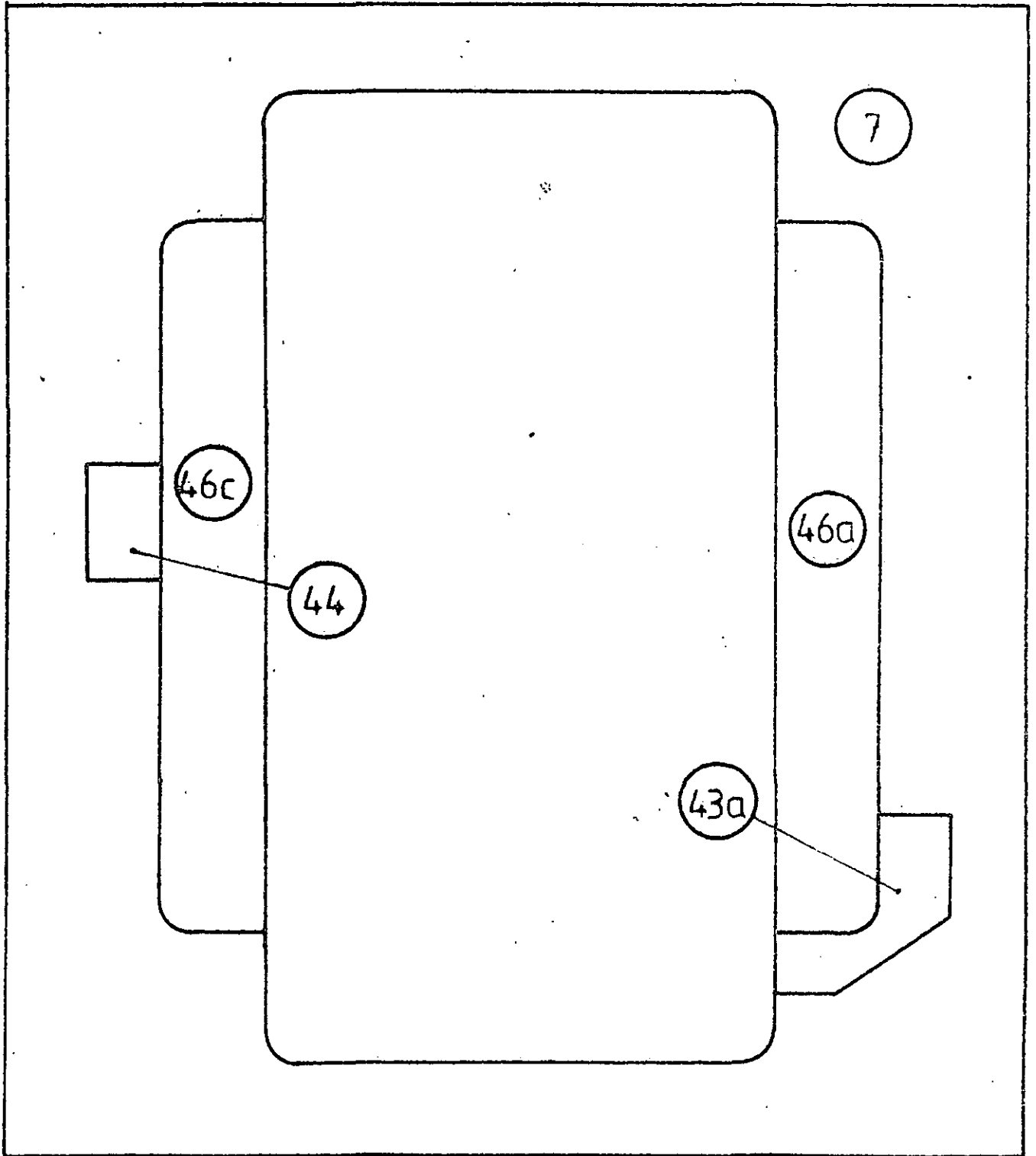


Fig. 8. 9    INSERTS FOR RECTANGULAR CAVITY

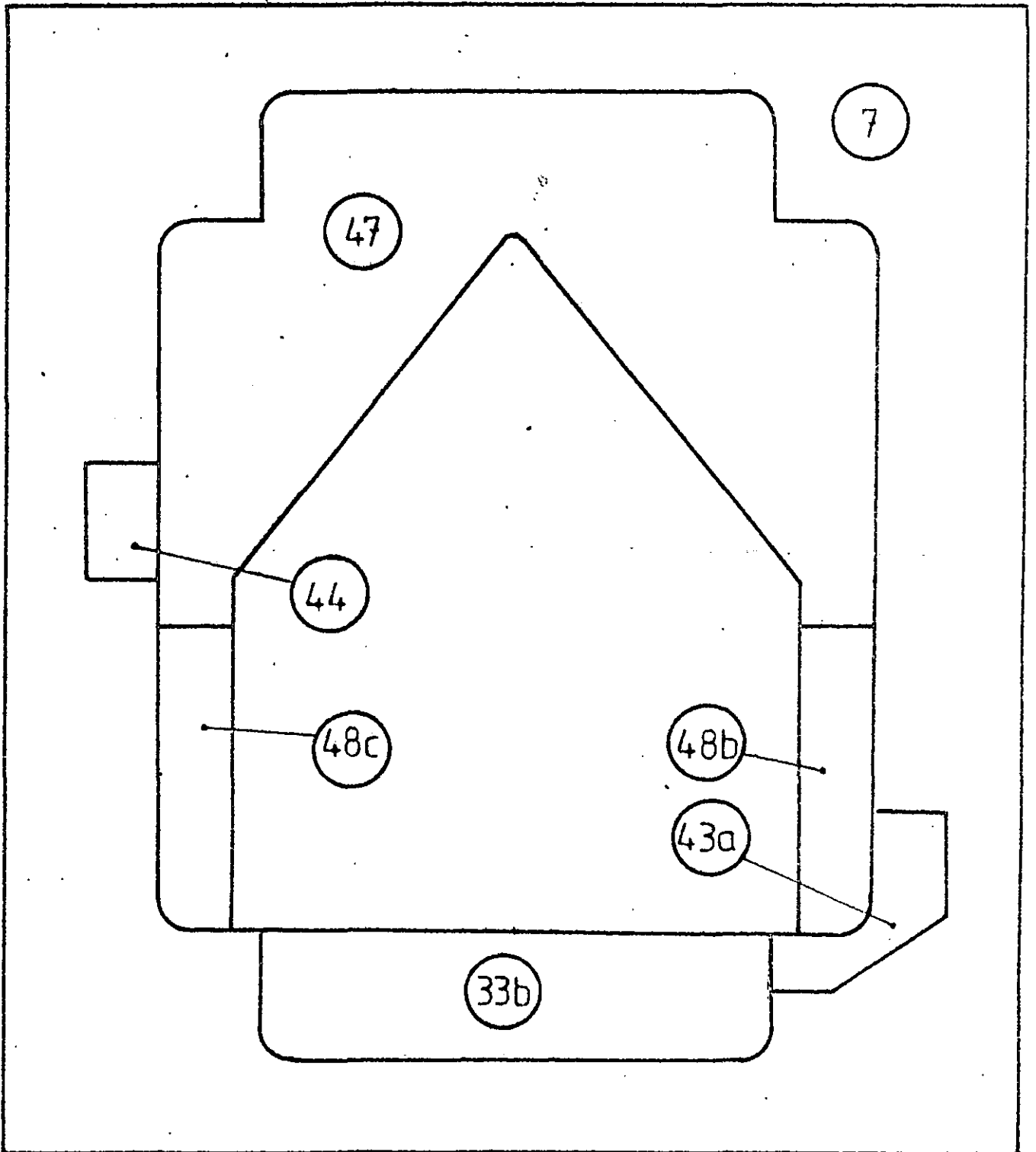


Fig. 8.10 INSERTS FOR SQUARE & TRIANGLE  
CAVITY

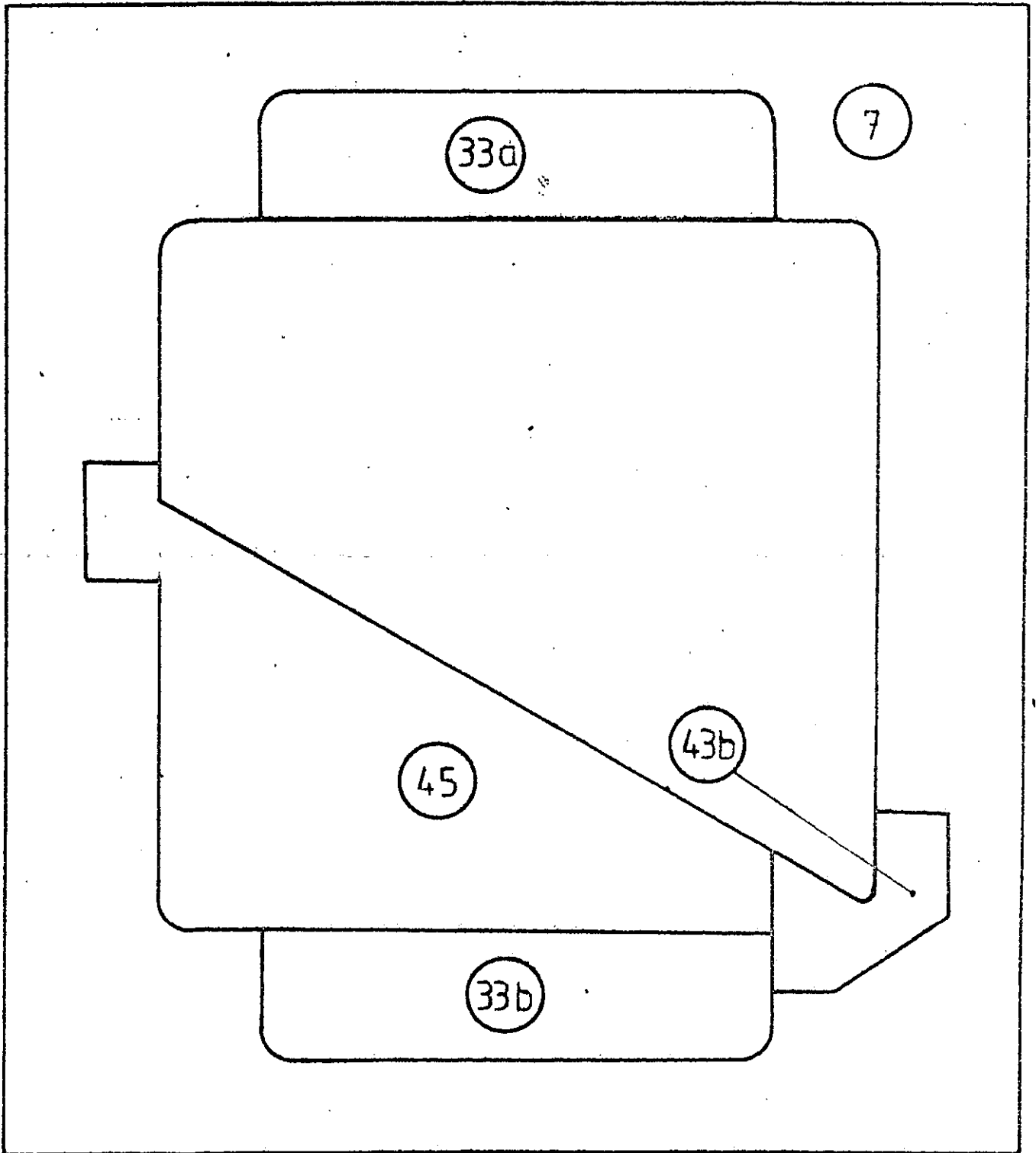


Fig. 8.11 INSERTS FOR TRAPEZOIDAL CAVITY

Such fitting was also checked at 160°C. The steel used on the cavity was the same as for the punches (21 Mn Cr 5), to avoid problems of different expansion coefficients.

Other manufacturing considerations were associated with the fact that the mould was not going to be used in a compression-moulding press for moulding the SMC plates; thus attention had to be given to the following points.

Firstly to guide the punch and also to ensure parallelism of the punch with the base of the mould cavity during closure, the guide pillars had to be thicker than for the usual moulds and had to pass through the top plate to ensure guidance when the mould was fully open. Thus the top plate was in contact with the guide pillars during the whole cycle. (This is not the case when a mould is designed for a compression moulding machine).

Also the mould ejection system had to be activated manually. Therefore a simple taper-wedge and ejector-pin was incorporated into the mould design.

The mould was equipped with its own electric heaters. The size of the heaters for moulding was determined by calculating the amount of heat required to heat the mould from 20°C to 160°C in 30 minutes. This calculation took into account the amount of heat lost by convection and radiation, the heat required by the SMC for curing (for a moulding cycle of 120 seconds) and the heat generated during the exothermic reaction. The calculation was carried out following the work of Herman (H3). Syndanyo plates on the top and the bottom of the mould were used to insulate the mould from the Denison testing machine.

Since the Denison testing machine could only be used in compression the mould was fitted with four 16 mm diameter screws to open the mould after curing. The opening procedure was to lift the punch 4 mm with the screws and then use a small hydraulic crane to continue the opening of the mould. The light weight of the top plate helped this procedure.

The mould is equipped with two lifting rings for transport purposes, and also to help with opening the cavity. It also has two safety bars which should be screwed together, fixing the top part to the lower one, every time that the mould is required to be moved.

Because of the lightness of the mould design, it would be advisable for future work using a compression moulding press to screw one plate (396 x 396 x 12 mm) to both the top and bottom of the mould. Also, attaching the electric heaters to this top plate would make it easier to remove the pressure transducers and mould cavity inserts.

Finally, the mould cavity surface has not been chromed because of reasons of time and cost. However, this is not a limitation when comparing the moulding work of this project with that under the moulding conditions in industry. This work was not aiming to mould plates with high quality surface finishes: the surface finish of the mould affects flow only slightly (M9). In this case the mould cavity surface was polished as much as possible in order to avoid possible surface friction forces. The surface finish used was a mean rough surface of  $10\mu$ .

The mould has been equipped with stops, but the actual moulding was done off the stops by placing slightly more material in the cavity than that needed to completely fill it.

### 8.3 Mould Instrumentation and Control Equipment

The mould is heated electrically by two sets of heaters, one set in the top platen and the other in the bottom platen. Approximately 1.1 kW of heat per platen is provided, with temperature control at  $160^{\circ}\text{C} \pm 1.25 \text{ deg C}$ .

The control box (see Figure 8.2) contains the four heat controllers (Eurotherm model 101-003-03-020-19-21-00), two for each platen. For the bottom platen, one of them controls the heat for the external part of the cavity and the other is for the centre of the cavity. Figure 8.12 shows the layout of the heat supply. The control box also contains the amplifiers for the mould-cavity pressure transducers and the amplifier voltage supplies (3 supplies of 30 volts each).

Together with associated amplifiers, the mould instrumentation consists of 6 piezo-electric pressure transducers (Kistler type 6153), 3 displacement transducers (R.D.C. Electronics DC-LVDT-D5/1000C), 8 Cr-Al thermocouples per platen for controlling the heaters, and 5 Cr-Al thermocouples for measuring the temperature near the cavity.

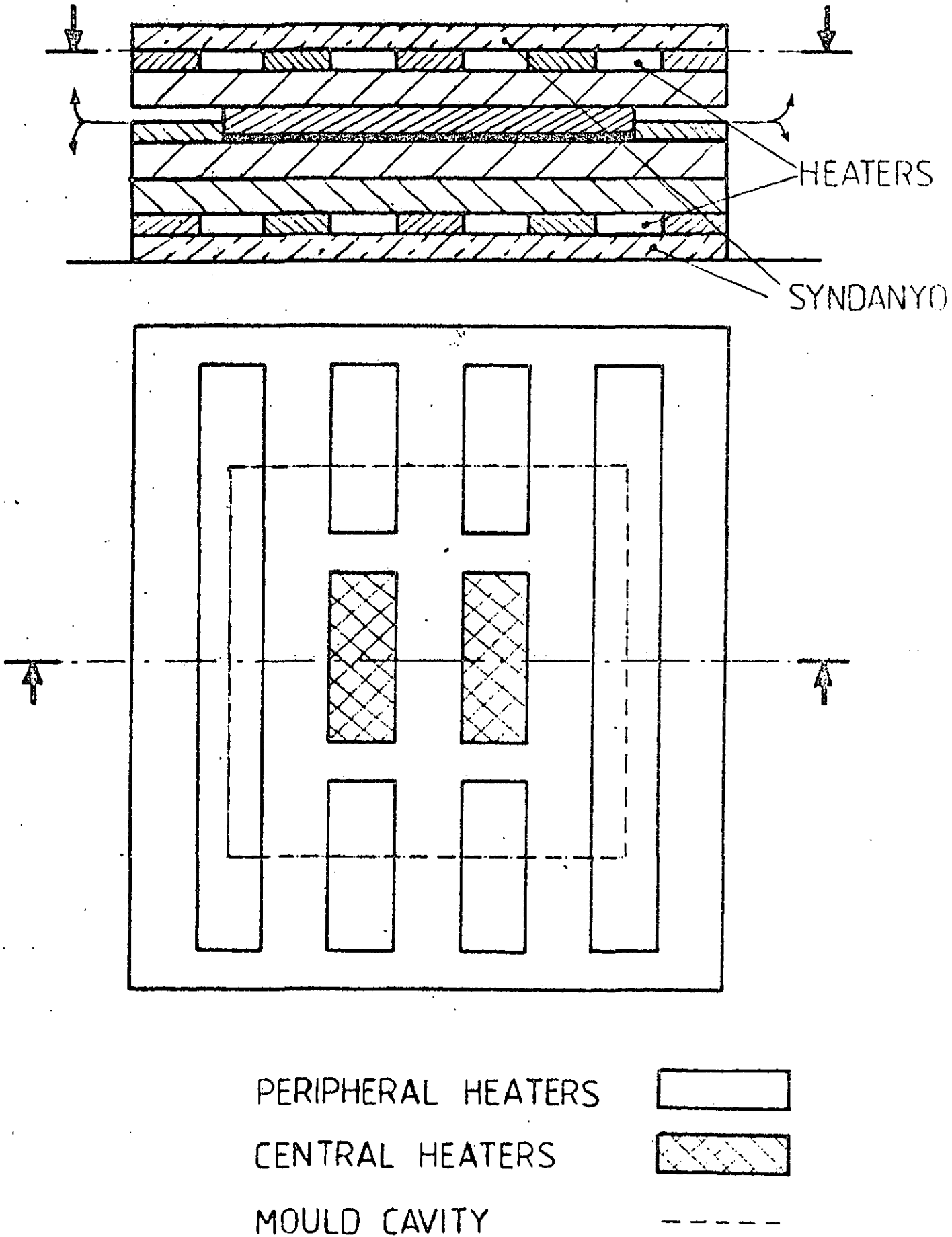


Fig. 8.12 LAYOUT OF HEAT SUPPLY

Figures 8.13 and 8.14 show the positions for the square and trapezoid plates of the pressure and displacement transducers, and the thermocouples for measuring the temperature near the cavity. Similar arrangements apply for the rectangle and the square plus triangle plates.

The mould has 34 holes for changing the positions of the 6 pressure transducers in the mould cavity. The holes are filled with pins when they are not used for the pressure transducers. This solution has been taken, due to the high price of every pressure transducer (about £250.00 each in August 1978).

During moulding, the pressure, temperature, displacement and mould compression-force data were collected on-line using a PDP-11/05 computer. There were 15 channels of input data. The mould compression-force was measured on-line from the Denison testing machine load scale indicator. The voltage range for the displacement and pressure transducers were 1V/1 cm and 0.21 V/bar respectively. The thermocouple voltage range was from 0.76 mV to 6.54 mV for a temperature range from 0°C to 160°C.

#### 8.4 Calibration Procedure, Before Moulding

The experimental work of this project was carried out for one set of moulding-process conditions (see Chapter 9). Thus to obtain repeatability of these moulding conditions from one test series to another, it was important that the correct sequence of steps for the experimental work was followed in each case. Part of that sequence involves checking the calibration of the instrumentation by following manufacturers' instructions, as well as ensuring that the moulding process conditions (for example, moulding temperature, force and closure speed) remained unaltered.

Checks on moulding temperature, force and closure speed for each mould closure were made from the data collected on-line during the tests (see section 9.2). To ensure that the mould and instrumentation were correctly set-up for each test series, the following setting-up procedure was followed:

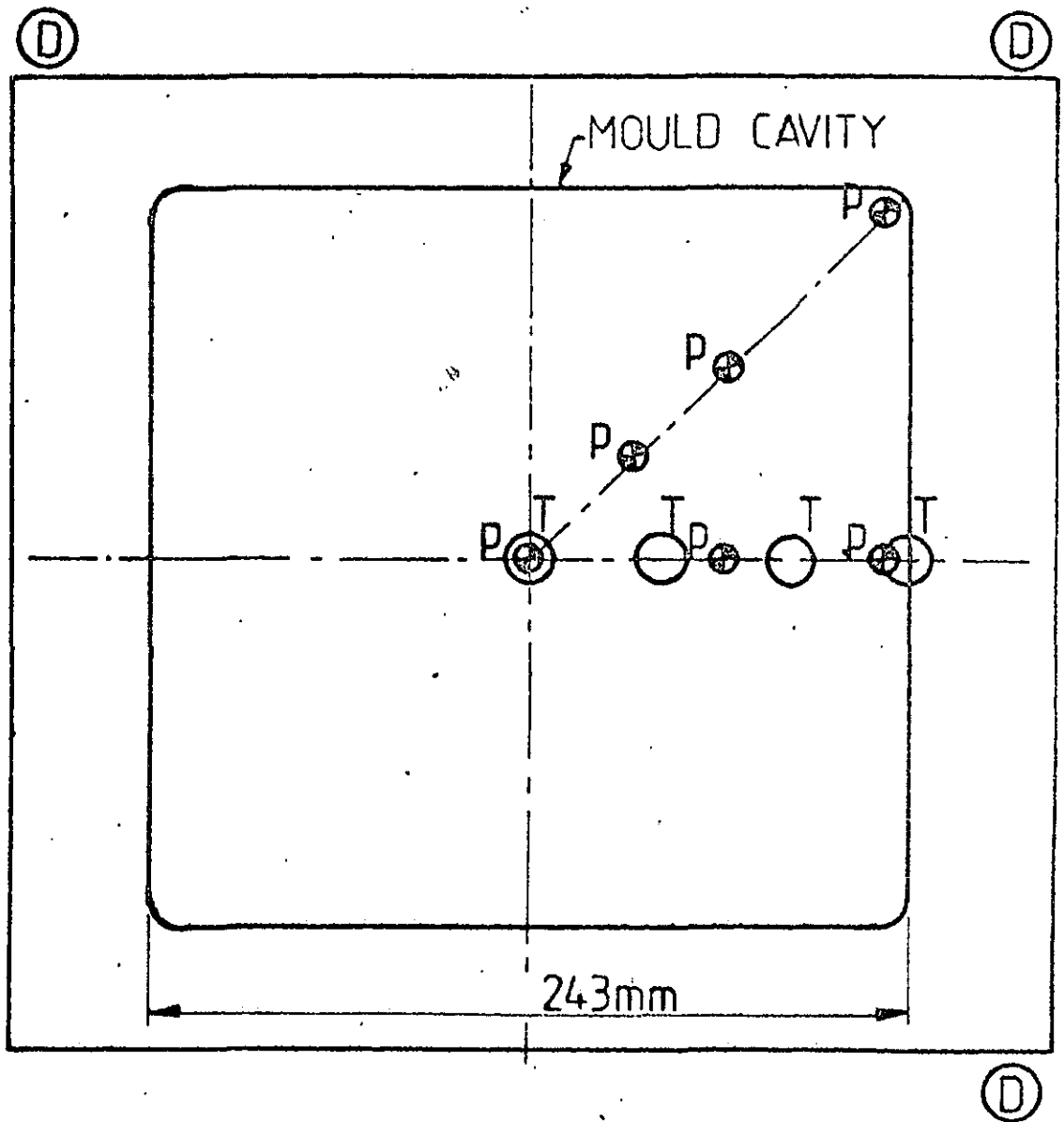


Fig.8.13 SQUARE CAVITY

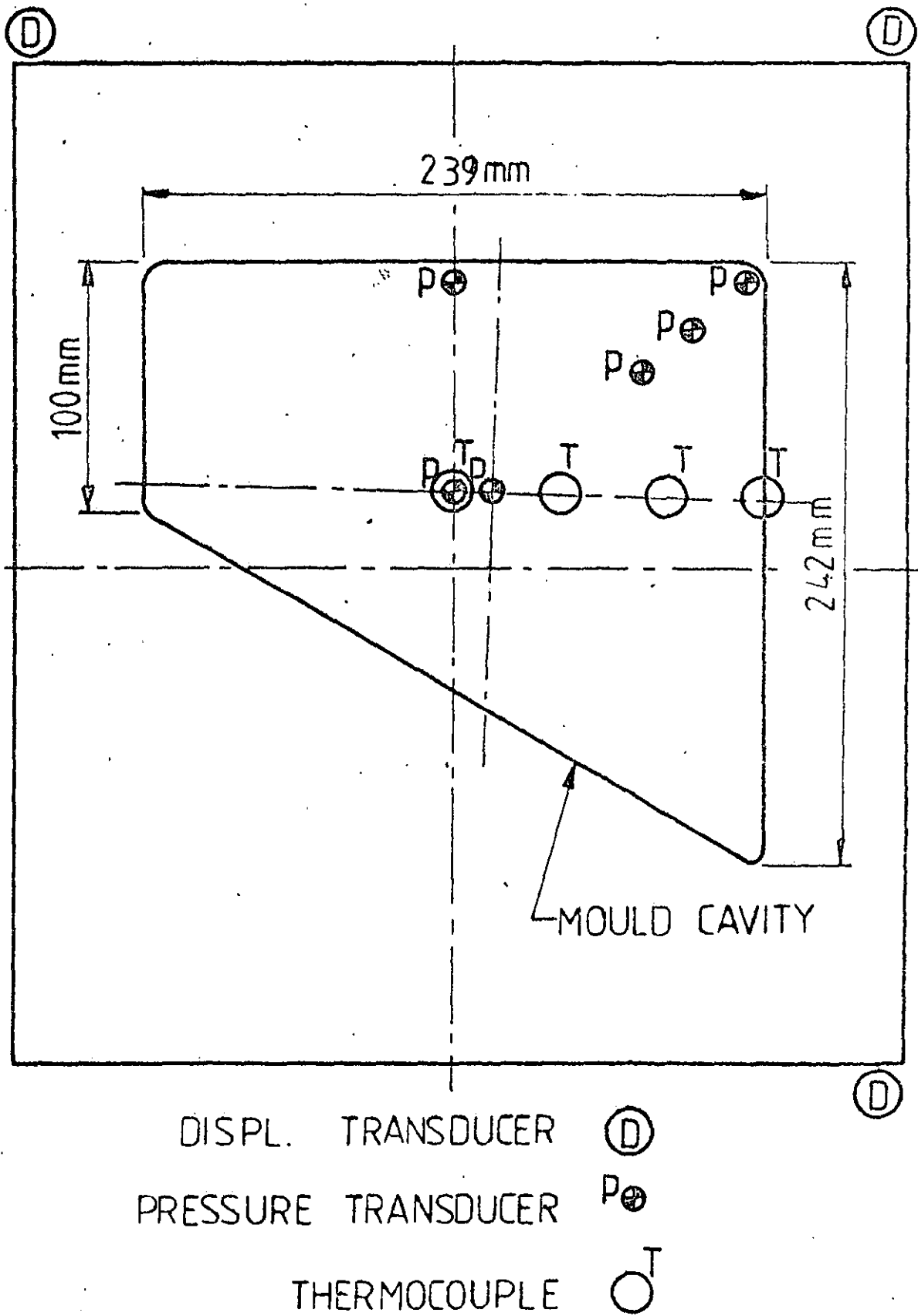


Fig.8.14 UNSYMMETRICAL CAVITY

- Place the mould in position
- Unscrew the safety bars to allow the punch to be lifted
- With the mould closed, check the zero level of the mould with a spirit level
- Take the mobile hydraulic crane and attach the lifting rings of the mould to the hook using a rope sling. Open the mould and check the zero level of the cavity.
- Check the linearity and calibration of the displacement transducers alone by using steel slip-gauges and plotting output voltage against displacement. Allow at least 30 minutes for the LVDT transducers to warm up
- Fasten the displacement transducers to the mould and connect them to their respective amplifiers.- Connect the amplifiers to the mains supply and switch on
- Zero the LVDT transducers with the mould closed. The top plate should be in contact with the moulding stops.
- Check the displacement of the mould as measured by the transducers, using steel slip gauges.
- Connect the pressure transducer terminals from the mould to the amplifiers in the control box
- Before connecting the control box to the mains supply, check that all the switches on the box are in the off-position, especially for the pressure transducer amplifiers. *THESE AMPLIFIERS COULD BE DAMAGED if the switches are on.* Now connect the main supply to the control-box.
- Switch on the amplifiers of the pressure transducers. Leave the pressure transducers and amplifiers for at least 30 minutes to warm up and stabilize.
- Open the mould and check that all the pressure transducers are working properly by pressing each one and observing the voltage variation.
- Close the mould, select the 160°C moulding temperature and switch on the heaters. Leave the mould for a minimum of 30 minutes to reach the required moulding temperature
- Check the temperature readings of the five thermocouples that are located in the punch, using an electronic thermometer.
- Open the mould and check the temperature on the cavity and punch surfaces with an electronic-thermometer. Close the mould again.

- Connect the Denison ram-force plug, the ~~six~~ pressure transducers, the five thermocouples and the three LVDT transducers to the computer scanner terminal. Connect also the remote control switch to the scanner terminal. This remote control will send the signal to the computer to start the scanning
- Load the computer program which controls the on-line collection of the moulding data (a suitable computer program is shown in Appendix 7, with full explanation for its use). Run the program setting the scanning time to about 10 seconds.
- Press the remote control and check that the readings of the scanner printed by the teletype correspond with those set during calibration, for example:

<u>Equipment</u>	<u>Readings</u>
3 LVDT Transducers	≈ 0.0
6 Pressure Transducers	≈ 0.0
5 Thermocouples	6.5 mV ≈ 160°C
Ram force	≈ 0.0

If the readings correspond with the calibration settings then the equipment and the mould are ready for moulding.

## CHAPTER 9

EXPERIMENTAL WORK9.1 Introduction

The main aim of the experimental programme was to check that flow from appropriately calculated charge shapes does not form weld-lines during SMC moulding. To do this the experimental programme was designed in which a series of square and trapezoidal plates were moulded. There were three parts to the experimental work.

The first part of the work involved checking the initial assumptions (see section 6.3), of material uniformity, homogeneity and planar isotropy (before moulding) by measuring the glass fibre distribution in the SMC matrix. The second part was to mould the plates from the predicted charge shapes while recording the moulding-process variables, such as pressures in the cavity, temperatures and closure speeds. The last part of the work involved checking that no weld-lines were present in the plates moulded using the predicted charge shapes. The planar isotropy of the moulded plates was also checked in this last part, to see if flow from 70% charge area induced anisotropy.

The first material to be used in this experimental work was a 2.5 mm thick general purpose SMC (type No. SV273), but the initial analysis showed that this SMC had a non-uniform fibre distribution and anisotropic properties in the plane of the sheet before moulding. Thus another material was selected. This was a 2.5 mm thick low profile SMC (type SY-19/25L). Its approximate composition (without fibre glass) by weight is:

Unsaturated polyester (diluted in styrene)	23%
Low profile additive (diluted in styrene)	15%
Filler (calcium carbonate)	57%
Thickening agent	1.5%
Release agent	2.5%
Catalyst	0.3%

The percentage of fibre glass is 25% by weight for the whole mixture. The fibre glass strands are 25 mm long, and made from bundles of 108 strands.

During the experimental work for moulding plates the material used was always 30 days old ( $\pm 5$  days).

## 9.2 Analysis of the SMC Before Moulding

The aim of this section of the work was to check that the supplied SMC was uniform, homogeneous and isotropic in the plane of the sheet.

Samples were cut from fresh SMC sheet. Figure 9.1 shows the three positions in the SMC manufactured sheet, from where the samples were cut. Sample size was 233 x 156 mm, which completely filled a rectangular cavity mould. To cure the samples, a force of approximately 10 kN was applied to the mould while its temperature was held at 160°C for one minute. There was no flow of the SMC matrix during curing. This technique was selected to avoid changing the fibre-glass distribution. Therefore it was possible to check not only the initial assumptions as explained above, but also to establish a reference for the mechanical properties of the SMC without flow.

Three experimental techniques were used to analyse the material homogeneity and isotropy. Firstly, tensile tests were made using specimens taken from the samples, and cut parallel and perpendicular to the SMC manufacture direction. The maximum strength of the specimens before failure was determined using the test procedure described in BS 2782 (B8). The tests were carried out in an Instron TT-CM machine with a force range of 10 kN, at 0.016 mm/sec test speed. Room temperature was at 20°C.

Table 9.1 shows the results for the LP-SMC, while Figures 9.2 and 9.3 compare the results for the two types of material used (general purpose SMC and LP-SMC).

Secondly the orientation of the glass fibre in the cured SMC samples was determined using an X-ray technique with a Cambridge S2A Stereoscan (H2). Specimens between 0.25 mm and 0.5 mm thick were cut to examine the through-the-thickness fibre orientation (along a section

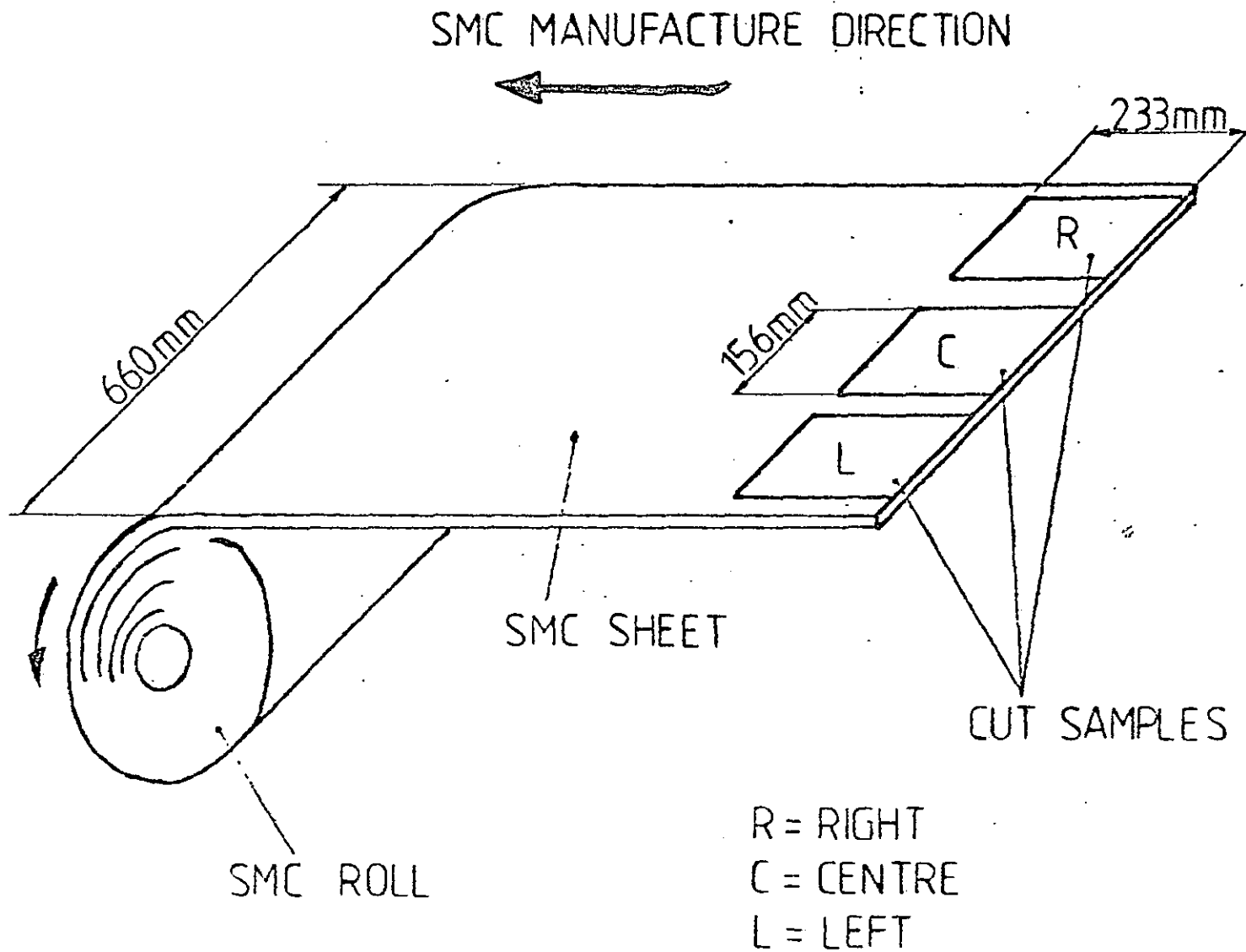


Fig.9.1 SMC SHEET MANUFACTURE AND SAMPLE POSITIONS

TABLE 9.1

Location	Ref	Stress (MN / m <sup>2</sup> )	Mean (MN/m <sup>2</sup> )	S.D.
Left side parallel to the flow	I11	58.6	57.78	2.24
	I12	*42.0		
	I13	55.6		
	I31	55.7		
	I32	58.0		
	I33	61.0		
Centre parallel to the flow	C11	71.0	63.88	5.89
	C12	59.5		
	C13	71.5		
	C21	59.3		
	C22	59.0		
	C23	63.0		
Right side parallel to the flow	R31	56.8	57.62	1.02
	R32	56.9		
	R33	59.1		
	R11	57.0		
	R12	*40.8		
	R13	58.3		
Left side perpendicular to the flow	I41	70.6	61.41	4.78
	I42	59.6		
	I43	58.5		
	I51	60.9		
	I52	57.2		
	I53	61.7		
Centre perpendicular to the flow	C51	64.1	58.01	5.61
	C52	62.3		
	C53	58.0		
	C61	61.1		
	C62	50.5		
	C63	52.0		
Right side perpendicular to the flow	R41	50.4	58.65	6.86
	R42	57.4		
	R43	55.0		
	R51	55.3		
	R52	65.3		
	R53	68.5		

\* Values not considered for the calculation of the mean. The breaking point was in the grips.

perpendicular to the manufacturing direction), and also the fibre orientation in the plane of the SMC sheet. Figures 9.4 and 9.5 show the orientation of the glass fibre bundles in the general purpose SMC and Figures 9.6 and 9.7 show the orientation in the LP-SMC.

Finally the percentage weight of glass fibre per-unit-area of SMC sheet - neglecting the effects caused by variations in SMC sheet thickness - was determined using Whybrew's experimental technique (W2), see Appendix 6. Checks were made for each sample position of Figure 9.1. Table 9.2 shows the results obtained for the LP-SMC, and Figure 9.8 compares the fibre glass variation for the two materials analysed.

### 9.3 Measurements during SMC Moulding

A compression mould was designed, manufactured and instrumented (see Chapter 8) to provide the experimental data for testing the charge shape calculation method, and also to enable comparisons to be made with moulding process data - cavity pressure and temperatures, platen displacement, closure speed and ram forces - from previous work (M2, T8). Full details of mould design and instrumentation are given in Chapter 8.

Four different plate shapes can be moulded by using mould inserts, although only two shapes - the square and trapezoid - were moulded for this work. The following plates were moulded using differently shaped charges:

<u>Plate Shape</u>	<u>Charge Shape</u>	<u>% Mould Cover</u>
Square	Circle	57%
Square	Two rectangles (placed at opposite sides of the mould)	60%
Square	Calculated (see Fig. 9.9)	70%
Trapezoid	Calculated (see Fig. 9.10)	70%

TABLE 9.2

Location	Ref	Wt/Area (kg/mm <sup>2</sup> )	% Fibre Glass	Mean	S.D.
Left Side	L1	4.25 x 10 <sup>-6</sup>	27.0	26.36	0.37
	L2	4.18 x 10 <sup>-6</sup>	26.3		
	L3	4.86 x 10 <sup>-6</sup>	26.2		
	L4	4.76 x 10 <sup>-6</sup>	26.0		
	L5	4.69 x 10 <sup>-6</sup>	26.3		
Centre	C1	4.52 x 10 <sup>-6</sup>	28.4	27.42	0.57
	C2	4.89 x 10 <sup>-6</sup>	27.0		
	C3	4.72 x 10 <sup>-6</sup>	27.0		
	C4	4.77 x 10 <sup>-6</sup>	27.4		
	C5	4.71 x 10 <sup>-6</sup>	27.3		
Right Side	R1	4.68 x 10 <sup>-6</sup>	25.1	26.20	0.67
	R2	4.72 x 10 <sup>-6</sup>	26.9		
	R3	4.26 x 10 <sup>-6</sup>	26.3		
	R4	4.46 x 10 <sup>-6</sup>	26.5		
	R5	4.60 x 10 <sup>-6</sup>	26.2		

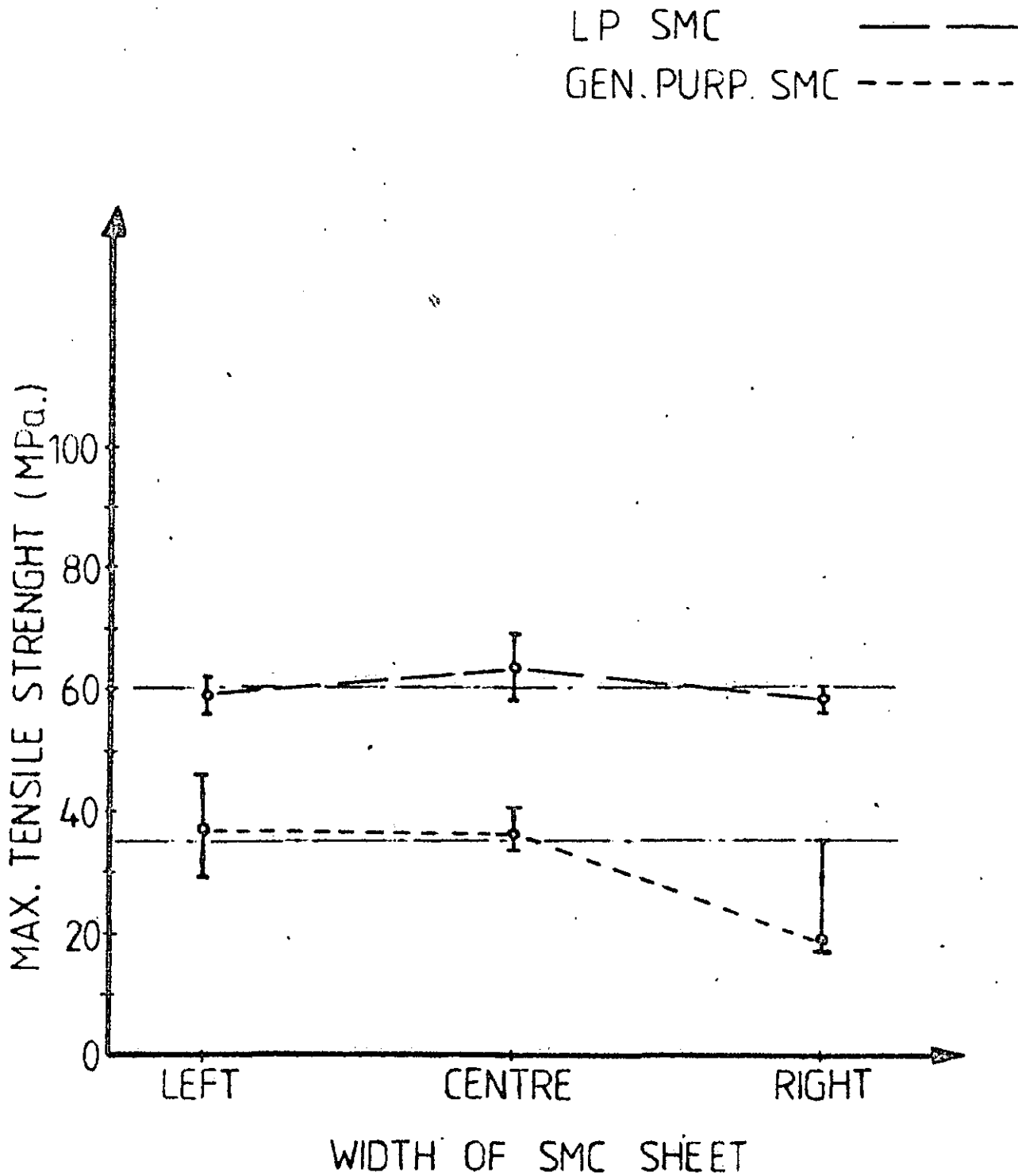


Fig.9.2 TENSILE TEST RESULTS PARALLEL TO SMC MANUFACTURING DIRECTION

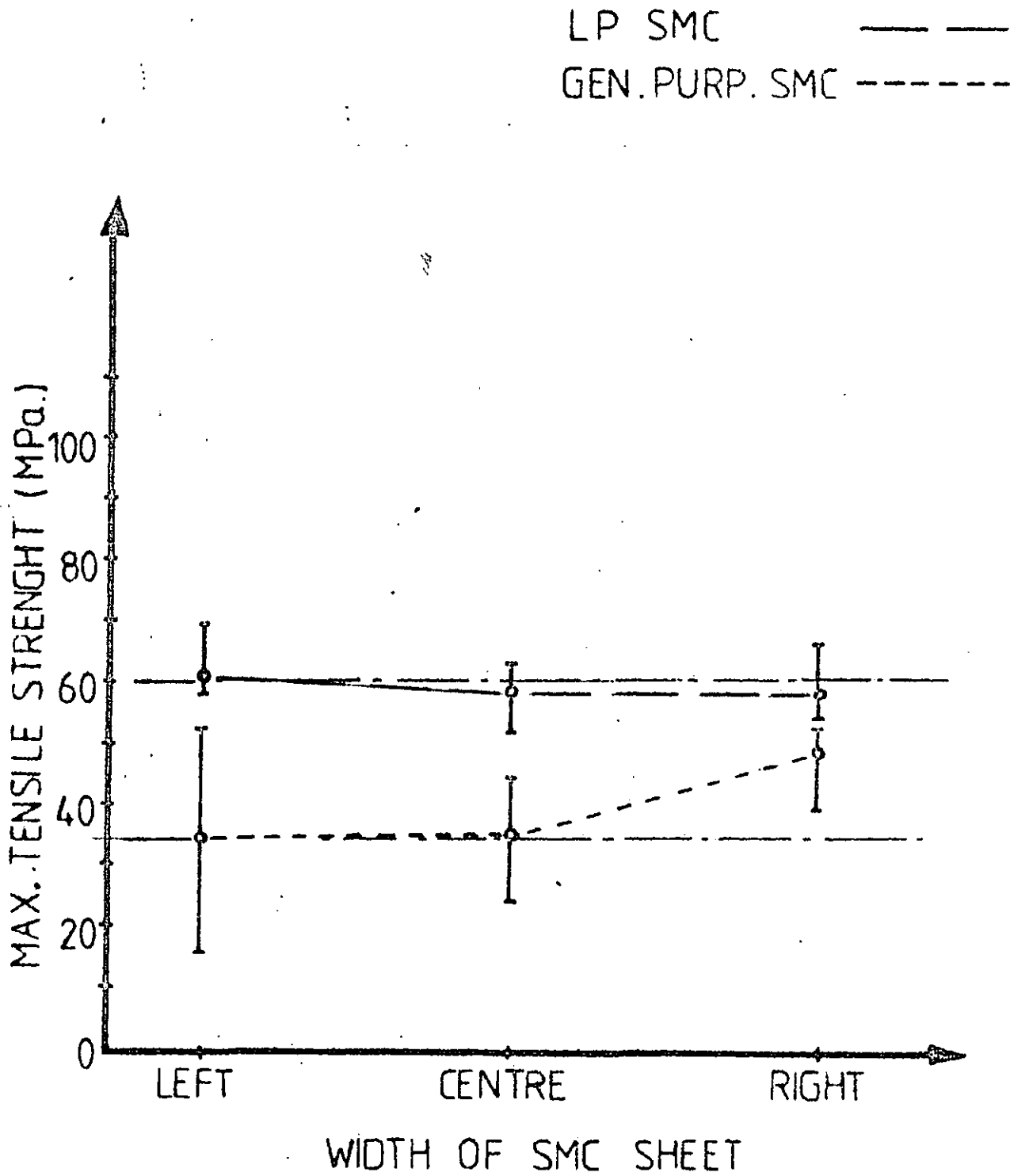


Fig.9.3 TENSILE TEST RESULTS PERPENDICULAR TO SMC MANUFACTURING DIRECTION



FIGURE 9.4 Fibre distribution in the plane of the SMC sheet (general purpose SMC). Magnification x 6.

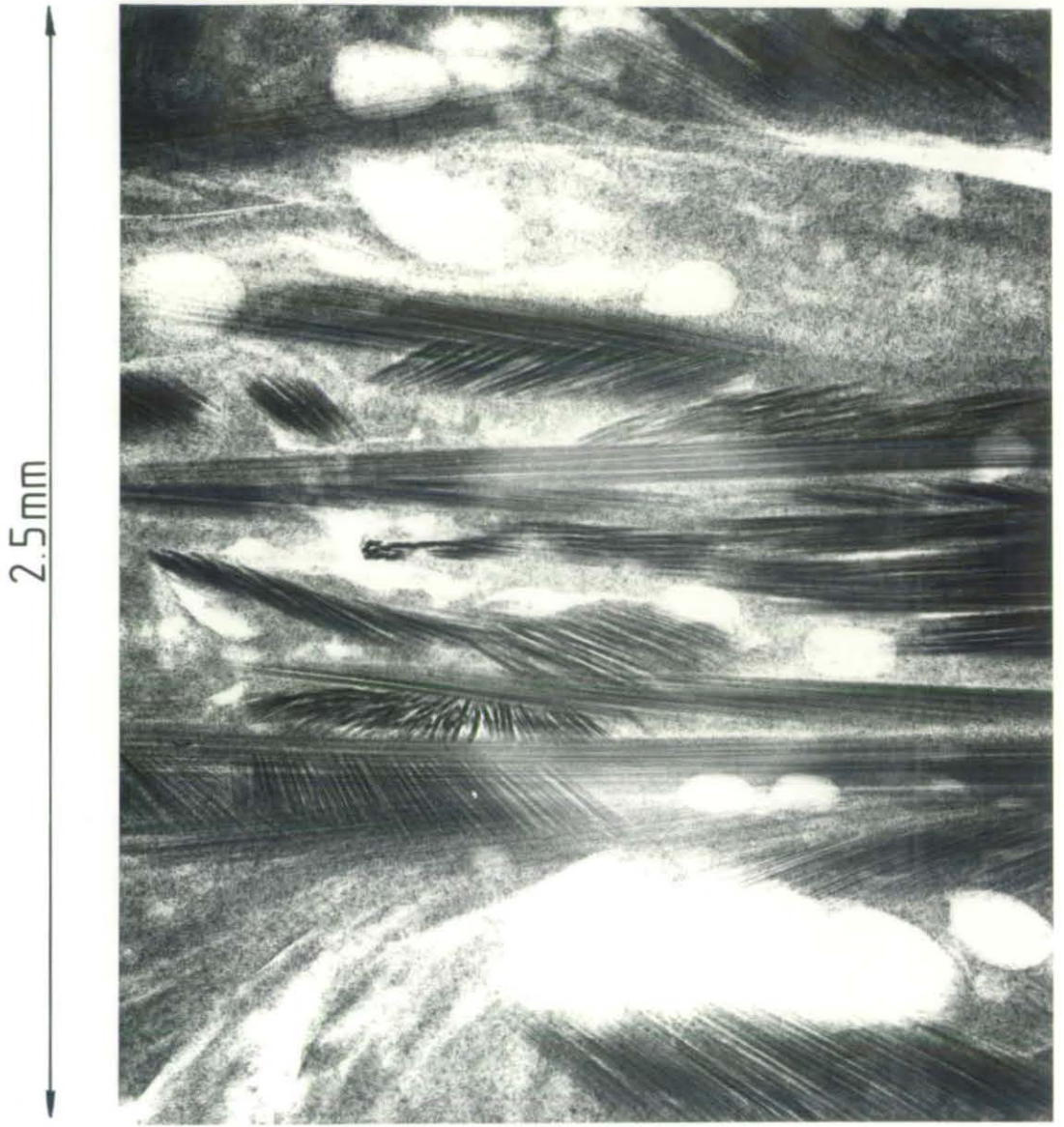


FIGURE 9.5 Fibre distribution in the SMC sheet thickness (general purpose SMC)



FIGURE 9.6 Fibre distribution in the plane of the SMC sheet (LP-SMC). Magnification x 6.

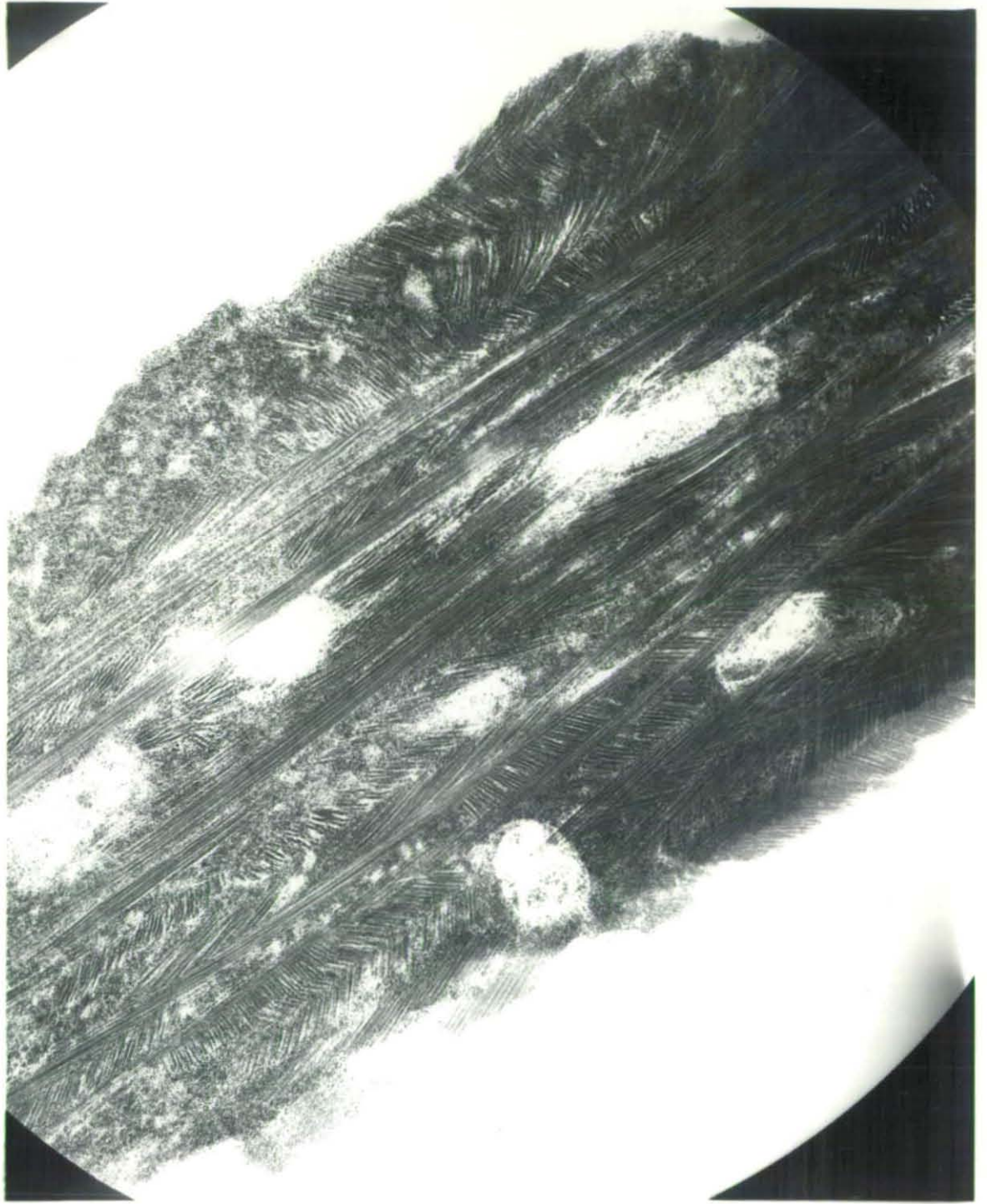


FIGURE 9.7 Fibre distribution in the SMC sheet thickness (LP-SMC)

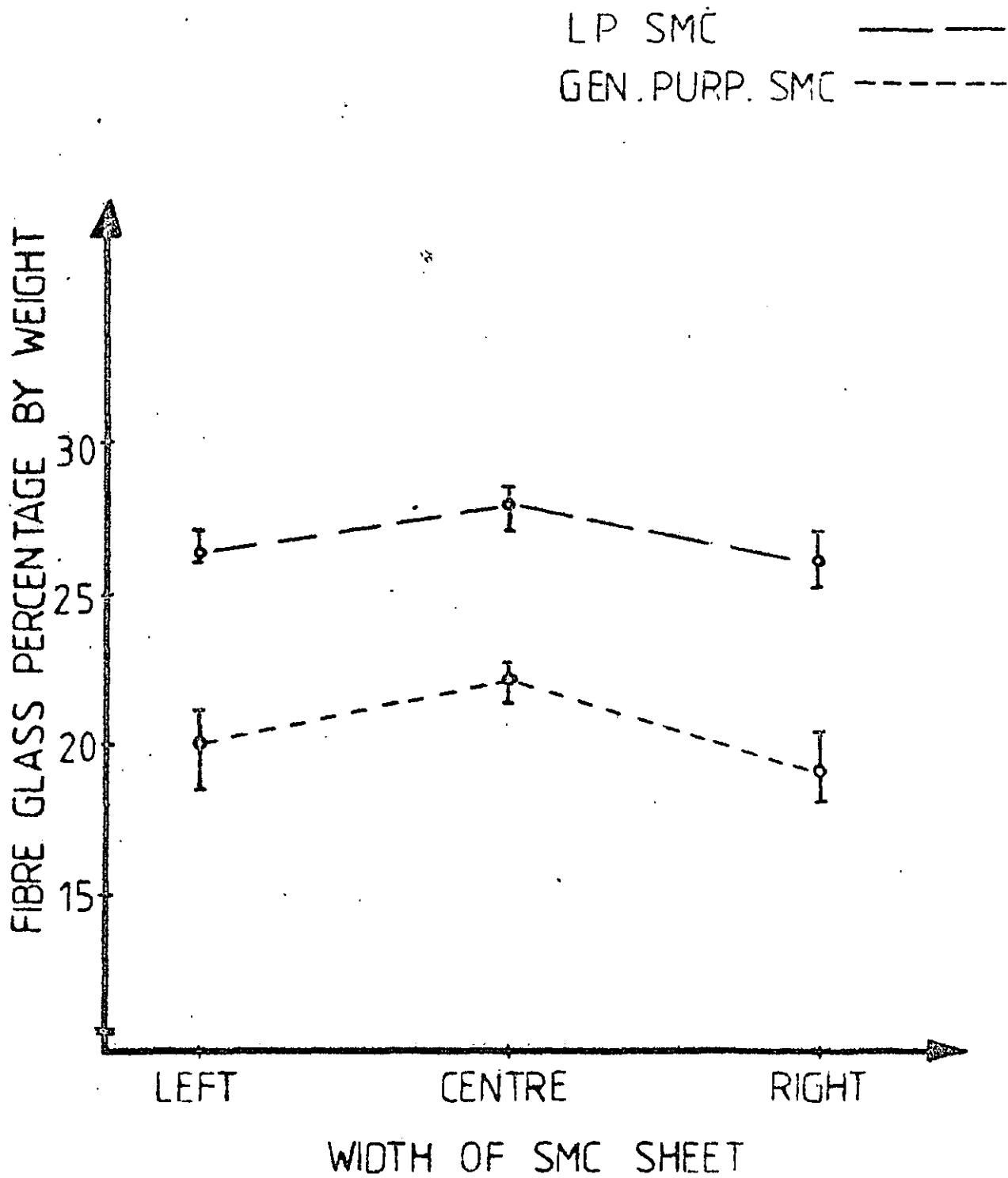
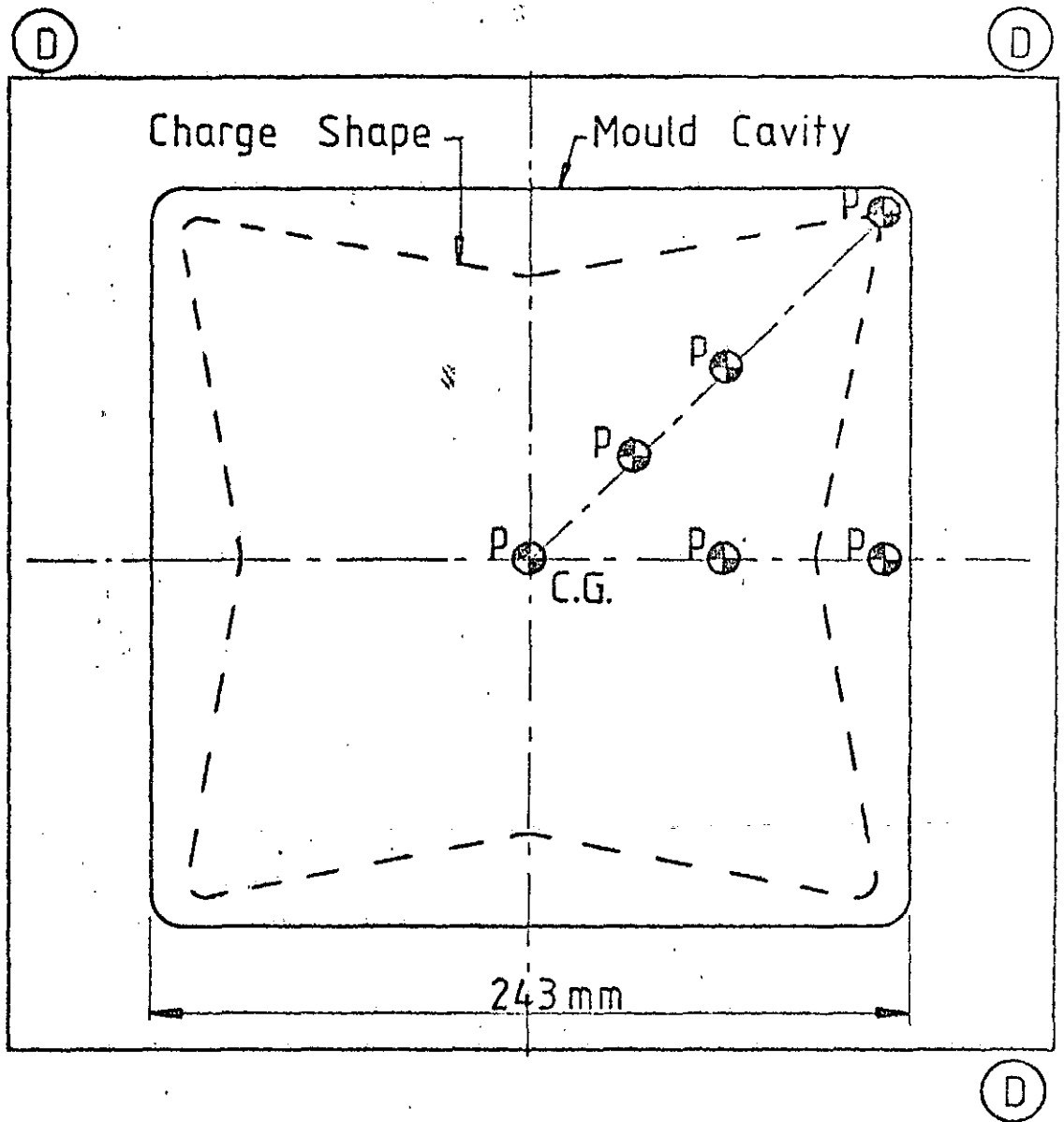


Fig.9.8 PERCENTAGE WEIGHT OF FIBRE GLASS



Displacement Transducer (D)

Pressure Transducer P

Fig.9.9 MOULD AND CHARGE SHAPE FOR SQUARE PLAQUE

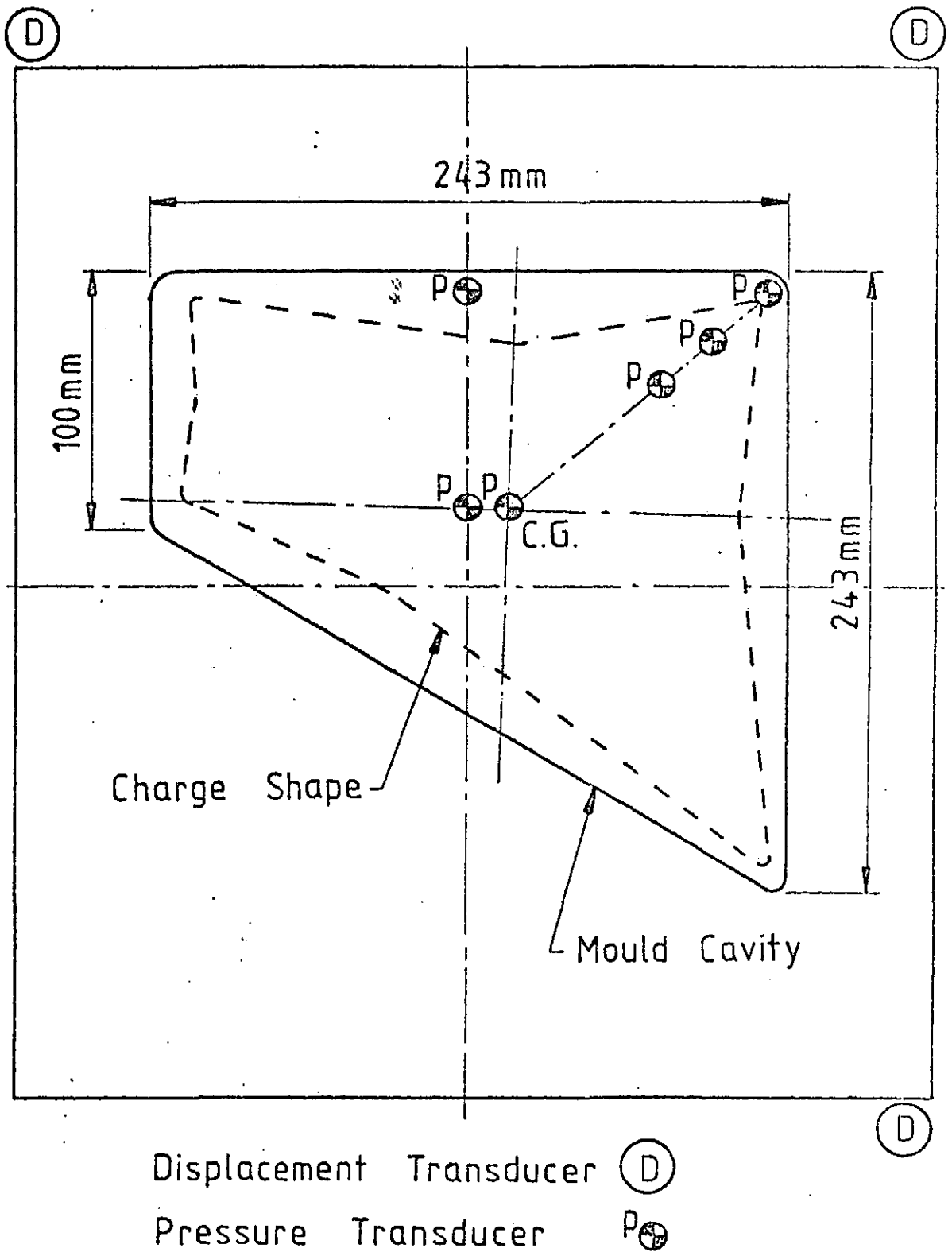


Fig.9.10 MOULD AND CHARGE SHAPE FOR ASYMMETRICAL PLAQUE

For all the mouldings, nominal moulding pressure was 3.0 MPa, the moulding temperature was held approximately at 160°C and the curing time was 1 minute. Figure 9.11 shows typical ram-force and platen displacement traces, which follow the form shown in previous work (M2). There was no significant out-of-parallelism of the platens, and therefore the displacement trace is the average of the readings from the three LVDT's.

Pressure readings from the transducers for the moulded square plate are shown in Figure 9.12 compared against the calculated pressure distribution given by equation 6.40.

Figure 9.13 shows the variation of pressure at various positions during moulding cycle for the square plate. These data follow the form shown in previous work (M2). Figure 9.14a shows the pressure variation during closure for the square plate and Figure 9.14b shows the pressure variation during closure obtained by Marker and Ford (M2) when moulding a circle with 32% of area covered.

#### 9.4 Analysis of the Moulded SMC

The aim of this part of the experimental work was to test for weld-line formation, and also check that there was no significant fibre reorientation due to flow, i.e. that moulded SMC material remained uniform, homogeneous and isotropic in the plane of the moulding flow. The three experimental techniques described in section 9.1 were used. Only the X-ray technique was changed, because the sample size of the technique used in section 9.1 covers only a very small area (approximately 625 mm<sup>2</sup>). Another X-ray technique was used (E2) which allowed a bigger area (approximately 62500 mm<sup>2</sup>) to be examined.

Figures 9.15 and 9.17 show the position of the tensile test specimens, together with the results of the tests, for the square and trapezoidal plates moulded from calculated charge shapes. Figure 9.16 compares the strength of specimens cut from the edge of each of the three square plates.

The percentage weight of fibre glass per-unit-area of moulded SMC was determined (W2) for the square plate moulded from the calculated

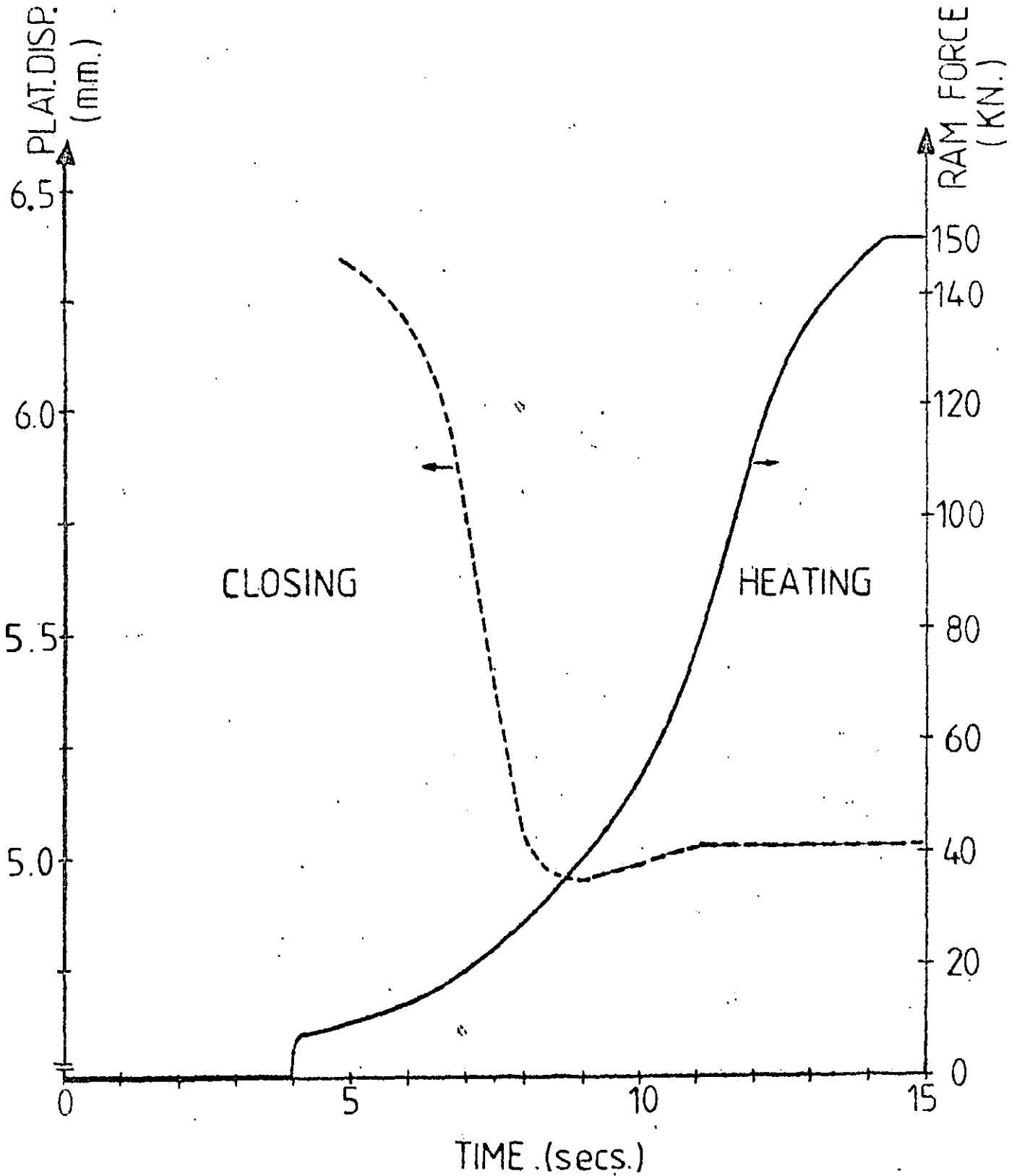


Fig.9.11 PLATEN DISPLACEMENT AND RAM FORCE VARIATION FOR SQUARE-PLATE MOULDING CYCLE, USING CALCULATED CHARGE SHAPE

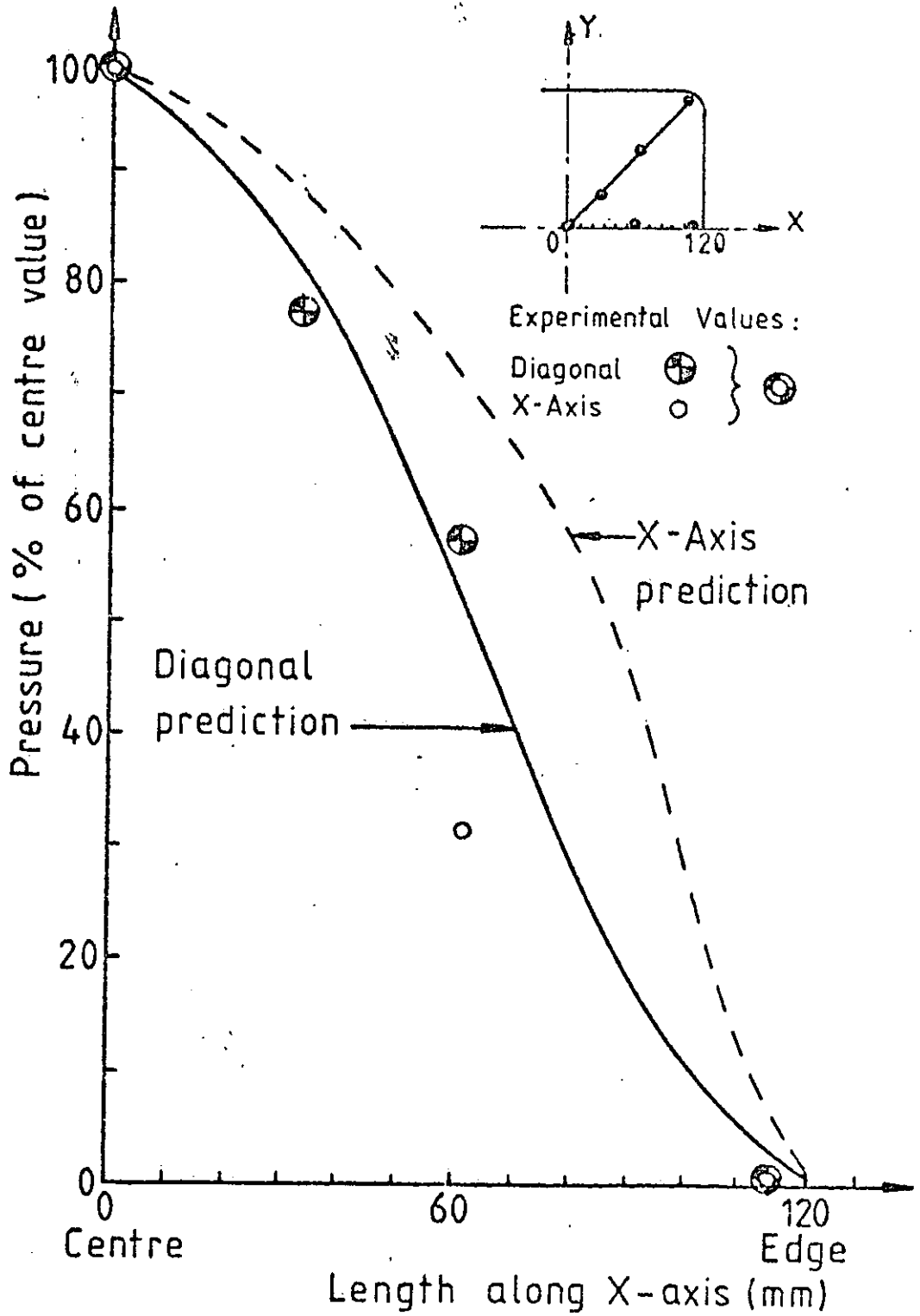


Fig.9.12 PRESSURE DISTRIBUTION FOR SQUARE PLAQUE

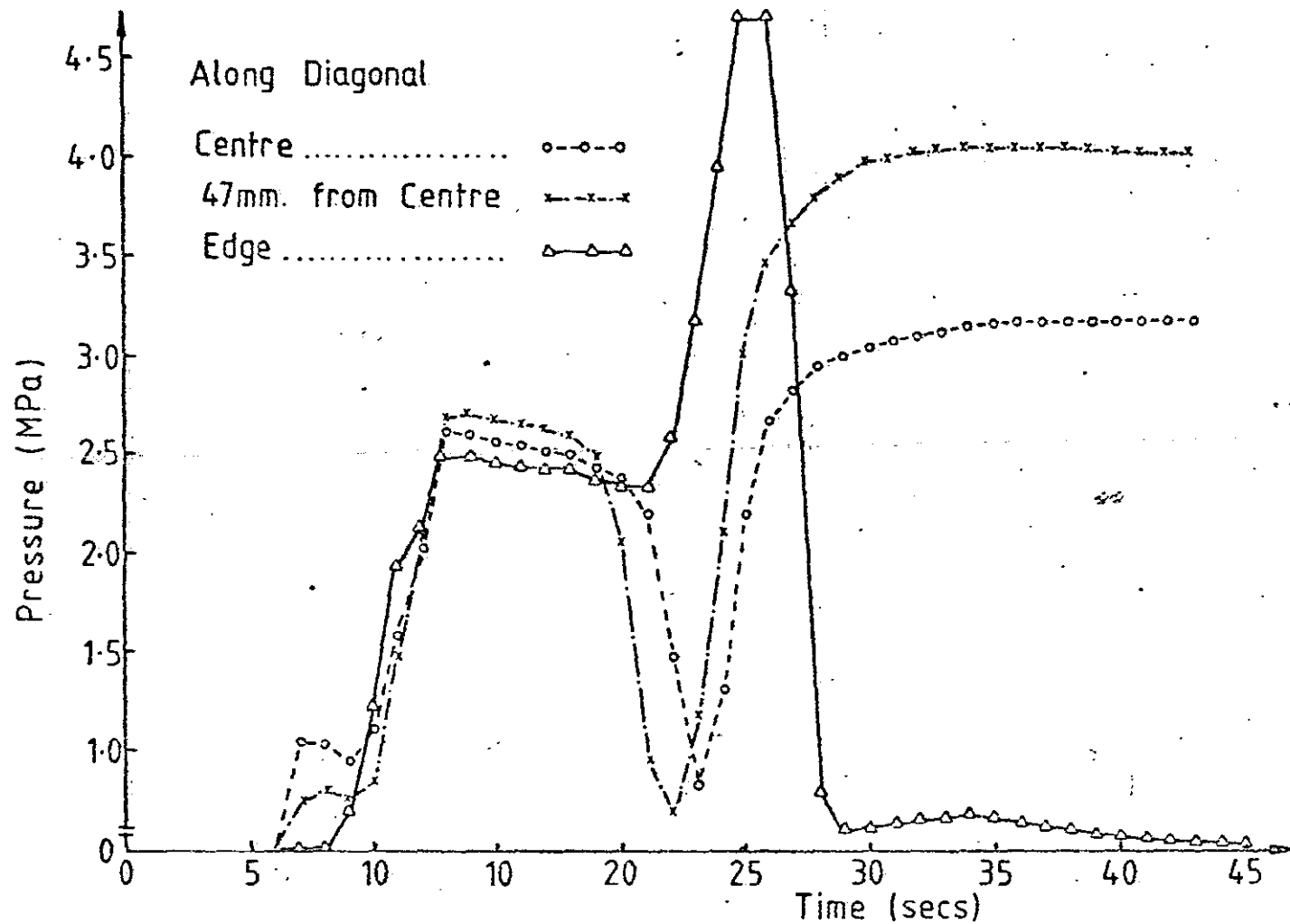
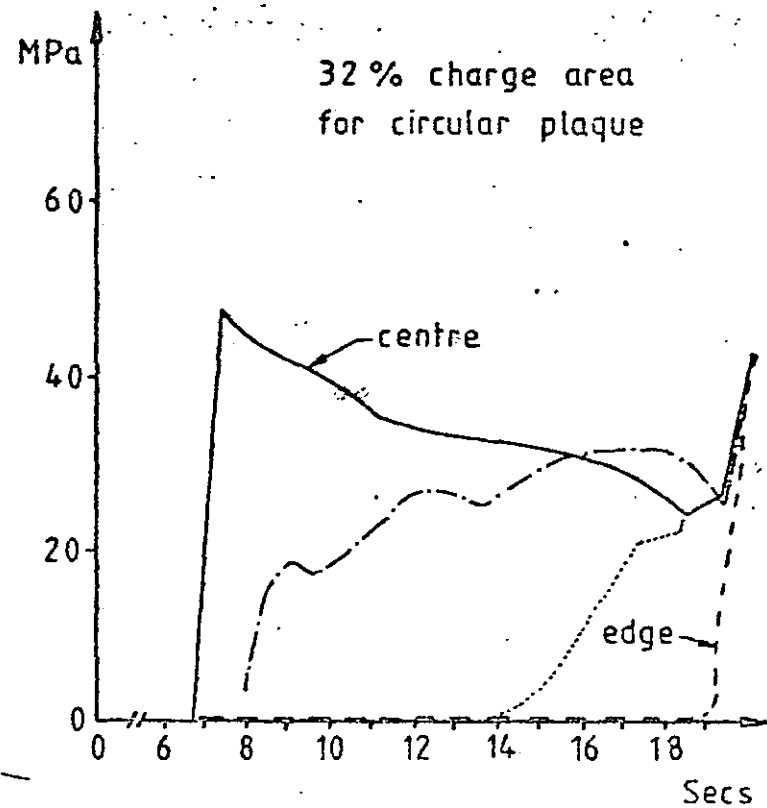
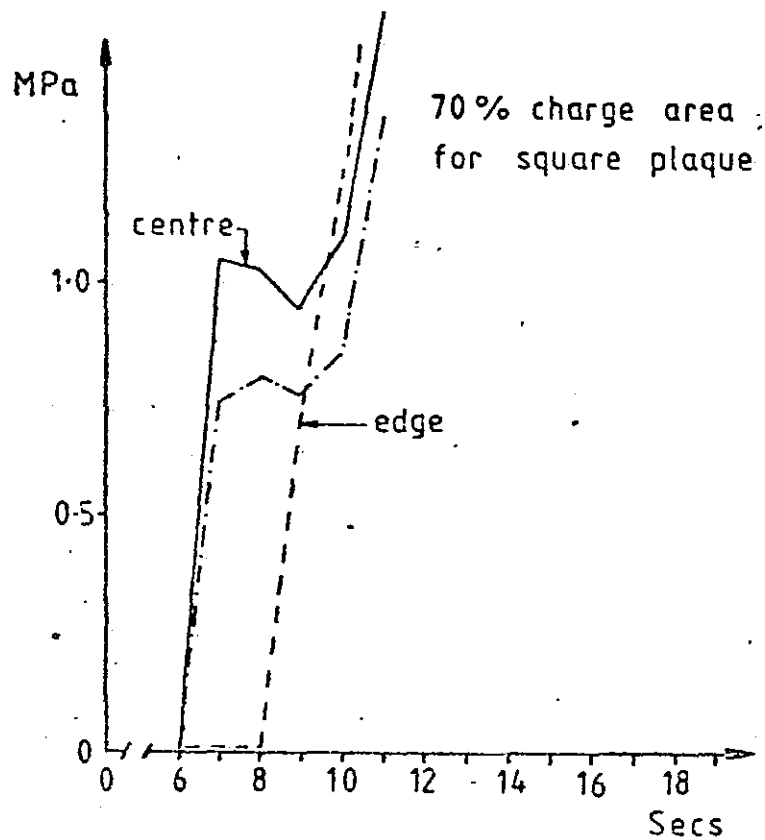


Fig.9.13 PRESSURE VARIATIONS DURING MOULDING OF A SQUARE PLAQUE



Marker and Ford (SPI 32nd Conf. 1977)

Fig.9.14 PRESSURE DURING MOULD CLOSURE

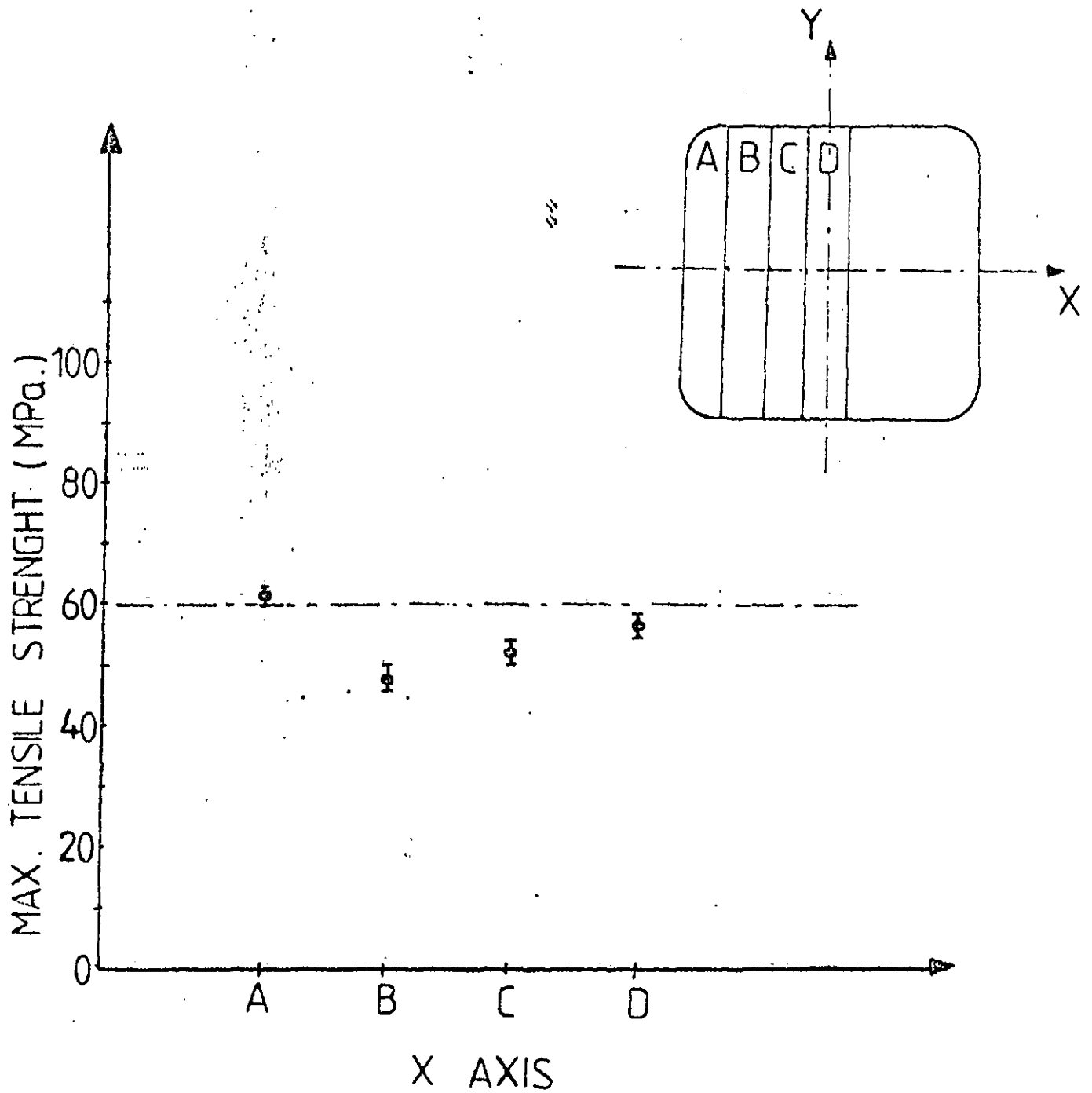


Fig.9.15 TENSILE TEST RESULTS FOR SQUARE PLATE MOULDED USING CALCULATED CHARGE SHAPE

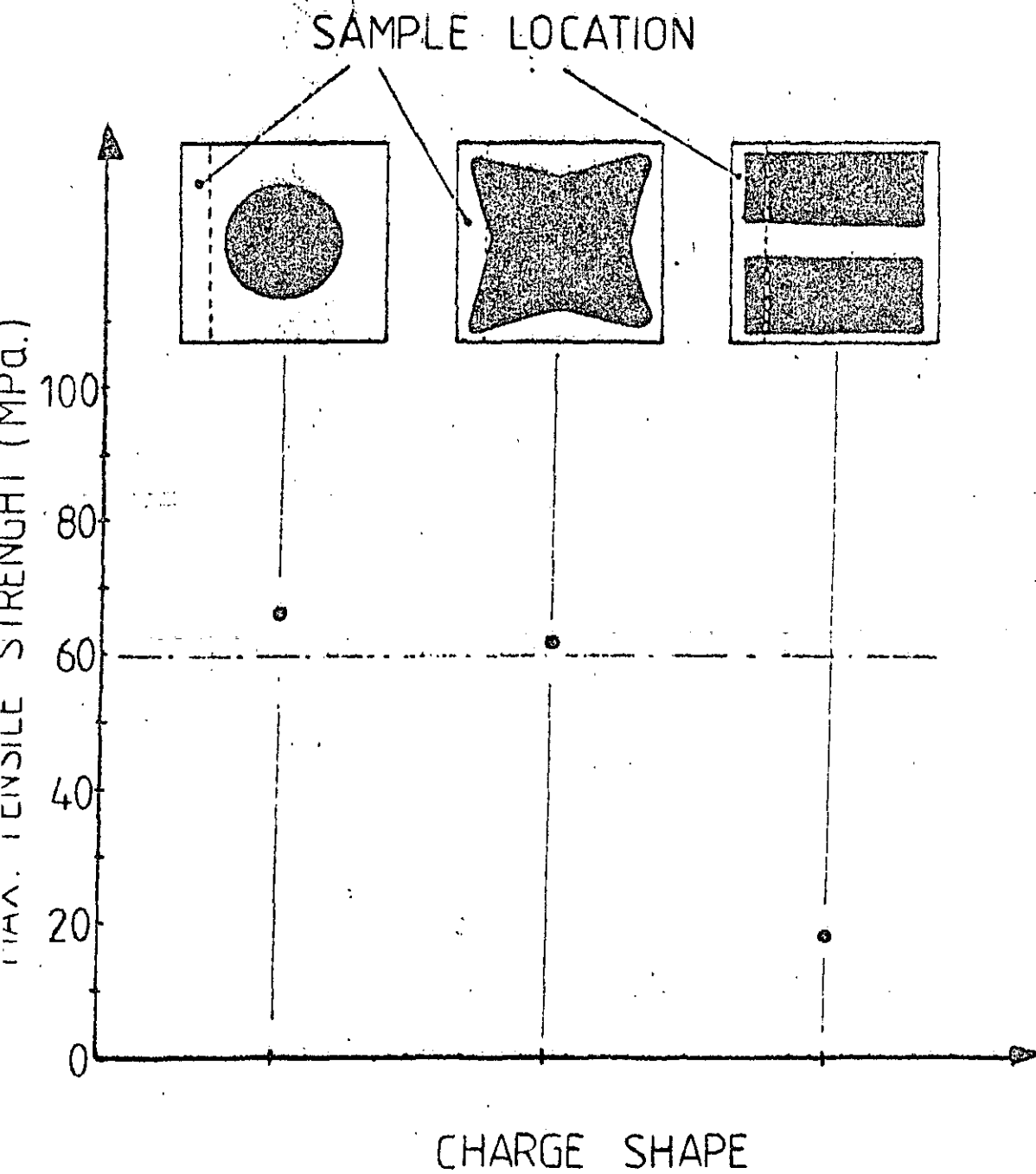


Fig.9.16 TENSILE TEST RESULTS FOR SQUARE PLATES USING DIFFERENT CHARGE SHAPES

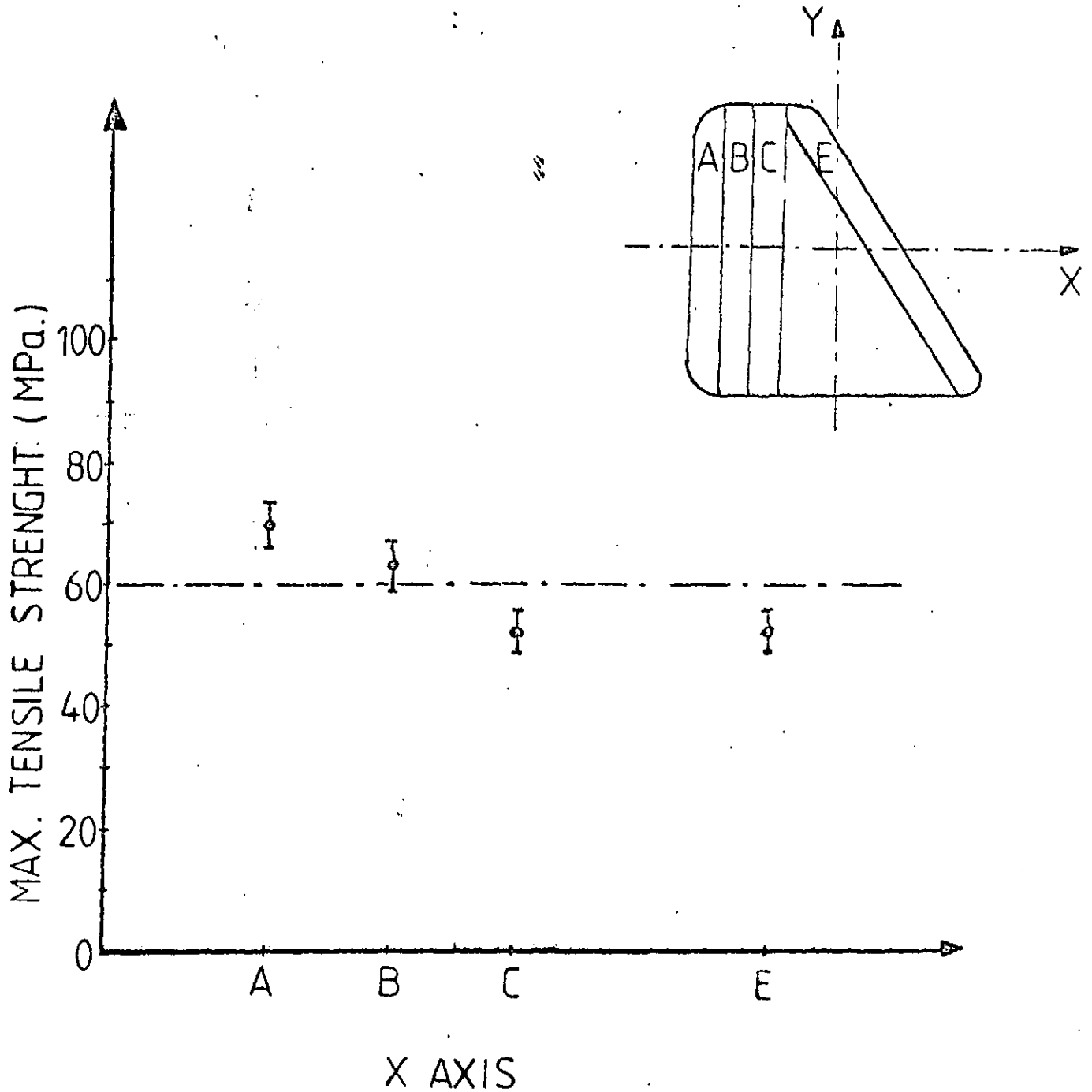


Fig.9.17 TENSILE TEST RESULTS FOR TRAPEZOIDAL PLATE MOULDED USING CALCULATED CHARGE SHAPE

charge shape. The position of the samples for this test together with the results are shown in Figure 9.18.

The X-ray technique for examining glass fibre orientation was used to check the moulded plates for weld-line formation. A weld-line was found across the centre, from edge to edge, of the square plate which had been moulded using the two SMC rectangles, i.e. where the two flow fronts met. Figure 9.20 shows this weld-line in a sample taken from the plate edge. Also a weld-line was detected in each corner of the square plate which had been moulded from the circular charge shape. This is shown in Figure 9.21.

By comparison, no weld-lines were found in the square and trapezoidal plates moulded from the calculated charge shapes. X-ray photographs of glass fibre orientation at the region of longer flow path of the two calculated charge shapes are shown in Figures 9.22 to 9.23.

## 9.5 Discussion

### 9.5.1 Analysis of the SMC before Moulding

The results presented in Figures 9.2 and 9.8 justify the assumption that the LP-SMC material is uniform, homogeneous and planar isotropic in its uncured state. This assumption does not apply to the general purpose SMC used in this work.

Figures 9.2 and 9.3 show that the unflowed but cured LP-SMC material has almost constant tensile strength parallel and perpendicular to the SMC manufacturing direction. Across the SMC sheet there is a variation of about 5% from a nominal 60 MN/m<sup>2</sup> maximum strength value. Although Figure 9.8 shows for the LP-SMC that the weight of glass fibre/unit area can be slightly higher in the centre than at the edges, this variation does not significantly affect tensile strength.

On the other hand the variation in the tensile strength of the general purpose SMC is of the order of 8% from a nominal 36 MN/m<sup>2</sup> maximum strength value. The variation in the amount of fibre glass per-unit-area is not significant except at the left hand side, where the variation reaches a value of 27% from the mean. This variation is due to one sample having a very low fibre content, otherwise the variation would be 10%.

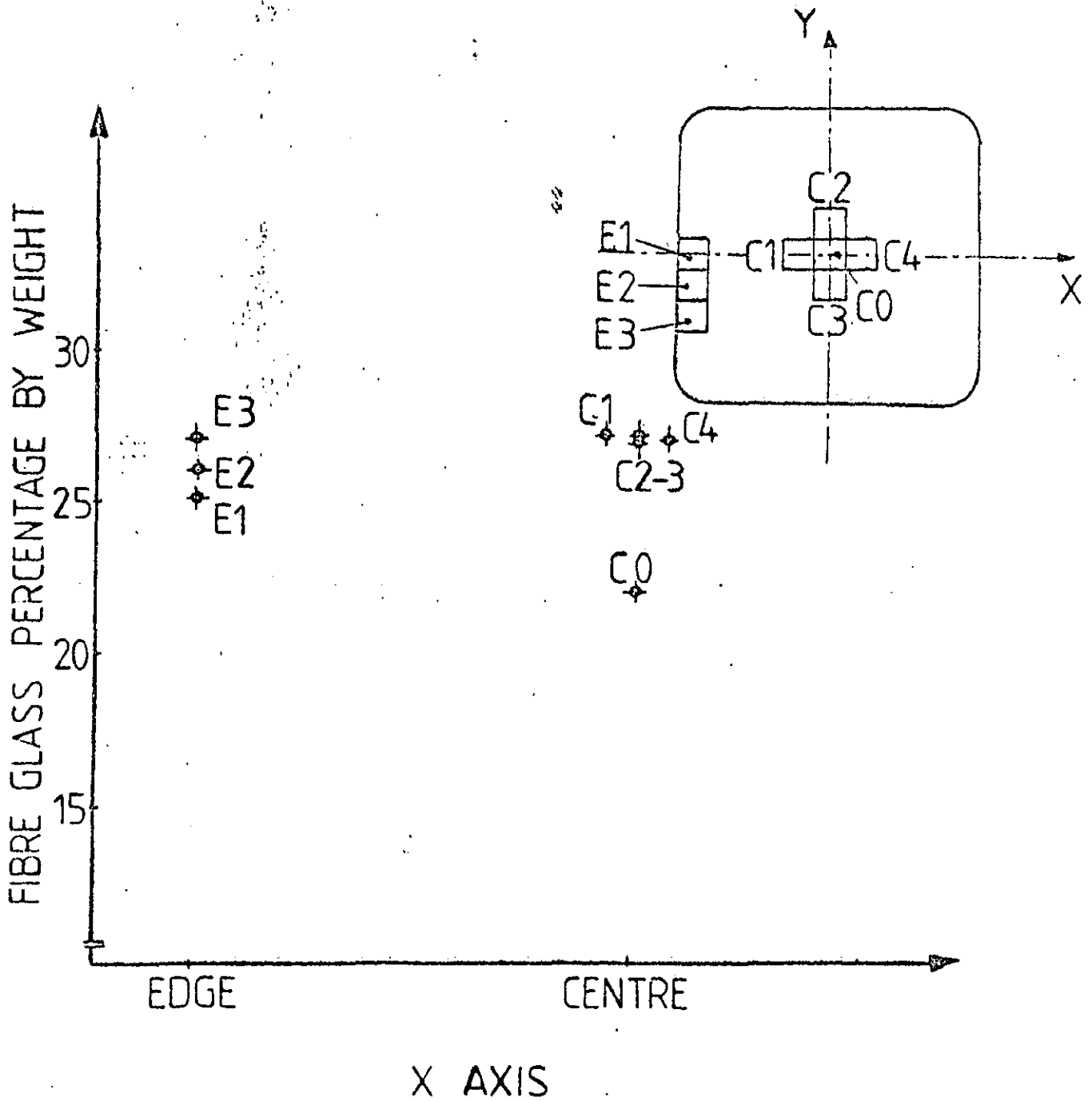
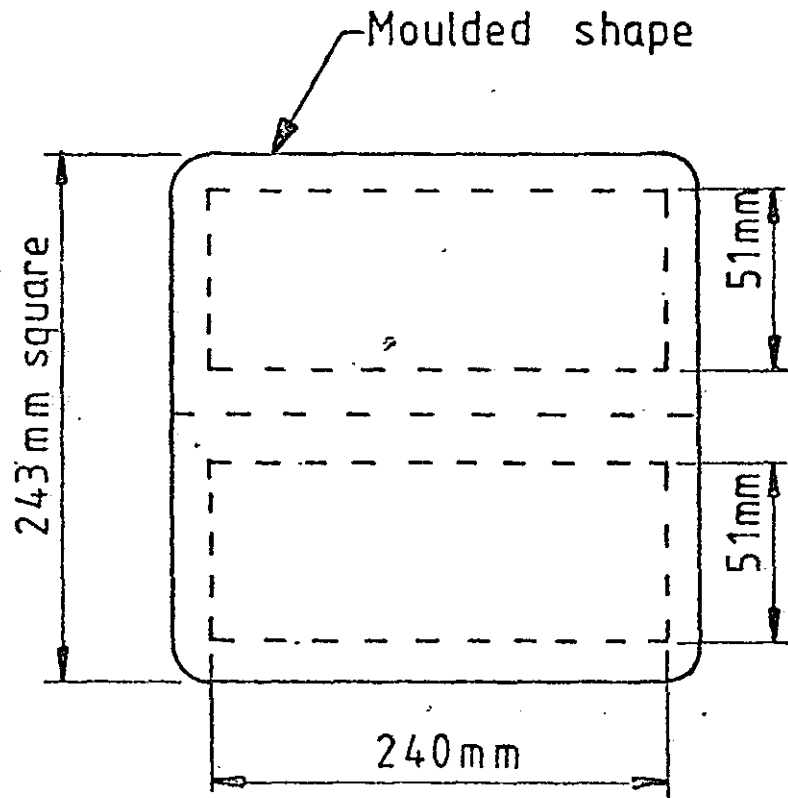
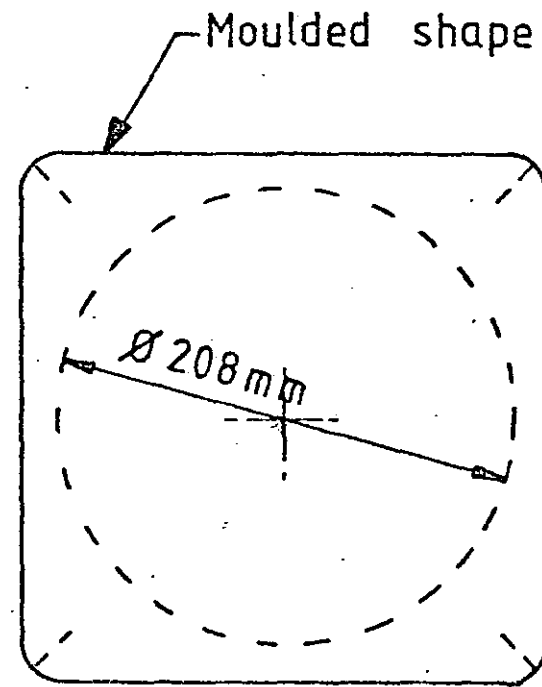


Fig. 9.18 PERCENTAGE WEIGHT OF FIBRE GLASS FOR THE SQUARE PLATE, MOULDED USING THE CALCULATED CHARGE SHAPE



Charge shape: 2 rectangles.

Centre weld line.



Charge shape: circle.

Corner weld line.

Fig.9.19 WELD-LINE FORMATION: SQUARE PLAQUE



FIGURE 9.20 Weld-line across centre of square plate, moulded with a two rectangle charge shape. Magnification x 6.



FIGURE 9.21 Weld-line at corner of square plate, moulded with a circular charge shape. Magnification x 6.



FIGURE 9.22 Fibre distribution for square plate, moulded using calculated charge shape. Magnification x 6.



---

FIGURE 9.23 Fibre distribution for unsymmetrical plate, moulded using calculated charge shape. Magnification x 6.

---

Figures 9.4 and 9.6 show no preferential orientation of glass fibre bundles in the x-y plane of the general purpose SMC and LP-SMC. Figures 9.5 and 9.7 show the alignment through-the-thickness for the general purpose SMC and LP-SMC. The white spots in Figures 9.5 and 9.7 are voids in the material formed from air trapped by curing the SMC under low pressure. The three-dimensional picture obtained by combining the distributions in the x-y plane and the through-the-thickness direction for each material indicates no preferential orientation of the fibre bundles lying in the plane of the SMC sheet.

### 9.5.2 Measurements during SMC Moulding

The moulding parameters followed the same pattern of variation as those reported in previous work (M2, T8). Figure 9.11 shows a typical analysis of ram-force and platen-displacement experimental data during moulding. The ram-force starts increasing when the mould punch touches the material. During mould closure the force increases slowly, but when the mould has filled the force increases rapidly because of the compaction of the material and the thermal expansion of the SMC. The platen displacement curve shows this expansion.

Figure 9.12 compares for the square mould the discrete experimental pressure measurements with the theoretical pressure distribution given by equation 6.40 at the instant of mould closure. The data have been plotted as a percentage of the pressure at the mould centre. There is good correlation for the four pressure measurements along the diagonal of the square (see Table 9.3). The correlation is poor for one of the other two pressure measurements. I do not have an explanation for this. (Even so, it is perhaps relevant to mention here that the calculated charge shapes do mould weld-line free plates, see section 9.5.3).

Figure 9.13 shows the time variation of pressure in the square cavity during the complete moulding cycle. This figure is different to the one obtained by Marker and Ford (M2) for the mould closure part of the cycle (see Figure 9.14). The curves of Marker and Ford (Figure 9.14b) show a higher pressure at an intermediate radius than at the mould edge and centre. This may be because Marker and Ford used a

TABLE 9.3

Distance (mm)	Theoretical Pressure (%)	Experimental Pressure (%)	Correlation Factor
0.0	100.00	100.00	0.995
37.5	81.17	77.35	
60.8	52.05	57.05	
115.0	3.52	1.00	

small SMC charge area (32%). This required an increased mould closure time, which is the likely reason for the difference in the last part of the mould-closure pressure measurements. Comparing only the initial part of the Marker and Ford curve (Figure 9.14b) with the whole of Figure 9.14a shows that both curves follow a similar pattern (the percentage of area used in Figure 9.14a was 70%). For the work here the centre pressure was always the greatest, which adds validity to using equation 6.40 to describe the mould pressure distribution.

### 9.5.3 Analysis of the Moulded SMC

Figure 9.16 shows the variation in tensile strength for specimens cut from the three square moulded plates. The plate which has the weld-line across its centre gives the lowest strength: the specimen broke at the weld-line. The reason is that no fibres are crossing that line; they are oriented parallel to the weld-line. The tensile strength results for the other two plates show almost equal values of tensile strength because the weld-line formed from the circular charge-shape did not lie in the specimen test section.

There is more variability in the tensile strength distribution for the plates moulded from the calculated charge shapes - see Figures 9.15 and 9.17 - than for the cured but unflowed SMC sheet (see Figures 9.2 and 9.3). The range of variation in strength values is not large - about 10% of the nominal strength value (see Figs. 9.15 and 9.17) and it is probably due to the effect of flow on glass fibre distribution.

For example, Figure 9.18 shows results for the percentage weight of glass fibre at various points in the square plate moulded from a

calculated charge. There is a scatter in the results at the plate centre, but along the edge the fibre content increases slightly towards the corners from the middle. This can be understood by observing the shape of the calculated charge. Such a charge induces less SMC flow at the cavity corners than on the middle of the cavity edges.

Figure 9.19 shows the place where the weld-lines were expected to form for the square plates moulded from the two rectangle charges and the circular charge. (Figures 9.20 and 9.21 show the actual positions of the weld-lines). There are qualitative explanations for the formation of the weld-lines shown in Figures 9.20 and 9.21. For the weld-line formation shown in Figure 9.20, since pressure in the mould is higher towards the centre, most of the early SMC flow would be expected to occur along the mould edges. Flow fronts would meet at the middle of the edges and then move towards the mould centre, thus forming a weld-line across the square plate. For the circular charge shape, material flows outwards to meet the middle of the cavity edges first and then move towards the corners where four weld-lines are formed when the flow fronts meet (see Figure 9.21).

A similar explanation applied to the calculated charge shapes (see Figures 9.10 and 9.11) would predict least flow at the mould corners, and most flow in the middle regions of the mould edges. Qualitatively it therefore seems reasonable to expect the flow front to meet the mould edges simultaneously thus giving weld-line free mouldings; as indicated by the results in Figures 9.22 and 9.23.

## CHAPTER 10

CASE STUDY USING CHARGE SHAPE  
PREDICTION PROCEDURE

10.1 Introduction

In addition to designing the experimental programme in Chapter 9 to test the validity of the charge shape prediction procedure, it was decided to test the prediction procedure by moulding an engineering product under industrial production process conditions. The experimental programme had shown that for realistic moulding conditions in the laboratory, it was possible to mould plates without weld-lines, and without significant reorientation of fibres during flow. Thus BTR-Permalit RP Ltd, Gloucester, were approached and arrangements made to use predicted charge shapes to make trial mouldings of "Teresa" grills (see Figure 10.1) for the Ford Cortina car. The Teresa grill was an appropriate product to choose because it is essentially two-dimensional in shape (disregarding the small bosses) and because it was being produced using production presses. This allowed evaluation under compression moulding conditions as used in industry.

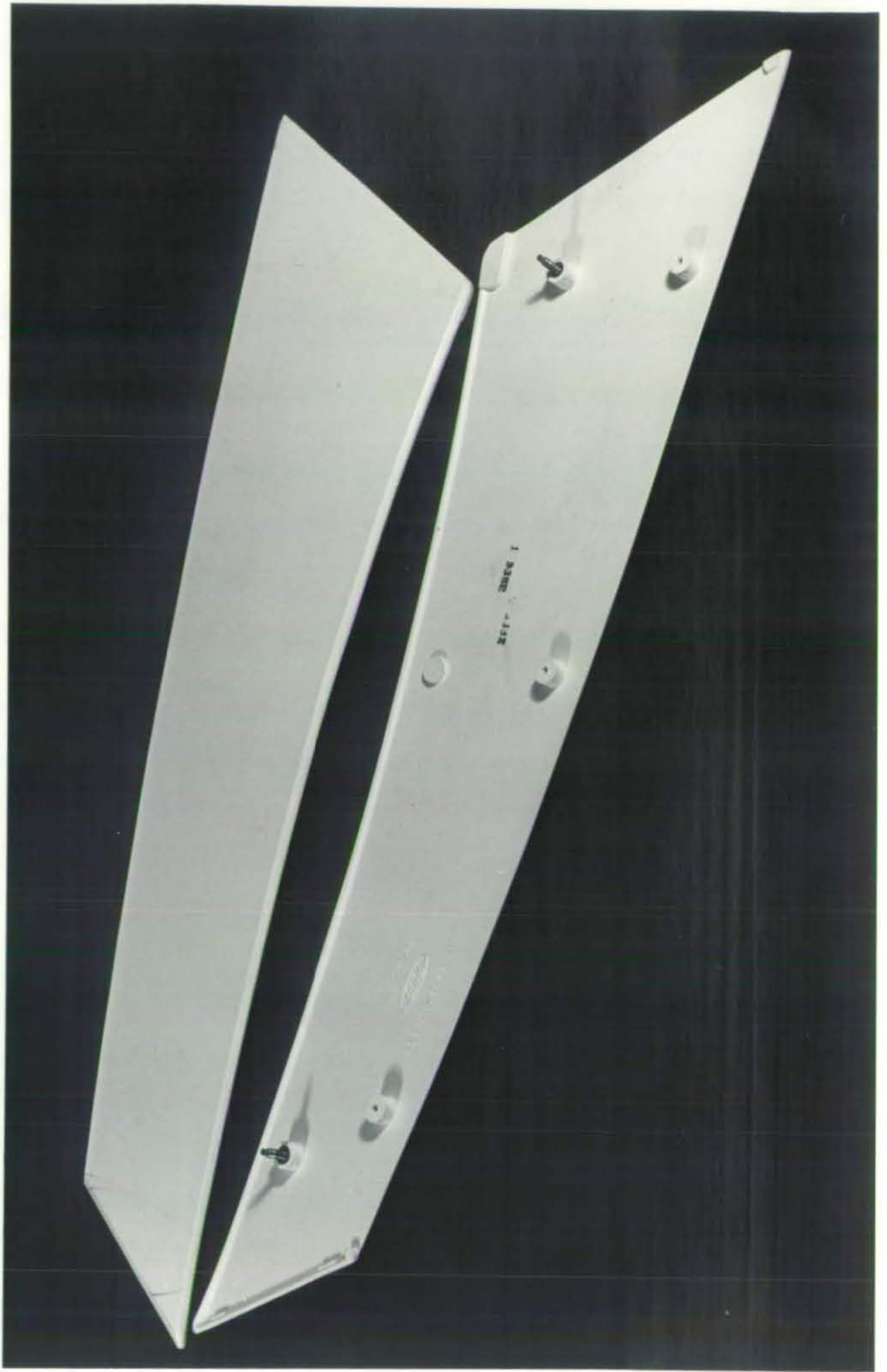
10.2 Charge Shape Prediction

The charge shape for the Teresa grill has been determined using the computer program outlined in section 7.3. Figure 10.2 shows the mesh used for the calculation of the charge shape, the general dimensions of the Teresa grill, and the position of centre of area.

The parameters of equation 7.2 used for the evaluation of the pressure contours are:

Viscosity	0.02 N-sec/mm <sup>2</sup> (20 x 10 <sup>6</sup> cps)
Thickness	3.0 mm
Moulding Speed	2.5 mm/sec
Distance between nodes	29.2 mm

The first three parameters were supplied by BTR-Permalit; the fourth one was selected according to the limits of the computer program.



---

FIGURE 10.1 View of the Teresa grill on both sides

---

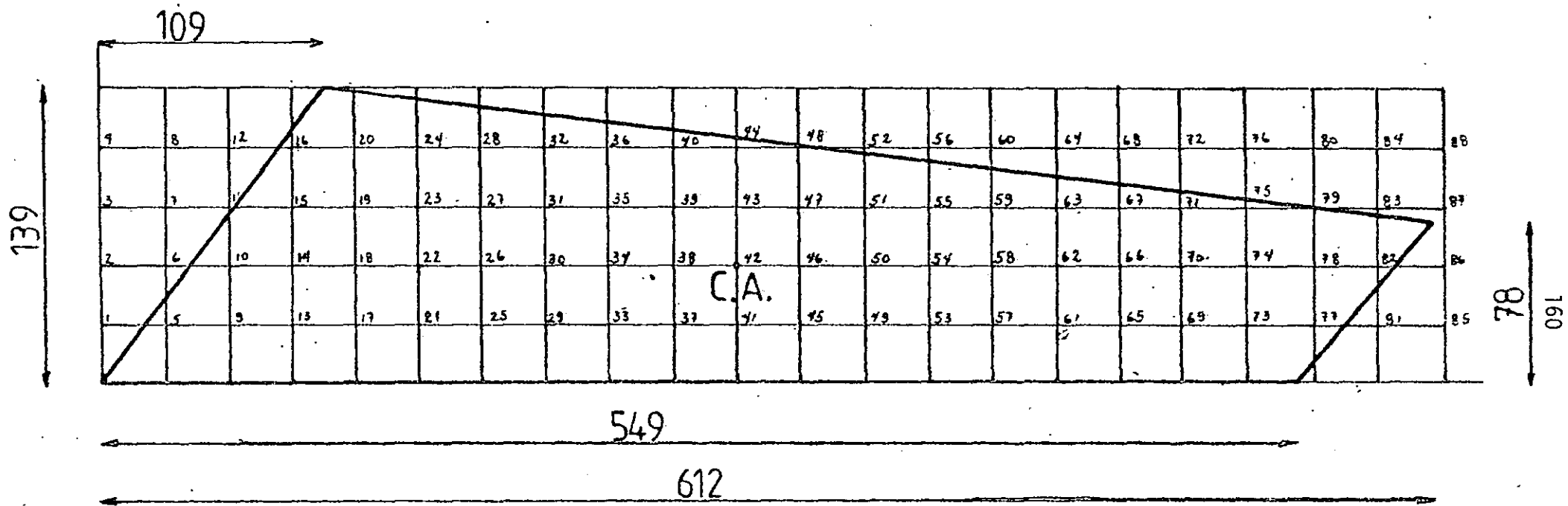


Fig.10.2 MESH NODES; NUMBERING AND DIMENSIONS

Table 10.1 shows the production process conditions being used at the time.

TABLE 10.1

PRODUCTION PROCESS CONDITIONS	
Moulding speed	2.5 mm/sec
Moulding pressure	250 tons/pair
Moulding temperature	150° - 160°C
Opening time	30 - 40 sec
Charge weight	314g
Material	LP-SMC
Press capacity	250 tons

Figure 10.3 shows the pressure contours for the grill at the instant before completion of closure, together with stream-lines. The centre of pressure dictates the position of the charge in the mould cavity.

The percentage cover of the mould by the charge shapes was governed from constant volume conditions required by the final thickness (3 mm) of the Teresa grill and the initial thickness (2.8 mm) of the SMC. Two layers of SMC gave charge cover of 54% and three layers gave 35% cover. Figure 10.4 shows the predicted shapes for these charges. It was not possible to use a charge area of about 70% because this would have given a finished thickness greater than 3 mm (using two layers), which was not possible in the production situation. Also, grills were moulded with the charge completely covering the mould. This needed a single layer of material which covered 107% of the area, to ensure that grill bosses were filled and final thickness attained. Table 10.2 shows the charge thickness, charge areas and volumes of material in each case.

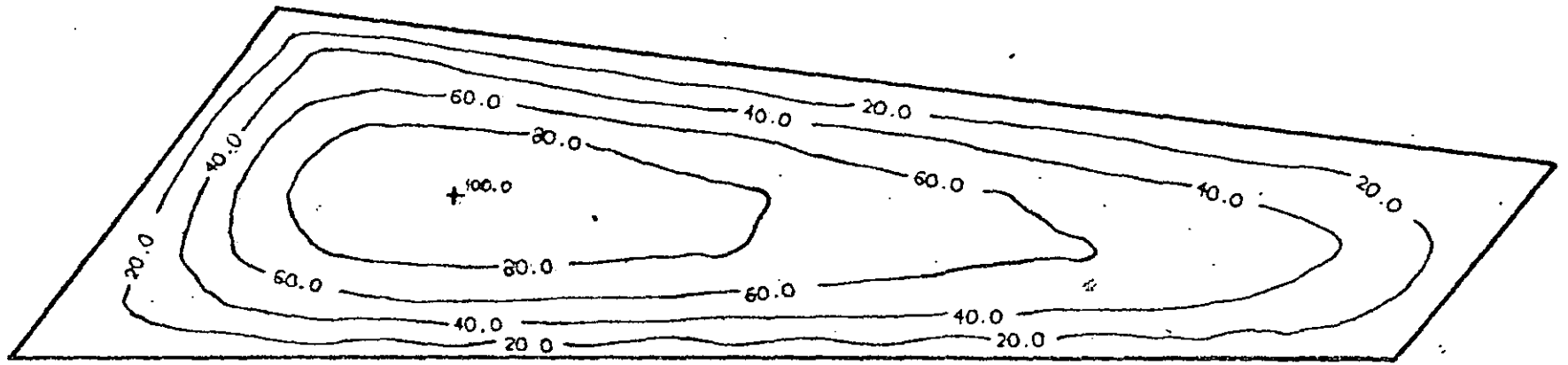
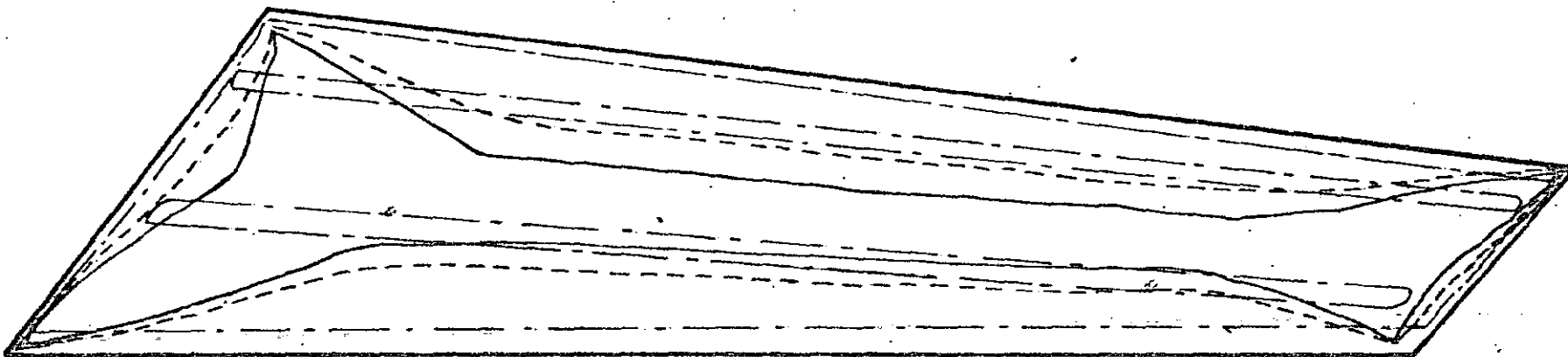


Fig.10.3 PRESSURE CONTOURS IN PERCENTAGE



FINAL SHAPE (100%)

107%

54%

35%

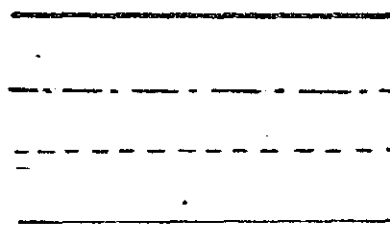


Fig.10.4 DIFFERENT CHARGE SHAPES

TABLE 10.2

Charge Thickness (mm)	Charge Area (mm <sup>2</sup> )	Charge Volume (mm <sup>3</sup> )	Area Covered (%)	Samples Moulded
2.8	63957	179082	*107	4
5.6	31978	179082	53.5	4
8.4	21319	179082	35.7	4

\* The area of the mould cavity = 59694 mm<sup>2</sup>

### 10.3 Discussion of Moulding Results

To examine the effect of flow on fibre orientation and weld-line formation, X-ray photographs of moulded grills were made using a System 125 Rank Xerox X-ray machine at 50 kVa with 3 second exposure time for System 125 Rank Xerox film material. Figures 10.5 to 10.7 show the photographs for grills moulded with the 107% charge area and the 54% and 35% predicted shapes respectively.

Figure 10.5 shows the orientation of fibre glass without flow, and Figures 10.6 and 10.7 show the effect of progressively increasing the amount of flow. Most flow occurs at the centre part of the charge shape - this is the narrowest part of the charge shape with the lobes going into the mould cavity corners - and fibres have aligned with the direction of flow across the grill width. As expected, this effect is more pronounced with the 35% charge area mouldings. Structurally this gives a greater tensile strength in the transverse direction than the longitudinal direction. Single tensile test specimen results cut from the 107%, 54% and 35% charge area mouldings in the transverse and longitudinal directions at the centre section are shown in Figures 10.8 and 10.9 respectively. Test specimen size was 3 x 25 x 95 mm and cross head speed was 0.016 mm/sec. The samples cut from the Teresa grill (TG) moulded with the charge shape used by BTR-Permalii show the highest tensile yield strength in the longitudinal direction and the lowest in the transverse direction. This is due to the high degree of orientation parallel to the flow direction, i.e. the longitudinal direction, produced by flow.



FIGURE 10.5 X-ray photograph of the Teresa grill, moulded with a charge of 107%



FIGURE 10.6 X-ray photograph of the Teresa grill, moulded using calculated charge shape of 54%

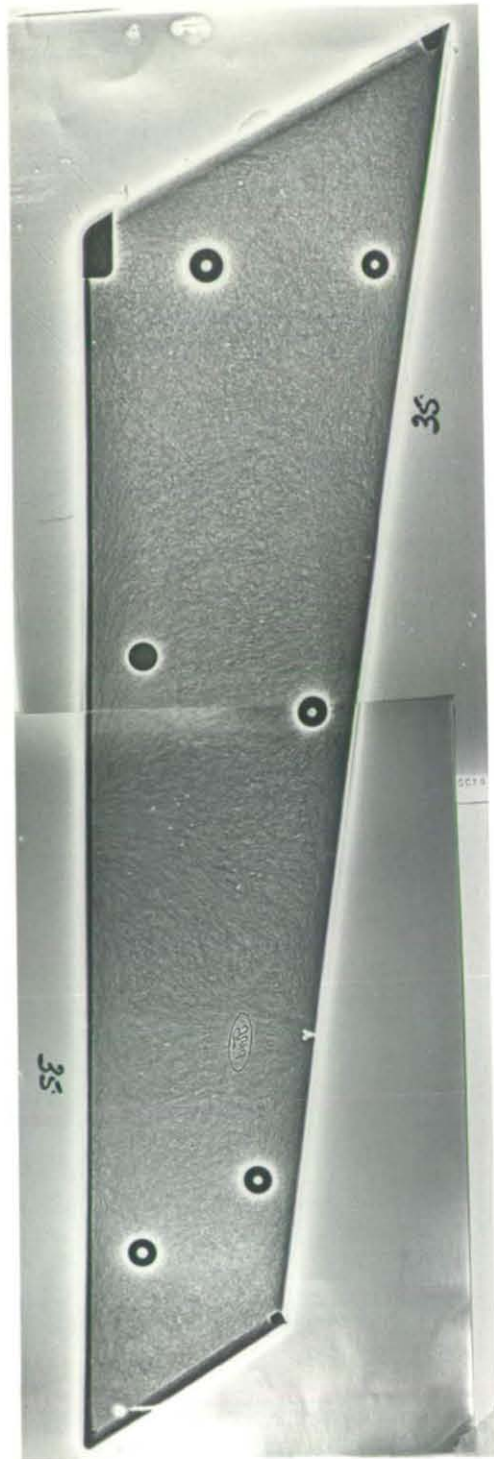


FIGURE 10.7 X-ray photograph of the Teresa grill, moulded using calculated charge shape of 35%

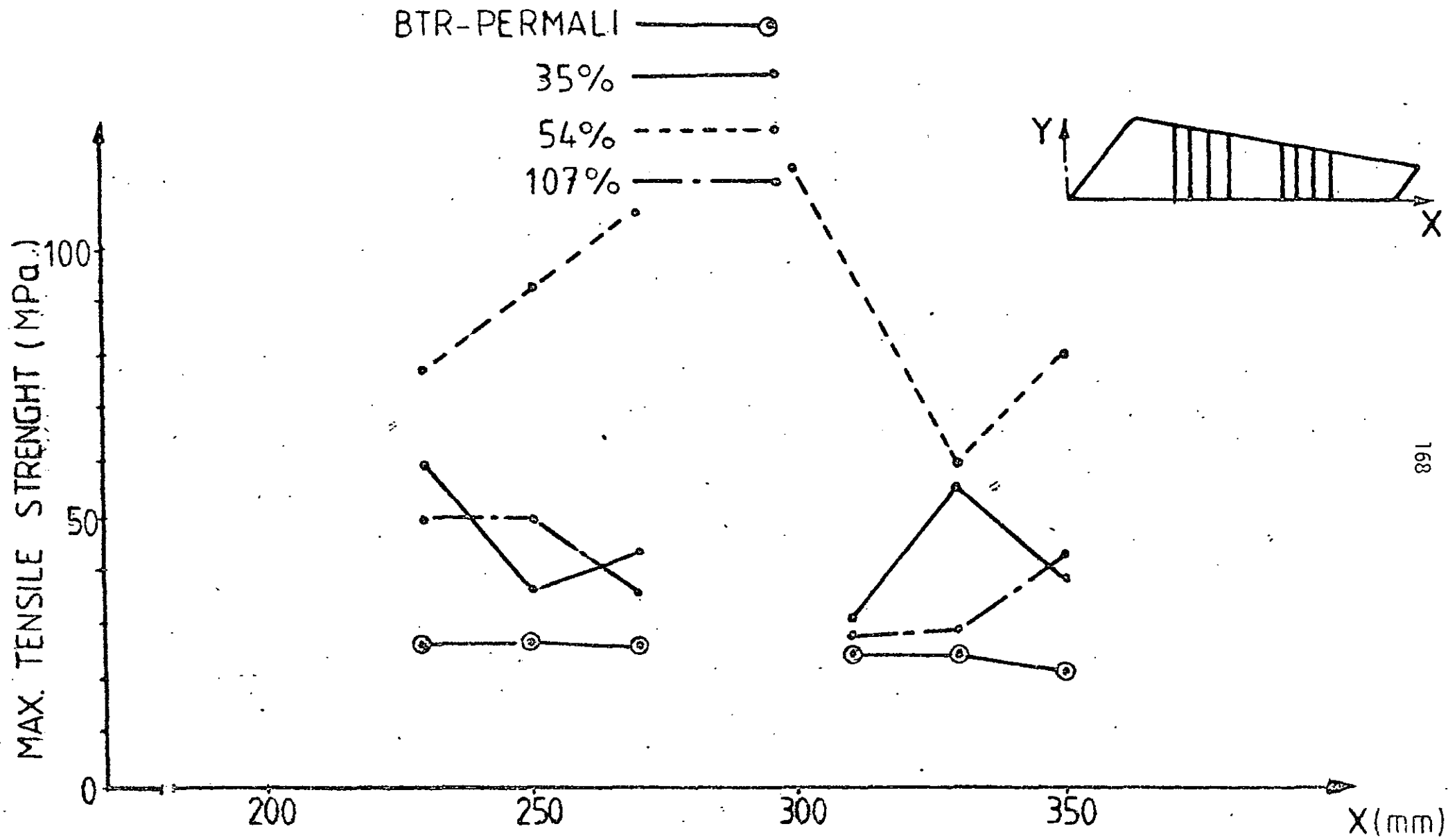


Fig.10.8 TENSILE TEST RESULTS

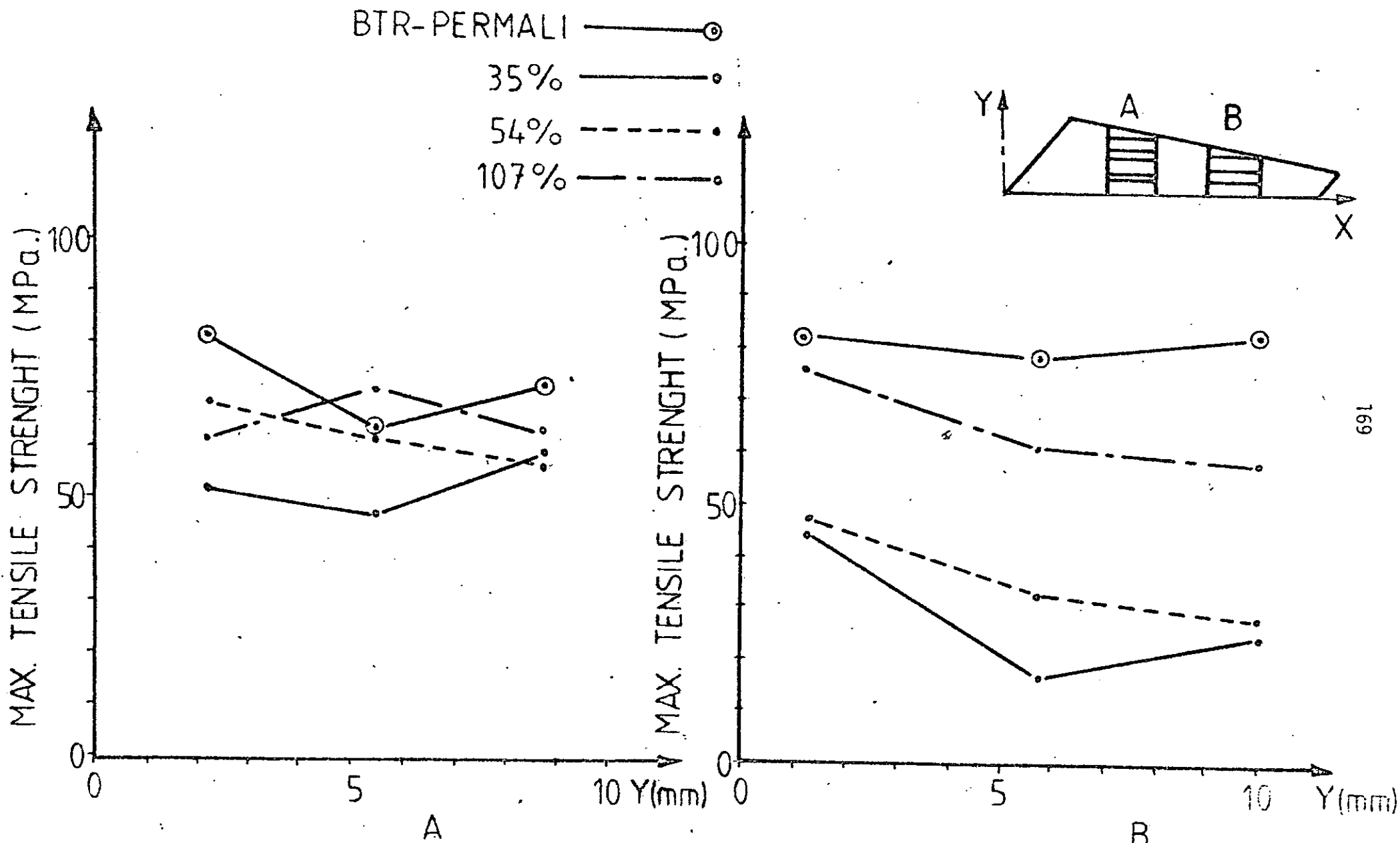


Fig.10.9 TENSILE TEST RESULTS

The samples cut from the TG moulded with 107% show a high tensile yield strength in the longitudinal direction and a low in the transverse direction. This is due to the way in which the charge has been placed on the mould. Approximately 90% of the mould area was covered and the other 17% extra were strips placed on top and along the 90% (see strip marks in Figure 10.5). Such strips reinforced the material in the longitudinal direction, but reduce the strength in the transverse direction.

The samples cut from the TG moulded with the 54% predicted charge shape show high tensile yield strength in the transverse and longitudinal direction, although in the longitudinal direction some data present a low tensile yield strength. This low strength is in the area of high orientation (see Figure 10.6).

The samples cut from the TG moulded with 35% predicted charge shape show a low tensile yield strength in the longitudinal direction and a higher strength in the transverse direction. This results from a high orientation in the transverse direction due to flow (see Figure 10.7).

Because of the orientation effects indicated by the yield strength test results, the method for predicting the charge shape is at the moment perhaps more useful for load-bearing applications where the percentage of area covered is about 70%. For the cases of cosmetic applications a smaller charge is required, and then the method is useful for predicting the position of the charge shape. But despite these expected orientation effects, the grills have been moulded without forming weld-lines. It is most likely that if mouldings had been made from 70% charge areas they would have shown no significant fibre reorientation, as did the laboratory plate moulding test (see Chapter 9).

Two other aspects which are important from the compression moulding production process point of view are the cutting of charge shapes and the surface finish of moulded products. A lot of waste is associated with cutting the predicted shapes although this should not be a limitation for the future use of this method since some of the charge's curved shape could perhaps be transformed by using straight cuts.

The charge shape given by the computer prediction process is very different to that actually used during production. A main reason for

this is that qualities of surface finish and appearance are more important for this "cosmetic" component than its structural qualities. Unfortunately for reasons of commercial security the shape of the production charge cannot be given in this work. However, its shape does promote more mould flow than that given by the predicted charge shape of corresponding area. This leads to a better surface finish, a technique which has been described in the literature (G4, T8).

Nevertheless, the trial-and-error procedure which was used to determine the shape and position of the production charge to give acceptable mouldings took a long time, and wasted a lot of material that could not be recycled. The interesting point which emerges from this work is that the centre of pressure for the predicted charge shape is exactly coincident with that for the production charge shape.

Qualitative assessments of the surface finish of the moulded grills were made and compared with the surface finish of the production grill. The grill surface finish given by the predicted charge shapes were slightly inferior to that of the production grill, probably because of the previously mentioned reason but also because a longer mould opening time was used - 80 seconds compared with the 30 to 40 seconds production process time. This would have caused a slight decrease in the mould cavity and punch temperatures.

#### 10.4 Conclusions

The use of the charge shape prediction procedure with a flat product shows that mouldings can be produced without weld-lines. However, the surface finish of the mouldings are not class A which is required for cosmetic parts.

## CHAPTER 11

GENERAL CONCLUSIONS AND FUTURE WORK

A method has been developed for predicting and characterising two-dimensional compression-mould flow for unsaturated polyester resin SMC.

The method for calculating the position and geometry of the SMC charge has proved to produce weld-line free mouldings, despite of the fact that it assumes an essentially Newtonian behaviour. This method can be used to predict the position and geometry of the SMC charge for load-bearing applications using an area covered by 70% or more. However the method can also be used to determine the position of the SMC charge in cosmetic applications. Further work is needed to determine the geometry of the charge for cosmetic applications.

The squeeze flow method of flow characterization, using a parallel plate plastometer, gives a good understanding of the basic rheological behaviour of SMC for the compression moulding of flat parts. This conclusion is based on tests at 20° and 160°C using one formulation of SMC. The squeeze flow behaviour of discs at 20°C is predicted accurately by the mathematical model which describes the time variation of compression force, but the model does not take into account variations due to number of layers, different physical stages through which the material passes when compressed, and age of the material. The model is based on an equation of state with equally strained viscous, elastic and yield elements. Satisfactory explanations of flow behaviour are given in terms of four-stage physical model of flow.

Experimental data provided by the parallel plate plastometer from 160°C tests show how the moulding force, closure speed, SMC temperature, and gel and cure times are interrelated during compression moulding.

The recommendations for future work are as follows:

1. Develop the mathematical analysis for the compression-injection mode of flow during compression moulding, and integrate this

analysis with that for the compression-compression mode. This development will be necessary for the charge shape prediction of three-dimensional products.

2. Continue the work on the equation of state by applying the mathematical model to each of the four-stages of SMC flow at 200°C, and develop a mathematical model for 160°C. However such work may prove not to be directly applicable to the charge shape prediction procedure because the resulting equation of state will be more complicated than the already assumed Newtonian one and it will involve a more difficult mathematical analysis to predict charge shapes.
3. Study ways of relating the flow behaviour to the mechanical properties of moulded products. One approach would be to model fibre alignment due to flow, combined with the charge-shape prediction procedure, and use flow factors to scale the values of the mechanical properties of the moulded article from those of moulded but unflowed material.

REFERENCES

- A1 Ackley, R H and Carley, E P; "*XMC-3 composite material structural moulding compound*", 34th Annual Tech. Conf., SPI Reinf. Plast/Comp. Inst., 1979, Section 21-0.
- A2 Amptor, F J, Humnski, F M, Lowry, J R, Marple, R K and Trimble, S M; "*Chemical thickening and maturation control for production SMC*", 33rd Ibid, 1978, Section 9-E.
- A3 Anon: "*New kneading bed design improves SMC wet out*"; Mod. Plast. Int., 8, 9, (1978), 41.
- A4 Anon: "*Hybrid reinforcement: low cost route to premium performance*"; Ibid, 8, 5, (1978), 62-64.
- A5 Anon: "*New resin for tougher sheet moulding compound*"; Reinf. Plast., 23, 1, (1979), 10-11.
- A6 Anon: "*Applications in SMC*"; Plast. Paint. Rubb., 21, 7, (1976), 23-27.
- A7 Atkins, K E and Sollman, K J; "*Resines de compensation pour systemes polyesters renforces de fibre de verre*"; Verre Text.-Plast. Renf., 15, 9, (1977), 28-31.
- B1 Bastone, A L and Beck, R H Jr; "*Structural new design horizon for reinforced plastics*", Plast. World, 36, 2, (1978), 64-67.
- B2 Batchelor, G K; "*An introduction to fluid dynamics*", Cambridge University Press, 1967, Chapters 3 and 4.
- B3 Bert, C W; "*Composite material mechanics: prediction of properties of planar-random fibre composites*", 34th Annual Tech. Conf., SPI Reinf. Plast/Comp. Inst., 1979, Section 20-A.
- B4 Bird, R B; "*Analysis of squeezing flow between parallel disks using the Goddard-Miller model*", Research Rheology Center, Univ. of Wisc., October 1974.

- B5 Bowyer, E G; *"Recent advances in technology of polyester resins and their use in moulding compounds"*, Int. Symp. on Polyester Moulding Compound, Geneva, May 1977, paper 5.
- B6 Braun, D and Quella, F; *"High temperature curing of unsaturated polyester resins with peroxide free initiators"*, *Kunststoffe* 69, 2, (1979), 15-17.
- B7 Brindley, G, Davies, J M and Walters, K; *"Elastico-viscous squeeze films. Part I"*, *J. Non-Newtonian Fluid Mechanics*, 1, 1, (1976), 19-37.
- B8 B S 2782; Part 3; Method 320E: 1976. British Standard Institution, Brit. Standards House, London.
- B9 Brown, B and Bowyer, G; *"The achievement of improved quality in unsaturated polyesters for dough and sheet moulding compound"*, Reinf. Plast. Cong., British Plast. Fed., Brighton, November 1978, pap.15/117-122.
- B10 BTR-Permalit Ltd; *"GRP technology and practice"*, Gloucester, U.K. 1974.
- B11 Burns, R, Gandhi, K S, Hankin, A G and Lynskey, B M; *"Variability in sheet moulding compound (SMC): Part I: Thickening reaction and effect of raw materials"*, *Plastics and Polymer*, 43, 168, (1975), 228-235.
- B12 Burns, R and Gandhi, K S; *"The rheology of glass reinforced polyester moulding compounds"*, 32nd Annual Tech. Conf., SPI Reinf. Plast/Comp. Inst., 1977, Section 7-C.
- B13 Burns, R; *"Polyester moulding compound - review of progress"*, *Polym. Plast. Technol. Eng.*, 10, 2, (1978), 165-198.
- B14 Buttler, M J; *"Moulds and machinery"*, Int Symp. on Polyester Moulding Compound, Geneva, May 1977, paper 11.
- C1 Cassoni, J P Gallagher, R B and Kamath, V R: *"Curing unsaturated polyesters with peroxyketals effect of compounding variables"*, 34th Annual Tech. Conf., SPI Reinf. Plast/Comp. Inst., 1979, Section 14-F.

- C2 Chamis, C C; *"Design properties of randomly reinforced fibre composites"*, 27th Annual Conf., SPI Reinf. Plast/Comp. Div, 1972.
- C3 Clavadetscher, D J and Brandish, F W Jr; *"Competition for new applications pushes improvements in SMC and BMC"*, Plast. Des. and Processing, 17, 3, (1977), 43-48.
- C4 Collister, J and Powell, R; *"Permi-Glas energy - absorbing SMC"*, 32nd Annual Tech. Conf., SPI Reinf. Plast/Comp. Inst., 1977, Section 16-B.
- D1 Davey, F M; *"History of tooling, an encapsulation case; proto-type through high production"*, 21st Annual Meeting, SPI Reinf. Plast. Div., 1966; Section 6-C.
- D2 Del Valle, C J; *"The right filler saves in flame-retardant SMC"*, Plast. Tech., 24, 10, (1978), 85-87.
- D3 Delano, T and Shayota, M; *"Computer design of structural body components station wagon tailgate"*, 33rd Annual Tech. Conf., SPI, Reinf. Plast/Comp. Inst., 1978, Section 18-A.
- D4 Denton, D L; *"Mechanical properties characterization of an SMC-R50 composite"*, 34th Ibid., 1979, Section 11-F.
- D5 Denton, D L; *"The mechanical properties of an SMC-R50 composite"*, Owens-Corning Fibreglas Co., 1979.
- D6 Diens, G J and Klumm, H F; *"Theory and applications of parallel plate plastometer"*, J Appl. Phys, 17, (1946), p.485.
- D7 Drapper, N R and Smith, H; *"Applied regressional analysis"*, John Wiley and Sons, London, 1966.
- E1 Edelman, R and McMahon, P; *"A new polyester system for automotive composite applications"*, 34th Annual Tech. Conf., SPI Reinf. Plast/Comp. Inst., 1979, Section 2-A.
- E2 Ehnert, G; *Nouveaux procédés pour l'étude du comportement au moulage des préimprégnés (SMC)"*, Verre Textile - Plast. Renf. 16, 8, (1978), 15-21.

- E3 Eisenberg, M A; *"Theory of fabrication-induced anisotropy of chopped-fibre/resin panels"*, GMR Research Publication GMR-2633, Warren Michigan, 1977, 18p.
- E4 Enos, J H, Errott, R L, Francis, E and Thomas, R E; *"Structural performance of vinyl ester compression moulded high strength composites"*, 34th Annual Tech. Conf., SPI Reinf. Plast/Comp. Inst., 1979, Section 11-E.
- F1 Frappa, A L, Le Coz E and Libert, J C; *"Agents d'épaississement pour l'industrie des polyesters préimprégnés"*, Verre Textile-Plast. Renf., 15, 4 (1977), 14-22.
- F2 Ferrarini, J, Longenecker, D M; Shah, N N, Feltzin, J and Greth, G G; *"Development of a unique method for the preparation of high quality SMC"*, 33rd Annual Tech. Conf., SPI Reinf. Plast/Comp. Inst., 1978, Section 9-D.
- F3 Fock, K; *"Service type test methods for polyester prepregs and bulk moulding compounds"*, Kunststoffe, 68, 3 (1978), 20-22.
- F4 Freeman Chemicals Ltd; *"Freeman Chemicals, SMC and DMC and you"*, Merseyside, U.K.
- G1 Gandhi, K S and Burns, R; *"Rheological properties of glass fibre-reinforced DMC"*, Trans. of the Soc. of Rheology, 20, 4, (1976), 489-502.
- G2 Gary, L W; *"Lower moulding pressures brighten outlook for shorter-run SMC parts"*, Plastics World, 34, 6, (1976), 47-50.
- G3 Gracewski, A S, Mandell, J F and McGarry, F J; *"Factors affecting the impact resistance of SMC materials"*, 34th Annual Tech. Conf., SPI Reinf. Plast/Comp. Inst., 1979, 23-D.
- G4 Griffiths, R M and Shanoski, H; *"The effect of compounding and processing on interlaminar strength and blister formation in SMC mouldings"*, SPE, Eng. Prop. and Struct. Div., Div. Tech. Conf., Hudson, Ohio, 1975, 117-125.

- G5 Grim, R J; *"Squeezing flows of polymeric liquids"*, Research Rheology Center, Univ. of Wiśc. October 1975.
- G6 GINOSURF, GINOSURF MANUAL, University of Selford, June 1979, version Mk 1.0.
- H1 Harrier, J L; *"Sheet moulding compound - state of art"*, Reinf. Plastc., 20, 7, (1976), 196-198.
- H2 Hemsley, D and Hayles, M; *"The development of a microradiography stage for use in the SEM and its applications"*, Inst. Physics Conf. Ser. No 36, 1977, Chapter 1.
- H3 Herman, E A; *"Heat transfer phenomena in compression moulding glass fibre reinforced sheet moulding compound"*, 33rd Annual Tech. Conf., SPI Reinf. Plast/Comp. Inst., 1978, Section 14-F.
- H4 Hillman, S L, Palmer, M and David, J H; *"Corrosion resistance of new unsaturated polyester formulations based on TMPD<sup>(R)</sup> glycol with isophthalic acid or dimethyl terephthalate"*, 34th Ibid, 1979, Section 4-F.
- H5 Hull, N A and Bergstrom, D H; *"High strength reinforced plastic bumpers for passenger car applications"*, 34th Ibid, 1979, section 21-B.
- J1 Jacobs, E F and O'Hearn, T P; *"A new resin and new concept for high performance vinyl ester premix moulding"*, 34th Ibid, 1979, Section 6-E.
- K1 Kamens, E R, Gallagher, R B and Kamath, V R; *"Novel initiator blends for curing unsaturated polyester resins"*, 34th Ibid 1979, Section 16-B.
- K2 Klunder, J; *"Fabrication des préimprégnés en particulier, des prémixes et mats préimprégnés"*, Verre Textile-Plast. Renf. 10, 6 (1972), 18-21.
- L1 Labonne, M; *"Situation et perspective du préimprégné"*, Ibid, 16, 8, (1978), 10-13.

- L2 Langlois, W E; *"Slow viscous flow"*, Collier-Macmillan Ltd., London, 1964.
- L3 Lawonn, H and Hesse, A; *"Fast maturing of unsaturated polyester resin prepregs"*, *Kunststoffe*, 65, 10, (1975), 678-680.
- L4 Lawonn, H and Hesse, A; *"The economic mass production of components for vehicle construction from UP-resin mats"*, *Ibid* 68, 10, (1978), 679.
- L5 Leider, P J and Bird, R B; *"Squeezing flow between parallel disks, Part I"*, *Ind. & Eng. Chem. Fund.*, 13, (1974), 336-341.
- L6 Leider, P J; *"Squeezing flow between parallel disks, part II"*, *Ibid*, 13, (1974), 342-346.
- L7 Loud, S N; *"Fibre glass reinforced plastic sheet moulding compounds (SMC) for productivity"*, *Tech. Rep. Syst. ASM* n.76-61, 1976, 7p.
- L8 Luchini, A; *"SMC design and moulding criteria"*, *Int. Symp. on Polyester Moulding Compounds*, Geneva, May 1977, paper 10.
- L9 Lundenberg, J A and Coats, C E; *"Energy absorbing polyester for low profile SMC"*, 32nd Annual Tech. Conf., SPI Reinf. Plast/Comp. Inst., 1977, Section 16-A.
- M1 Mandy, F; *"Market and applications of sheet moulding compounds: new developments in low profile formulations"*, *Reinf. Plast. Cong.*, British Plast. Fed., Brighton, November 1974, p.33-39.
- M2 Marker L and Ford, B; *"Rheology and moulding characteristics of glass fibre reinforced sheet moulding compound"*; 32nd Annual Tech. Conf., SPI Reinf. Plast/Comp. Inst., 1977, Section 16-E.
- M3 Maxel, J M; *"Rheology of SMC at moulding temperatures"*, 32nd *Ibid*, 1977, Section 2-E.
- M4 McLellan, D R and Warner, G; *"Application of RP/C to the Corvette"*, 34th *Ibid*, 1979, Section 18-B.

- M5 McGarry, F J, Rowe, E H and Rien, C K; *"Improving the crack resistance of BMC and SMC"*, 32nd Ibid, 1977, Section 16-C.
- M6 McLaughlin, McAssey Jr and Dietrich R; *"Non-destructive examination of fibre composite structures by thermal field techniques"*, 34th Ibid, 1979, Section 22-D.
- M7 Methven, J; *"The flow behaviour of SMC and DMC"*, *Plastics and Rubber: Processing*, 1, 4, (1976), 149-157.
- M8 Methven, J M; *"L'utilisation des microspheres creuses dans les compounds et imprégnés polyester"*, *Verre Textile-Plast.Renf.* 17, 3 (1979), 12-18.
- M9 Mohar, J G, Oleski, S S, Shook, D G and Meyer S L; *"SPI Handbook of technology and engineering of reinforced plastics/composites"*, Van Nostran Reinhold Co. New York 1973, 175-239.
- M10 Morris, J J; *"The mathematical simulation of the flow of sheet moulding compound in compression moulding processes"*, ICI Petrochemicals Division, Technical and Planning Resource Department, Wilton, Teeside, U.K. 1979.
- M11 Moulson, T J and Mathur, K K; *"Low viscosity limestone fillers for SMC"*, 32nd Annual Tech. Conf., SPI Reinf. Plast/Comp. Inst., 1977, Section 3-F.
- M12 Murfitt, P S; *"Fillers for the automotive industry: their selection and quality"*, *Reinf. Plast. Cong.*, British Plast. Fed., Brighton, 1978, pap. 28/199-201.
- M13 Myers, F A and Maxel, J M; *"Visco-elastic properties of sheet moulding compound"*, 33rd Annual Tech Conf., SPI Reinf. Plast/Comp. Inst., 1978, Section 19-D.
- N1 Nelb, R G; *"Auto parts manufacture - a new dimension"*, 34th Ibid, 1979, Section 18-C.
- N2 Newman, S, Pink, F and Fesko, D; *"Processing plastics - make a production part from a test mould"*, *Plast. Eng.*, 33, 1, (1977), 22-24.

- N2 Nightingale, R J; *"GRP mouldings from SMC - their process and markets"*, *Europlastics*, 45, 10, (1972), 70-75.
- N4 Nottingham Algorithm Group, NAG Library Manual, November 1974
- 01 Oka, S and Ogawa, S; *"Theory of a parallel plate plastometer for a Bingham-body"*, *Japan J. Appl. Phys.*, 3, 6, (1964), 347-350.
- 02 Okuto, H, Hirand, H and Yotsuzuka, M; *"Having trouble evaluating processability of SMC? Here are some handy approaches you can try"*, *Plastics Technology*, 19, 9, (1973), 43-45.
- 03 Owens-Corning Fibreglas Co; *"Sheet moulding compound"*, Ohio, USA, June 1976, Pub No. 5-TM-6991-A.
- 04 Owens-Corning Fibreglas Co; *"Spray metal prototype tooling"*, Ohio, USA, September 1978, Pub. No. 5-EL-8365-A.
- P1 Pastorino, R L; *"Guide to sheet moulding catalyst"*, *SPE J.* 28, 5, (1972), 18-21.
- P2 Peterson, P; *"New procedures to study flow behaviour of SMC"*, 33rd Annual Tech. Conf., SPI Reinf. Plast/Comp. Inst., 1978, Section 24-E.
- P3 Powell, R; *"Characterization of high glass polyester composites through the use of dynamic mechanical testing"*, 34th Ibid, 1979, Section 7-A.
- R1 Rapp, R S; *"Sheet moulding compounds: the effects of isophthalic polyester processing"*, 34th Ibid, 1979, Section 16-F.
- R2 Rheometrics, Inc., Marketing Department, 2438 U.S. Hwy.22, Union, N.J. 07083, USA.
- R3 Rowe, E H; *"Developments in improved crack resistance of thermoset resins and composites"*, 34th Annual Tech.Conf., SPI Reinf.Plast/Comp. Inst., 1979, Section 23-B.

- R4 Rudy, A J; *"Total approach to tooling"*, 33rd Ibid, 1978, Section 4-D.
- S1 Scott, J R; *"Theory and application of the parallel plate plastimeter"*, Trans. Inst. Rubb. Ind., 7, (1931), 169-186.
- S2 Scott, J R; *"Theory and application of the parallel plate plastimeter"*, Ibid, 10, (1935), 481-493.
- S3 Seamark, M J; *"Quality and consistency of sheet moulding compound (SMC) related to optimum material usage in production"*, Reinf. Plast. Cong., British Plast. Fed., Brighton, November 1978, pap. 26/183-188.
- S4 Shaw, F S; *"Relaxation methods"*, Dover Publications Inc., 1953.
- S5 Shenk, W; *"How matched die moulded fibreglass prototypes of SMC business equipment mouldings benefit both the customer and the moulder"*, 33rd Annual Tech. Conf., SPI Reinf. Plast/Comp. Inst., 1978, Section 3-A.
- S6 Sieglaff, C F; *"Use of flow properties to improve bulk and sheet moulding operations"*, *Plastics Design and Processing*, 11, (1972), 16-18.
- S7 Silva-Nieto, R J, Fisher, B C and Birley, A W; *"Predicting mould flow for unsaturated polyester resin sheet moulding compounds"*, 34th Annual Tech. Conf., SPI Reinf. Plast/Comp. Inst., 1979, Section 7-B.
- S8 Silva-Nieto, R J, Fisher, B C and Birley, A W; *"Rheological characterization of unsaturated polyester resin sheet moulding compound"*, 35th Ibid, 1980, Section 2-E.
- S9 Simko, T D; *"Automotive and commercial high strength moulding compounds"*, 33rd Ibid, 1978, Section 18-G.

- S10 Smith K L and Suh, N P; *"An approach towards the reduction of sink marks in SMC"*, SPE, 36th Annual Tech. Conf., Washington, D.C., 1979, 796-799.
- S11 Smith R J and Jutte R B; *"The sources and nature of mechanical property variability in sheet moulding compound"*, 32nd Annual Tech. Conf., SPI Reinf. Plast/Comp. Inst., 1977, Section 7-E.
- S12 Sommers, D J; *"Effects of wetting agents on clay filled sheet moulding compound"*, 34th Ibid, 1979, Section 16-D
- S13 Spaay, A; *"New development in compression moulding with continuous SMC"*, 33rd Ibid., 1978, Section 9-G.
- S14 Stanley, A; *"Wheel wells of structural SMC for transportation industry"*, 34th Ibid, 1979, Section 21-C
- S15 Synthetic Products Co; *"New FRP release agent improves cost performance"*, Plast. Tech., 24, 3, (1978), 10.
- T1 Tadmor, A and Gogos C G; *"Principles of polymer processing"*, John Wiley and Sons, London, 1979, Chapter 5.
- T2 Tetlow, P D, Mandell, J F and McGarry, F J; *"Effects of rubber addition on the fracture toughness of a polyester resin"*, 34th Annual Tech. Conf., SPI Reinf. Plast/Comp. Inst., 1979, Section 23-F.
- T3 Thomas, A, Roskott, L, Groenendaal, A A M and Kolczynski, J R; *"The use of peroxyketals as initiators for curing unsaturated polyester sheet moulding compound"*, 33rd Ibid, 1978, Section 5-E.
- T4 Thomas, D H; *"Consistency control in sheet moulding compounds: the key to component design"*, Conf. Proceedings: "Chemistry in Industry - the Way Ahead", Wembley, London, November 1976.

- T5 Thomas, D H; *"Weight effectiveness and SMC rheology"*, 33rd Annual Tech. Conf., SPI Reinf. Plast/Comp. Inst., 1978, Section 19-F.
- T6 Thomas, D H; *"The relevance of a parallel plate type rheometer to the characterization of a class of discontinued materials"*, Conf. British Soc. of Rheology, Plymouth, September, 1978, 101-103.
- T7 Thomas, D H; private communication, while working for ICI Petrochemicals Division, Wilton, Teeside, U.K.
- T8 Thompson, S J; *"Instrumentation of SMC moulding"*, *Plastics and Rubber International*, 3, 4, (1978), 159-161.
- T9 Todd, W H; *"Control system promises to advance compression moulding technology"*, *Modern Plastics*, 53, 6, (1976), 54-56.
- T10 Truman, C M and Townsend, B; *"Sheet moulding compounds in commercial vehicles, a case study"*, 6th Cranfield Conf. Plast. Design Eng., January 1975, paper 6
- V1 Vlachopoulos, J; *"Should you use finite difference or finite element methods for polymer flow problems"*, SPE, 35th Annual Tech. Conf., Montreal Que., 1977, 519-520.
- W1 Warner, K N; *"Mechanism of the thickening of polyester by alkaline earth oxides and hydroxides"*, 28th Annual Tech. Conf., SPI Reinf. Plast/Comp. Inst., 1973, Section 19-E.
- W2 Whybrew, K; *"The effect of flow on the strength of polyester DMC"*, PhD Thesis, Nottingham University, 1972.
- W3 Wilkinson, J L and Reinsch, C; *"Handbook for automatic computation"*, Vol. II, Linear Algebra, Springer-Verlag, 1971, p.93-110.
- W4 Wilkinson, W L; *"GRP processing: a review of progress and future developments in understanding"*, *Plastics and Rubber: Processing*, 4, 1, (1979), 1-9.

- W5 Woelfel, J A, O'Neil, K B, Brede, A and Smith, R W; *"Reinforced composite wheels: light-wheel of the future"*, 34th Annual Tech. Conf., SPI Reinf. Plast/Comp. Inst., 1979, Section 21-A
- W6 Wood, E L, Rockwood, L, Foster, J E Jr. and Nelson G; *"Increase automotive reinforced plastic production and quality through automation of the SMC process"*, 34th Ibid, 1979, Section 18-E
- W7 Woodhams, R T and Xanthos, M; *"Viscosity behaviour of thickened polyester resin for use in HAR (high aspect ratio) mica thermoset moulding compounds"*, SPE, 35th Annual Tech. Conf., Montreal, Que. 1977, 292-295
- Y1 Yee, G Y; *"Innovative sheet moulding compound process"*, SAE Prepr. No. 790170, February-March 1979, 11p.

## APPENDIX 1

PROGRAM USED TO RECORD RHEOLOGY DATACOMPUTER PROGRAM (BASAC)A. Introduction

This program instructs the PDP-11/05 data logger during the compression of SMC discs (with the parallel plate plastometer) to record the voltage outputs from the displacement transducer, the thermocouple (or thermocouples), and the compression force. These three readings are recorded every second for a period specified at the beginning of the program. The program outputs the data to the teletype and paper tape punch.

B. Data

The following variables must be defined as the input:

D	=	Day of the experiment
H	=	Hour of the experiment
M	=	Minute of the experiment
S	=	Second of the experiment
J	=	Number of readings required (maximum 80)

C. Variables

A	=	Matrix where the data is stored (80 x 3)
C,V	=	Time in seconds
F	=	Force in volts
H1	=	Displacement of the plate in mm
R	=	Range of scanning speed (set at 25 channels/sec)
T	=	Time function in seconds (in array form)
TEMP	=	Temperature of the SMC disc in volts
U	=	Array
V1	=	Speed of compression in mm/sec
W	=	Variable used as control, to start the scanner from the test laboratory

- X = Block scanner function
- Y = Array
- Z = Function used for setting and reading the electric clock

#### D. Units

The units used in the program are in mm and seconds. The force and temperature values must be calculated using appropriate calibration tables. This facility has not been introduced into the program because of the storage limitations of the computer.

#### E. Channels

- 144 - This channel is the control to start the computer (W)
- 145 - Displacement channel
- 146 - Force channel
- 147 - Temperature channel

#### F. Flow Diagram

See following page.

#### G. Program

See following page.

#### H. Note

To use this program, delete from the compiler the extended and logarithmic functions (see manual of the computer). This is to increase the available memory size.

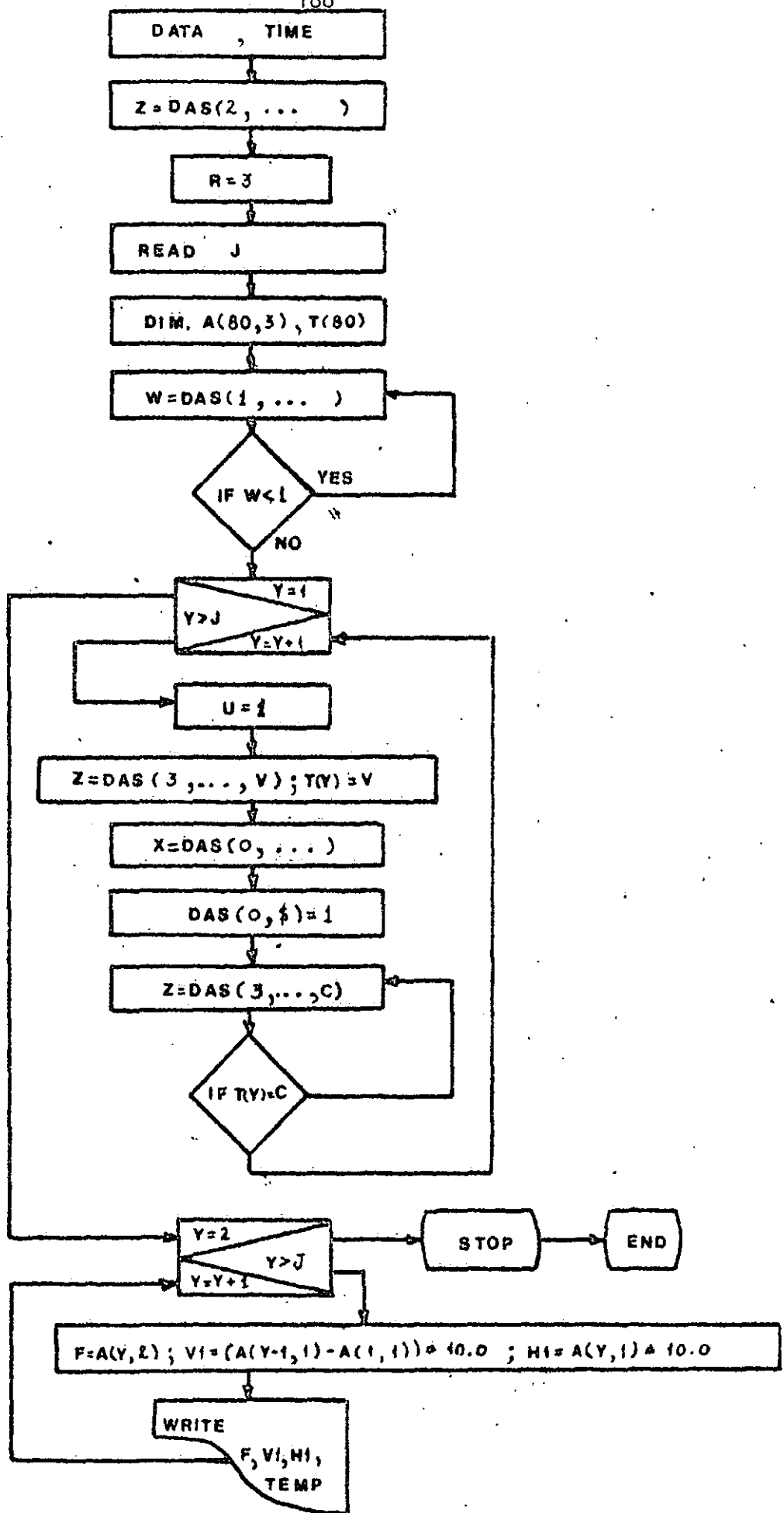


Fig.A1.1 BLOCK DIAGRAM

## LIST

```

1REM PROGRAM TO STORE THE DATA FOR THE RHEOLOGY WORK
30UT00"ENTER DATA AND TIME":IN00#31,D,#31,H,#31,M,#31,S
5LETZ=DAS(2,D,H,M,S)
8LETR=3
90UT00" NUMBER OF TIMES. = J ":IN00#31,J
10DIMA(80,3),T(80)
15REM          FORCE IN KG
16REM          SPEED IN MM/SEC
17REM          DISPLACEMENT IN MM
18REM          TIME IN SEC
20LETV=DAS(1,144,R,2)
25IFV<1.0GOTO20
40FORY=1TOJ
42LETH=1
43LETZ=DAS(3,D,H,M,V):LETT(Y)=V
44LETX=DAS(0,A(Y,U),145,147,R,4)
45IFDAS(0,S)=1GOTO45
46LETZ=DAS(3,D,H,M,C)
47IFT(Y)=CGOTO46
48NEXTY
49OUT00#7X,"Y",#6X,"T(Y)",#6X," HI ",#6X," VI ",#6X," F "
50OUT00#5X," TEMP ",#
51FORY=2TOJ
52OUT00#4X,#4I,Y,#5X,#3I,T(Y),#4X
54LETF=A(Y,2)
55LETVI=(A(Y-1,1)-A(Y,1))*10.0:LETHI=A(Y,1)*10.0
56OUT00#9E4,H1,#4X,#9E4,VI,#4X,#9E4,F,#4X,#9E4,A(Y,3),#
59OUT00#
60NEXTY
70LETF=A(1,2)
72LETVI=0.:LETHI=A(1,1)*10.0
74OUT00#9E4,H1,#4X,#9E4,VI,#4X,#9E4,F,#4X,#4I,Y,#
78LETT(1)=1
80FORY=2TOJ
81LETT(Y)=T(Y-1)+1
82LETF=A(Y,2)
83LETVI=(A(Y-1,1)-A(Y,1))*10.0:LETHI=A(Y,1)*10.0
84OUT00#15E4,F,#15E4,H1,#15E4,VI,#15E4,T(Y),#
86NEXTY
90STOP
100END

```

READY

## APPENDIX 2

PROGRAM USED TO ANALYSE DATACOMPUTER PROGRAM (FORTRAN)A. Introduction

The data recorded on paper tape using the program of Appendix 1, must be reproduced as another paper tape with even parity for every line of punched holes. This is necessary to process the data using the ICL-1904S. The data is stored on magnetic-disc of the ICL-1904S. The program evaluates the viscosity, elasticity and yield values for every experimental test for which data is stored on the magnetic-disc.

The method used to evaluate the viscosity, elasticity and yield values for each test is based on the least-squares solution to an over-determined set of equations (D7). The force-time experimental data for each test were substituted in turn into equation 4.34 and the functions  $f_1(t)$ ,  $f_2(t)$  and  $f_3(t)$  were evaluated with the parameters of the corresponding test. The functions  $f_1(t)$ ,  $f_2(t)$  and  $f_3(t)$  were each standardised to the range 0 to 1 for the fitting.

For the curve fitting, two subroutines are used: GØ2BDF and GØ2CHF (N4). The program will evaluate the coefficients of viscosity, elasticity and yield for the standardised data (see variables COEFFT). Those coefficients have to be transformed to cover the real range of the data (see variables COEFFI). If the data does not start from zero, a constant (COMP4) must be added in the equation 4.34.

The program evaluates the theoretical force using the functions  $f_1(t)$ ,  $f_2(t)$  and  $f_3(t)$ , the coefficients of viscosity, elasticity and yield and the constant COMP4. Then the experimental and theoretical values for the force (see experimental and fitted force in Appendix 10) are plotted.

The units of the coefficients are:

$\mu$	-	COEFFI (1,1)	kg-sec/mm <sup>2</sup>
K	-	COEFFI (2,1)	kg/mm <sup>2</sup>
f	-	COEFFI (3,1)	kg/mm <sup>2</sup>

The units for the forces F, F1 and F3 are kg.

B. Block Diagram

See following page for program structure.

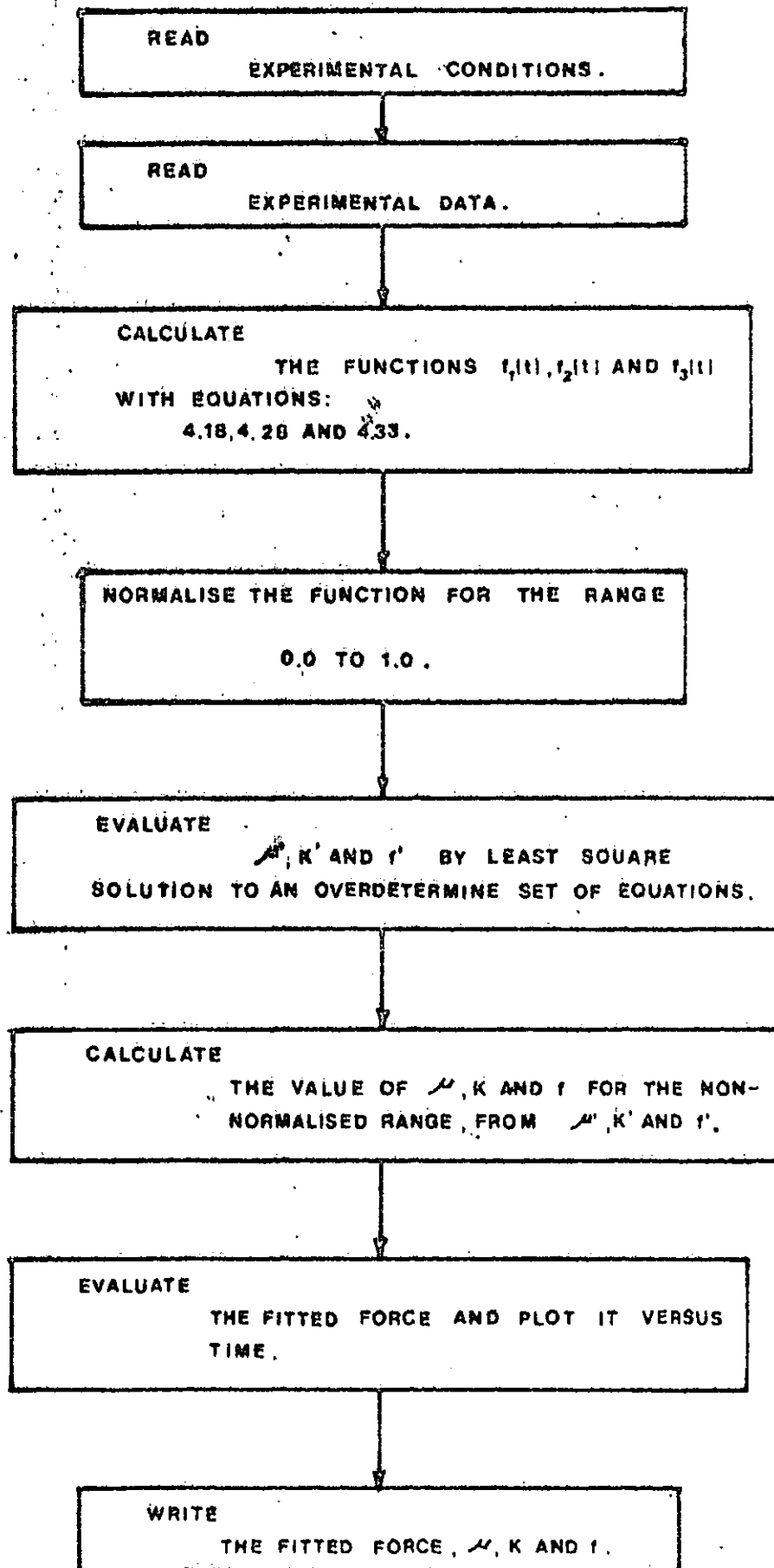


Fig.A2.1 BLOCK DIAGRAM

```

MASTER INITIAL
DIMENSION A(80,4),AMEAN(4),STD(4),SSP(4,4),CORR(4,4)
DIMENSION RESULT(12),COEFFT(4,3),RINV(3,3),C(3,3),W(3,3)
DIMENSION I1(12),F(85,12),H(85,12),V(85,12),Y(85,12),N1(12),N2(12)
*,P7(85,12),CON1(12),CON2(12)
DIMENSION VOL(12),H0(12),S(12),F1(85),Y1(85),F3(85)
DIMENSION B(80,4),COEFF1(4,3)
DIMENSION SR(12)
*****
C READ(1,3)L
5 FORMAT(I10)
CALL C1051N
CALL DEVICE(8,1H0)
CALL DEVPAF(210,297,1)
CALL WINDOW(2)
READ(1,10)(I1(J),J=1,L)
10 FORMAT(8I10)
DO 500 K=1,3
CALL AXIPL0(0,140,200,7,1,10,10,0,80,0,600,0,7,1,1MB,4,1,FORCE
*,5)
DO 100 J=1,L
IF(KS.GT.4)GO TO 42
READ(5,20)(F2(I,J),H(I,J),V(I,J),Y(I,J),I=2,I1(J))
20 FORMAT(4E0,0)
WRITE(2,26)(F2(I,J),H(I,J),V(I,J),Y(I,J),I=2,I1(J))
26 FORMAT(1H,4E15,4/)
READ(1,6)AN,M0,U1,M9
6 FORMAT(F10,5,I10,F10,5,I10)
READ(1,7)CON1(J),CON2(J)
7 FORMAT(2F10,5)
READ(1,28)H0(J),S(J),N1(J),N2(J)
28 FORMAT(2F10,5,2I10)
READ(1,8)SR(J)
8 FORMAT(F10,5)
VOL(J)=(W1/1.8)*1000
WRITE(2,30)
30 FORMAT(1H,/////)
DO 45 I=M0,I1(J)
F(I,J)=CON1(J)+F2(I,J)-CON2(J)
****
45 CONTINUE

```

```

AN=1.0
42 CONTINUE
Y1(J)=0.0
F1(J)=0.0
J0=2
DO 47 I=N1(J),N2(J)
F1(J0)=F(I,J)
Y1(J0)=(H0(J)-H(I,J))/S(J)
J0=J0+1
47 CONTINUE
C *****
C *****
46 K=0
C *****
WRITE(2,600)AN,AN1
600 FORMAT(1H , 'AN=',F10.5,10X, 'AN1=',F10.5////)
C ***
K=1
A(K,4)=0.0
T=0.0
A(K,2)=0.0
C ***
A(K,1)=0.
A(K,3)=0.
C *****
DO 48 I=N1(J),N2(J)
K=K+1
A(K,4)=F(I,J)
T=(H0(J)-H(I,J))/S(J)
T1=VOL(J)*((AN+3.0)/2.0)
T2=(2.*((AN+1.)))*((2.*AN)+1.)*AN/((AN+3.)*((2.*AN)+AN))
T3=(S(J)*AN)*0.001
T4=(3.9416)*((AN+1.)/2.)
T5=(H0(J)-S(J)*T)*((5.*AN)+5.)/2.5
A(K,1)=T1+T2+T3/(T4+T5)
WRITE(2,810)T1,T2,T3,T4,T5,VOL(J),S(J),H0(J),T
810 FORMAT(9(812.5,9X))
A(K,2)=((VOL(J)+1.5)*S(J)*T)/(1.7724+H0(J)+H(I,J)+2.5)
A(K,3)=(VOL(J)+1.5)*2./((5.31736+(H(I,J)+2.5))
C *****
48 CONTINUE
KONT=K
DO 49 I=1,KONT
B(I,1)=(A(I,1)-A(1,1))/(A(KONT,1)-A(1,1))
B(I,2)=(A(I,2)-A(1,2))/(A(KONT,2)-A(1,2))
B(I,3)=(A(I,3)-A(1,3))/(A(KONT,3)-A(1,3))
B(I,4)=A(I,4)
49 CONTINUE
M=4
N1=N2(J)+1+1

```

```

M2=M-1
WRITE(2,200)M,1,(K,K=1,M),(I,(A(I,K),K=1,M),I=1,M)
WRITE(2,200)M,1,(K,K=1,M),(I,(B(I,K),K=1,M),I=1,M)
IFAIL=1
*****SSSSB

CALL G02RDF(M1,M,B,R0,AMBAN,STD,SSP,4,CORR,4,IFAIL)

IF(IFAIL)90,55,50
50 WRITE(2,210)IFAIL
GO TO 100
65 WRITE(2,220) (I,AMBAN(I),STD(I),I=1,M)
WRITE(2,230) (I,(SSP(I,K),K=1,M),I=1,M)
WRITE(2,240) (I,(CORR(I,K),K=1,M),I=1,M)
200 FORMAT (32HNUMBER OF VARIABLES (COLUMNS) =, I1/10H NUMBER OF,
* 29H CASES (ROWS) =, I1/17H DATA MATRIX IS: /1H ,
* 4I12/(1H , 13, 4E12.4))
210 FORMAT (22HROUTINE FAILS, IFAIL=, I2)
220 FORMAT (24H VARIABLE MEAN ST. DEV. / (1H , 15 2E11.4))
230 FORMAT (46H SUM OF SQUARES AND CROSS-PRODUCTS ABOUT ZERO /1H ,
* 4I12/(1H , 13, 4E12.4))
240 FORMAT (30H CORRELATION-LIKE COEFFICIENTS /1H , 4I12/(1H , 13,
* 4E12.4))
IFAIL=1
CALL G02CMF(M1,M,M2,SSP,4,CORR,4,RESULT,COEFFT,4,RINV,3,C,3,W,3,IF
1011)

TEST IFOIL

IF(IFOIL)60,65,60
60 WRITE(2,250)IFOIL
GO TO 100
65 COEFFI(1,1)=COEFFT(1,1)/(A(KONT,1)-A(1,1))
COEFFI(2,1)=COEFFT(2,1)/(A(KONT,2)-A(1,2))
COEFFI(3,1)=COEFFT(3,1)/(A(KONT,3)-A(1,3))
COEFFI(1,2)=COEFFT(1,2)
COEFFI(2,2)=COEFFT(2,2)
COEFFI(3,2)=COEFFT(3,2)
COEFFI(1,3)=COEFFT(1,3)
COEFFI(2,3)=COEFFT(2,3)
COEFFI(3,3)=COEFFT(3,3)
WRITE(2,260) (I,(COEFFI(I,K),K=1,3),I=1,M2)
WRITE(2,260) (I,(COEFFI(I,K),K=1,3),I=1,M2)
*****
WRITE(2,270) (RESULT(I),I=1,13)
WRITE(2,280) (K,K=1,M2) (I,(RINV(I,K),K=1,M2),I=1,M2)
WRITE(2,290) (K,K=1,M2) (I,(C(I,K),K=1,M2),I=1,M2)
250 FORMAT (22H ROUTINE FAILS, IFOIL=, I2)
260 FORMAT (43H VARIABLE COEFFT STD ERR T=VALUE/2(1H ,
* 13, 3E13.4/))

```

```

C *****
270 FORMAT (32H)ANALYSIS OF REGRESSION TABLE :-//13H SOURCE,
* 55H SUM OF SQUARES D.F. MEAN SQUARE F-VALUE//
* 18H DUE TO REGRESSION, F14.4, F8.0, 2F14.4/14H ABOUT REGRES.
* 6HNSION, F14.4, F8.0, F14.4/18H TOTAL 7 F14.4.
* F8.0//29H STANDARD ERROR OF ESTIMATE #, F8.4/11H MULTIPLE C,
* 14HORRELATION (R) #, F8.4/29H DETERMINATION (R SQUARED) #.
* F8.4/29H CORRECTED R SQUARED #, F8.4//
280 FORMAT (50H)INVERSE OF CORRELATION MATRIX OF INDEPENDENT VARI.
* 6HABLES1/1H , 3I10/3(1H , 14, 3F10.4//)
290 FORMAT (25H)MODIFIED INVERSE MATRIX;1/1H , 3I10/3(1H , 14,
* 3R12.4//)
WRITE(2,300)
300 FORMAT(1H , 'THE FORCE EVALUATED THEORETICALLY'//)
WRITE(2,310)
310 FORMAT(1H , 5X, 'FORCE', 20X, 'TIME'//)
DO 75 I=1,M1
M3=I
C *****
COMP1=(COEFFY(1,1)*(-A(1,1)))/(A(KONT,1)-A(1,1))
COMP2=(COEFFY(2,1)*(-A(1,2)))/(A(KONT,2)-A(1,2))
COMP3=(COEFFY(3,1)*(-A(1,3)))/(A(KONT,3)-A(1,3))
COMP4=COMP1+COMP2+COMP3
F3(M3)=COEFFI(1,1)*A(I,1)+COEFFI(2,1)*A(I,2)+COEFFI(3,1)*A(I,3)+CO
1MP4
WRITE(2,325) COMP1,COMP2,COMP3,COMP4
WRITE(2,320)F3(M3),F1(M3),M3
325 FORMAT(1H , 4R20.4)
320 FORMAT(1H , 'F3=,E15.5,5X, 'F1=,E15.5,5X, I10)
75 CONTINUE
C *****
C *****
CALL GRAPOL(Y1,F1,M1)
CALL GRASV4(Y1,F3,M1,8.0)
C *****
100 CONTINUE
READ(1,800)AN
600 FORMAT(F10.5)
CALL PICCLE
500 CONTINUE
CALL DEVEND
STOP
END
FINISH

```

## APPENDIX 3

SAMPLE PREPARATION FOR ANALYSING THE CROSS-SECTION  
OF UNCURED SMC BY REFLECTIVE LIGHTA. Equipment

Araldite resin (CY212)  
Hardener (Dodecetyl succinic anhydride)  
Accelerator DMP-30 (2,4,6 Tri (dimethyl-amino-methyl) phenol)  
Dibutyl phthalate  
Plastic containers, size 8 ml  
Hearson oven 0° - 200°C (A4015)  
Struers polishing apparatus  
Wet and dry abrasive paper types 220, 320, 400 and 600  
Hyprez diamond alumina of 6 $\mu$ , 1 $\mu$  and 0.05 $\mu$   
Reichert Metavar microscope

B. Method

- Leave the samples for one month in open air
- Cut a section of 10 x 20 mm
- Prepare the embedding plastic by mixing 10% of Araldite, 10% of hardener, 0.5% of accelerator and 1% of Dibutylphthalate
- Place the sample in the plastic container and embed it with the mixture of Araldite
- Place the container in the oven at 80°C for 12 hours
- Polish the sample using water as a lubricant, starting with the 220 abrasive paper and finishing with the 600
- Place a thin layer of 0.1 mm of the Araldite mixture on the polished area to fill the holes of the sample
- Place the sample into the oven at 80°C for 12 hours
- Polish the sample with care using the 600 abrasive paper only. For the final polishing use the 6 $\mu$ , 1 $\mu$  and 0.05 $\mu$  "Hyprez" diamond alumina
- Examine the sample through the microscope.

## APPENDIX 4

COMPUTER PROGRAM FOR EVALUATING THE CHARGE SHAPECOMPUTER PROGRAM (FORTRAN)A. Introduction

This program calculates the charge shape for two-dimensional plates, and can be used for either symmetrical or unsymmetrical shapes.

The program is divided into four sections:

1. Calculation of pressure contours
2. Calculation of stream-lines
3. Calculation of flow-front position
4. Calculation of area covered by the new flow-front.

The following pages show block diagrams of the program structure. After each section, input data has to be calculated by hand and then supplied to the computer for the next calculation.

B. Method1. Calculation of pressure contours

This section of the program generates the Poisson's equation (6.1) in finite difference form at every node. This is obtained by supplying to the computer a number - called the node characteristic - which will select from 14 typical equations the required one depending on the node characteristic number (depending on the location of the node - see Section C). The program analyses a square mesh of  $n$  rows and  $m$  columns, therefore for the case of unsymmetrical shapes the matrix of coefficients will have complete rows of zeros. The rows of zeros are eliminated before the matrix-inversion. Then the remaining set of equations is solved by matrix-inversion using the subroutine F04ATF (N4). The pressure values of every node are interpolated to generate the contours of constant pressure. Such contours are calculated and plotted by using a computer package called GINO-SURFACE (G6).

## 2. Calculation of stream-lines

This section calculates the speed vector at every point supplied. The calculation is carried out using equations 7.3 and 7.4. Then the magnitude and angle of the speed are determined using classical vector analysis.

## 3. Calculation of flow-front position

This section evaluates the positions of the points of the flow-front on the stream-lines. The evaluation is based on equation 7.10 and 7.11. The flow-front points can be calculated by two methods: either with constant pressure difference  $\Delta p_{\alpha} = \Delta p_{\beta}$ , or with constant distance  $d_{\alpha} = d_{\beta}$ .

## 4. Calculation of the area covered by the new flow-front

This section evaluates the area of the charge shape. Four types of calculation can be made, depending on the number of axes of symmetry. In every case the area of each quadrant with respect to the centre of area is evaluated by dividing the area into small rectangular areas of length  $Y$  ( $Y$  is the distance from the x-axis to the flow-front) and width  $\Delta x$ . Then a negative area is calculated on the same basis. The total area is the sum of areas multiplied by twice the number of axes of symmetry.

Then the program evaluates the percentage of area covered by the charge.

## C. Node Characteristic Number

This number is used to select the finite difference form of Poisson's equation at each node. The node characteristic numbers are as follows:

$D(K) = 0$  Node outside the boundary of the plate

$D(K) = 1$  Node in vertical axis of symmetry

$D(K) = 2$  Node in horizontal axis of symmetry

$D(K) = 3$  Node next to the horizontal boundary

$D(K) = 4$  Node next to the horizontal boundary and node in vertical axis of symmetry

- D(K) = 5 Node next to the horizontal boundary and node in diagonal axis of symmetry
- D(K) = 6 Node next to the vertical boundary
- D(K) = 7 Node next to the vertical boundary and node in horizontal axis of symmetry
- D(K) = 8 Node next to the vertical boundary and node in diagonal axis of symmetry
- D(K) = 9 Node in diagonal axis
- D(K) = 10 Node in centre of area when analysing a plate with a vertical axis and horizontal axis of symmetry (for a rectangular plate)
- D(K) = 11 Internal or normal node
- D(K) = 12 Node in centre of area when analysing a plate with a horizontal axis of symmetry (for the "triangle + square" plate).
- D(K) = 13 Node in the centre of area when analysing a plate with a vertical and diagonal axis of symmetry (for the square plate)
- D(K) = 14 Node in an irregular star. In this case the value of the coefficients must be supplied and calculated according to Section 5 of this appendix.

- Note:
- (a) The nodes must always be numbered from bottom to top and from right to left.
  - (b) In the case of a square the area to analyse must be in the first quadrant of the centre of area axes between the vertical and diagonal axis
  - (c) In the case of rectangular shapes the area to analyse must be in the first quadrant of the centre of area axes.
  - (d) In the case of a plate with one axis of symmetry the area to analyse must be the fourth and first quadrants with respect to centre of area axis.
  - (e) In the case of an unsymmetrical plate the whole article will be considered in first quadrant of an axes of reference.

The examples in Figures A4-1 to A4-4 show the mesh with the node characteristic number in each node.

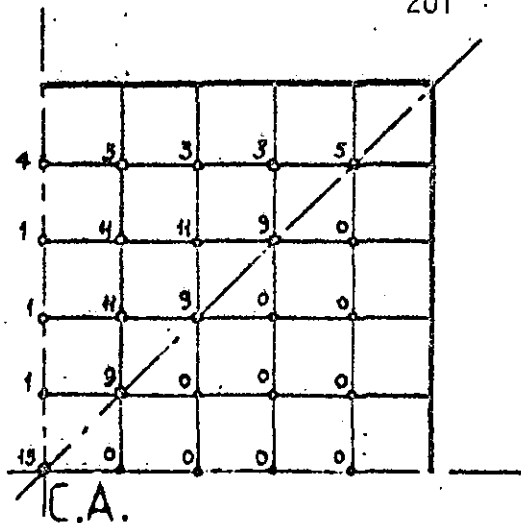


Fig.A4.1 NODE CHARACTERISTIC FOR A SQUARE

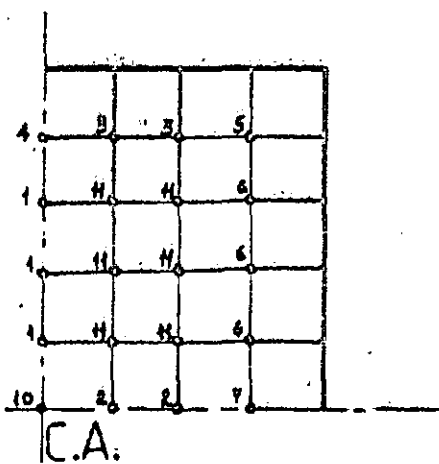


Fig.A4.2 FOR A RECTANGLE

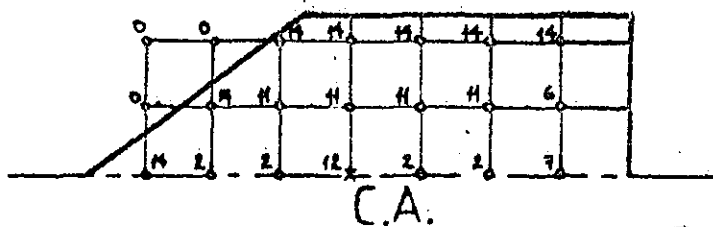


Fig.A4.3 FOR A SQUARE & TRIANGLE

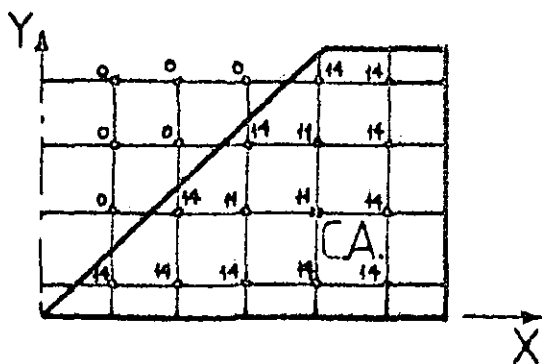


Fig.A4.4 FOR A TRAPEZOID

D. Evaluation of Coefficients for an Irregular Star (S4)

Figure A4-5 shows the general equation and values of coefficients for Poisson's equation. For the boundary conditions, the pressure is assumed to be 0.1 N/mm<sup>2</sup> (1 bar). Then the general equation may be written:

$$Cp_3 + Dp_4 - (E+F)p_0 = - \frac{12 \frac{1}{2}^2 \mu W_h}{h^3} - [A(0.1) + B(0.1)]$$

where the coefficients have to be evaluated by hand and then input to the computer.

E. Block Diagram

See following page for program structure.

$$\hbar^2 \left( \frac{\partial^2 p}{\partial x^2} + \frac{\partial^2 p}{\partial y^2} \right) = A p_1 + B p_2 + C p_3 + D p_4 - (E+F) p_0 = \hbar^2 (12 \mu W_h / h^3)$$

WHERE:

$$A = 2 / [a_1(a_1 + a_3)]$$

$$B = 2 / [a_2(a_2 + a_4)]$$

$$C = 2 / [a_3(a_3 + a_1)]$$

$$D = 2 / [a_4(a_4 + a_2)]$$

$$E = 2 / a_1 a_3$$

$$F = 2 / a_2 a_4$$

$$a_i = \hbar_i / \hbar \quad , i=1,2,3,4.$$

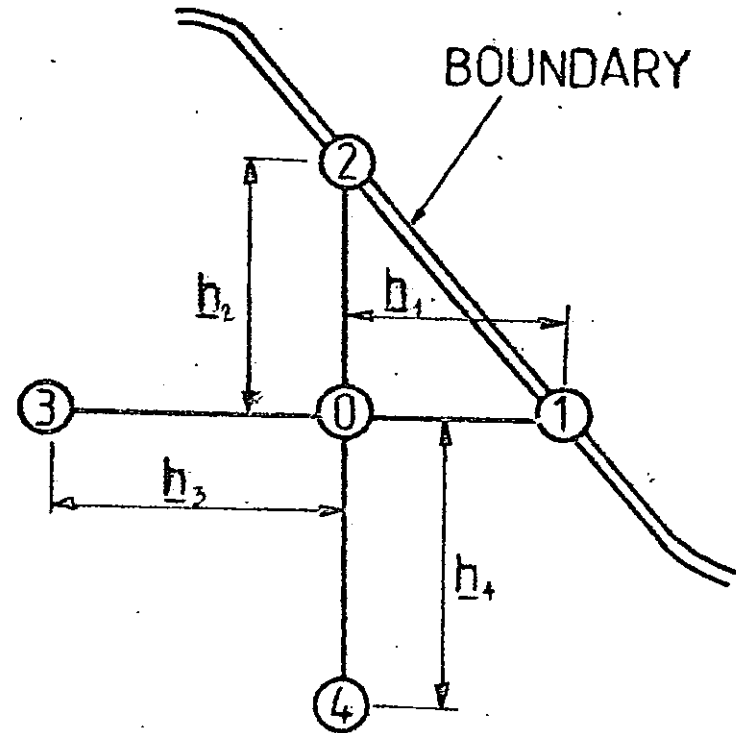


Fig.A4.5 COEFFICIENTS FOR AN IRREGULAR STAR

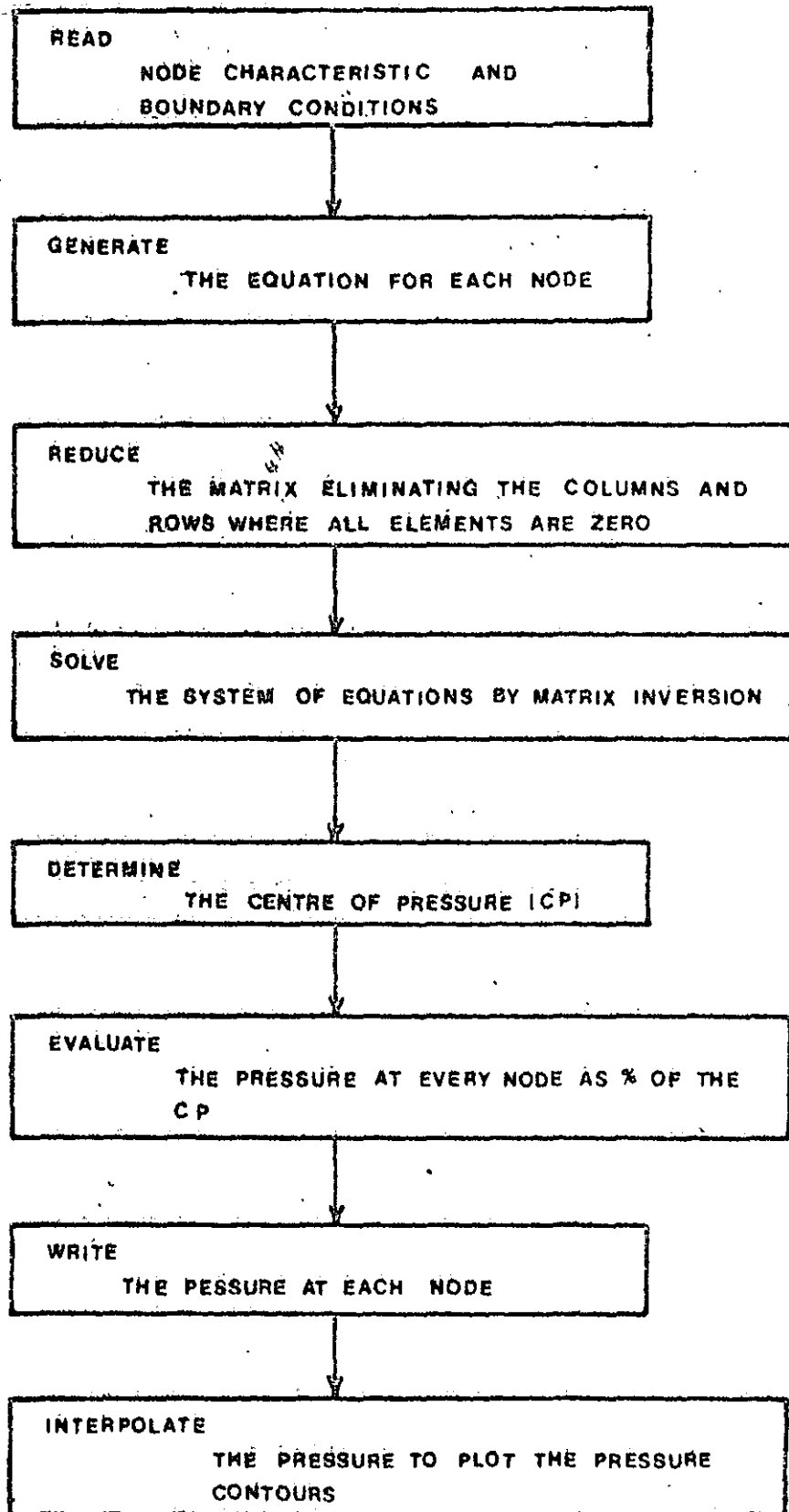


Fig.A4.6 BLOCK DIAGRAM  
PROGRAM 1

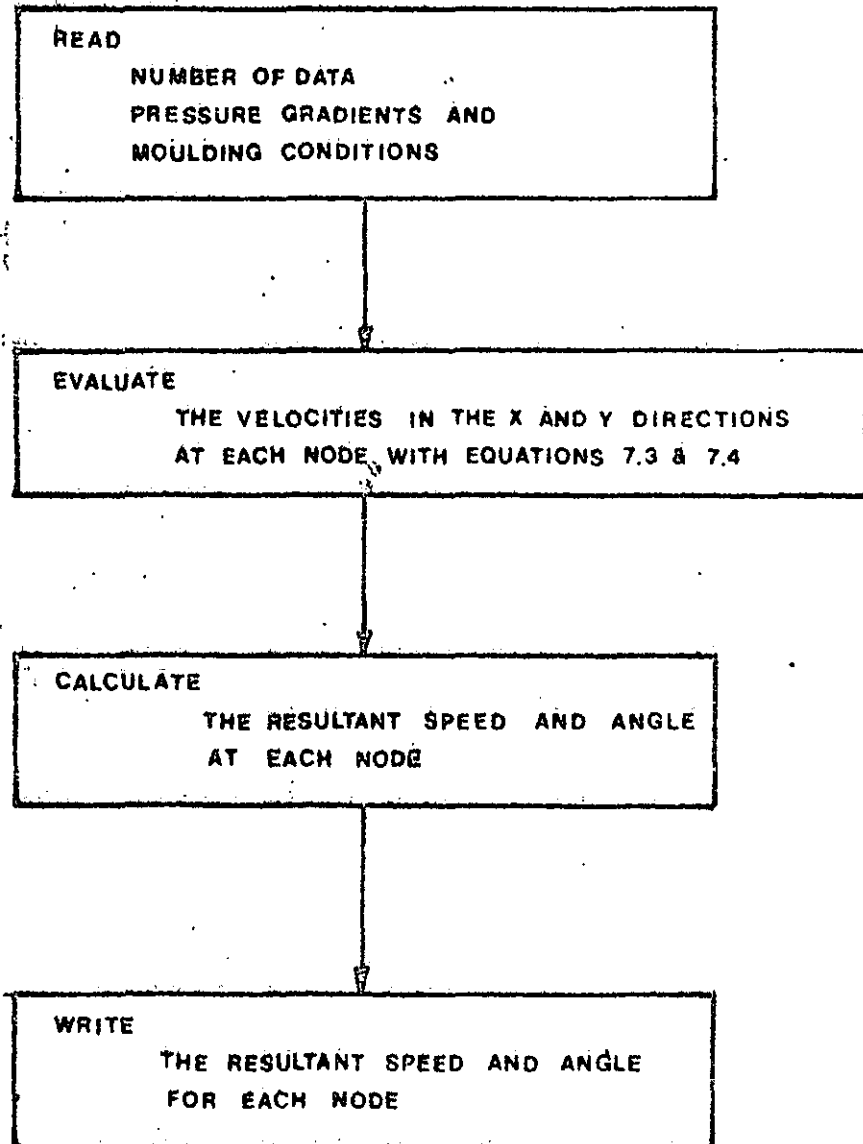


Fig.A4.7 BLOCK DIAGRAM  
PROGRAM 2

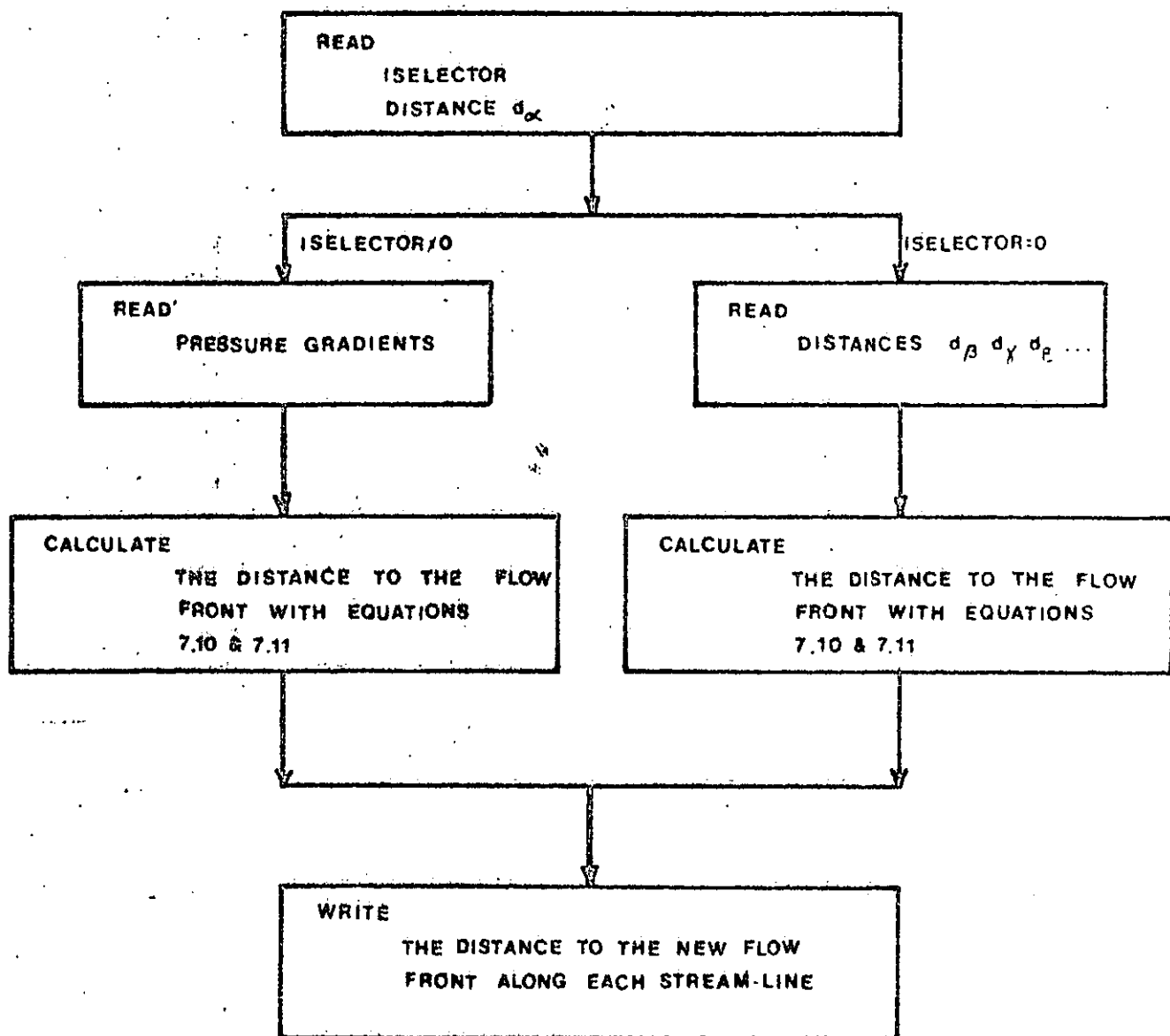


Fig.A4.8 BLOCK DIAGRAM  
PROGRAM 3

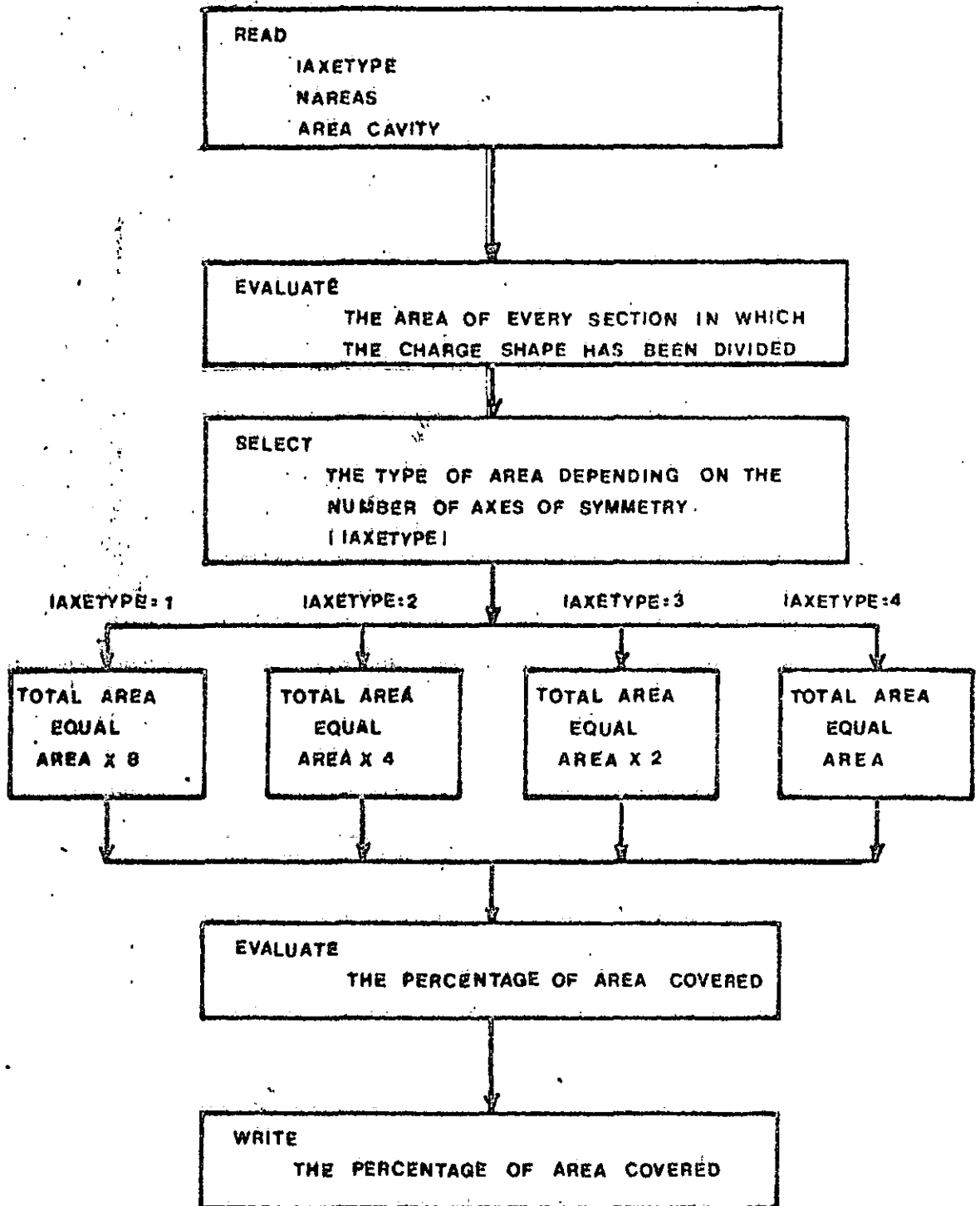


Fig.A4.9 BLOCK DIAGRAM  
PROGRAM 4

## APPENDIX 5

SAMPLE PREPARATION FOR X-RAY ANALYSIS OF  
THE CROSS-SECTIONA. Equipment

Cambridge S2A Stereoscan

"Struers" polishing apparatus

Wet and dry abrasive paper types 220, 320, 400 and 600

Double-sided tape

Glass slides

Cylindrical cork

Razor blade

B. Method

- Cut a 2 mm thick cross-section from the SMC of size 10 x 3 mm
- Stick a piece of the double-sided tape to one side of the glass-slide and another in the other side
- Stick the cylindrical cork to the glass-slide
- Stick the sample of 10 x 3 mm area to the other side of the glass-slide
- Polish the sample with the abrasive paper starting from 220 and finishing with 600, to reduce the 2 mm thickness to 0.25 mm.
- The sample is ready to place in the Cambridge S2A stereoscan (reference H2).

## APPENDIX 6

METHOD USED FOR THE EVALUATION OF  
FIBRE-GLASS PERCENTAGE

(Copied from Appendix 5, Ref. W2)

A. Equipment

Safety glasses

Rubber gloves

"Carbolite" furnace (1-2/70/T238)

"Vitrex" crucibles, 30 ml

"Saint Glass" filter-crucibles, 15 ml, porosity 4

Rubber sealing rings, size 7

Filter flask, 500 ml

Filter pump

Concentrated nitric acid

Distilled water

Squash bottle

Glass rod

Desiccator Pyrex, knob type, 20 cm diameter

"Belling" drying cabinet (000578)

"Unimatic" balance (S-32961)

B. Method

- Clean all the equipment, dry them in the oven for 2 hours at 120°C. Allow them to cool in a desiccator and store them until required
- Cut the samples of 10 x 10 mm from the SMC
- Weigh the "Vitrex" crucibles and lids (weight (1))
- Weigh each "Vitrex" crucible and lid plus sample (weight (2))
- Place covered crucibles containing the samples in "Carbolite" furnace at 625°C. Leave the samples for a minimum of 12 hours. Samples must be white, any greyness in the samples indicates unoxidised carbon
- When combustion is complete remove the crucibles from "Carbolite" furnace and allow to cool at room temperature
- Remove a filter-crucible from the desiccator and weigh (weight (3)). Assemble the filter-crucible, sealing ring, filter flask and filter pump. Start filter pump.

- Place the "Vitrex" crucible in a FUME CUPBOARD. Add 5 ml of water to the "Vitrex" crucible and then add sufficient concentrated nitric acid to cover the specimen. After 5 minutes stir with a glass rod and add 0.5 ml of nitric acid. The digestion of the calcium carbonate is complete when no further gas is released on adding acid.
- Empty the contents of "Vitrex" crucible into weighed filter-crucible. Rinse "Vitrex" crucible with a jet of distilled water from squash bottle and empty this into the filter-crucible. Repeat the rinse several times to ensure all of the residue is transferred to the filter-crucible. Filter to dryness.
- Dry the filter-crucible, "Vitrex" crucible and lid for 2 hours in the oven at 120°C.
- Cool in desiccator and reweigh the filter-crucible (weight (4)).
- Evaluate the percentage of glass content with the following equation:

$$\text{f.g.\%} = \frac{\text{weight (4)} - \text{weight (1)}}{\text{weight (2)} - \text{weight (1)}} \times 100$$

- Reweigh "Vitrex" crucible and lid. If all the residue has been transferred to the filter-crucible, this weight should be the same as weight (1).

### C. Safety

The acid digestion *MUST BE* performed in a *FUME CUPBOARD*. *SAFETY GLASSES* and *RUBBER GLOVES SHOULD BE* worn at all times when using nitric acid.

## APPENDIX 7

PROGRAM USED TO RECORD MOULDING DATA  
COMPUTER PROGRAM (BASAC)

A. Introduction

This program instructs the PDP-11/05 data logger to record during moulding the voltage outputs from the mould thermocouples, pressure transducers, displacement transducers and ram-force. Twenty readings (one control, 9 thermocouples, 6 pressure transducers, 3 displacement transducers and the compressive force) must be scanned simultaneously during each second. The readings must be recorded during the moulding cycle which lasts for approximately one minute.

The program has been written in such a way that when the memory of the computer is full, part of the data is released through the high speed puncher (72 characters per second) and hence more data can be stored. There is a compromise between the amount of data released through the high speed puncher and the time spent releasing the data. During the punching time no data can be recorded.

B. Data

The following variables must be defined in the input.

- D = Day of the experiment
- H = Hour of the experiment
- M = Minute of the experiment
- S = Second of the experiment

C. Variables

- A = Matrix where the data is stored (20 x 45)
- G = Counter of recordings
- J = Limit for the number of readings and punching data
- R = Range of scanning speed (set at 25ch/sec)
- T = Time function in seconds (in array form)
- U = Array
- V = Time in seconds

- W = Variable used as control to start the scanner  
from the test laboratory
- X = Block scanner function
- Y = Array
- Z = Function used for setting and reading the electric  
clock

#### D. Units

The units used in the program are in mm and seconds. The pressure, temperature and compressive force are in volts and must be transformed from tables into their proper units.

#### E. Channel

140 This channel is the control (W)

141 - 150 These are normal channels and can be used for pressure, displacement and compressive force

151 - 159 These channels are for temperature

#### F. Block Diagram

See following page.

#### G. Program

See following page.

#### H. Note

To use this program, delete from the compiler the extended and logarithmic functions (see manual of the computer). This is to increase the memory.



## LIST

```

10 INPUT "ENTER DATA AND TIME", I
20 INR#31, D, #31, H, #31, M, #31, S
30 LET Z=DAS(2, D, H, M, S)
40 LET I=3: LET G=1: LET J=45
50 DIM A(20, 45), T(45), X(45)
60 LET U=DAS(1, 140, 7, 2)
70 IF U<1.0 GOTO 20
80 FOR Y=1 TO J
90 LET U=0
100 LET Z=DAS(3, D, H, M, U): LET T(Y)=U
110 LET X(Y)=DAS(0, A(U, Y), 140, 159, R, 4)
120 NEXT Y
130 LET J=5
140 FOR Y=1 TO J
150 LET G=G+1: IF G>=6 GOTO 130
160 IF U=1 TO 20
170 OUT#2#41, U, #9E4, A(U, Y), I
180 NEXT Y
190 OUT#2#41, Y, #31, T(Y), I
200 NEXT Y
210 LET G=G+1: IF G>=3 GOTO 180
220 GOTO 140
230 IF J>=45 GOTO 190
240 LET J=45: GOTO 150
250 END

```

READY

APPENDIX 8  
USEFUL DATA CONCERNING THE WHOLE  
PROJECT

(For future users)

A. Introduction

The aim of this appendix is to supply information that has not been treated in the thesis, but that can be useful for future users.

This data is mainly concerned with the moulding of the four selected plates. It provides the shape of the charge for every plate and other useful information.

B. Data

The following table supplies the area of every cavity, the volume of material required and the force required based on a 3 MPa as moulding pressure.

TABLE A-8

Plate	Cavity Area (m <sup>2</sup> )	Volume of Material (m <sup>3</sup> )	Moulding Force (kN)	Charge Shape
Square	0.059	1.77 x 10 <sup>-4</sup>	177	Figure A-81
Rectangle	0.057	1.71 x 10 <sup>-4</sup>	171	Figure A-82
Square & Triangle	0.035	1.05 x 10 <sup>-4</sup>	105	Figure A-83
Trapezoid	0.042	1.24 x 10 <sup>-4</sup>	124	Figure A-84

The LP-SMC (SY19/25) has a density of 1.8 kg/dm<sup>3</sup>

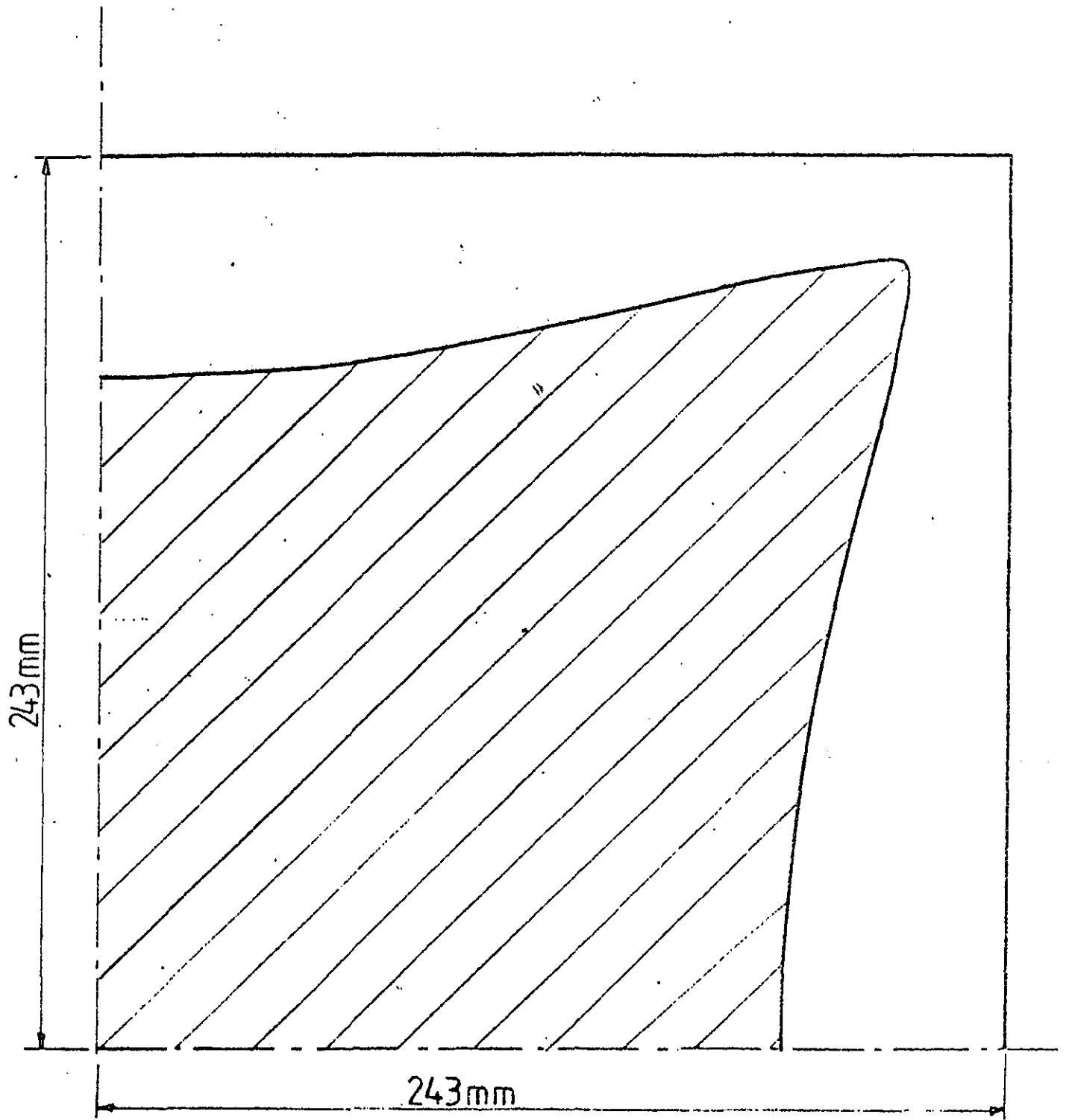


Fig.A81 CHARGE SHAPE FOR A SQUARE CAVITY

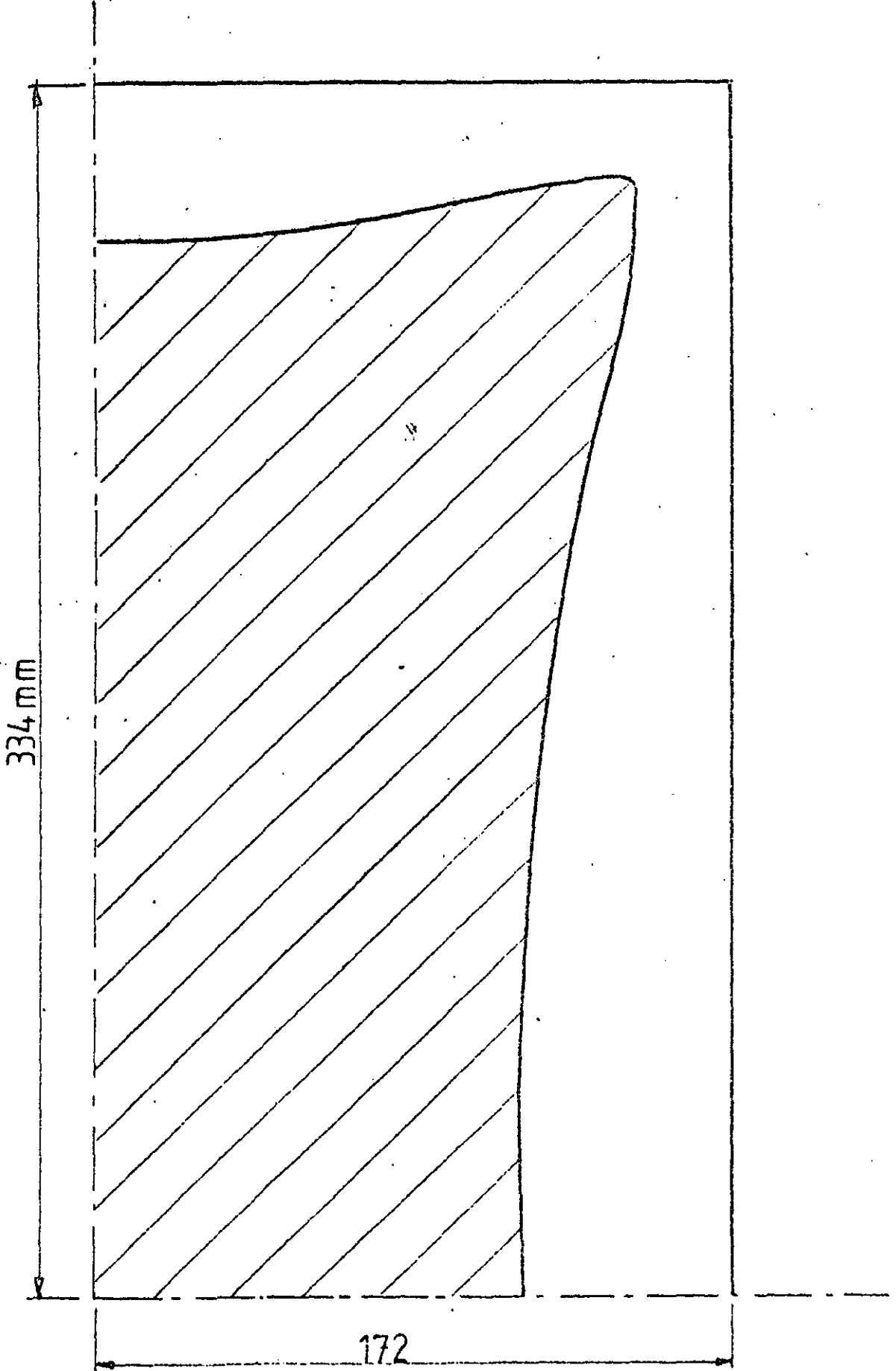


Fig.A8.2 CHARGE SHAPE FOR A RECTANGULAR CAVITY

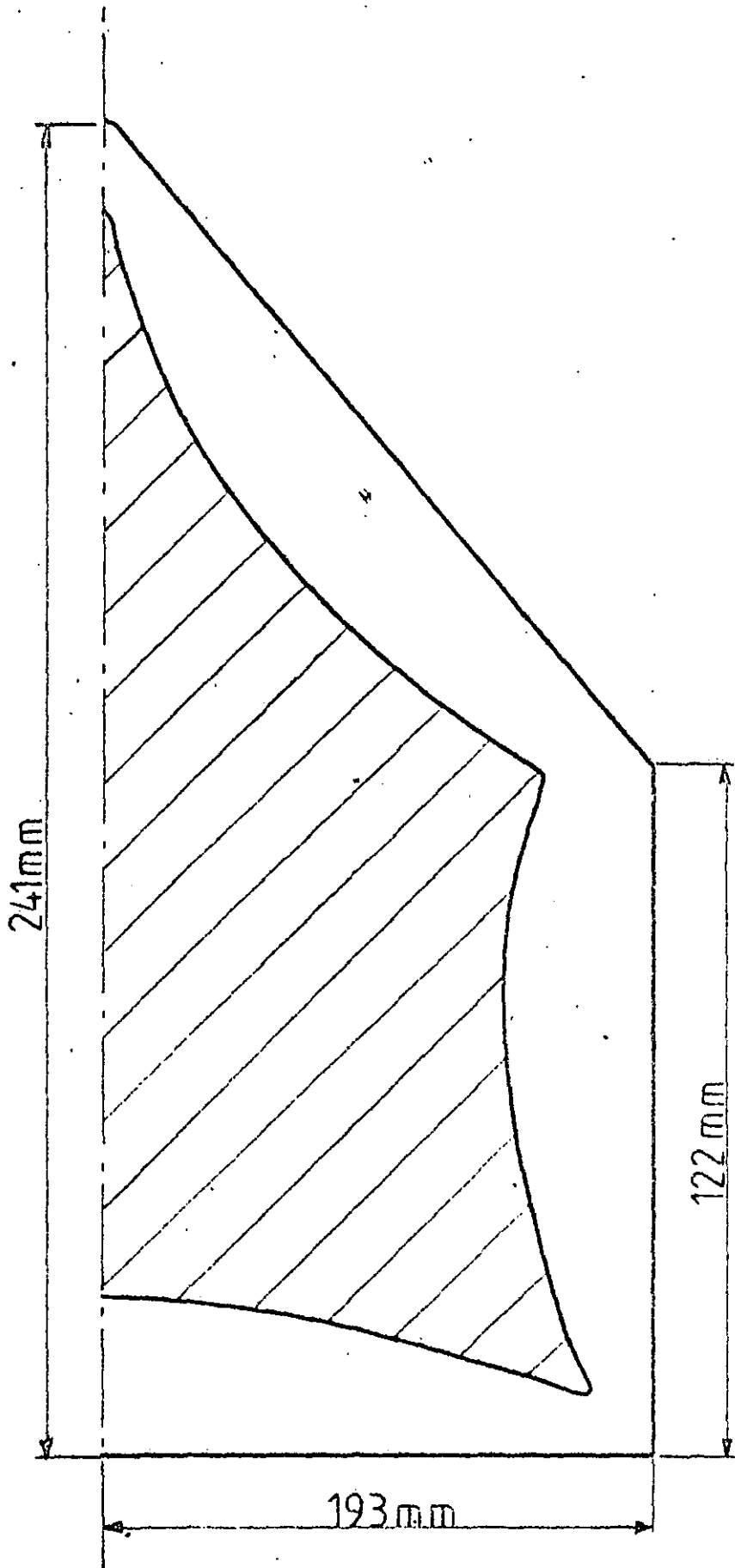


Fig.A8.3 CHARGE SHAPE FOR A SQUARE & TRIANGLE CAVITY

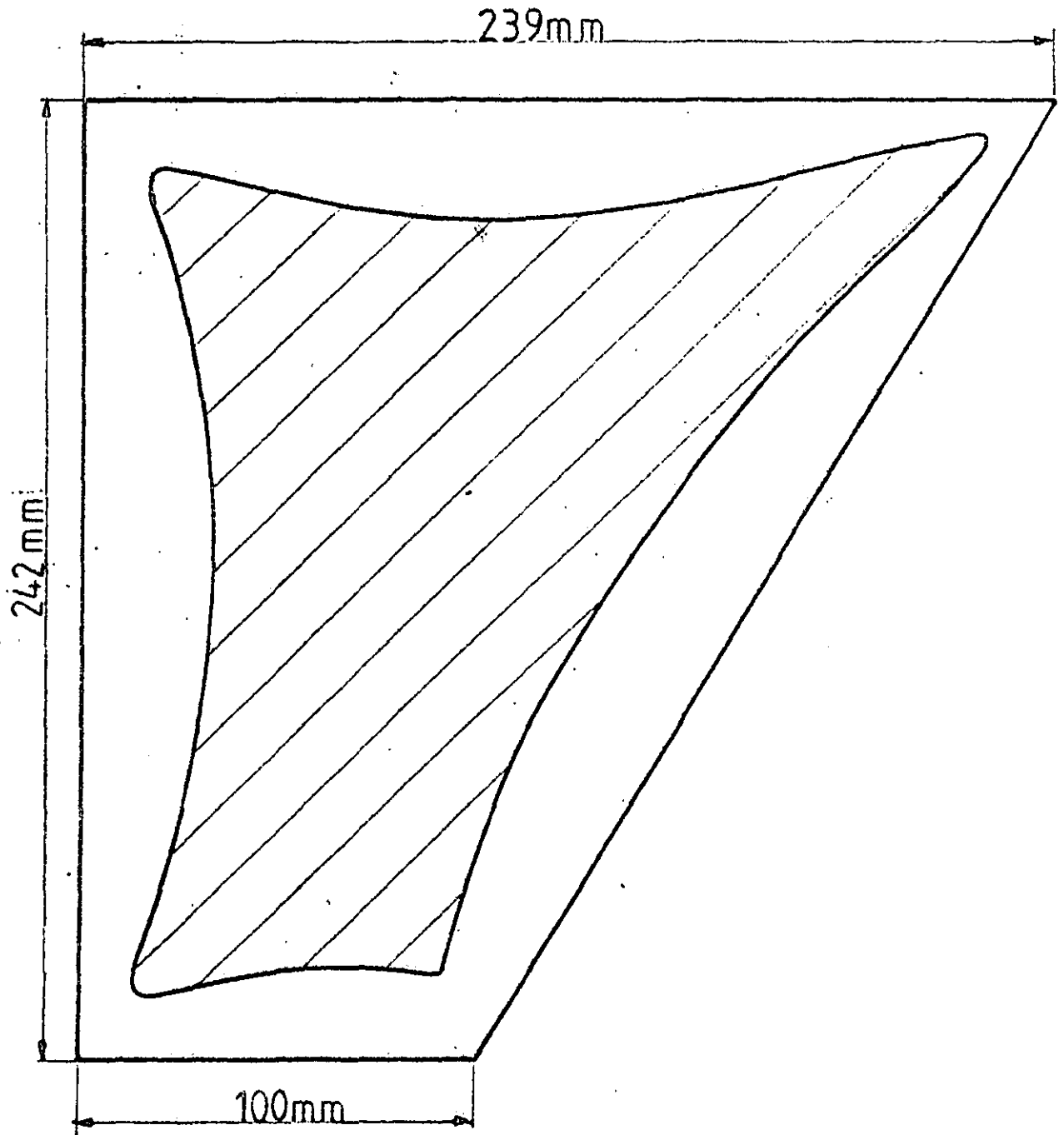


Fig.A8.4 CHARGE SHAPE FOR A TRAPEZOIDAL CAVITY

APPENDIX 9  
MOULD DRAWINGS

A. Introduction

The drawings for the manufacture of the mould are shown in this Appendix.

There are two reasons for including them in this thesis. Firstly they show the position of screws, ejectors, etc. so they are useful for future modifications of the mould. Secondly, the amount of work involved in drawing them was considerably important (4 months).

The general drawing is No. 1: in this plan all the parts are referred to with numbers. Those numbers are used in the description drawings of the corresponding part.

B. Drawings

The set of 18 drawings is shown in the following pages. Drawing No 1 is on the back of this thesis.

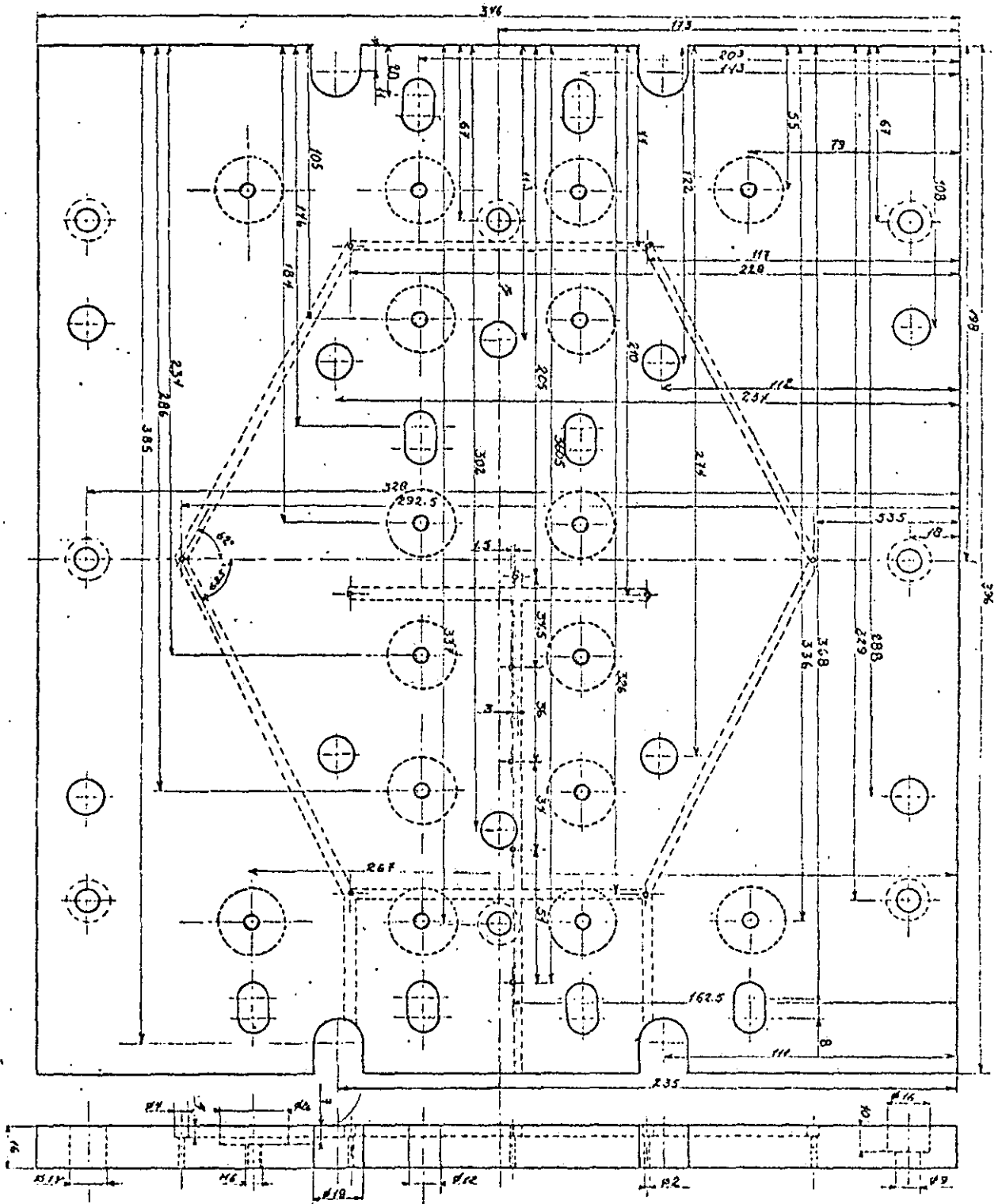
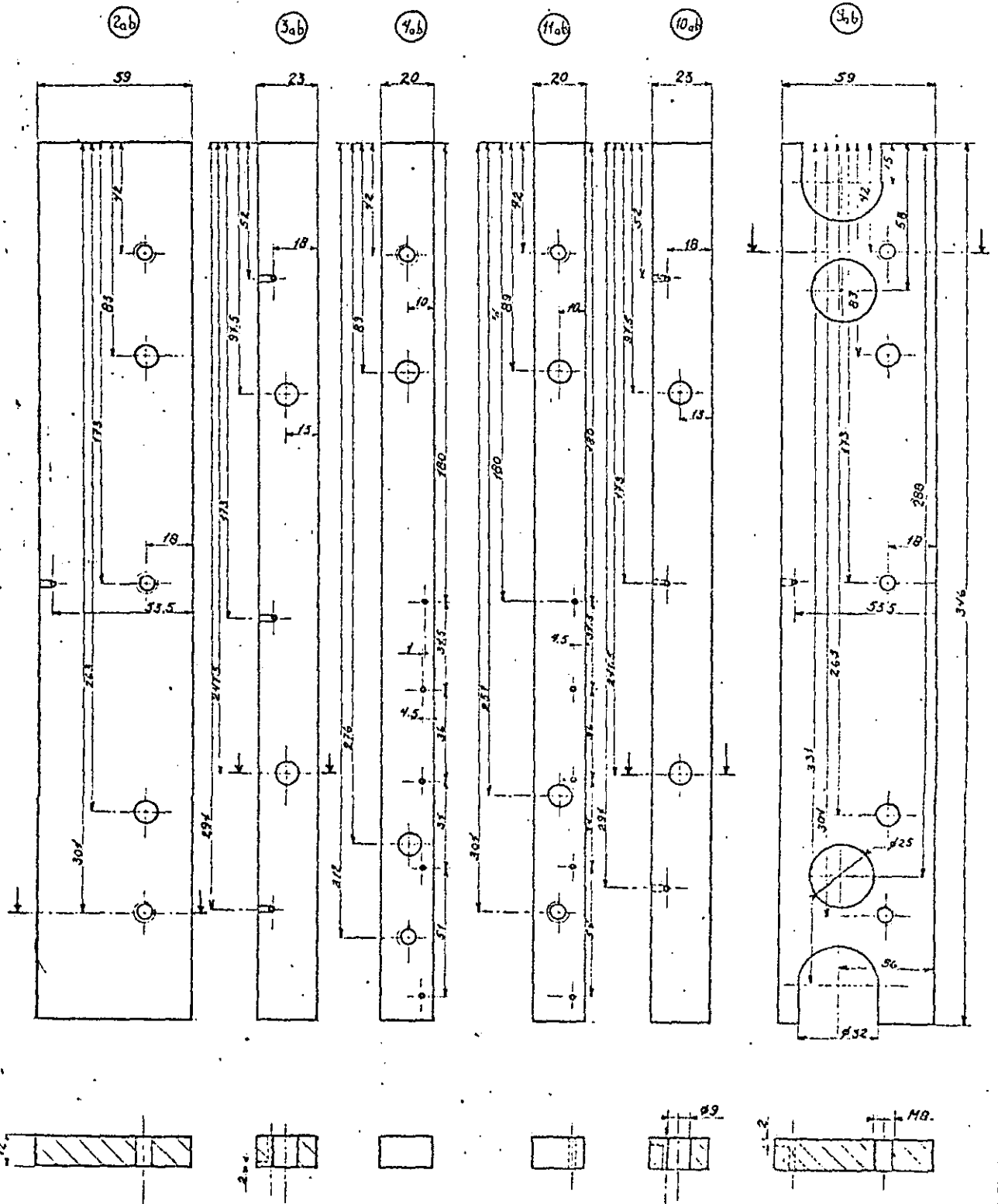
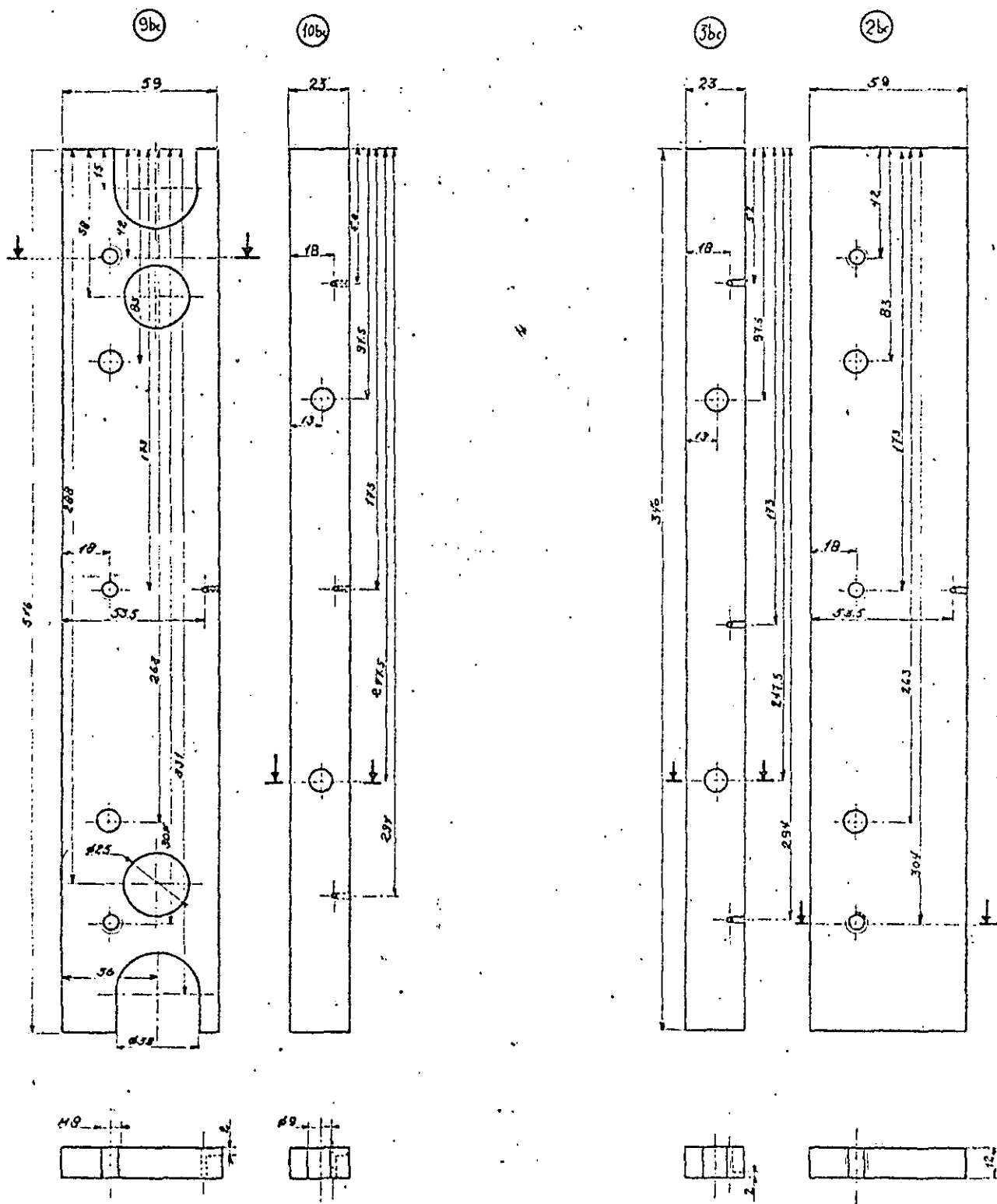


PLATE 1			IPT
Dim in mm. Scale 1:1			Pn.D. Theob
N° 2			R. S. S. S.



PLATES 2, 3, 4 (ad)			IPT
9, 10, 11			Ph D Thesis
Dim in mm	Scale 1:1	Nº 3a	R. S. S. N.



PARTS 2, 3 9, 10 (bc)			IPT
			PHOTOGRAPH
Dim in mm	Scale 1:1	N-56	R. S. VAN N.



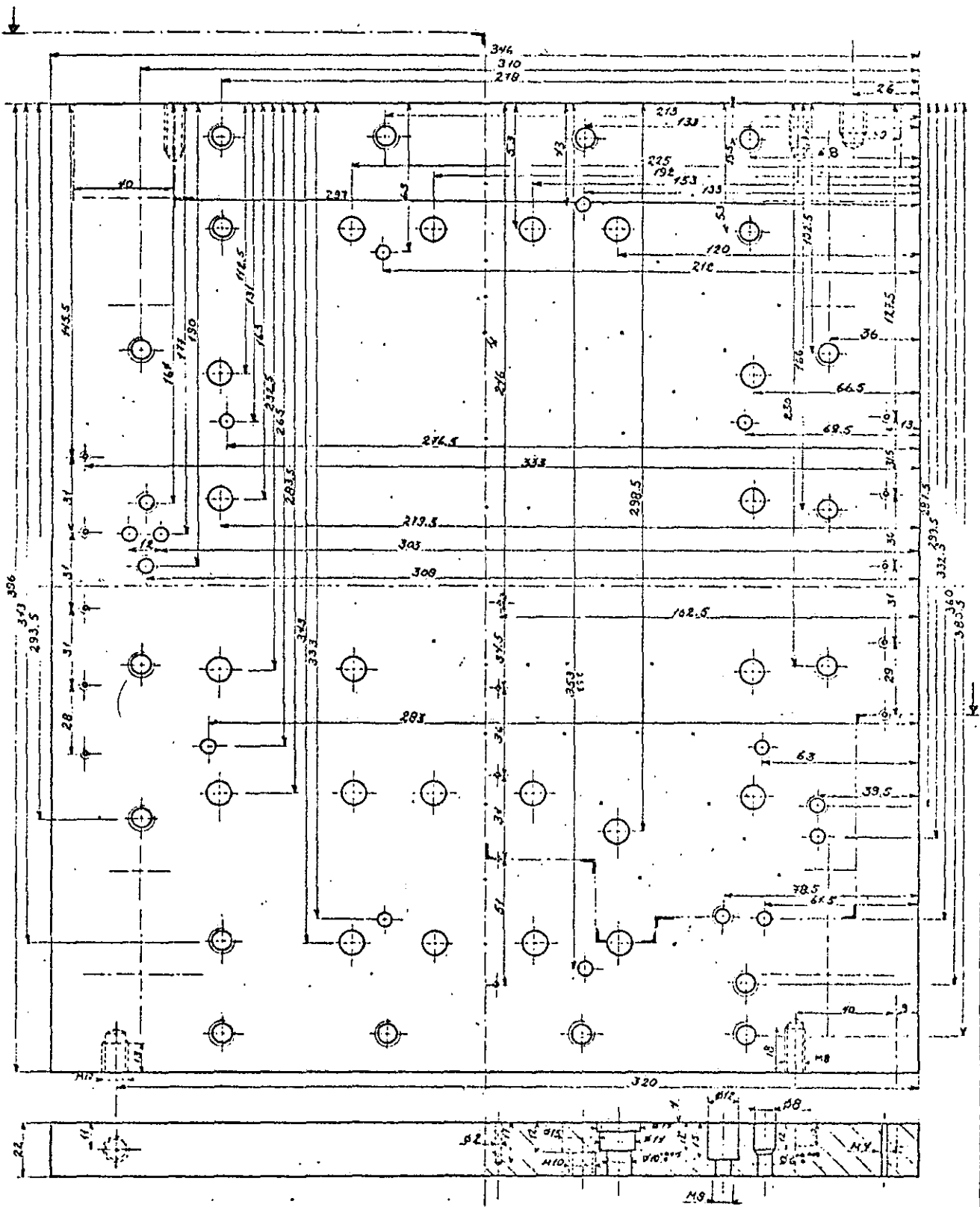


PLATE 6		IPT	
		Ph. D. Thesis	
Dim in mm	Scale 1:1	Nº 5	R SILVA-11



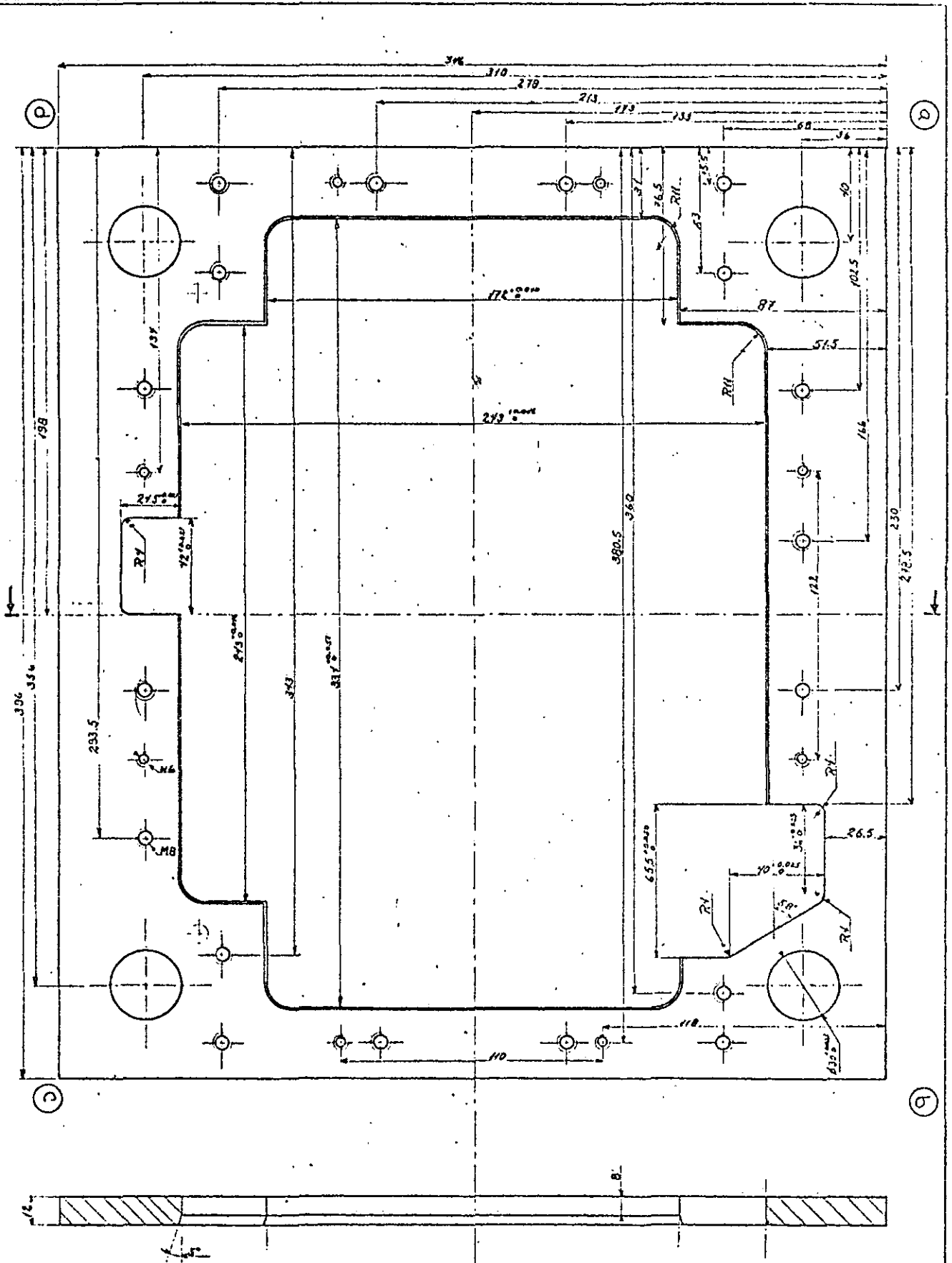


PLATE 7			IPT
			Ph. O. Thoms
Dm in mm	Scale 1:1	N. 7	R. S. v. 11



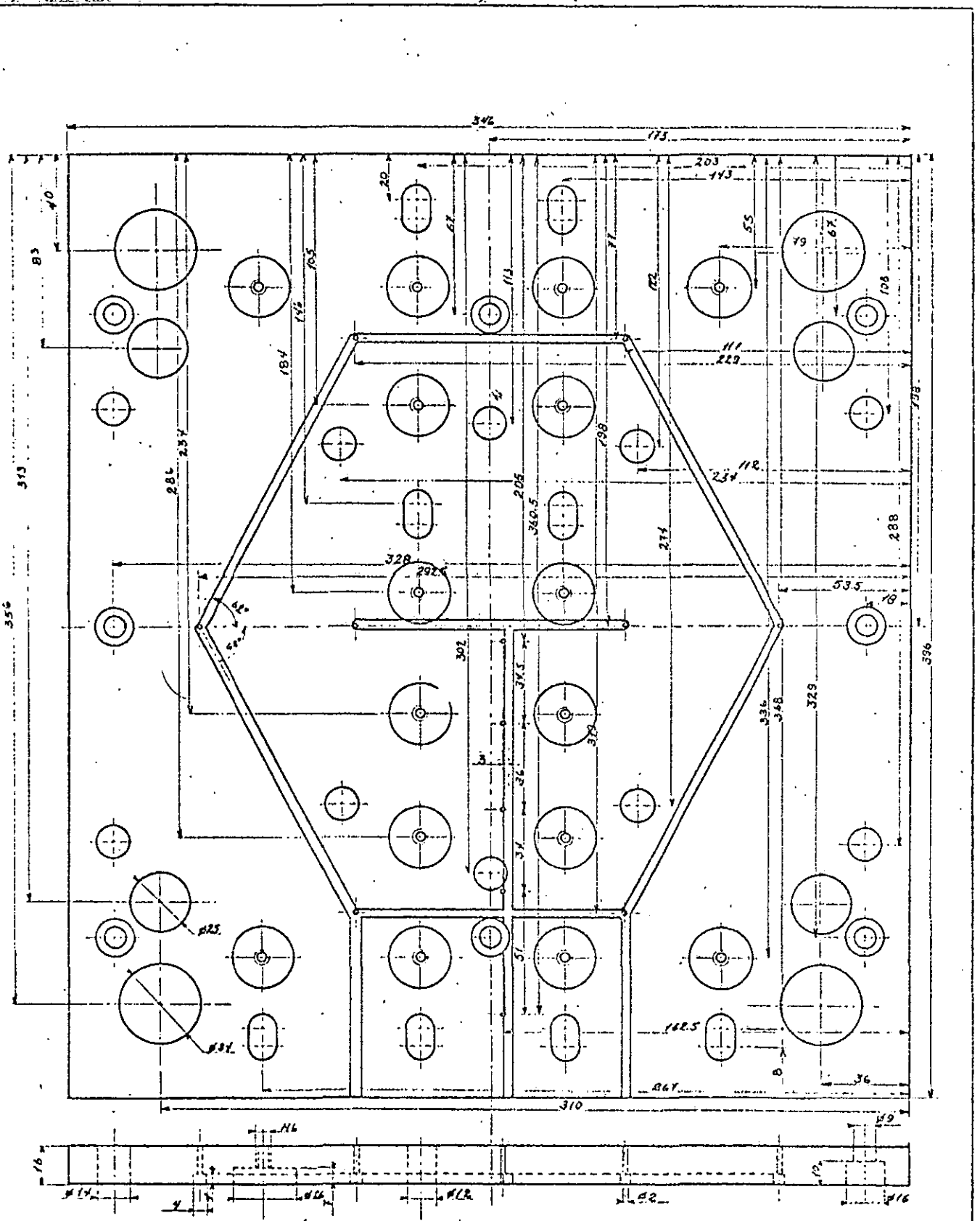
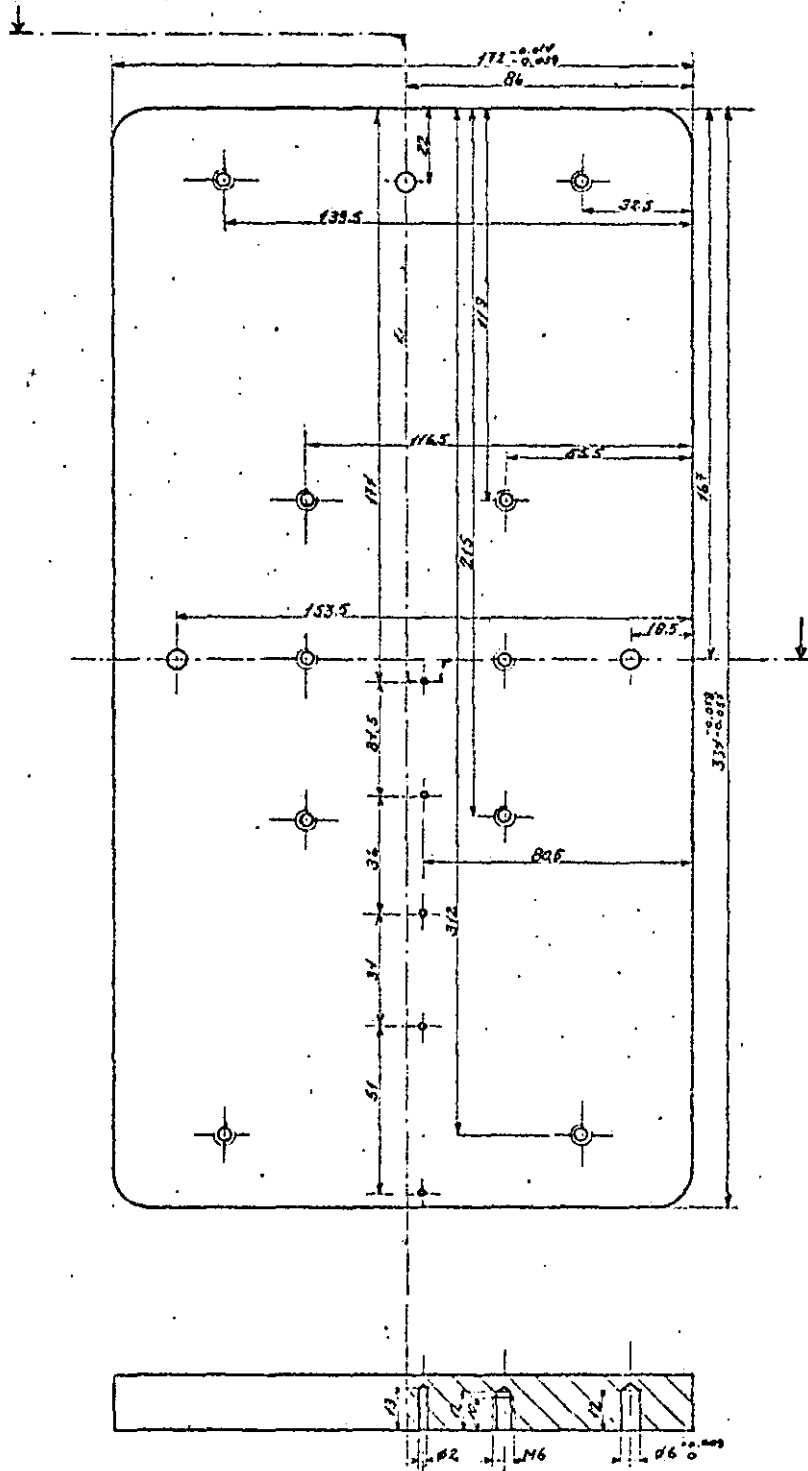


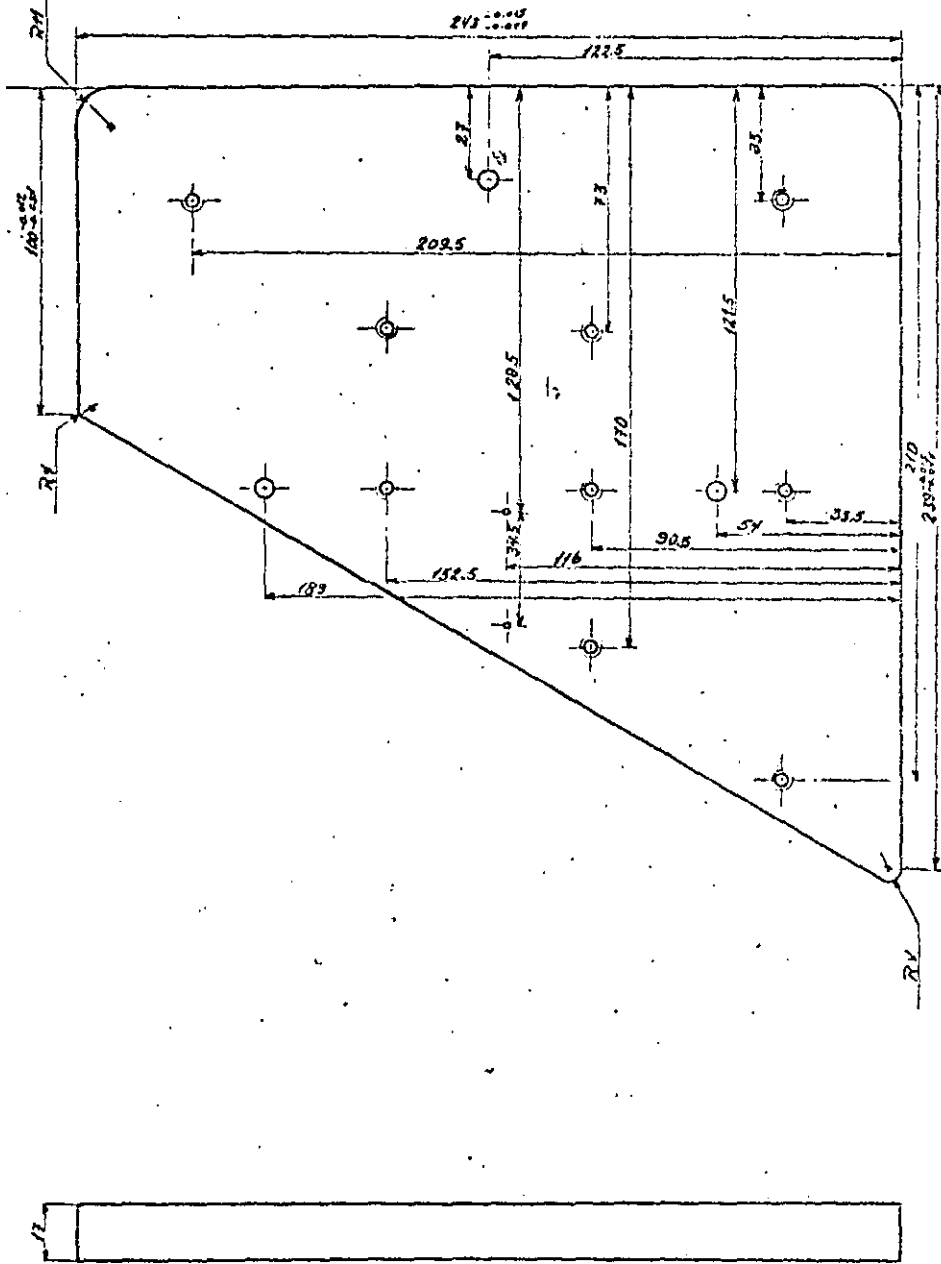
PLATE 12			IPT
			Ph D.T. 12/50
D. in mm	Scale 1:1	Nº 9	R. S. 11.11.



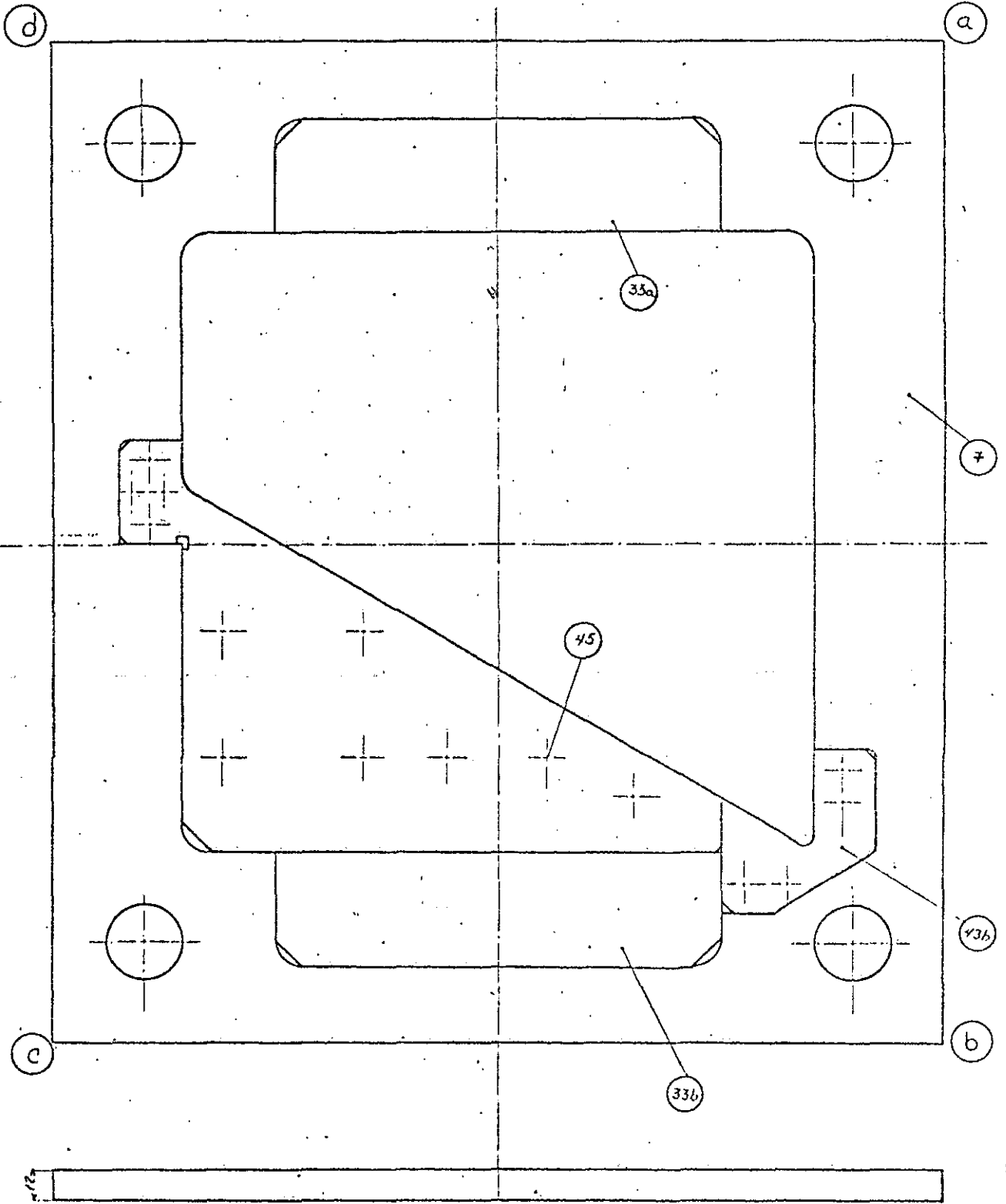


PUNCH "B" (19)			IP T
			Ph. D. Thesis
Dim in mm	Scale 1:1	N <sup>o</sup> 11	R. SILVA-N



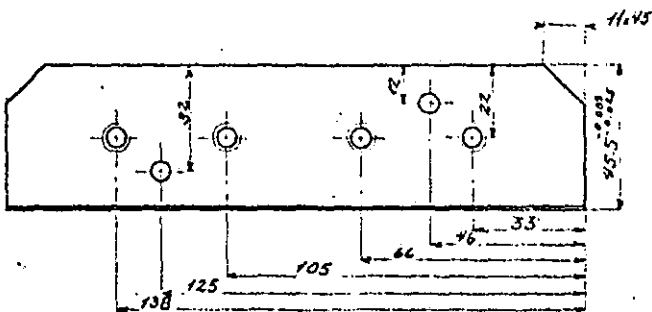
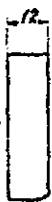


PUNCH "D" (19)			IPT
			Ph D Thresh
D= in mm	Scale 1:1	1/2" 13	R. S. S. S. S.

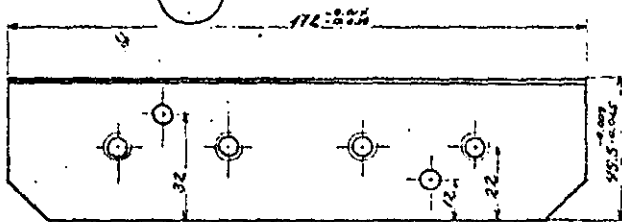
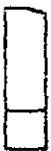


CAVITY FOR PUNCH "D"			I.P.T
			PH. D. THOMAS
Dim in mm	Scale 1:1	Nº 1/1	R. S. 11

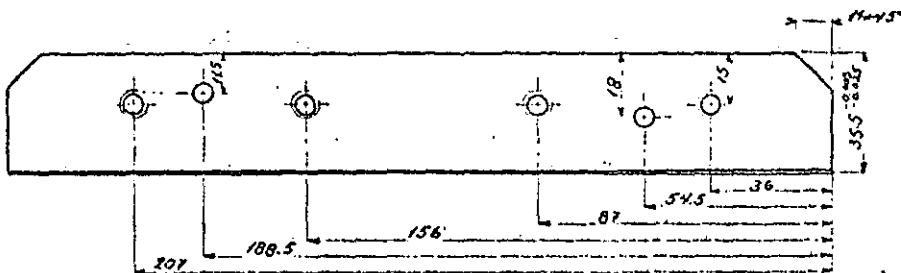
33ad



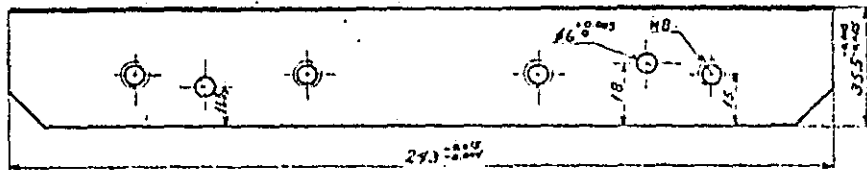
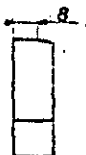
33bc



46ed



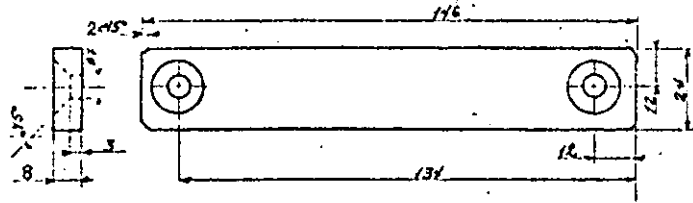
46ob



PLATES 33, 46			IPT
			PH. D. THOMAS
Dim in mm	Scale 1:1	N° 15	R. SILVA, N.

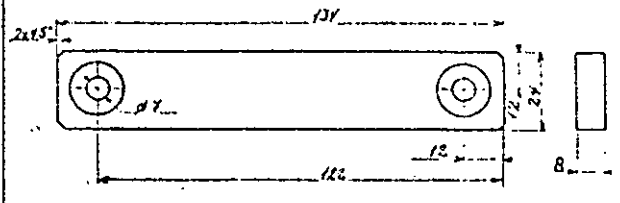






MAKE TWO PLATES (57ab, 57bc)

57ab

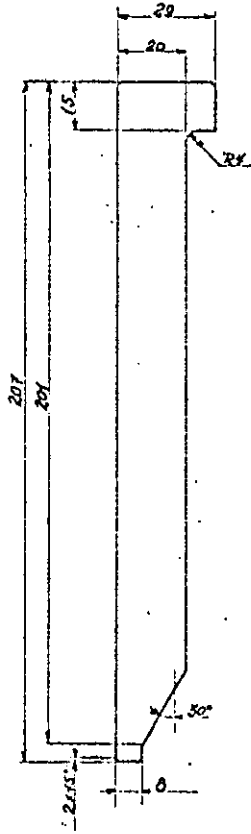


MAKE TWO PLATES (57ad, 57ba)

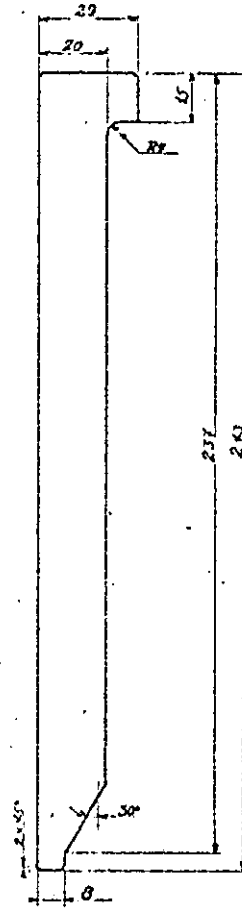
57bc

MAKE TWO PLATES (59ab, 59cd)

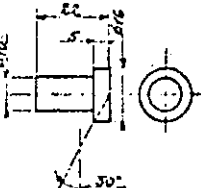
59ab



59



60



THREE Pcs

PIECES 57, 59, 60, 34			IPF
			Pl. D. Thrust
Dim in mm	Scale 1:1	N° 18	R. S. ...

APPENDIX 10  
COMPARISON OF EXPERIMENTAL FORCE V. FITTED FORCE AND  
PREDICTED FORCE

DATA:

AGE 1 MONTH OLD  
TEMPERATURE 20  
NUM OF LAYERS 1 LAYER  
WEIGHT 6.332 GRs.  
DIAMETER 40.0 MM  
COMPRESSION SPEED 0.5 CM/MIN

THE VALUE OF THE FUNCTIONS OF EQUATION 4.34

T	F1(T)	F2(T)	F3(T)
0.00000	0.0000E 00	0.0000E 00	0.0000E 00
0.94838	0.2814E 01	0.2435E 03	0.5934E 04
1.87275	0.3234E 01	0.5154E 03	0.6361E 04
2.84514	0.3759E 01	0.8442E 03	0.6858E 04

THE STANDARD ERROR OF ESTIMATE FOR THE FITTED FORCE 0.00

COMPARISON OF FORCES

T	EXP. FORCE	FITTED FORCE	PREDICTED FORCE
0.00000	0.0000E 00	0.0000E 00	0.0000E 00
0.94838	0.1957E 02	0.1956E 02	0.5801E 03
1.87275	0.4543E 02	0.4543E 02	0.7230E 03
2.84514	0.9587E 02	0.9587E 02	0.9263E 03

\*\*\*\*\*

DATA:

AGE 1 MONTH OLD  
TEMPERATURE 20  
NUM OF LAYERS 1 LAYER  
WEIGHT 6.078 GRs  
DIAMETER 40.0 MM  
COMPRESSION SPEED 0.5 CM/MIN

THE VALUE OF THE FUNCTIONS OF EQUATION 4.34

T	F1(T)	F2(T)	F3(T)
0.00000	0.0000E 00	0.0000E 00	0.0000E 00
0.19208	0.5746E 01	0.1013E 03	0.5874E 04
0.98439	0.7347E 01	0.5869E 03	0.6642E 04
1.89076	0.9885E 01	0.1308E 04	0.7705E 04

THE STANDARD ERROR OF ESTIMATE FOR THE FITTED FORCE 0.07

COMPARISON OF FORCES

T	EXP. FORCE	FITTED FORCE	PREDICTED FORCE
0.00000	0.0000E 00	0.0000E 00	0.0000E 00
0.19208	0.1304E 02	0.1304E 02	0.7694E 03
0.98439	0.6348E 02	0.6347E 02	0.1088E 04
1.89076	0.1628E 03	0.1628E 03	0.1675E 04

\*\*\*\*\*

DATA:

AGE 1 MONTH OLD  
 TEMPERATURE 20  
 NUM OF LAYERS 2 LAYER  
 WEIGHT 12.462 GRS.  
 DIAMETER 40.0 MM  
 COMPRESSION SPEED 0.5 CM/MIN

THE VALUE OF THE FUNCTIONS OF EQUATION 4.34

T	F1(T)	F2(T)	F3(T)
0.00000	0.0000E 00	0.0000E 00	0.0000E 00
0.98439	0.3171E 00	0.5946E 02	0.2795E 04
1.99280	0.3416E 00	0.1249E 03	0.2900E 04
3.02521	0.3690E 00	0.1971E 03	0.3014E 04
3.98559	0.3969E 00	0.2693E 03	0.3126E 04

THE STANDARD ERROR OF ESTIMATE FOR THE FITTED FORCE 1.86

COMPARISON OF FORCES

T	EXP. FORCE	FITTED FORCE	PREDICTED FORCE
0.00000	0.0000E 00	0.0000E 00	0.0000E 00
0.98439	0.4348E 01	0.3709E 01	0.1660E 02
1.99280	0.1065E 02	0.1244E 02	0.2804E 02
3.02521	0.2891E 02	0.2718E 02	0.4441E 02
3.98559	0.4652E 02	0.4709E 02	0.6451E 02

\*\*\*\*\*

DATA:

AGE 1 MONTH OLD  
 TEMPERATURE 20  
 NUM OF LAYERS 2 LAYER  
 WEIGHT 12.547 GRS  
 DIAMETER 40.0 MM  
 COMPRESSION SPEED 1.0 CM/MIN

THE VALUE OF THE FUNCTIONS OF EQUATION 4.34

T	F1(T)	F2(T)	F3(T)
0.00000	0.0000E 00	0.0000E 00	0.0000E 00
0.91236	0.6845E 00	0.1149E 03	0.2913E 04
1.88475	0.7921E 00	0.2554E 03	0.3134E 04
2.85714	0.9207E 00	0.4174E 03	0.3379E 04

THE STANDARD ERROR OF ESTIMATE FOR THE FITTED FORCE 0.27

COMPARISON OF FORCES

T	EXP. FORCE	FITTED FORCE	PREDICTED FORCE
0.00000	0.0000E 00	0.0000E 00	0.0000E 00
0.91236	0.1217E 02	0.1217E 02	0.3571E 02
1.88475	0.4870E 02	0.4869E 02	0.7043E 02
2.85714	0.1413E 03	0.1413E 03	0.1239E 03

\*\*\*\*\*

DATA:

AGE 1 MONTH OLD  
 TEMPERATURE 20  
 NUMBER OF LAYERS 2 LAYER  
 WEIGHT 12.343 GRs  
 DIAMETER 40.0 MM  
 COMPRESSION SPEED 2.0 CM/MIN

THE VALUE OF THE FUNCTIONS OF EQUATION 4.34

T	F1(T)	F2(T)	F3(T)
0.00000	0.0000E 00	0.0000E 00	0.0000E 00
0.88836	0.1469E 01	0.2288E 03	0.2993E 04
1.77671	0.1936E 01	0.5252E 03	0.3436E 04

THE STANDARD ERROR OF ESTIMATE FOR THE FITTED FORCE 0.30

COMPARISON OF FORCES

T	EXP. FORCE	FITTED FORCE	PREDICTED FORCE
0.00000	0.0000E 00	0.0000E 00	0.0000E 00
0.88836	0.8239E 02	0.8239E 02	0.7412E 02
1.77671	0.3072E 03	0.3072E 03	0.1801E 03

\*\*\*\*\*

DATA:

AGE 1 MONTH OLD  
 TEMPERATURE 20  
 NUM OF LAYERS 3 LAYERS  
 WEIGHT 18.815 GRs.  
 DIAMETER 40.0 MM  
 COMPRESSION SPEED 0.5 CM/MIN

THE VALUE OF THE FUNCTIONS OF EQUATION 4.34

T	F1(T)	F2(T)	F3(T)
0.00000	0.0000E 00	0.0000E 00	0.0000E 00
0.48019	0.9052E-01	0.1269E 02	0.1835E 04
1.45258	0.9489E-01	0.3930E 02	0.1878E 04
2.40096	0.9939E-01	0.6648E 02	0.1922E 04
3.38535	0.1043E 00	0.9604E 02	0.1970E 04
4.44178	0.1100E 00	0.1294E 03	0.2022E 04
5.28211	0.1147E 00	0.1571E 03	0.2065E 04

THE STANDARD ERROR OF ESTIMATE FOR THE FITTED FORCE 1.61

COMPARISON OF FORCES

T	EXP. FORCE	FITTED FORCE	PREDICTED FORCE
0.00000	0.0000E 00	0.0000E 00	PROGRAM
0.48019	0.4348E 01	0.3742E 01	IFAIL
1.45258	0.5000E 01	0.6984E 01	PREDICT
2.40096	0.1783E 02	0.1614E 02	NEGATIVE FOR
3.38535	0.3326E 02	0.3264E 02	
4.44178	0.5761E 02	0.5919E 02	
5.28211	0.8826E 02	0.8759E 02	

\*\*\*\*\*

DATA:

AGE 1 MONTH OLD  
 TEMPERATURE 20

NUM OF LAYERS 3 LAYER  
 WFIGHT 19.424 GRG  
 DIAMETER 40.0 MM  
 COMPRESSION SPEED 1.0 CM/MIN

THE VALUE OF THE FUNCTIONS OF EQUATION 4.34

T	F1(T)	F2(T)	F3(T)
0.00000	0.0000E 00	0.0000E 00	0.0000E 00
0.99040	0.1844E 00	0.5243E 02	0.1881E 04
1.95678	0.2024E 00	0.1085E 03	0.1971E 04
2.89316	0.2219E 00	0.1680E 03	0.2064E 04

THE STANDARD ERROR OF ESTIMATE FOR THE FITTED FORCE 0.27

COMPARISON OF FORCES

T	EXP. FORCE	FITTED FORCE	PREDICTED FORCE
0.00000	0.0000E 00	0.0000E 00	PROGRAM
0.99040	0.9130E 01	0.9130E 01	IFAIL
1.95678	0.4022E 02	0.4021E 02	PREDICT
2.89316	0.9630E 02	0.9630E 02	NEGATIVE FOR

\*\*\*\*\*

DATA:

AGE 1 MONTH OLD  
 TEMPERATURE 20  
 NUM OF LAYERS 3 LAYER  
 WEIGHT 19.182 GRG  
 DIAMETER 40.0 MM  
 COMPRESSION SPEED 5.0 CM/MIN

THE VALUE OF THE FUNCTIONS OF EQUATION 4.34

T	F1(T)	F2(T)	F3(T)
0.00000	0.0000E 00	0.0000E 00	0.0000E 00
1.36685	0.1645E 01	0.4810E 03	0.2490E 04
2.43970	0.3048E 01	0.1169E 04	0.3389E 04

THE STANDARD ERROR OF ESTIMATE FOR THE FITTED FORCE 0.40

COMPARISON OF FORCES

T	EXP. FORCE	FITTED FORCE	PREDICTED FORCE
0.00000	0.0000E 00	0.0000E 00	0.0000E 00
1.36685	0.5635E 03	0.5635E 03	0.7962E 02
2.43970	0.7491E 03	0.7491E 03	0.4272E 03



STOR-A-FILE IMAGING LTD

---

**PLANS  
TAKEN  
FROM  
HERE**

Date: 12/02/08

Authorised by: Simon Cockbill

Issue 2

Page 1 of 1

**If in hard copy, this page is UNCONTROLLED and only valid on date of issue 22-Feb-08**